UC Davis

UC Davis Electronic Theses and Dissertations

Title

Epigenetic Signatures of Prenatal Exposures and their Relevance to Autism Spectrum Disorders

Permalink

https://escholarship.org/uc/item/408372kv

ISBN

9798189235177

Author

Williams, Logan Allan

Publication Date

2026-06-25

Peer reviewed|Thesis/dissertation

eScholarship.org Powered by the California Digital Library
University of California

Epigenetic Signatures of Prenatal Exposures and their Relevance to Autism Spectrum Disorders

By

LOGAN ALLAN WILLIAMS

DISSERTATION

Submitted in partial satisfaction of the requirements for the degree of

DOCTOR OF PHILOSOPHY

in

Integrative Genetics and Genomics

in the

OFFICE OF GRADUATE STUDIES

of the

UNIVERSITY OF CALIFORNIA DAVIS

Approved:

Janine M. LaSalle, Chair

Rebecca J. Schmidt

C. Titus Brown

Committee in Charge

2026

Table of Contents

ACKNOWLEDGEMENTS ..... **VI**

ABSTRACT ..... **XI**

ABBREVIATIONS ..... **XIII**

LIST OF TABLES ..... **XV**

LIST OF FIGURES ..... **XV**

CHAPTER 1: INTRODUCTION **1**

1.1 Preface 1

1.2 Authorship 1

1.3 An overview of Autism Spectrum Disorder 1

1.4 On genetic etiologies of Autism Spectrum Disorder 3

1.5 Environmental exposures, epigenetics, and Autism Spectrum Disorder 4

1.5.1 Epigenetic markers of ASD in the brain *6*

1.5.2 Epigenetic markers of ASD in peripheral tissue *9*

1.6 Research objectives and contributions 12

CHAPTER 2: PRENATAL CELL-FREE DNA METHYLOME DETECTS ASSOCIATION WITH AUTISM AND MATERNAL OBESITY **14**

2.1 Preface 14

2.2 Authorship 14

2.3 Abstract 15

2.4 Introduction 15

2.5 Results 18

2.5.1 Study design and subject characteristics *18*

2.5.2 Fetal sex-stratified cfDNA methylomes reveal ASD-associated DMRs enriched in neurodevelopmental pathways. *20*

2.5.3 CfDNA ASD DMR genes are enriched for known autism risk genes and developmentally dynamic loci. *23*

2.5.4 CfDNA methylation patterns mirror ASD-associated DMRs in placenta and cortex. *24*

2.5.5 MO DMRs in cfDNA are detectable in ASD relevant gene pathways and enriched in ASD DMRs of both fetal sexes. *29*

2.6 Discussion 34

2.7 Methods 40

2.7.2 Cell-free DNA extraction and whole-genome bisulfite sequencing (WGBS) *41*

2.7.3 WGBS alignment and quality control *42*

2.7.4 Detection of DMRs *43*

2.7.5 Principal component analysis of smoothed DMR methylation *46*

2.7.6 Global methylation averages between male and female samples *47*

2.7.7 DMR enrichment analysis *47*

2.7.8 DMR overlap analysis *48*

2.7.9 SFARI enrichment analysis *49*

2.7.10 Developmentally differentially methylated genes overlap analysis *49*

2.7.11 Chromatin state enrichment analysis *50*

2.8 Data and Code Availability 50

2.9 Supplemental Material 51

2.9.1 Supplemental Figures *51*

2.9.2 Supplemental Tables *94*

CHAPTER 3: PLACENTAL DNA METHYLATION GENE NETWORKS ASSOCIATE WITH WILDFIRE PARTICULATE MATTER EXPOSURE AND CHILD NEURODEVELOPMENTAL OUTCOMES. **96**

3.1 Preface 96

3.2 Authorship 96

3.3 Abstract 96

3.4 Introduction 98
3.5 Methods 102
3.5.1 Study cohort *102*
3.5.2 Wildfire air pollution measurement *105*
3.5.3 DNA isolation from placenta and whole genome bisulfite sequencing *106*
3.5.4 WGBS alignment and quality control *108*
3.5.5 Placental cell type composition estimates *109*
3.5.6 Comethylation network generation and annotation *109*
3.5.7 Correlating comethylation module eigennodes with sample traits *112*
3.5.8 Differentially methylated region detection *112*
3.5.9 Global methylation averages *114*
3.5.10 DMR enrichment analysis *114*
3.5.11 Gene list overlap analysis, SFARI enrichment analysis, and DMR region overlap analysis *115*
3.5.12 Chromatin state enrichment analysis *116*
3.6 Results 117
3.6.1 Comethylation networks were identified in placenta and displayed expected topologic features *117*
3.6.2 Wildfire air pollution is correlated with modules of placenta comethylation in patterns distinct from non-wildfire derived air pollution *119*
3.6.3 Placenta comethylation networks correlate differently with preconception versus pregnancy wildfire-informed particulate exposures *125*
3.6.4 Comethylation modules associated with air pollution and child developmental outcomes contain multiple genes previously tied to autism etiology. *128*
3.6.5 Sex-stratified placental methylomes reveal wildfire exposure associated differentially methylated regions enriched in neurodevelopmental pathways *132*
3.7 Discussion 136
3.8 Conclusion 142

3.9 Data and code availability 143

3.10 Supplemental Material 144

3.10.1 Supplemental Figures *144*

3.10.2 Supplemental Tables *176*

CHAPTER 4: CONCLUSION 177

4.1 Summary of Work 177

4.2 Future Directions 178

4.2.1 Longitudinal analysis of the cfDNA methylome in relation to ASD *178*

4.2.2 Identifying markers of smoke exposure in adult blood plasma, with a focus on cancer risk assessment *179*

4.2.3 Future prospects for epigenetics in Autism Spectrum Disorder *180*

4.3 Conclusion 189

REFERENCES 191

Acknowledgements

First and foremost, I would like to extend my deepest gratitude to Dr. Janine LaSalle and Dr. Rebecca Schmidt, my co-PI's throughout the entirety of my graduate degree. From year one to year six, both asked essential questions and provided critical feedback that enabled me to perform the best experiments I possibly could. Janine's eternal wellspring of relevant publications in combination with her ability to focus on the most interesting questions our set of data could answer elevated my research and my writing substantially. Rebecca, thank you for your eternal patience in explaining the intricacies of epidemiological research to a complete novice such as myself. Your management prowess facilitated the connection of epidemiologic data to epigenomic data, and without that none of the research in this dissertation would have been possible. Furthermore, both Rebecca and Janine were stalwart advocates for me and my career interests throughout graduate school, even when those interests diverged from their own experiences. I am exceptionally privileged to have been their student.

In addition to my co-PI's, I am deeply grateful for the support of Dr. C. Titus Brown, who served both on my Dissertation Committee and my Qualifying Exam Committee. Titus combines a remarkable technical expertise with a stalwart devotion to student well-being and reproducible analysis that improves the quality of research of everyone who works with him. Without his reassurance that bioinformatics was accessible to anyone with the will to learn it, I may never have been able to ask the kinds of questions central to this dissertation.

Also deserving of acknowledgment is Dr. Dag Yasui, who supported and assisted my wet lab experiments in innumerable ways throughout my graduate school career. No matter what unexpected technical or logistical problem I encountered while performing my experiments, Dag was always able to provide a clear-headed suggestion of the next best steps. All the experiments done in the LaSalle lab are improved by Dag's feedback and recommendations, and I'm grateful my own experiments are among this list.

Beyond my mentors at UC Davis, I would also like to thank Dr. Javin Oza for offering me my first real opportunity to be a part of the scientific process as an undergraduate research assistant. Javin entrusted undergraduates with a remarkable amount of responsibility, and my wet lab skills would not be what they are today without my experiences in his lab.

While their influence on my career took place outside of the halls of academia, I would also like to thank my coworkers and mentors at Roche Sequencing Solutions and DuPont Industrial Biosciences. Specifically, I would like to thank Dr. James Blau and Dr. Virgil Rhodius for serving as my mentors during my time at Roche and DuPont, respectively. James and Virgil provided me all the support a summer intern could ask for and made my brief industry experiences disproportionately impactful. My belief in the power of biotechnology to make peoples' lives better is derived from these experiences, and I look forward to turning that belief into reality throughout the course of my career.

I am fortunate to have been surrounded by many remarkable peers in the LaSalle Lab, and their support has been a boon to my research and mental health alike. There are too many names and too little paper to properly recognize everyone in full, but I would like to thank a few individuals specifically. Dr. Yihui Zhu, whose work on placenta WGBS

laid the groundwork for my own and whose commitment to her research remained even after she completed her PhD. Dr. Antonio Gomez, who provided an example of rigorous science and healthy mentorship coexisting. Dr. Osman Sharifi, a man with near-infinite patience for my early bioinformatic stumbling. He has a knack for asking insightful questions about whatever research project is being presented to him, and his questions have improved my work more times than I can count. Dr. Aron Judd Mendiola, who is perhaps the most mentorship-focused scientist I have had the pleasure of working with. AJ's wholehearted belief that the best science is done in an environment of peers with diverse viewpoints engaging in intellectually rigorous analysis is an inspiration to myself, and I can think of no one better suited to engage in the work of science policymaking. Dr. Julia Mouat, who exemplified intense commitment to one's research. Dr. Viktoria Haghani, who joined the LaSalle Lab at the same time as me, has proven herself time and time again to be an exceptional computational biologist with a deep drive for teaching others. Thank you for answering all my computational queries without fail, from the astute to the absurd. Dr. Jessica Huang, who balances demanding cell culture work with the demands of her students. Her passion for teaching and care for her students gives me faith in the future of academia. Dr. George Kuodza, who has shown adaptability and tenacity in his transition from M.D to postdoctoral researcher. Dr. Ensieh Habibi, whose contributions to my analysis of cell-free DNA data are invaluable. The LaSalle Lab would not be able function without the tireless efforts of our lab manager, and I would like to recognize Christina Torres, Abigail Humphries, and Sophia Hakam for their essential work in this role. All three of them are superb scientists and organizers whose diligent work supports the entire lab team. Additional thanks to Kelly Chan, He Yang, Judy Abuel, Giovanni

Pimentel-Solorio, Matt Kramer, Taylor Tran, Emily Thrall, Rohan Marde, Sylvia Holesinger, and Vanessa Su for all their questions and commentary on my research.

In addition to my mentors and peers throughout the scientific community, I am deeply grateful for the support of my friends, who have shaped me both as a scientist and as a person over many decades. I would like to thank my longtime friends Kyler Silverman, Sijay Liu, and Adrian Huang, all of whom have pushed me to be the best possible version of myself whether in the lab or around the board game table. To all my brothers in Alpha Chi Sigma's Gamma Zeta chapter at Cal Poly SLO, thank you for accepting a biologist into your chemistry fraternity and for cultivating an environment of academic excellence with connections as strong as a double bond. To all the members of the Florilegium Collaborative, for welcoming a newcomer to Davis into your community with open arms and joyful hearts. I would also like to highlight the Presbyterian Church of Los Gatos and thank both the staff and the congregation for welcoming a teen with an overabundance of questions into their community and always making him feel like he had a home there.

Also deserving of thanks are my family, who have helped mold me into the man I am today. My grandparents, Bob Kaercher, Pat Kaercher, Steve Williams, and Ann Williams, all of whom nurtured my curiosity about the world throughout my life. My aunts and uncles, Mark Williams, Stacy Williams, Kirsten Bookman, Tommy Bookman, Megan Winger, and Andy Winger, who cheered me on through every step of my academic odyssey. Thanks as well to the entirety of the Khoobyarian family, who have supported and mentored me for decades.

Words are insufficient to express my gratitude for my parents, Ron and Patrice Williams. Both have supported my development as a scientist and as a human being in ways too myriad to fully recall, and I am infinitely grateful for their presence in my life. Dad, thank you for promoting my curiosity by saving me every newspaper clipping and online article about new scientific advancements you knew I might find fascinating. Mom, thank you for encouraging me to think about my future more actively, and for helping me realize that a career in the sciences was possible.

I would also like to express my appreciation for my brother, Jared Williams, who has been my lifelong mentor and advocate in fields innumerable. Jared has taught me many things throughout my life, from how to play more assertive defense in basketball to the most optimal route back home from high school. However, I am most grateful for the lesson he taught by example: how to be a caring and impactful mentor to those who look up to you.

Finally, my endless gratitude and love belong to my wife, Kathryn Williams. Kathryn, your presence in my life is the source of countless joys. For over a decade, you have been my greatest supporter, my constant confidant, and my best friend. You endure my endless excited ramblings on the progress of my research, asking questions and giving me grace when I forget to explain an acronym for the umpteenth time. You are my wellspring of laughter and hope in hard times, never letting me stew over setbacks for too long. You are my reminder to appreciate every finite moment of happiness that comes our way, and you are the origin of more of those moments than you could possibly know. All the components of our life together, including my research, are made better by your influence, and it is the greatest fortune of my life to call myself your husband.

Abstract

After decades of investigation into the genetics of autism spectrum disorder (ASD), a consensus in the field persists that ASD likelihood is too heterogenous to be diagnosed by a single set of genetic variants. A growing catalogue of environmental exposures have been found to associate with ASD likelihood, though the biological mechanisms driving potential interactions between these exposures and ASD remain elusive. This dissertation investigates epigenetics, specifically DNA methylation, as a potential biological mediator between environmental exposures linked to ASD, with the aim of identifying epigenetic signatures of these prenatal exposures and examining their overlap with and relevance to ASD neurodevelopment.

Chapter 1 provides an overview of the known genetic and epigenetic etiologies of ASD, discussing previously discovered epigenetic markers linked to ASD development to frame expected findings in later chapters.

Chapter 2 reports whole genome bisulfite sequencing of cell-free DNA from a prospective ASD cohort study, identifying overlapping differentially methylated regions (DMRs) associated with both ASD diagnosis and maternal obesity (MO). Comparing ASD-associated methylation profiles in cell-free DNA to those identified in placenta and cortex, it highlights conserved epigenetic markers of ASD across tissues. Functional pathway enrichment analysis of the ASD and MO-associated DMRs reveals concentration in pathways critical to synapse development and cell signaling, biological pathways whose potential epigenetic dysregulated by MO could confer increased likelihood of ASD.

Chapter 3 describes whole genome bisulfite sequencing of placenta DNA from both a prospective ASD cohort study and a prenatal wildfire exposure study, used to generate comethylation networks and detect clusters of genomic regions with methylation patterns associated with both neurodevelopmental outcomes and air pollution. This chapter dissects the different modules of comethylated regions associated with ambient air pollution compared to wildfire-derived air pollution and identifies DMRs corresponding to prenatal exposure to extreme wildfire events. Examining the gene ontology of comethylated modules associated with both ASD and air pollution, it describes epigenetic dysregulation of pathways involved in cell signaling, chromatin architecture, and neurodevelopment broadly as potential axes of increased ASD likelihood.

Chapter 4 summarizes these findings and extrapolates on future lines of inquiry into the characteristics and impacts of epigenetic profiles linked to environmental exposures and ASD.

Abbreviations

ADI-R = Autism Diagnosis Interview - Revised

ADOS = Autism Diagnostic Observation schedule

ASD = autism spectrum disorder

BMI = body-mass index

B-SAFE = Bio-Specimen Assessment of Fire Effects

CBCL = Child Behavior Check List

CfDNA = cell-free DNA

CffDNA = cell-free fetal DNA

CpG = cytosine-phosphate-guanine site

DhMRs = differentially hydroxymethylated regions

DMR = differentially methylated region

DSM = Diagnostic and Statistical Manual of Mental Disorders

GO = gene ontology

GREAT = Genomic Regions Enrichment of Annotations Tool

KEGG = Kyoto Encylopedia of Genes and Genomes

MARBLES = Markers of Autism Risk in Babies – Learning Early Signs

MO = maternal obesity

MSEL = Mullen Scales of Early Learning

$PM_{2.5}$ = particulate matter of less than 2.5 micrometer diameter

SFARI = Simons Foundation Autism Research Initiative

WGBS = whole-genome bisulfite sequencing

WUI = wildfire-urban interface

List of Tables

2.1 DMRs in the five genes from the female-specific cross-tissue ASD DMR gene list which have concordant genic annotation and methylation directionality

List of Figures

1.1 Epigenetic profiles of ASD across tissues

2.1 WGBS of cfDNA in a prospective autism cohort study enables prenatal detection of ASD-associated differentially methylated regions (DMRs)

2.2 ASD DMRs are detectable in cfDNA and show strong enrichment for synaptic gene pathways

2.3 ASD DMRs identified from placenta and cortex WGBS exhibit shared characteristics with cfDNA DMRs

2.4 Overlap analysis of cfDNA ASD DMRs with placenta and cortex ASD DMRs

2.5 MO DMRs in cfDNA share substantial overlaps with ASD DMRs, while maintaining unique enrichments for inflammatory pathways

3.1 A flowchart describing sample inclusion in this study from MARBLES and B-SAFE participants.

3.2 Visualization of the placenta comethylation network

3.3 Comethylation network module ~ trait heatmap correlations

3.4 Highlight module ~ trait correlations of a module with divergent associations with wildfire and ambient air pollution exposures

3.5 Highlighted air pollution-associated module ~ trait correlations and GO enrichments

3.6 Highlighted air pollution and neurodevelopment outcome-associated module ~ trait correlations and GO enrichments

3.7 Wildfire exposure DMR visualization and enrichment analysis

4.1 A model for epigenetic substratification of ASD

4.2 A model for epigenetic biomarker-mediated early intervention in ASD cases

4.3 A model for mechanistic investigation of epigenetic variants in ASD

Chapter 1: Introduction

1.1 Preface

Sections 1.3-1.5 of this chapter adapt material from the manuscript *Future Prospects for Epigenetics in Autism Spectrum Disorder* by myself and Dr. Janine M. LaSalle, published in Molecular Diagnosis & Therapy on August 13th, 2022. Janine M. LaSalle and I conceived, planned, and wrote the manuscript together. It has been modified to meet the formatting requirements of this dissertation.

1.2 Authorship

Logan A. Williams and Janine M. LaSalle

1.3 An overview of Autism Spectrum Disorder

Autism spectrum disorder (ASD) is a diagnosis that encompasses a group of neurodevelopmental disorders characterized by persistent impairments in social interaction and language together with repetitive patterns of behavior and interests (1). While the term autism was first coined by Eugen Bleuer in 1911 to describe a purported symptom of schizophrenia characterized by a fixation on a fantastical and imaginative inner life, the contemporary definition of ASD as described in the Diagnostic and Statistical Manual of Mental Disorders (DSM)-5 acts as an amalgamation of numerous

conditions defined as pervasive developmental disorders under the DSM-4 (2,3). As such, while people diagnosed with ASD exhibit shared impairments to social interaction, communication problems, restricted interests, and stereotyped behaviors, the magnitude of each of these symptoms can vary dramatically between individuals.

Despite this heterogeneity, decades of epidemiologic studies have revealed numerous details of ASD's prevalence and impact. ASD is the second most common neurodevelopmental disorder observed in the United States, with 1 in every 31 children being diagnosed with ASD by 8 years of age (4,5). This represents a nearly 5-fold increase in ASD prevalence from when the CDC first began reporting in 2000 (6). ASD is approximately 3.4 times as common in male children than female children (5). Nearly 70% of individuals with ASD have psychiatric comorbidities, including social anxiety and attention deficit/hyperactivity disorder, whose own behavioral traits can mask underlying ASD (7–9). True to its name as a 'spectrum' disorder, outcomes for individuals with ASD are varied, and many adults with ASD live independently and find full-time employment (10,11). Nevertheless, adults with ASD are more likely to be unemployed (12), less likely to live independently (13), are more likely to suffer from mental health disorders than the neurotypical population (14).

Early diagnosis and behavioral interventions have been shown to improve quality of life outcomes for individuals with ASD (15). However, diagnosis of ASD is entirely behavioral, making early life diagnosis difficult and subject to interpretation even under the application

of “gold standard” diagnostic tools with the Autism Diagnostic Observation Schedule (ADOS) and the Autism Diagnostic Interview-Revised (ADI-R) (16). Considering this challenge, increased focus has been applied to potential underlying biological etiologies of ASD development, and their potential to act as quantifiable biomarkers of ASD likelihood and severity

1.4 On genetic etiologies of Autism Spectrum Disorder

While a sizable body of literature has firmly established a genetic component of ASD, an exact estimate of the condition’s heritability remains elusive. ASD exhibits a 58%-90% concordance rate in monozygotic twins (17,18), though heritability estimates and specific genetic risk factors for ASD vary dramatically between studies (19–22). While many chromosomal rearrangements and single-gene disorders have been definitively associated with ASD, each of these more discrete genetic causes are attributable to less than 2% of the total ASD population (23). This suggests an understanding of ASD’s genetic component as deeply polygenic, with ASD development being attributable to the cumulative effects of numerous impacted loci acting in concert to produce an atypical developmental phenotype. Delineation of the genetic architecture underlying ASD, particularly in syndromic forms attributable to single-gene causes, has been critical for identifying etiologic mechanisms of the disorder; however genetic variation alone cannot account for the full phenotypic variation, variable penetrance, and population-level prevalence of ASD (24,25).

Epigenetics, literally meaning “on top of genetics”, is defined as alterations to DNA or chromatin that can alter gene expression without a change to the DNA sequence. DNA methylation, which collectively refers to methyl groups added at cytosine bases in DNA, is the most investigated epigenetic mark in human tissues, and as such will be the focus of further discussion in this manuscript. As a multifactorial disorder, ASD development is often a result of the interplay between genetic and environmental factors, which is what DNA methylation marks are frequently reflecting. Thus, a complete understanding the molecular etiology of ASD requires knowledge of both genetics and epigenetics associated with the condition.

1.5 Environmental exposures, epigenetics, and Autism Spectrum Disorder

The insufficiency of solely considering genetic risk factors for the purpose of understanding ASD etiology has prompted a plethora of investigations into the environmental factors contributing to ASD development (26). Various maternal medical conditions, including maternal pre-pregnancy BMI (27), diabetes (28), and hypertension (29) have been shown to increase risk of ASD. Perinatal exposure to some common environmental pollutants, such as air pollution (30), and pesticides (31) have also shown an association with increased ASD risk. Some differences in maternal nutrients, including maternal iron supplement consumption (32) and maternal use of folic acid and multivitamin supplements (33), have also been shown to have potential protective effects against ASD development. These environmental exposures are often hypothesized to act

at least partially through epigenetic mechanisms (34–38), though the tissue-specific and temporally-influenced nature of epigenetic modifications can make repeated observation of epigenetic markers of ASD difficult. Despite these inherent challenges, some progress has been made in identifying DNA methylation patterns from multiple tissue sources that distinguish ASD from typically developing controls (Figure 1.1).

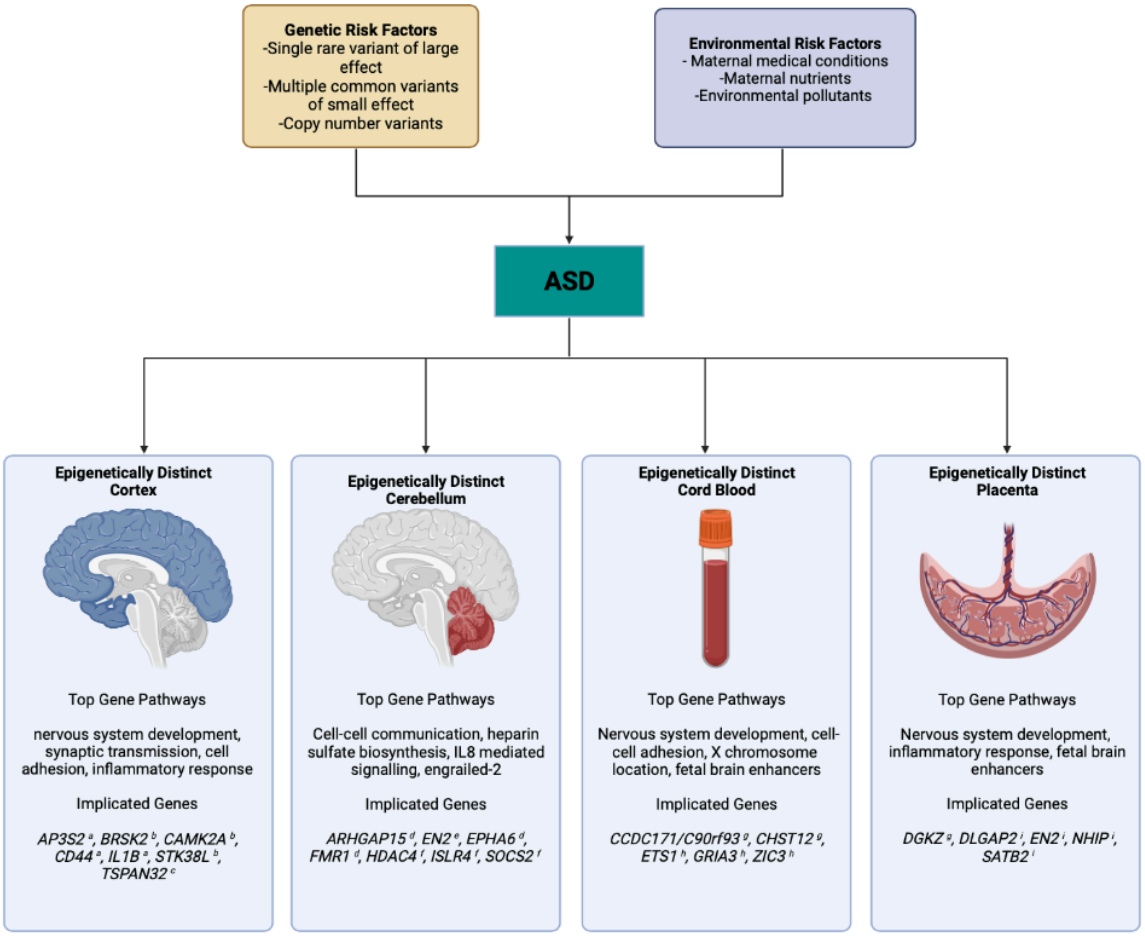


Figure 1.1: A summary of multiple genetic and environmental risk factors implicated in ASD that can be informed by distinct epigenetic profiles in both postmortem brain and perinatal tissues collected prior to diagnosis. *ASD* autism spectrum disorder, *AP3S2*

adaptor related protein complex 3 subunit sigma 2, *ARHGAP15* Rho GTPase activating protein 15, *BRSK2* brain-specific serine/threonine-protein kinase 2, *CAMK2A* calcium/calmodulin dependent protein kinase II alpha, *CCDC1171/C90rf93* coiled coil domain containing 171, *CD44* CD44 molecule (Indian blood group), *CHST12* carbohydrate sulfotransferase 12, *DGKZ* diacylglycerol kinase zeta, *DLGAP2* DLG associated protein 2, *EN2* engrailed homeobox 2, *EPHA6* EPH receptor A6, *ETS1* ETS proto-oncogene 1 transcription factor, *FMR1* fragile X messenger ribonucleoprotein 1, *GRIA3* glutamate ionotropic receptor AMPA type subunit 3, *HDAC3* histone deacetylase 3, *IL1B* interleukin 1 beta, *ISLR4* immunoglobulin superfamily containing leucine rich repeat, *NHIP* neuronal hypoxia inducible placenta associated, *SATB2* SATB homeobox 2, *SOCS2* suppressor of cytokine signaling 2, *STK38L* serine/threonine kinase 38 like, *TSPAN32* tetraspanin 32, *ZIC3* Zic family member 3. a.) Wong, C. C. Y. et. al (2019). b.) Nardone, S., et. al (2017). c.) Ladd-Acosta, C. et. al (2014). d.) Cheng, Y. et. al (2018). e.) James, S. J., et. al (2013). f.) Corley, M. J. et. al (2019). g.) Bakulski, K. M. et. al (2021). h.) Mordaunt, C. E. et. al (2020). i.) Zhu, Y. et. al (2022).

1.5.1 Epigenetic markers of ASD in the brain

The neurodevelopmental origin of ASD makes post-mortem human brain tissue the most relevant tissue to provide direct epigenetic links between environmental exposures and altered genes in ASD. Insights gained from epigenetic changes associated with ASD in the brain therefore serve as the standard against which epigenetic data from other tissues are compared. Epigenomic analysis of post-mortem ASD brain DNA has focused largely on the cortex and cerebellum, as these regions of the brain have been implicated in prior

examination of neural abnormalities associated with ASD and are more commonly available from public brain banks. Among the most common methods for studying ASD epigenetics is the methylation array, which is manufactured to target regions of epigenetic interest in humans and uses hybridization-based fluorescent signaling to determine whether a given target nucleotide is methylated (39–44). Despite the relative scarcity of available ASD brain tissue for investigations, methylation array-based analyses of epigenetic changes in the ASD brain have revealed many differences at individual CpGs or differentially methylated regions (DMR). These analyses rarely identify global differences in DNA methylation between ASD and control brains, regardless of the brain region surveyed.

Cerebral cortex has been the brain tissue of focus for multiple array-based ASD methylome analyses. For instance, Wong *et al*. (2019) extracted DNA from post-mortem prefrontal cortex and temporal cortex to perform region co-methylation network analysis, revealing multiple co-methylation modules significantly associated with ASD diagnosis (41). Gene ontology (GO) pathway analysis of these co-methylation modules revealed them to be enriched for pathways relating to immune functionality, synaptic signaling and regulation, and post-synaptic density, with these enrichments reflecting the known dual contributions of immune and neuronal dysregulation associated with ASD (45,46). Using an alternative approach of whole genome bisulfite sequencing (WGBS), Vogel Ciernia *et al.* found similar gene pathway enrichments in ASD cortex, focusing on microglia as the source of the inflammatory signal (47). Other array-based methylomic studies of ASD cortex have similar findings. Ladd-Acosta *et al.* (2014) reported three differentially

methylated regions (DMRs) in ASD temporal cortex, with these DMRs being proximal to genes involved in neuronal and immune pathways as well as maintaining imprinting patterns (48). Nardone *et al.* (2014) identified differentially methylated CpGs in ASD prefrontal cortex samples, with GO analysis revealing hypomethylated CpGs enriched for immune functions and hypermethylated CpGs enriched for neuron-neuron synaptic activity (49). Further ASD methylomic analysis of the sorted nuclei from frontal cortex neurons revealed differential regions of comethylation that were enriched for synaptic, neuronal, GABAergic and immune processes (50).

Methylomic analyses of cerebellum has shown similar general findings, with differences in genic locations of ASD differences. Corley et. al (2019) performed DNA methylation analysis of the subventricular zone, a component of the cerebellum that serves as a source of neuronal stem cells, and reported differentially methylated loci (DML) in ASD samples (43). The observed DML were underrepresented at promoter regions and overrepresented at gene bodies and intergenic sequences, with GO analysis of the ASD-related DMLs showing enrichment of genes involved in neuron proliferation, differentiation, and migration. A targeted investigation of the ASD-associated and neurodevelopmentally linked *EN2* gene by James et. al (2013) identified significant hypermethylation in the *EN2* promoter region of ASD cerebellum samples relative to non-ASD samples (51). In addition to ASD DMRs being identified in the cerebellum, differentially hydroxymethylated regions have been observed as well. Hydroxymethylated cytosines are the result of Tet protein interaction with methylated cytosines, and have been implicated to function in a manner unique from methylated cytosines in some

biological functions (52). In Cheng et. al (2018), the authors screened for differentially hydroxymethylated regions (DhMRs) between ASD and non-ASD cerebellum, and identified 797 DhMRs (53). GO analysis of the 181 DhMRs that were identified in intragenic regions were found to be significantly enriched for ASD-implicated pathways like ‘cell-cell communication’ and ‘heparan sulfate biosynthesis’, and *cis* functionality of the 599 intergenic DhMRs associated with ASD was predicted.

1.5.2 Epigenetic markers of ASD in peripheral tissue

While studies of ASD-specific differential methylation in the brain are limited due to low sample availability, methylomic analysis of peripheral tissues do not suffer this same limitation. A wide range of investigations into DNA methylation patterns associated with ASD in non-neuronal tissue have been performed, with many of these studies using either ASD blood or maternal placenta as sources of DNA. While these peripheral tissue studies are less informative about consequential methylomic changes associated with ASD than studies on brain tissue, blood methylation levels at specific loci have been shown to be correlative with brain tissue methylation in prior studies (54,55), and placental methylation levels have likewise been shown to associate with child ASD diagnosis (56–59).

Blood samples from individuals diagnosed with ASD versus matched controls offer an easily accessible sample type for interrogating the ASD epigenome, but questions have been raised about how well alterations in blood reflect the brain. ASD blood samples were

demonstrated to have an impaired metabolic capacity for methylation (60), sparking further interest. Investigations of potential associations between blood DNA methylation and ASD have shown modest associations (61–63). Of particular note is Andrews et. al (2018), where the authors conducted a the largest methylome wide association study on blood DNA ever performed, using samples from 1,654 children (61). No single CpG surveyed in this study was identified as being significantly associated with ASD, though seven CpGs passed the much lower threshold for suggestive association. A study from a fairly small subset of ASD-discordant monozygotic twin pairs showed some significant differentially methylated genes, with the significance of association decreasing when comparing ASD to non-ASD individuals more broadly (64). Furthermore, the methylation chip used in this study screened for nearly 19X fewer CpG sites than the chips used in future studies, including Andrews et. al 2018 (65). While blood DNA methylation profiles may well contain ASD-associated DMRs in small subsamples of highly genetically similar individuals, contemporary studies have shown them to be ill-suited to examining large and heterogenous groups.

In contrast to the somewhat limited utility of blood methylation studies from ASD patients, recent prospective investigations into the methylome of ASD placental, cord blood, and maternal blood samples have identified some consistent epigenetic changes that exist prior to the diagnosis of ASD. This is not particularly surprising given the importance of the placental *in utero* environment for fetal neurodevelopment (66,67). Mordaunt et. al (2020) performed whole genome bisulfite sequencing (WGBS) of cord blood from a high risk ASD cohort and identified 2,299 DMRs across male and female samples, with ASD-

associated DMRs being significantly enriched for methyl-sensitive developmental transcription factors that play a role in fetal neurodevelopment (68). Sex-stratified DMRs associated with ASD were found to be highly enriched for X chromosome location, implying a potential epigenetic etiology to ASD's male bias. Further implication of the role of the methylome in ASD development was reported by Zhu et. al (2022), where the authors performed WGBS of placenta samples and observed an ASD-associated 118kb hypomethylated region at 22q13.33 (59). This hypomethylated region was comprised of ASD-associated DMRs that were significantly enriched for multiple fetal brain enhancers and a novel gene named *NHIP*, for neuronal hypoxia-inducible, placenta associated. Bakulski et. al (2021) assessed the methylomes of both cord blood and placenta, finding nominally ASD-associated DMPs that corelated across both tissues (58). Additionally, these DMPs were highly enriched for SFARI ASD risk genes. The authors also assessed the methylation of maternal whole blood DNA and found ASD DMPs that overlapped with those identified in placenta and cord blood. These results contribute to emerging evidence of conserved regions of cross-tissue methylomic profiles associated with neuropsychiatric disorders like ASD (55,56,68,69)

It is noteworthy that much of the existing methylomic analyses of ASD DNA (both in brain and peripheral tissues) are limited by the relatively narrow focus of the commercially available methylation array platforms. The vast majority of contemporary methylomic studies assess methylation with Illumina HumanMethylation450 or Infinium MethylationEPIC platforms, which provide coverage of only ~1.5-3% of all CpG sites in the human genome (65). The targeted regions were determined by expert panels prior to

whole methylome maps based on sequencing, introducing additional bias for particular regions of the genome with the least variation in methylation (70,71). As an example, >80% of the ASD-associated DMRs identified in cord blood by WGBS did not overlap with a single probe represented on the Illumina HumanMethylation450 or Infinium MethylationEPIC platforms (68). While these methylation array platforms do provide broad coverage of Refseq genes and CpG islands, the limited scope of their query should be kept in mind when considering potential ASD-differential methylation patterns outside of these locations.

1.6 Research objectives and contributions

The primary objective of the research presented in this dissertation is to investigate the epigenetic markers of ASD both in isolation and in the context of possible environmental risk factors. To this end, this manuscript details the identification of differentially methylated genomic regions in cell-free DNA from ASD pregnancies, explores the degree to which those regions replicate epigenetic signals of ASD observed in other tissues, and compares them to differentially methylated regions identified in associated with the known ASD risk factor of maternal obesity (MO) to identify potential pathways of convergent epigenetic dysregulation tying MO exposure to ASD outcomes (Chapter 2). Additionally, I describe the results of placenta comethylation network analysis in association with wildfire-informed air pollution measures, report on a subset of comethylation modules associated with both air pollution and neurodevelopmental outcomes, and discuss a shared implication of cell signaling and signal transduction that may connect air pollution exposure to increased likelihood of ASD development (Chapter 3). The findings presented

here provide new insights into the epigenetic connections between prenatal environmental exposures and ASD development, presenting a plethora of candidate regions and loci for future mechanistic studies to target, ultimately improving our understanding of ASD etiology at the molecular level.

Chapter 2: Prenatal cell-free DNA methylome detects association with autism and maternal obesity

2.1 Preface

This chapter contains original research that is currently undergoing peer review for publication. It has been modified to meet the formatting requirements of this dissertation. I isolated cfDNA and prepared whole genome bisulfite sequencing libraries for all samples described in this manuscript and executed all bioinformatic and statistical analyses related to the identified DMRs. Ensieh Habibi performed enrichment analyses of the DMRs relative to chromatin state. Meghan Miller oversaw all behavioral assessments of MARBLES participants used in this manuscript's analyses. Irva Hertz-Picciotto conceived of the MARBLES study itself. Cheryl K. Walker assisted with the recruitment of MARBLES participant mothers and the sample collection. Rebecca J. Schmidt, Janine M. LaSalle, and I conceived of the experiments and analyses described in this manuscript.

2.2 Authorship

Logan A. Williams, Ensieh Habibi, Meghan Miller, Irva Hertz-Picciotto, Cheryl K. Walker, Rebecca J. Schmidt, and Janine M. LaSalle

2.3 Abstract

Early identification of autism spectrum disorder (ASD) remains a critical challenge, particularly in utero when non-genetic factors such as maternal obesity (MO) are implicated. Here, we report results of whole-genome bisulfite sequencing of cell-free DNA (cfDNA) from third-trimester maternal plasma in a high-likelihood ASD pregnancy cohort associated with child (3 y) ASD diagnosis and/or MO. Differentially methylated regions (DMRs) between ASD and control cfDNA were strongly enriched for synaptic functions and genes previously implicated in ASD. These cfDNA ASD DMRs recapitulated those observed in ASD placenta and postmortem cortex and significantly overlapped with MO DMRs. Our findings establish cfDNA methylation derived from maternal blood as a minimally invasive window into fetal brain ASD etiology, providing a framework for future mechanistic and early intervention studies. Future studies could investigate additional prenatal environmental exposures interacting with genetics during neurodevelopment.

2.4 Introduction

In the United States, autism spectrum disorder (ASD) is diagnosed in 1 in 31 children, a figure representing a more than four-fold increase in prevalence over the last two decades (5,72). Characterized by persistent deficits in social communication in combination with restrictive and repetitive patterns of behavior and interests, ASD is one of the most common neurodevelopmental disorders diagnosed in U.S children (73). While ASD is variable in its severity and manifestation between individuals, children with ASD also show increased rates of attention deficit disorder, obesity, epilepsy, anxiety, depression,

and intellectual disability (5,74–80). However, effective early life behavioral interventions can dramatically improve quality of life outcomes for people with ASD (81–83). Identifying early molecular indications of ASD may enable more effective early interventions and therapeutics, thereby improving the lives of people with ASD (84,85).

The etiology of ASD development includes both genetic and environmental contributions (86–89). Twin studies report 58%-90% concordance among monozygotic twins, but ASD is highly polygenic, involving both rare large-effect and common small-effect variants (18,20,90,91). To fully capture potential molecular predictors of ASD, it is necessary to also consider environmental exposures that may interact with genetic susceptibility to increase the likelihood of ASD development (92). One known environmental factor is maternal obesity (MO), defined by having a pre-pregnancy BMI of $\geq$30kg/m^2 and currently estimated to affect up to 29% of pregnant women (93,94). MO has been associated with a 36%-54% increase in risk of ASD offspring (95–99). MO is hypothesized to increase ASD risk though inflammation, specifically changes to proinflammatory cytokine levels, which cross the placenta and induce fetal neuroinflammation that dysregulates developmental gene regulatory networks (100–103). Acting as the interface between environmental stimuli and gene network regulation, epigenetic mechanisms integrate environmental exposures like MO to gene networks contributing to ASD etiology (104). Reproducible DNA methylated regions and signatures of ASD have been observed in human brain and placenta (59,105–110). MO in rhesus macaque studies revealed differential methylation in infant brain connecting MO to social behavior through gene

networks enriched for functions in neurodevelopment (111). Similar effects were observed in mice with perinatal high-fat diet exposure (112,113).

Human studies on epigenetic ASD markers have been limited by the inaccessibility of fetal tissue prior to diagnosis. The onset of abnormal brain development and dysregulated gene expression profiles characteristic of ASD begin *in utero* as early as the 1st trimester, but due to the risks of invasive fetal sampling, research has historically been limited to investigating accessible perinatal tissues such as placenta and newborn blood (114–117). However, advances in the field of noninvasive prenatal testing provide a means to examine fetal genetic material from cell-free fetal DNA (cffDNA) isolated from maternal blood (118,119). Originating from developmental apoptosis in the placenta, cffDNA are predominantly short fetal-derived nucleic acids, representing a fraction of the total plasma cell-free DNA (cfDNA), coexisting with maternal circulating nucleic acids derived from hematopoietic cells and adipose tissue (120–127). The fraction of cffDNA within cfDNA is variable between pregnant women, but increases throughout pregnancy and peaks at 21.6%-41.0% in the 3rd trimester (128). Notably, cffDNA retains a placental methylomic signature in maternal circulation, making it ideal for non-invasive testing of the fetal epigenome during pregnancy (129). Some progress in assaying the prenatal cfDNA methylome has been made, though it has predominantly been constrained to lower-resolution methods, limited to individual case studies, or performed on pooled samples (129–132).

To test the efficacy of cfDNA methylomes as environmentally-sensitive predictors of ASD *in utero*, whole-genome bisulfite sequencing (WGBS) was performed on cfDNA isolated from maternal blood plasma in a high-likelihood prospective ASD cohort (133). Comprehensive methylome analysis of cfDNA enabled the identification of differentially methylated regions (DMRs) of cfDNA associated with ASD or MO that were enriched for synaptic functions. These DMRs shared substantial similarity to ASD DMRs in placenta and cortex, supporting the applicability of cfDNA methylation to the methylomes of other ASD relevant tissues.

2.5 Results

2.5.1 Study design and subject characteristics

To investigate fetal epigenomic signatures associated with ASD, we leveraged samples from the MARBLES cohort, a prospective longitudinal study of pregnancies at elevated ASD risk (133). All participants contributed biological samples and detailed questionnaire data from preconception through early childhood, culminating in standardized neurodevelopmental assessments of all offspring at age three years.

A subset of 51 MARBLES pregnancies was selected to capture variability in fetal sex (n = 33 male; n = 18 female), maternal BMI (BMI; n = 33 control [BMI 18.5 – 29.8], n = 18 MO [BMI 30.2 – 51.2]) and ASD diagnosis (n = 27 non-ASD controls; n = 24 ASD) [Supplemental Tables 2.1-2.4]. Our major inclusion criteria were the availability of 1 ml stored maternal plasma collected at delivery (36–41 weeks gestation) from MARBLES

participants with existing placental WGBS data to facilitate multi-tissue comparison [Supplemental Figure 2.1]. CfDNA (4.1 ng–37.4 ng) was isolated and subjected to WGBS, enabling methylome-wide interrogation of cfDNA at single-base resolution [Figure 2.1].

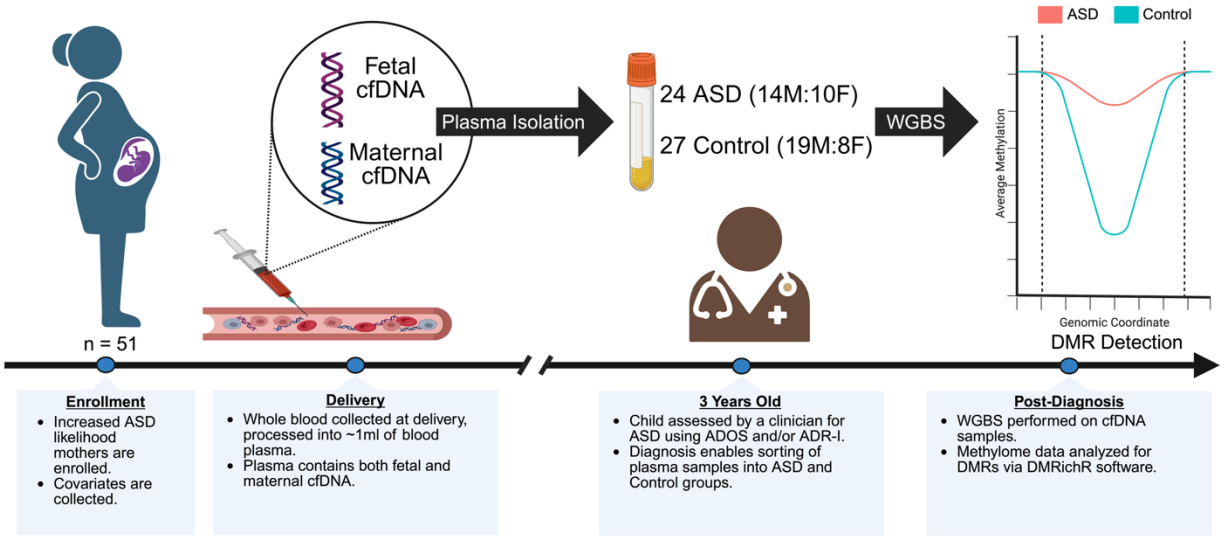


Figure 2.1: WGBS of cfDNA in a prospective autism cohort study enables prenatal detection of ASD-associated differentially methylated regions (DMRs). This experimental diagram details the process by which study participants were selected for cfDNA sampling, the subsequent diagnostic follow-up, and the computational method by which WGBS data was investigated for DMRs associated with ASD diagnosis. Image made in Biorender.com.

2.5.2 Fetal sex-stratified cfDNA methylomes reveal ASD-associated DMRs enriched in neurodevelopmental pathways.

Differentially methylated regions (DMRs) between ASD and non-ASD controls after adjustment for MO were identified in a sex-stratified manner, yielding 1,436 DMRs in male and 3,113 in female pregnancies [Figure 2.2A, Supplemental Tables 2.5-2.6]. ASD DMRs were detected in greater numbers in the female pregnancies than the male pregnancies, and also displayed a significantly greater magnitude of change [Supplemental Figure 2.2], consistent with what we have previously observed for ASD DMRs from newborn blood spots and cord blood (109,134). Many ASD DMRs displayed opposing methylation directionality by fetal sex, with male DMRs skewed towards hypomethylation and female DMRs towards hypermethylation, a pattern not observed at the global methylome level [Figure 2B]. Combining both sexes and correcting for sex reduced ASD DMR detection sensitivity, despite greater power, resulting in only 377 DMRs that exhibited no significant enrichment for expected neuronal gene pathways [Supplemental Table 2.8, Supplemental Figure 2.3]. Despite sex-specific directionality, both male and female ASD DMRs were similarly enriched in genic (promoters and exons) versus intergenic regions and preferentially localized to CpG-rich regions [Supplemental Figure 2.4].

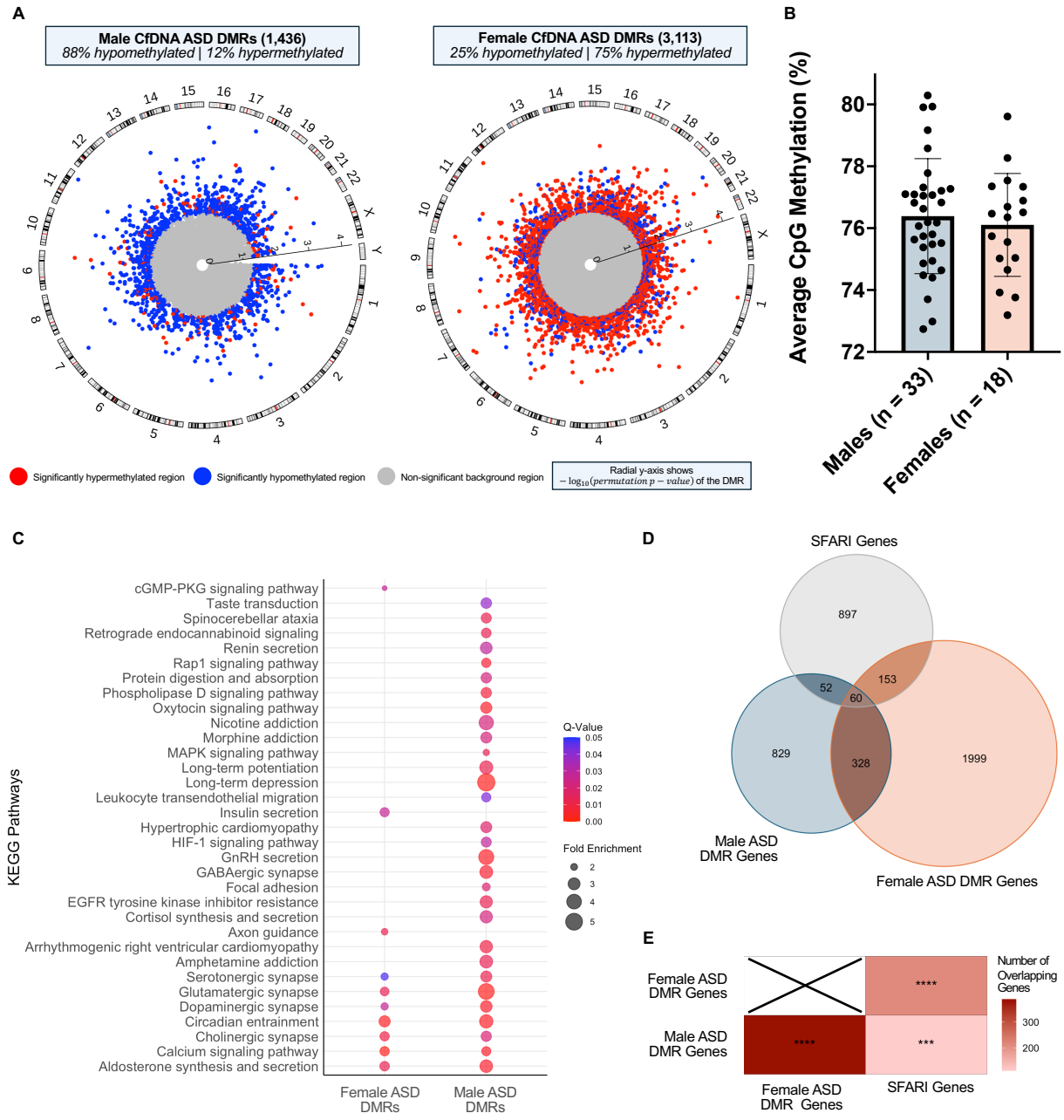


Figure 2.2: ASD DMRs are detectable in cfDNA and show strong enrichment for synaptic gene pathways. (A) Circos plots of the identified ASD DMRs in cfDNA from sex-stratified analyses and plotted against the human genome. DMR directionality with respect to ASD diagnosis is denoted by dot color, with red indicating a hypermethylated DMR and blue indicating and hypomethylated DMR. Significance of a given DMR is

shown by its placement on the radial y-axis. **(B)** Bar plot average of global CpG methylation across all sequenced sites, separated by fetal sex. Error bars show standard deviation from the mean. No significant difference was identified between groups by application of a two-tailed t-test ($p = 0.536$). **(C)** Dot plot of all significant KEGG pathway enrichments for the male and female cfDNA ASD DMR genes. Significance indicated by dot color, and fold enrichment indicated by dot size. **(D)** Venn diagram of the overlapping genes between both sets of cfDNA ASD DMRs and the SFARI gene list. **(E)** Heatmap displaying the significance of gene overlap between both cfDNA ASD DMR gene lists and the SFARI gene list. Number of overlapping genes in each comparison is indicated by tile color. Significance of the overlap between two gene sets determined by Fisher's Exact Test. Asterisks denote p-value as follows: *** $p < 0.001$, **** $p < 0.0001$.

Genes mapped to these DMRs were analyzed for KEGG pathway enrichment. Male ASD DMRs were enriched for 30 pathways and female DMRs for 10, with 7 shared pathway enrichments across both groups [Figure 2.2C, Supplemental Tables 2.9-2.10]. These included multiple neuronal synaptic pathways such as glutamatergic, serotonergic, and cholinergic synapses; calcium signaling; and circadian entrainment. Gene ontology enrichment analysis corroborated these findings, though with greater divergence between sexes [Supplemental Figure 2.5].

2.5.3 CfDNA ASD DMR genes are enriched for known autism risk genes and developmentally dynamic loci.

Both sex-specific ASD DMR gene lists significantly overlapped with the SFARI Gene database [Figure 2.2D and 2.2E], with 112 genes in common for males and 213 for females, though fetal fraction-adjusted female cfDNA DMRs did not replicate this significant SFARI overlap [Supplemental Figure 2.6] Male ASD DMRs were selectively enriched for SFARI genes categorized as “strong candidate” genes, while Female ASD DMRs exhibited enrichment for both SFARI “high confidence” and “strong candidate” genes [Supplemental Table 2.11]. The two gene lists were also significantly enriched for each other (388 overlapping genes), and their DMRs showed significant proximity in the genome beyond random expectation [Supplemental Figure 2.7]. Notably, 60 genes appeared in both cfDNA ASD sets and the SFARI database, including prominent autism risk genes such as *ANK2*, *CACNA1C*, and *GRIN2B* [Figure 2.2D, Supplemental Table 2.12] (135–137).

DMR genes were also enriched for loci undergoing dynamic methylation changes across pregnancy [Supplemental Figure 2.8], suggesting temporal relevance (138). Enrichment was further observed in Polycomb-repressed and weakly repressed chromatin states, including those in brain and placental tissues [Supplemental Figure 2.9; Supplemental Tables 2.13-2.14], indicating potential developmental regulation consistent with neurodevelopment risk genes like *AUTS2* (139–142).

2.5.4 CfDNA methylation patterns mirror ASD-associated DMRs in placenta and cortex.

To assess the tissue relevance of cfDNA methylation patterns, we compared cfDNA ASD DMRs to those identified from previous WGBS data from matched term placenta samples from MARBLES, as well as WGBS from unrelated ASD and control post-mortem cortex (59,105). Using identical DMR pipelines as for cfDNA, we identified 2,678 DMRs (male) and 8,447 DMRs (female) in placenta, and 5,191 DMRs (male) and 16,644 DMRs (female) in cortex [Figure 2.3A and 2.3B, Supplemental Tables 2.15-2.18].

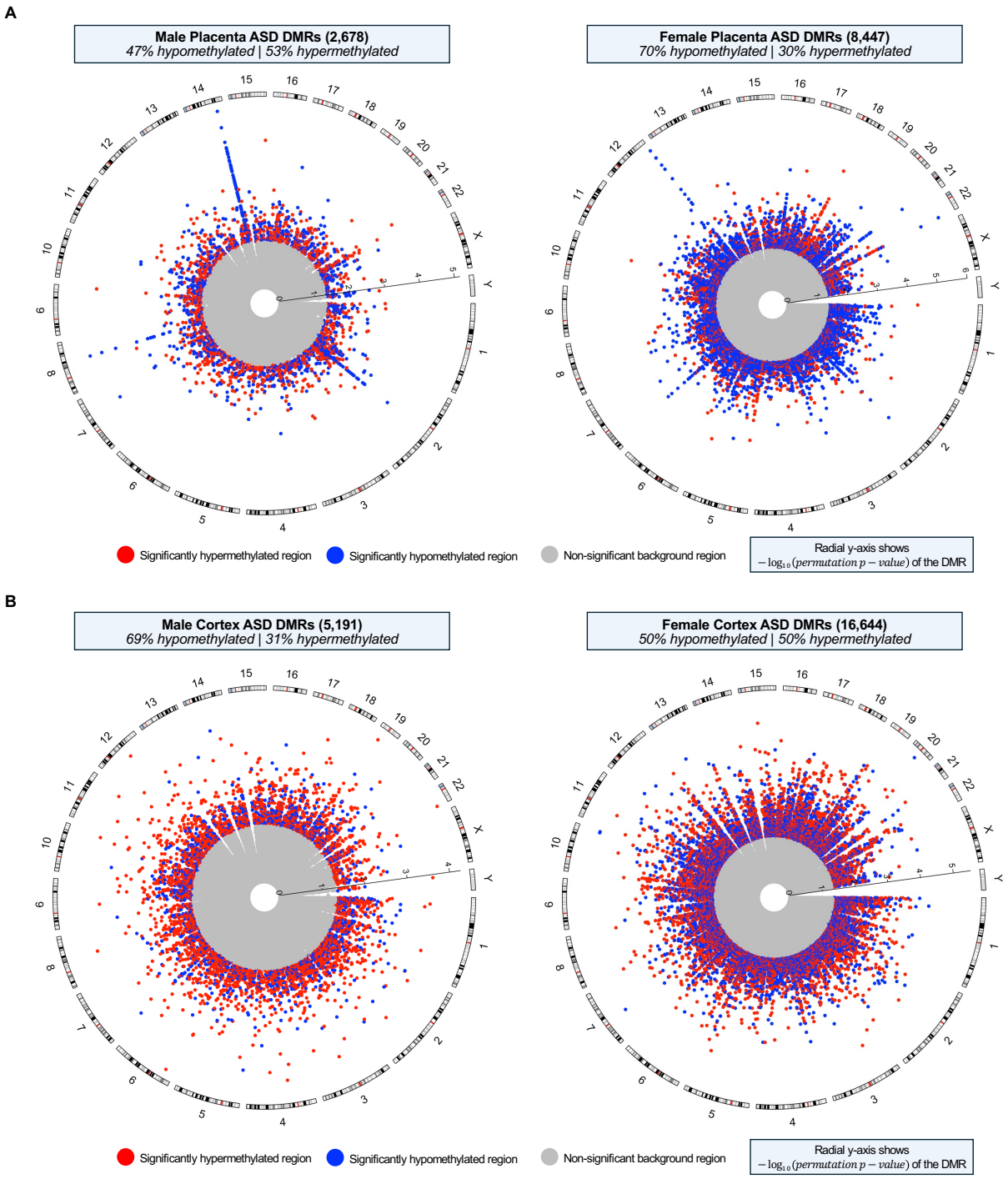


Figure 2.3: ASD DMRs identified from placenta and cortex WGBS exhibit shared characteristics with cfDNA DMRs. Circos plots mapping the genomic locations and significance of all DMRs from the sex-stratified analyses of **(A)** placenta and **(B)** cortex

WGBS. DMR directionality with respect to ASD diagnosis is denoted by dot color, with red indicating a hypermethylated DMR and blue indicating and hypomethylated DMR. Significance of a given DMR is shown by its placement on the radial y-axis.

All tissues shared a uniform genomic distribution of DMRs, and consistent enrichment in gene bodies and CpG islands [Supplemental Figures 2.10-2.11], though the fetal sex difference in methylation directionality observed in cfDNA were less pronounced in placenta and cortex than was observed for cfDNA [Figure 2.2A]. Cross-tissue gene-level overlap was substantial, with all six ASD DMR gene lists showing significant intersections [Figure 2.4A and 2.4B, Supplemental Figures 2.12-2.17]. KEGG analysis across all DMR gene sets identified four pathways that were enriched in all six tissue/sex groups: glutamatergic synapse, cholinergic synapse, calcium signaling, and circadian entrainment [Supplemental Figures 2.18-2.20], pointing to convergent methylomic alteration in synaptic gene pathways implicated across tissues and sexes.

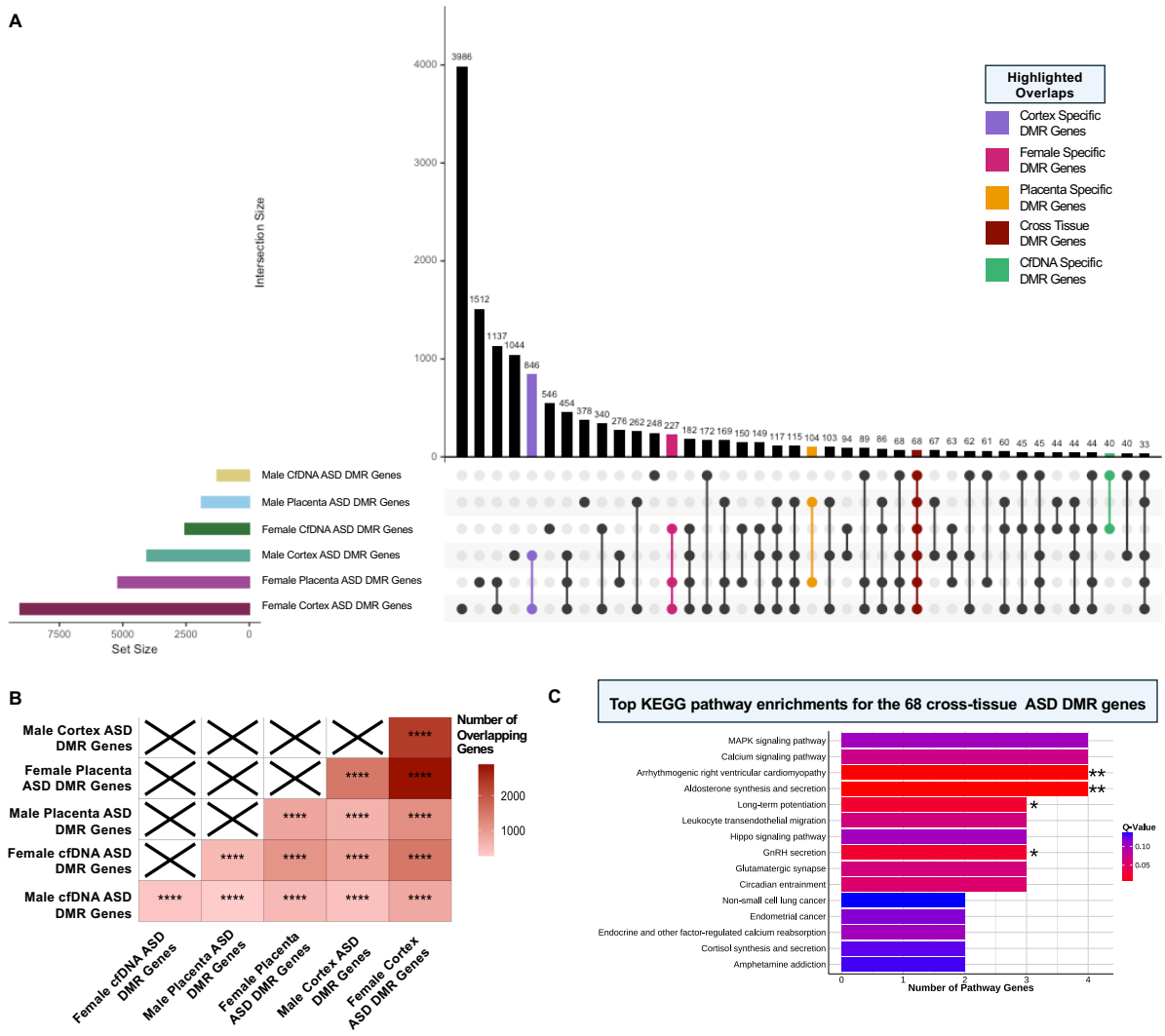


Figure 2.4: (A) Upset plot of the intersections between the six ASD DMR genes lists. Some intersections of interest are highlighted with specified colors. **(B)** Heatmap of the significance of gene overlap between the six DMR gene lists. Significance of the overlap between two gene sets determined by Fisher's Exact Test. Asterisks denote p-value as follows: **** $p < 0.0001$. **(C)** Bar graph of the top 15 most significantly enriched KEGG pathways for the list of 68 genes that appear in all six ASD DMR gene lists. Significance determined via Fisher's Exact Test with Benjamini-Hochberg correction. Asterisks denote q-value as follows: * $q < 0.05$, ** $q < 0.01$.

A shared set of 68 genes was present in all six tissue/sex differentially methylated gene lists [Supplemental Table 2.19]. These were enriched for pathways including long-term potentiation, GnRH signaling, circadian entrainment, and aldosterone synthesis [Figure 4C, Supplemental Table 2.20]. The novel gene neuronal hypoxia inducible, placenta associated (*NHIP*) that we previously identified as ASD associated from MARBLES placenta was included in this cross-tissue/sex differentially methylated gene list, consistent with its described function in both placenta and brain (59). No ASD DMR genes were shared among male-only DMR lists, but 227 were exclusive to female-specific DMRs, encompassing known risk loci such as *AUTS2*, *NRCN1*, and *SCN2A*, although no KEGG enrichments were identified for this female-specific set [Supplemental Table 2.21, Supplemental Figure 2.21]. All placenta and cortex DMR gene lists exhibited significant enrichment for SFARI genes [Supplemental Figures 2.22-2.23]. Among the 227 female-specific cross-tissue DMR-associated genes, 20 overlapped with established SFARI risk genes. Notably, five of these exhibited differentially methylated regions consistently localized within identical genic features and demonstrating concordant methylation alterations across all three tissues [Table 2.1]. This persistent, cross-tissue epigenetic signature is specifically associated with ASD diagnosis in females and is detectable prenatally in cfDNA.

Gene	SFARI Gene Score	Annotation	Direction	DMR Positions	Tissue	% Methylation Difference	P-Value
NRXN2	1	Intron	Hypermethylated	chr11:64,637,874-64,637,983	CfDNA	14	0.0476
				chr11:64,711,585-64,712,063	Placenta	10	0.0179
				chr11:64,611,402-64,612,258	Cortex	18	0.0103
				chr11:64,613,813-64,614,998	Cortex	15	0.0183
				chr11:64,645,890-64,646,102	Cortex	19	0.0203
ERG	2	Intron	Hypermethylated	chr21:38,436,804-38,437,438	CfDNA	12	0.0141
				chr21:38,384,196-38,384,517	Placenta	9	0.0460
				chr21:38,395,695-38,395,950	Cortex	17	0.0270
				chr21:38,647,306-38,648,469	Cortex	15	0.0458
PTBP2	2	Distal Intergenic	Hypermethylated	chr1:96,919,158-96,919,901	CfDNA	12	0.0075
				chr1:96,833,633-96,834,747	Placenta	10	0.0397
				chr1:96,592,914-96,594,274	Cortex	21	0.0132
SF3B1	2	Distal Intergenic	Hypermethylated	chr2:197,371,759-197,372,113	CfDNA	13	0.0057
				chr2:197,369,767-197,370,324	Placenta	11	0.0343
				chr2:197,368,831-197,369,767	Cortex	23	0.0014
TBX22	3	Distal Intergenic	Hypomethylated	chrX:79,843,148-79,845,059	CfDNA	-14	0.0091
				chrX:79,956,019-79,957,534	Placenta	-8	0.0409
				chrX:80,139,730-80,139,990	Cortex	-18	0.0195
				chrX:79,749,789-79,750,252	Cortex	-30	0.0369

Table 2.1: Summary of DMRs in the five genes from the female-specific cross-tissue ASD DMR gene list which have concordant genic annotation and methylation directionality. Each entry specifies the DMR gene, SFARI gene score, genic annotation, methylation directionality, chromosomal coordinates, tissue source, % methylation difference between ASD and Control samples, and the p-value of the DMR call. These loci may represent a female-specific cross-tissue epigenetic signature of ASD detectable early in development.

2.5.5 MO DMRs in cfDNA are detectable in ASD relevant gene pathways and enriched in ASD DMRs of both fetal sexes.

The identification of ASD-associated methylation signatures in cfDNA provides a foundation for exploring convergent epigenetic mechanisms linking ASD with a common prenatal exposure, MO. To explore this hypothesis, we identified DMRs on the same group of cfDNA WGBS but stratified by MO rather than ASD. MO was defined

categorically, with a pre-pregnancy BMI of 30 kg/m^2 separating obese mothers (n=18, 9 females and 9 males, 9 non-ASD and 9 ASD) from non-obese mothers (n=33, 9 females and 24 males, 18 non-ASD and 15 ASD).

We identified 6,677 MO DMRs in cfDNA from male pregnancies and 7,748 MO DMRs in female pregnancies [Supplemental Tables 2.22 and 2.23]. Samples were stratified by fetal sex to maintain comparability with sex-specific ASD DMR profiles. Unlike ASD DMRs, MO DMRs did not display marked differences in global methylation directionality between sexes [Figure 2.5A]. Like ASD findings, MO DMRs exhibited preferential localization within gene bodies and promoters, but de-enrichment over intergenic regions [Supplemental Figure 2.24].

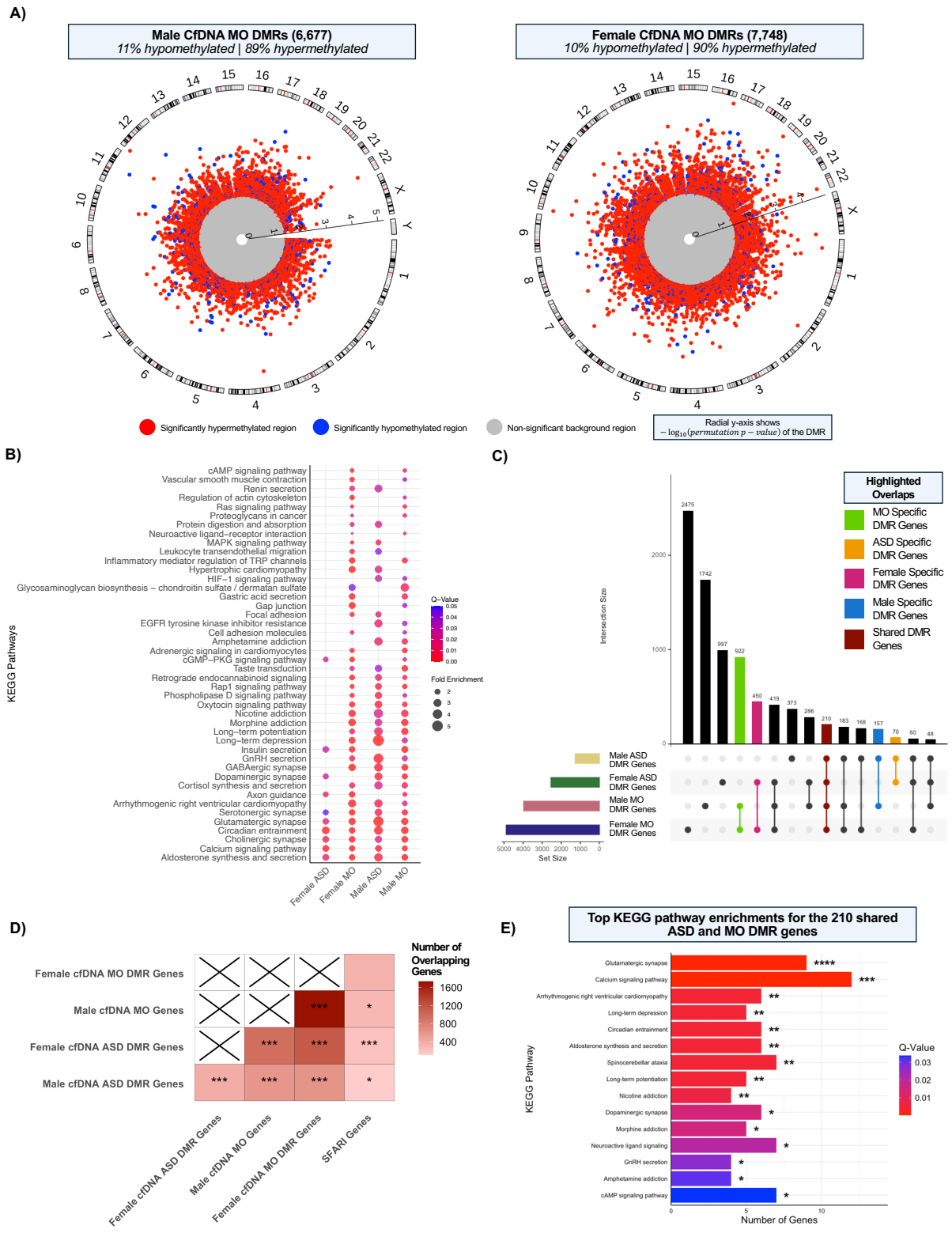

A)
Male CfDNA MO DMRs (6,677)
11% hypomethylated | 89% hypermethylated
Female CfDNA MO DMRs (7,748)
10% hypomethylated | 90% hypermethylated
Significantly hypermethylated region
Significantly hypomethylated region
Non-significant background region
Radial y-axis shows
$-\log_{10}(permutation\ p-value)$ of the DMR
B)
KEGG Pathways
cAMP signaling pathway
Vascular smooth muscle contraction
Renin secretion
Regulation of actin cytoskeleton
Ras signaling pathway
Proteoglycans in cancer
Protein digestion and absorption
Neuroactive ligand–receptor interaction
MAPK signaling pathway
Leukocyte transendothelial migration
Inflammatory mediator regulation of TRP channels
Hypertrophic cardiomyopathy
HIF−1 signaling pathway
Glycosaminoglycan biosynthesis – chondroitin sulfate / dermatan sulfate
Gastric acid secretion
Gap junction
Focal adhesion
EGFR tyrosine kinase inhibitor resistance
Cell adhesion molecules
Amphetamine addiction
Adrenergic signaling in cardiomyocytes
cGMP−PKG signaling pathway
Taste transduction
Retrograde endocannabinoid signaling
Rap1 signaling pathway
Phospholipase D signaling pathway
Oxytocin signaling pathway
Nicotine addiction
Morphine addiction
Long−term potentiation
Long−term depression
Insulin secretion
GnRH secretion
GABAergic synapse
Dopaminergic synapse
Cortisol synthesis and secretion
Axon guidance
Arrhythmogenic right ventricular cardiomyopathy
Serotonergic synapse
Glutamatergic synapse
Circadian entrainment
Cholinergic synapse
Calcium signaling pathway
Aldosterone synthesis and secretion
Female ASD
Female MO
Male ASD
Male MO
Q−Value
Fold Enrichment
C)
Highlighted Overlaps
MO Specific DMR Genes
ASD Specific DMR Genes
Female Specific DMR Genes
Male Specific DMR Genes
Shared DMR Genes
Intersection Size
Male ASD DMR Genes
Female ASD DMR Genes
Male MO DMR Genes
Female MO DMR Genes
Set Size
D)
Female cfDNA MO DMR Genes
Male cfDNA MO Genes
Female cfDNA ASD DMR Genes
Male cfDNA ASD DMR Genes
Number of Overlapping Genes
Female cfDNA ASD DMR Genes
Male cfDNA MO Genes
Female cfDNA MO DMR Genes
SFARI Genes
E)
Top KEGG pathway enrichments for the 210 shared ASD and MO DMR genes
KEGG Pathway
Glutamatergic synapse
Calcium signaling pathway
Arrhythmogenic right ventricular cardiomyopathy
Long−term depression
Circadian entrainment
Aldosterone synthesis and secretion
Spinocerebellar ataxia
Long−term potentiation
Nicotine addiction
Dopaminergic synapse
Morphine addiction
Neuroactive ligand signaling
GnRH secretion
Amphetamine addiction
cAMP signaling pathway
Number of Genes
Q-Value

Figure 2.5: MO DMRs in cfDNA share substantial overlaps with ASD DMRs, while maintaining unique enrichments for inflammatory pathways. (**A)** Circos plots mapping the genomic locations and significance of all MO DMRs from the sex-stratified analyses of cfDNA WGBS. **(B)** Dot plot of all significant KEGG pathway enrichments for cfDNA ASD and MO DMRs. Significance indicated by dot color, and fold enrichment indicated by dot size **(C)** Upset plot of gene overlaps between cfDNA ASD and MO DMRs. Some intersections of interest are highlighted in specified colors. **(D)** Heatmap of the significance of gene overlap between the cfDNA DMR gene lists and the SFARI gene list. Significance of the overlap between two gene sets determined by Fisher's Exact Test. Asterisks denote p-value as follows: *** $p < 0.001$, * $p < 0.05$. **(E)** Bar graph of the top 15 most significantly enriched KEGG pathways for the list of 210 genes that appear in all cfDNA DMR gene lists. Significance determined via Fisher's Exact Test with Benjamini-Hochberg correction. Asterisks denote q-value as follows: **** $q < 0.0001$, *** $q < 0.001$, ** $q < 0.01$ * $q < 0.05$.

To assess shared genomic features, we compared MO and ASD DMRs from cfDNA by intersecting their genomic coordinates within matched sex strata. This analysis revealed highly significant overlap in both male and female MO and ASD DMRs comparisons relative to permutation-based expectations using matched control region sets (Supplemental Figures 2.25 and 2.26). Functional enrichment of DMR-associated genes via KEGG pathway analysis revealed six pathways consistently enriched across all four cfDNA DMR datasets: aldosterone synthesis and secretion (hsa04925), calcium signaling (hsa04020), cholinergic synapse (hsa04725), circadian entrainment (hsa04713),

glutamatergic synapse (hsa04724), and serotonergic synapse (hsa04726) (Figure 2.5B). These pathways reflect convergent epigenetic alterations within neurodevelopmentally critical signaling networks implicated in both MO and ASD contexts. Additional enrichments unique to MO DMRs, such as inflammatory mediator regulation of TRP channels (hsa04750), suggest a broader engagement of immune and regulatory systems in MO exposure compared to ASD.

To further delineate trait-specific and shared epigenetic signatures, we examined the intersection of the four cfDNA DMR genes lists corresponding to ASD and MO [Figure 2.5C]. Pairwise comparisons using Fisher's Exact Test revealed significant mutual enrichment among all four DMR gene lists [Figure 2.5D]. Notably, three of the four DMR gene lists exhibited significant overlap with the SFARI Gene database, with only the female MO DMR gene list not passing our significance threshold. However, female cfDNA MO DMRs with adjustment for estimated fetal fraction do display significant overlap with the SFARI Gene database [Supplemental Figure 2.6]. When stratified by SFARI Gene evidence thresholds, Male MO DMRs were selectively enriched for "strong candidate" SFARI genes, while female MO DMRs approached significant enrichment for the same SFARI subcategory [Supplemental Table 2.11].

To resolve trait-specific biological associations, KEGG pathway enrichment analysis was performed separately on genes unique to either MO or ASD DMRs. Among the 922 genes specific to MO DMRs, significant enrichment was observed for pathways involved in

morphine addiction (hsa05032) and neuroactive ligand signaling (hsa04080), implicating neuromodulatory signaling systems in the context of maternal metabolic influence [Supplemental Figure 2.26]. By contrast, analysis of the 70 genes uniquely associated with ASD DMRs identified enrichment for pathways related vitamin digestion and absorption (hsa04977), pancreatic secretion (hsa04972), and motor proteins (hsa04814), suggesting an alternative axis of neurodevelopmental disruption [Supplemental Figure 2.28].

Finally, we interrogated the 210 genes common to all four cfDNA DMR lists to identify shared epigenetically perturbed pathways [Supplemental Table 2.24]. KEGG analysis of these overlapping genes revealed significant enrichment across 15 pathways [Figure 2.5E], including glutamatergic synapse (hsa04724), circadian entrainment (hsa04713), and calcium signaling pathway (hsa04020) — three of the four pathways consistently identified as enriched in the ASD DMR sets across multiple tissue types, highlight convergent neurodevelopmental mechanisms across etiologically distinct maternal exposures and fetal outcomes.

2.6 Discussion

Our study presents evidence that cfDNA collected from late 3rd trimester maternal blood reflects epigenomic signatures associated with ASD diagnosis. Remarkably, we demonstrate that cfDNA methylation patterns distinguishing ASD from non-ASD are sex-specific and occur at genes with functions at fetal neuronal synapses, despite originating

from maternal blood. ASD DMRs overlapped across cfDNA, matched placenta, and postmortem cortex, reinforcing that ASD etiology begins *in utero* and converges on placental-brain pathways. WGBS of cfDNA identified ASD and MO associated DMRs, uncovering both distinct and convergent molecular pathways across sexes. These findings advance our understanding of ASD etiology as being rooted in early developmental dysregulation, emphasizing maternal metabolic health as a modifiable factor which may shape the prenatal epigenomic landscape in ways that modulate synaptic development.

Epigenetic modifications, particularly DNA methylation, mediate gene-environment interactions during fetal development. Our detection of ASD-associated DMRs in 3rd trimester cfDNA—before the manifestation of behavioral symptoms—supports a model in which prenatal epigenetic programming contributes to ASD susceptibility. These ASD DMRs were enriched in genes involved in synaptic signaling, transcriptional regulation, and neuronal connectivity, consistent with prior sex-combined studies of post-mortem ASD brain tissues, and with reports of fetal origins of neurodevelopmental conditions (48,49,143). These pathway enrichments are consistent with a contemporary understanding of ASD as developing from systemic alteration to general neurodevelopmental pathways (144). Epigenetic profiles of ASD in cfDNA appear to mirror genetic profiles of ASD in this regard, as they implicate numerous loci with convergent neurodevelopmental relevance as opposed to singular high-penetrance variants (145–147). ASD etiology is characterized by the cascading effects of alterations to synaptic development, brain energy and metabolism, inflammatory response, and

myriad other biological pathways acting in concert to produce a broad neurodevelopmental phenotype, and our reported ASD DMRs in maternal cfDNA reflect this diverse etiology.

Substantial sex-specific divergence in ASD-associated methylation signatures aligns with male-biased ASD prevalence and with sex-specific placenta and fetal epigenomic regulation (148,149). Particularly in cfDNA, we observe substantial sex differences in the directionality of methylation associated with ASD, though the downstream effects of such differences are difficult to predict. The subset of cfDNA DMRs in genes shared between males and females with diverging methylation patterns at the same genic elements show a significant enrichment for the MAPK signaling pathway (hsa04010), potentially implicating altered MAPK signaling as interacting with fetal sex [Supplemental Figure 2.29A]. MAPK signaling pathways are rhythmic in the developing brain and function to entrain the brain's activity to maternal feeding and activity cues (150,151). MAPK and circadian entrainment pathways are also known to be sexually dimorphic (152,153). In contrast, the genes that showed concordance in the direction of methylation's association with ASD between fetal sexes, were significantly enriched for canonical neurodevelopmental pathways including calcium signaling (hsa04020), glutamatergic synapse (hsa04724), and cGMP-PKG signaling (hsa04022) [Supplemental Figure 2.29B]. Divergent methylation of MAPK signaling gene pathways in association with ASD in males versus females may be a byproduct of more general sex differences in the timing or rhythmicity of prenatal neuronal development, though future studies are needed to assess this hypothesis (154–156).

Overlapping epigenetic alterations in ASD and MO-associated DMRs suggest convergent mechanisms linking maternal metabolic disruption and ASD development. Multiple maternal metabolic conditions—including diabetes, hypertension, and obesity—have been linked to increased ASD risk in offspring across epidemiological cohorts, yet the biological intermediaries of these associations have remained poorly defined (95–99,157–160). Pre-pregnancy BMI was shown to associate with altered methylation of 27 loci in placenta that were significantly enriched for oxidative stress-induced signaling pathway genes, and has been shown to associate with hypermethylation of the *LEP* promoter and reduced leptin expression, possibly making the placental environment more susceptible to inflammation (161,162). Our findings fortify existing hypotheses that tie MO and ASD risk through shared genetic and epigenetic impacts on convergent biological pathways, particularly those related to inflammation (163–165). For example, the shared KEGG enrichment in some ASD- and MO-associated DMR sets for pathways such as Rap1 signaling, retrograde endocannabinoid signaling, and Phospholipase D signaling highlight shared epigenetic profiles between ASD and MO concentrated in immune activation and cellular stress response. The presence of *NHIP* in all four cfDNA DMR gene lists suggests oxidative stress as an axis of potential MO-influenced ASD susceptibility (59). While inflammation and oxidative stress have previously been proposed as mechanistic links between MO and ASD, our findings provide evidence that this connection is epigenetically encoded during prenatal development, supporting future studies into the regulatory consequences of DNA methylation changes on inflammation, reactive oxygen species levels, and synaptic development.

Crucially, our use of maternal cfDNA, which includes DNA from fetal trophoblast cells of the placenta, demonstrates the feasibility of capturing fetal epigenetic regulation *in vivo* using noninvasive methods (119–121). Prior cfDNA studies in cancer, transplantation, and aging demonstrate broad utility, and we now extend this to the interrogation of a neurodevelopmental outcome (123–125,166–168). Leveraging WGBS, we move beyond array-based coverage limitations and identify DMRs across both genic and intergenic regions, enhancing our ability to capture regulatory elements implicated in disease. These methodological advances open new avenues for investigating a range of prenatal exposures beyond MO, including maternal stress, infection, environmental toxicants, and other modifiable factors recognized as contributors to ASD and related outcomes (169).

Moreover, the capacity to stratify cfDNA-based epigenetic signatures by fetal sex adds a critical dimension to biomarker development and mechanistic inference. Sex differences in placental development may interact with maternal exposures to yield differential risk, and our findings underscore the importance of sex-stratified analyses in perinatal epigenetic studies (170–172).

Our limitations warrant acknowledgment. Firstly, we did not adjust for estimated fetal fraction while defining our DMRs, and thus we cannot attribute differences in methylation between our cases and controls to fetal or maternal DNA. This was an intentional choice, arising both from the unreliability of fetal fraction estimation for WGBS data as well as an

interest in both maternal and fetal cfDNA as an aggregate source of potential etiological insight. Whether our reported ASD DMRs are driven by changes to maternal or fetal cfDNA is a question to be interrogated by future studies. A set of cfDNA DMRs where an attempt was made to correct for fetal fraction despite unreliable quantification has been provided for comparison [Supplemental Tables 2.26-2.29]. Furthermore, cfDNA reflects a mixture of placental and fetal tissues, and although the ASD epigenomic signature was highly reflective of synaptic functions in brain, it does not provide direct brain-specific resolution. Future integration with placental and fetal tissues from ASD animal models will clarify the functional consequences of observed methylation changes on brain and behavior. Additionally, we were limited in sample size due to the high volume of plasma required for cfDNA isolation. Larger studies are needed to confirm DMR reproducibility. Finally, the association of any single DMR reported in this study should be replicated in other populations, as the definition of DMRs by the passing of an empirical permutation p-value threshold holds the potential for Type 1 errors.

In conclusion, our work supports a model in which both inherited and environmental risk factors for ASD converge in altered DNA methylation at synaptic gene pathways in the fetal brain. The ability to detect epigenetic signatures of fetal brain in maternal blood via cfDNA provides a minimally invasive approach to discover the origins of neurodevelopmental conditions and their modulation by the intrauterine environment. This framework could be extended to interrogate other prenatal risk factors and conditions, expanding our understanding of how maternal physiology shapes fetal neurodevelopment. As methods for cfDNA profiling continue to mature, they may

ultimately inform diagnostic biomarkers aimed at rapid detection of ASD early in life, maximizing the efficacy of early interventions.

2.7 Methods

2.7.1 Sample population and diagnostic classification

All samples in this study were taken from participants in the Markers of Autism Risk in Babies – Learning Early Signs (MARBLES) prospective cohort study, which recruits women of enriched risk for ASD pregnancies in order to study etiologic factors of ASD (133). The MARBLES study enrolls women who are either pregnant or planning an additional pregnancy and already have a child diagnosed with ASD. Women whose children would be the half-sibling of a child with ASD are also enrolled. Additional inclusion criteria are as follows: the mother is 18 years of age or older; the mother speaks, reads, and understands English proficiently enough to complete the protocol and the younger sibling will be taught to speak English; and the mother lives within 2.5 hours of the Davis/Sacramento region at time of enrollment. Recruitment into the MARBLES study is performed primarily via the California Department of Developmental Services (DDS). ASD diagnosis in the proband (older affected sibling or half-sibling) is confirmed during the enrollment process. Enrolled mothers participate in phone interviews and complete questionnaires both pre-pregnancy and during pregnancy, collecting demographic, diet, and medical information, including maternal pre-pregnancy BMI. After the child is born, ASD symptomatology is assessed at 6, 12, 24, and 36 months of age by trained psychologists and study staff applying age-appropriate instruments. Participant children

were not screened for any specific chromosomal abnormalities or copy number variants known to be associated with ASD, and were not excluded from consideration in this study based on the presence or absence of ASD-associated genetic variants. The final neurodevelopmental outcome of the child is determined by an outcome algorithm based on ADOS score and MSEL score results, using methods previously published (173). Children classified as non-Typically Developing but not ASD were grouped with Typically Developing children into a “non-ASD” group for the purpose of DMR identification.

For this analysis, MARBLES participants were chosen based on the availability of blood plasma samples of sufficient volume (≥1 ml) for cfDNA extraction. Actual sample volumes in the 0.6-1 ml range were able to yield sufficient cfDNA for 93.7% (59/63) of samples. Plasma samples were derived from 2 ml whole blood collected in EDTA storage tubes. Whole blood samples were collected at time of delivery and stored on ice for no more than 4 hours prior to centrifugation. Samples were centrifuged at 1000*g* for 15 min to separate out the plasma, which was subsequently aliquoted in 0.5 ml amounts into fresh cryovials. Plasma aliquots were stored at -80°C. Two frozen plasma aliquots from selected participants were thawed and pooled for cfDNA isolation.

2.7.2 Cell-free DNA extraction and whole-genome bisulfite sequencing (WGBS)

CfDNA was extracted from the supplied plasma aliquots with the QIAamp Circulating Nucleic Acids Kit (QIAGEN, 55114) by following recommended procedures and quantified with the Qubit DNA Assay Kit (ThermoFisher Scientific, Q32851). All purified cfDNA

samples were also analyzed with the Bioanalyzer High Sensitivity DNA Kit (Agilent, 5067-4626) to verify sample concentrations and validate that samples contained only the small nucleic acids typical of cfDNA. Any samples containing nucleic acids of ≥200bp length were subjected to a size-selective clean-up with SPRIselect (Beckman Coulter, B23317) beads.

CfDNA was bisulfite-converted using the EZ-DNA Methylation Direct Kit (Zymo Research, D5020) according to manufacturer recommendations. No fragmentation was performed, as cfDNA are naturally of a short length amenable to library preparation (174). Whole genome bisulfite sequencing libraries were then prepared from the bisulfite-converted cfDNA using the xGen Methylation-Sequencing DNA Library Preparation Kit (IDT, 10009860) with UDI Primer Pairs (IDT, 10005922) and an 11-cycle indexing PCR. Libraries were assessed for uniform size with Bioanalyzer High Sensitivity DNA Kit and pooled to 10nM concentration with a 10% PhiX spike-in. Pooled libraries were sequenced on 4 lanes with 150bp paired end reads of Illumina NovaSeq 6000 S4 (Illumina, 20012850) by the DNA Technologies Core at UC Davis, producing an average 209M sequences per sample and an average of 9.6X CpG coverage.

2.7.3 WGBS alignment and quality control

Raw sequencing files were preprocessed, aligned to hg38, and used to generate cytosine reports with Epigenerator (175). In short, Epigenerator provides a user-friendly means of generating cytosine reports from fastq files by applying the FASTQ_Me and CpG_Me

workflows in tandem (176,177). Merged reads were trimmed of adaptors, corrected for potential methylation bias at the 5' and 3' ends, and aligned to hg38. The aligned reads were then deduplicated and CpG methylation was extracted with to generate cytosine reports for further analysis. FastQC and MultiQC were also applied to check sequencing quality of all samples (178,179). Fetal fraction was estimated by calculating ChrY:ChrX reads and via SeqFF, although these estimates should be interpreted cautiously due to the nature of WGBS libraries defying many of the assumptions of conventional fetal fraction estimation (180,181) [Supplemental Figure 2.30]. While the SeqFF-derived estimate of fetal fraction varied substantially from expected values for third trimester plasma, it did demonstrate a positive linear correlation with ChrY:ChrX read ratios, thus indicating a rough relationship to true fetal fraction in aggregate even if individual sample estimates are suspect [Supplemental Figure 2.31].

2.7.4 Detection of DMRs

Differentially methylated region (DMR) calling and some downstream enrichment analyses were performed with DMRichR v1.7.1 (182). DMRichR combines dmrseq and bsseq tools to enable the inference of differentially methylated regions based on user-supplied variables of interest. The dmrseq algorithm pools the differences in CpG methylation between the case (ASD) and control (non-ASD) groups and performs smoothing to assemble background regions. Possible regions were defined as sections of the genome that a minimum of 5 CpGs with a maximum gap of 1000 bp, with each CpG being required to have at least 1X coverage in 75% of our sample group. A statistic for each possible region was then estimated through a generalized least squares

regression, and permutations test were used to identify regions with significantly differential methylation between case and control groups. No curated regions of the genome were masked in the process of calling DMRs, enabling DMRs to be called from any regions in the genome meeting the specified coverage standards. This includes regions of known high variance. A methylation difference of 5% was used as the minimum threshold for magnitude of difference between regions to be considered significant as a DMR.

DMRs were identified for both ASD and MO in fetal sex-stratified groups, as prior investigations have shown sex-specific DNA methylation signatures in perinatal tissues (183). A child was defined as having ASD if their ADOS overall total score at 36 months surpassed the ADOS cutoff and the child met *DSM-5* criteria for ASD. All children not meeting these criteria, including those with developmental delays on the MSEL, were defined as non-ASD control. A mother was defined as having MO if her reported pre-pregnancy BMI in the intake questionnaire was $\geq$30kg/m^2, with all mothers of lesser BMI, including those meeting overweight criteria, classified as non-obese Control. Four distinct sets of cfDNA DMRs were identified: Male ASD DMRs (N=33, 14 ASD and 19 non-ASD control), Female ASD DMRs (N=18, 10 ASD and 8 non-ASD control), Male MO DMRs (N=33, 9 MO and 24 non-obese control), and Female MO DMRs (N=18, 9 MO and 9 non-obese control) [Supplemental Table 2.24]. The two ASD DMR sets were adjusted for MO as a significant covariate, as MO is a known upstream risk factor for ASD development, but the reverse causality was not expected, so there was no adjustment for ASD in MO versus Control (95). All DMRs were called with the default variable specifications with the

exception that the maximum number of permutations tested was increased to 33 for the males and 18 for the females to improve statistical rigor. Significant DMRs were defined as those with a permutation p-value of < 0.05. DMRs were annotated with their nearest known gene via the application of “one closest” rule of the Genomic Regions Enrichment of Annotations Tool (GREAT) (184). These DMR gene name lists were used in future enrichment analyses.

Despite concerns regarding the accuracy of SeqFF estimated fetal fraction, this metric was included as an adjusted for covariate in a separate group of DMRichR runs to identify ASD and MO DMRs from cfDNA. Region inclusion parameters for this batch of DMRs were identical to previous batches, and a minimum threshold of 5% difference between compared groups was still used as a cutoff to call a given region as a DMR. In both males and females, the ASD and MO DMRs identified after adjustment for SeqFF as a covariate did not exhibit sizable deviation from the previously identified DMRs [Supplemental Tables 26-29]. All SeqFF-adjusted ASD and MO DMRs exhibited significant overlap with the previously identified DMRs as quantified both by gene name overlap and genomic region overlap [Supplemental Figures 2.32-2.37]. Regardless of whether SeqFF is adjusted for during DMR identification, the resulting ASD DMR genes are significantly enriched for KEGG pathways involved in synapse development and cell signaling in both males and females [Supplemental Figure 2.38]. The inclusion of SeqFF as an explicit adjusted-out covariate also has no impact on whether the resulting cfDNA ASD DMRs are significantly enriched for placenta and cortex ASD DMRs [Supplemental Figure 2.39].

To visualize the correlations between the identified DMRs and other covariates of the sample set, regression analyses were conducted for every covariate ~ DMR combination, with significance of a given association reported as a p-value from a t-test of the regression coefficient [Supplemental Figures 2.40-2.43].

For the ASD DMRs identified from previously published placenta and cortex samples, data was acquired in the form of cytosine reports and subjected to sex-stratified DMR identification under the same parameters as previously described. Placenta and cortex DMRs were tested for overlap with age-predictive CpGs from previously published models using the GRanges package [Supplemental Table 2.30] (185,186). Average CpG coverage over placenta ASD DMRs was compared between ASD and Control groups to investigate whether copy number variants may be driving differences in methylation, although no significant associations ($q < 0.05$) were discovered [Supplemental Tables 2.27 and 2.28]. Fisher's exact tests of DMRs with nominally significant (p-value < 0.05) associations with CpG coverage were performed to identify potential overrepresentation of chromosomes [Supplemental Tables 2.33-2.34].

2.7.5 Principal component analysis of smoothed DMR methylation

The clustering of DMRs was visualized with PCA. Smoothed methylation values over significant cfDNA ASD DMRs were extracted with the "getMeth" function in the bsseq R package v1.36.0. PCA of these data was performed with the "prcomp" function in the stats R package v4.5.0 with centering set to 0 and units variables scaled to unit variance. PCA

plotted with the “ggplot” function from the ggplot2 R package v3.5.2, with an ellipse indicating a 95% confidence interval for the points as defined by ASD diagnosis under the assumption of a normal distribution. Point fill was specified by either ASD diagnosis, ADOS score, or Mullens Score.

2.7.6 Global methylation averages between male and female samples

Per sample global averaged methylation values per CpG were calculated for all cfDNA samples with the “globalStats” function from the DMRichR package. Samples were grouped by fetal sex and plotted with Prism v10.3.0. Significance of the difference between male and female groups was calculated by an independent two tailed t-test under the assumption of a normal distribution.

2.7.7 DMR enrichment analysis

Enrichment of DMR sets for genic and CpG annotations was performed with the “DMRichGenic” and “DMRichCpG” functions from the DMRichR package, respectively. In both cases a Fisher’s exact test was used to determine significant overrepresentation ($q < 0.05$) of a given genic or CpG annotation in the DMR set, with the background universe set as possible regions assessed for differential methylation within a given sample set. The resulting enrichments were then plotted with “DMRichPlot” from the DMRichR package.

Enrichment of DMR sets for gene ontology was performed with the “submitGreatJob” function from the rGREAT package v4.0.4 using the one closest rule to assign genes to regions and slimmed with the “slimGO” function from DMRichR. A binomial distribution is assumed, and the input region set was tested for overrepresentation of any ontologies relative to background regions. GREAT enrichments were plotted with “ggplot” from ggplot2.

KEGG pathway enrichments were determined with the “enrichKEGG” function from the clusterProfiler package v4.16.0. A Fisher’s exact test was used to test for overrepresentation, with all KEGG-annotated genes as the background universe. A Benjamini-Hochberg false discovery rate correction was applied, and a q-value threshold of 0.05 determined significance.

2.7.8 DMR overlap analysis

All testing of the significance of region level overlaps between sets of DMRs was performed using the “permTest” function of the regioneR package v1.32.0. Both numOverlaps and meanDistance used for evaluation of the number of region overlaps and the average distance between those overlaps, respectively. Regions were randomly reassigned across the entirety genome (hg38) and tested over 10,000 permutations. The results were then plotted with the “plot” function from the R base package v. 4.5.0.

2.7.9 SFARI enrichment analysis

All SFARI Gene database enrichments tests were performed with tools from the GeneOverlap package v1.44.0. First, the “newGeneOverlap” function was applied to all DMR gene lists, with the genome size defined as the length of the gene list containing all possible background regions from our sequencing data. Next, the “testGeneOverlap” function performed Fisher’s exact tests to determine whether a given input DMR gene list coincided with the SFARI gene list more frequently than expected by chance. The SFARI Gene list used for these enrichments tests was the 2023 Q4 release. Plotting of SFARI Gene intersections with DMR gene lists was performed with the “plot” function from R base package v4.5.0.

2.7.10 Developmentally differentially methylated genes overlap analysis

A list of 28,718 differentially methylated positions across fetal brain development was acquired from a pre-existing study of fetal epigenetic dynamics (138). The genic annotation of these positions was extracted, providing a list of 7,693 genes with positions of dynamic methylation throughout pregnancy. The “newGeneOverlap” and “testGeneOverlap” functions from the Gene Overlap package v1.44.0 were then used to perform Fisher’s exact tests on the enrichment of these 7,693 genes with the male and female cfDNA ASD DMR gene lists. For this test, the background universe for comparison was the intersecting genes between the Illumina Infinium HumanMethylation 450 BeadChip (Illumina WG-314) and the background regions from the appropriate cfDNA DMR set.

2.7.11 Chromatin state enrichment analysis

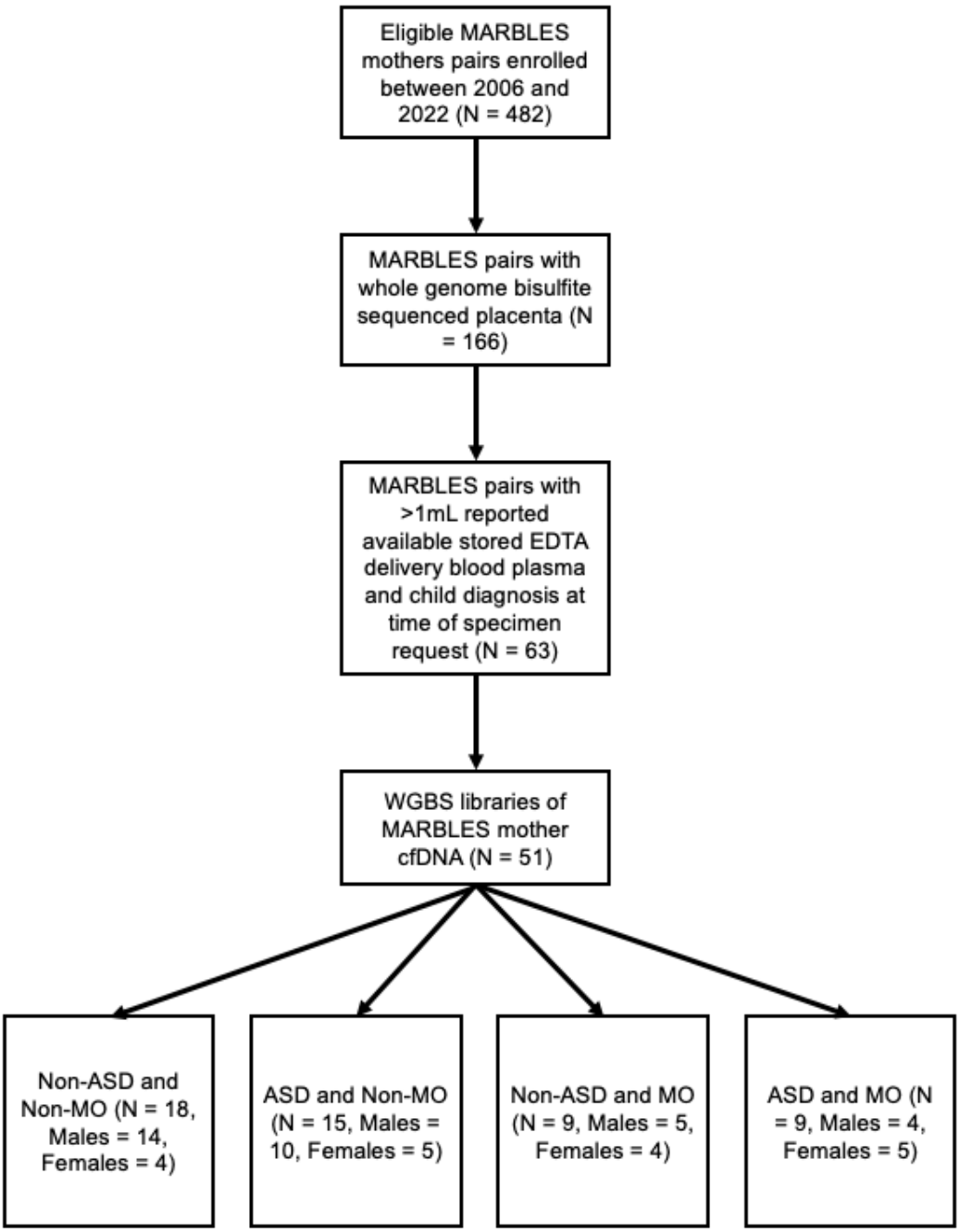
Chromatin state enrichment analysis was performed using the ChromHMM 15-state model for hg38 from the Roadmap Epigenomics Project via the LOLA framework (139,187). Significant cfDNA DMRs and matched background regions were submitted with the “runLOLA” function of the LOLA R package v1.38.0 with a reference database of ChromHMM segmentations across multiple tissue and cell types. Chromatin state enrichment p-values were computed using Fisher’s exact test. Chromatin states were annotated with human-readable labels, and infinite values were replaced with the highest finite odds ratio to enable plotting. Heatmaps of enriched states across tissues were generated with the “heatmap.2” function of the gplots R package v3.2.0.

2.8 Data and Code Availability

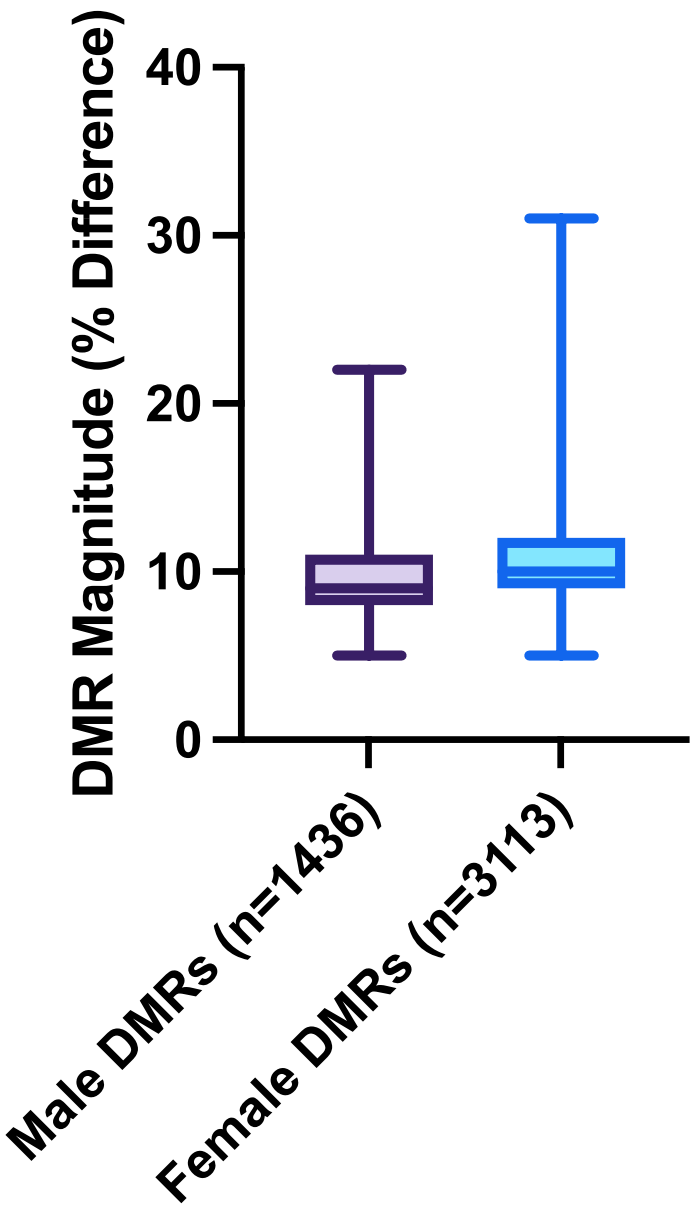
The sequencing data generated by this study from all subjects that have provided consent (n=48) have been deposited in the GEO database under accession code GSE307129. Interested parties can access GSE307129 by navigating to the following link: https://www.ncbi.nlm.nih.gov/geo/query/acc.cgi?acc=GSE307129. Enter token krgnyaeipfcxzij to view private data. Previously published WGBS data for placenta and cortex can be accessed in the GEO database under accession codes GSE178206 (placenta) and GSE119981 (cortex). All original code has been deposited on GitHub (https://github.com/lwilliams27/CfDNA_Methylome_AutismAndMaternalObesity) .

2.9 Supplemental Material

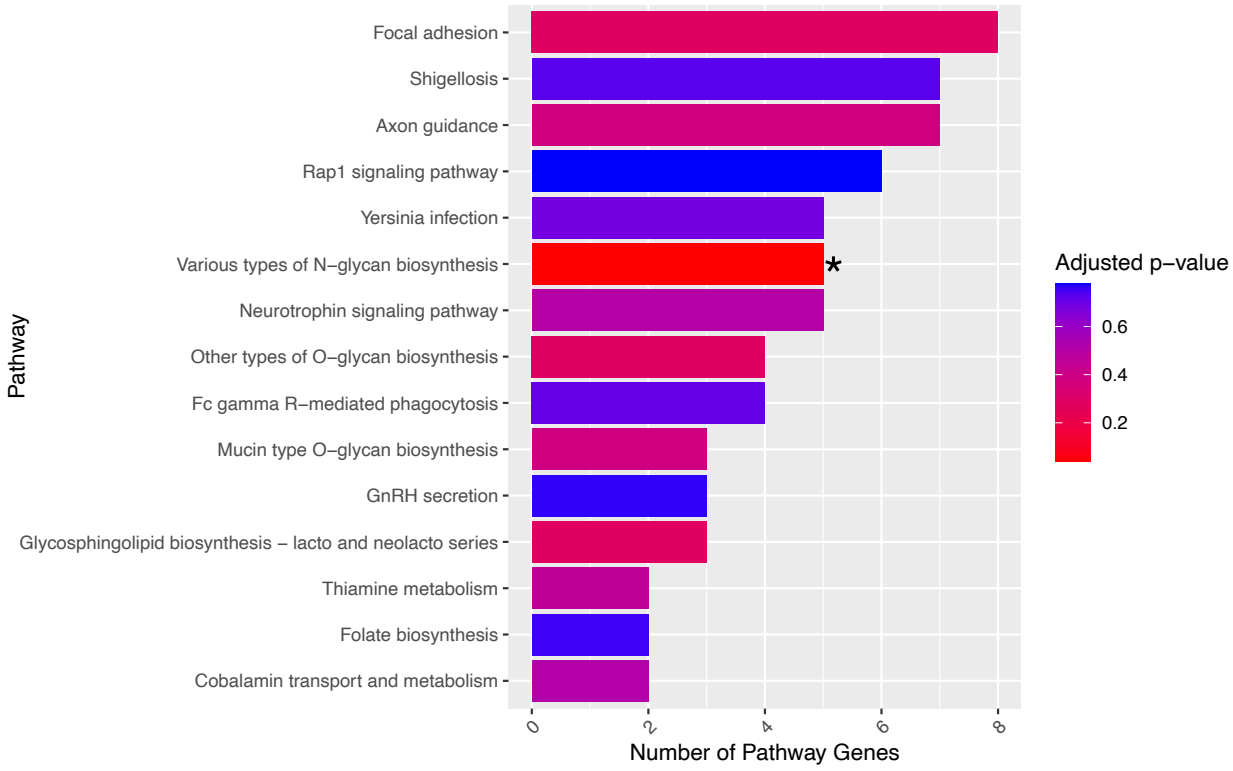
2.9.1 Supplemental Figures



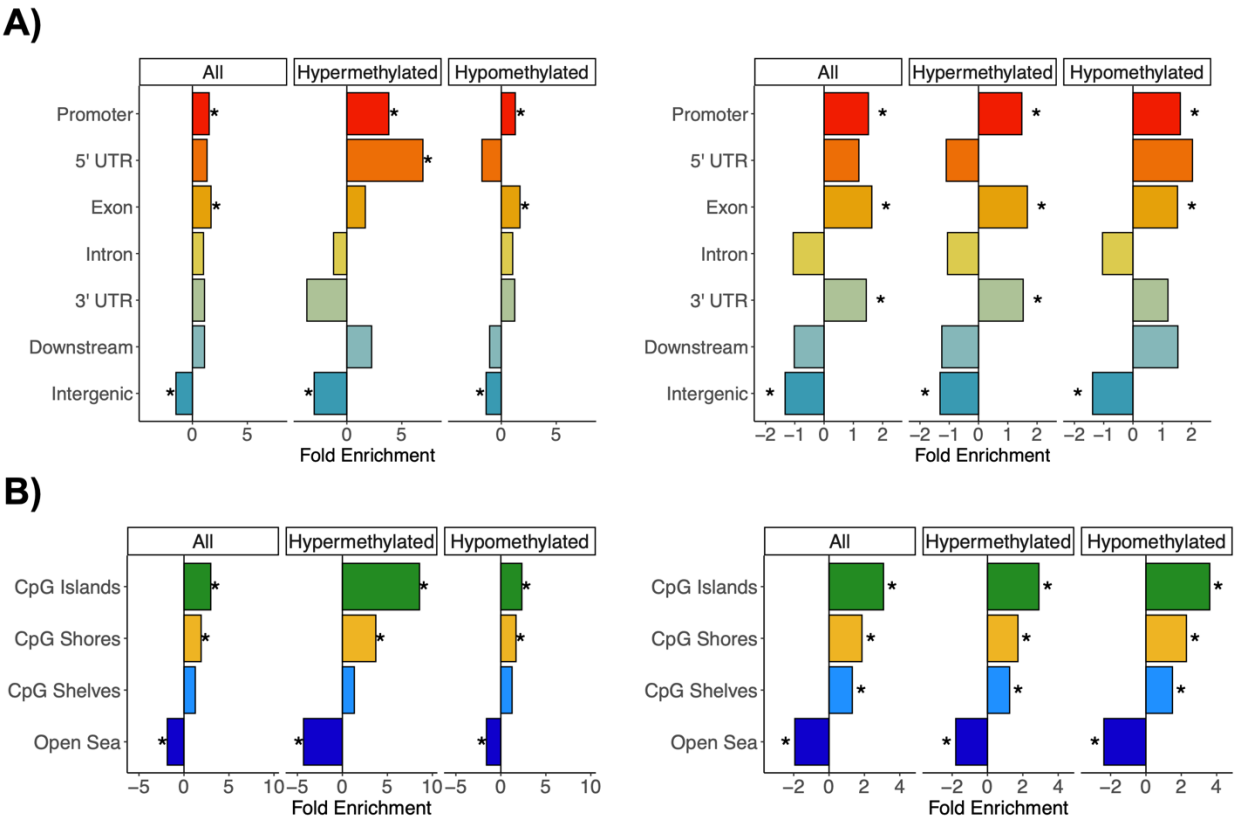
Supplemental Figure 2.1: Flowchart describing sample selection criteria and sample library covariates for the MARBLES samples used in this study.



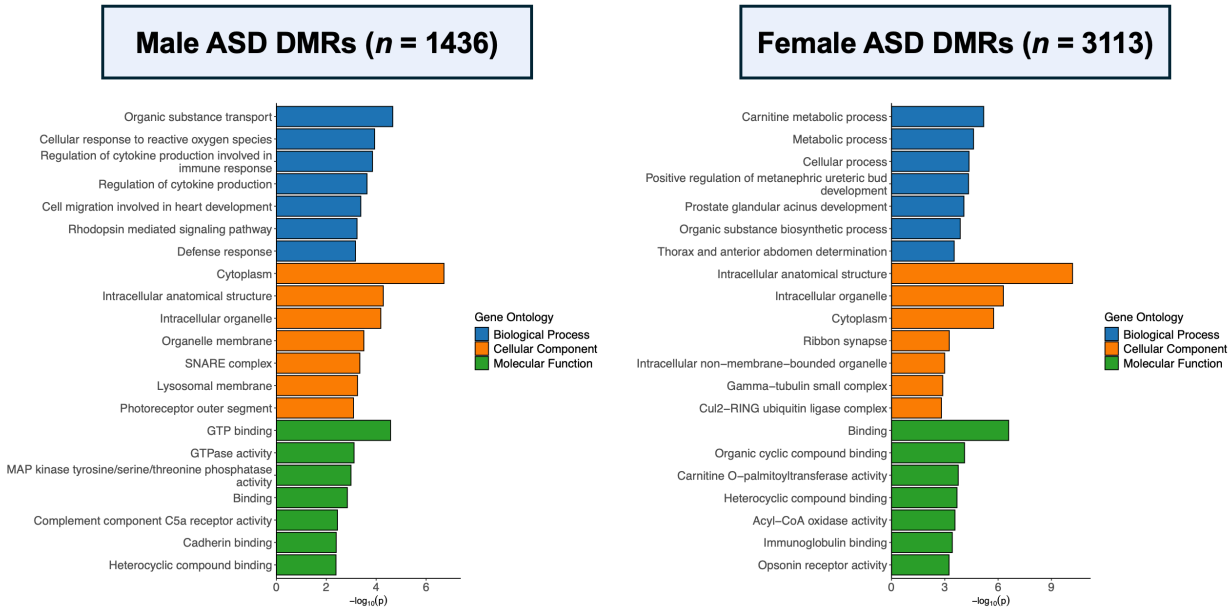
Supplemental Figure 2.2: Boxplot displaying the difference in DMR magnitude between male pregnancy ASD cfDNA DMRs and female pregnancy ASD cfDNA DMRs. The female DMRs are significantly larger than the male DMRs (Welch's t-test, $p < 0.0001$) by a factor of +1.345% on average.



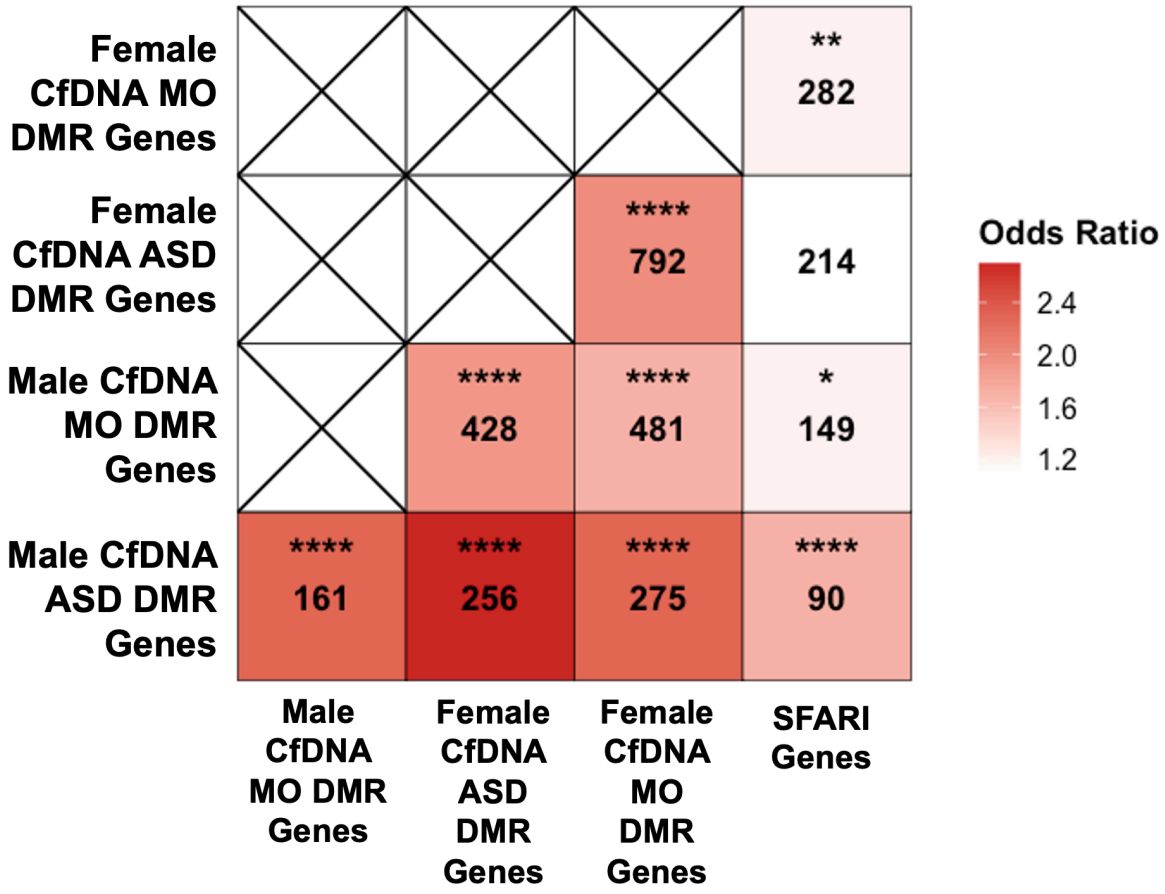
Supplemental Figure 2.3: The top 15 most significant KEGG pathway enrichments (by adjusted p-value) of the gene list from the cfDNA sex-combined ASD DMRs. The only significantly enriched pathway was “Various types of N-glycan biosynthesis” (hsa:00510).



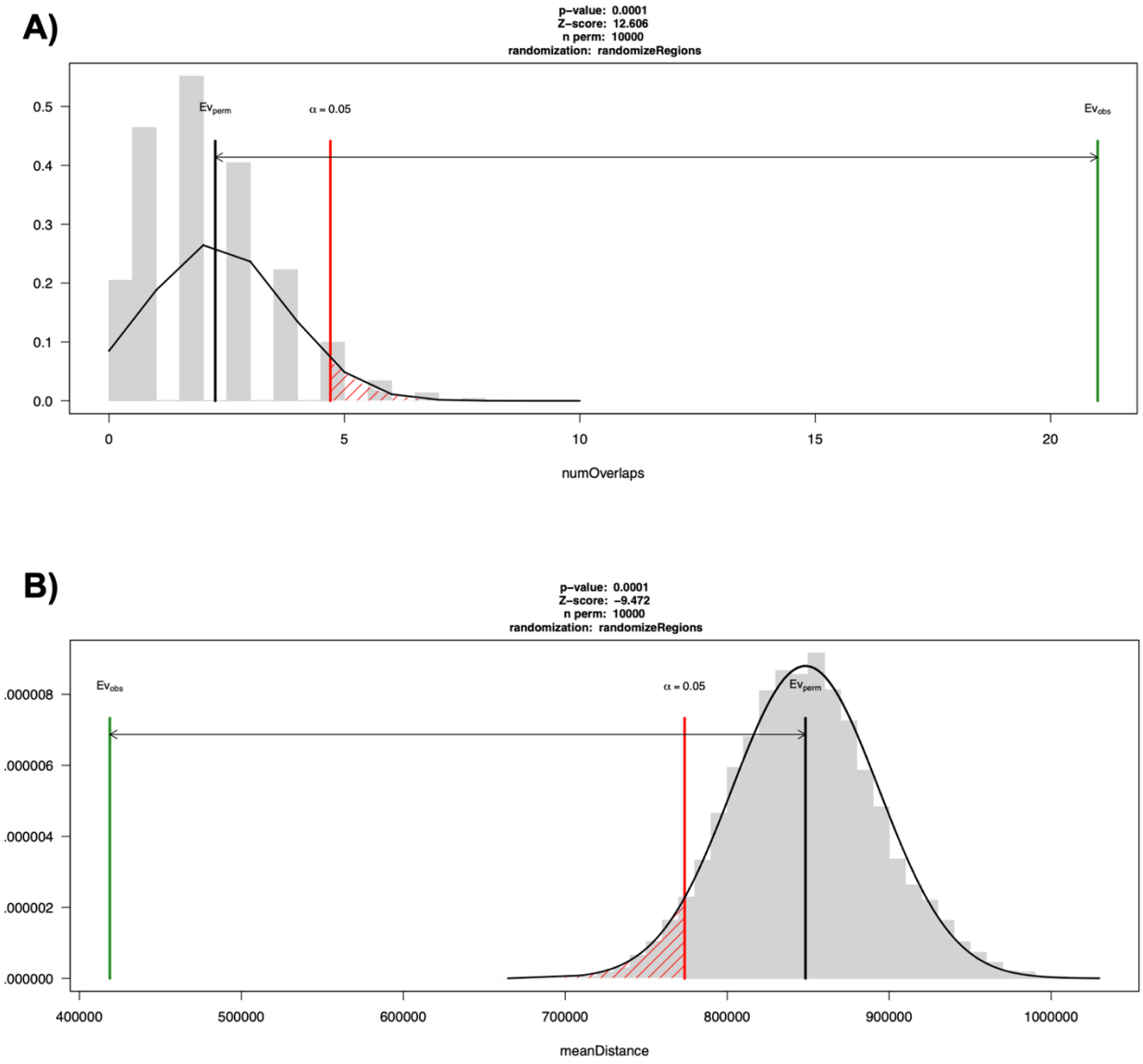
Supplemental Figure 2.4: Enrichment analyses of male and female cfDNA ASD DMRs (permutation p-value <0.05) for both **A)** genic annotations and **B)** CpG annotations as performed and plotted by DMRichR. DMRs were compared to background regions for each comparison, with significance determined by Fisher's test with FDR correction (* = q-value < 0.05).



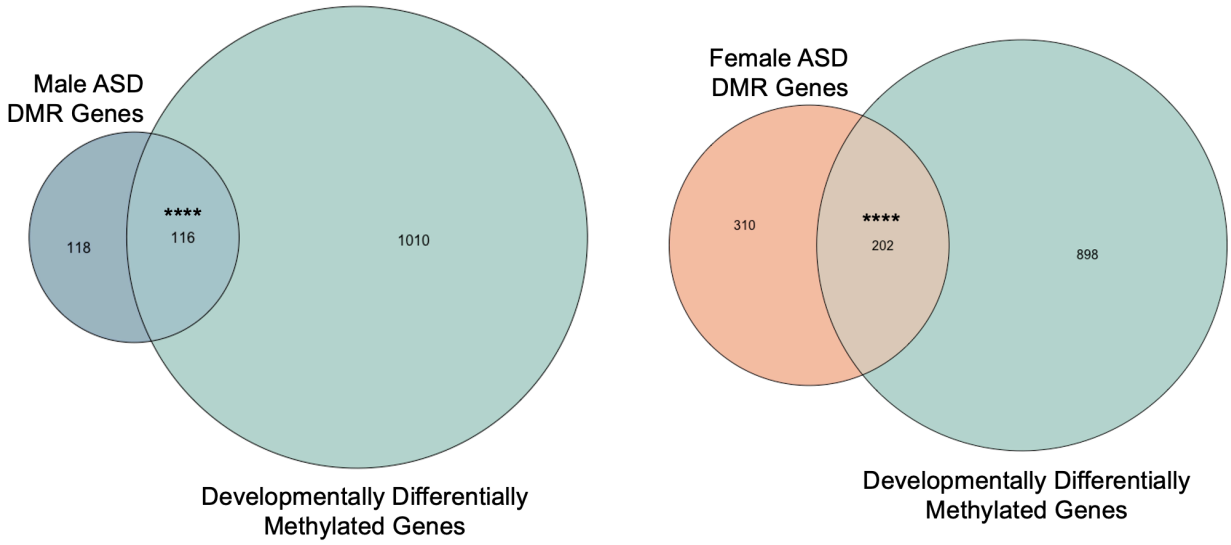
Supplemental Figure 2.5: The results of Gene ontology (GO) term enrichment analyses for male and female cfDNA ASD DMR gene lists, as performed by GREAT. The top seven most significantly enriched terms for each of the three gene ontologies are shown.



Supplemental Figure 2.6: Heatmap displaying the significance of gene-level overlap between all cfDNA DMRs with SeqFF fetal fraction adjustment and the SFARI Gene list. Significance determined by Fisher's Exact Test. The numbers shown on each tile correspond to the number of genes overlapping the two gene lists in question. Asterisks denote p-value as follows: * $p < 0.05$, ** $p < 0.01$, **** $p < 0.0001$.

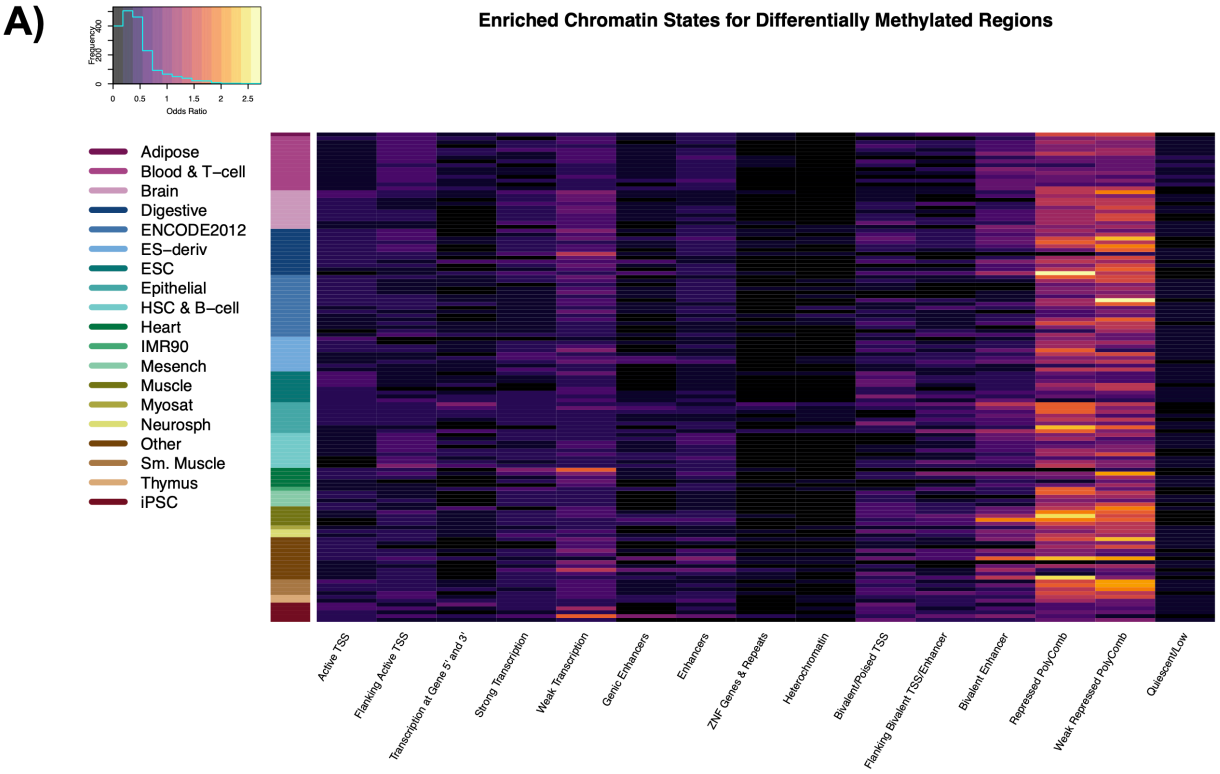


Supplemental Figure 2.7: Overlap analysis of the male and female cfDNA DMRs with the *regioneR* package. Analysis performed over 10,000 permutations, with the average number of **A)** overlaps between region sets and **B)** mean distance between region sets compared to the actual data, with significance calculated via permutation test.

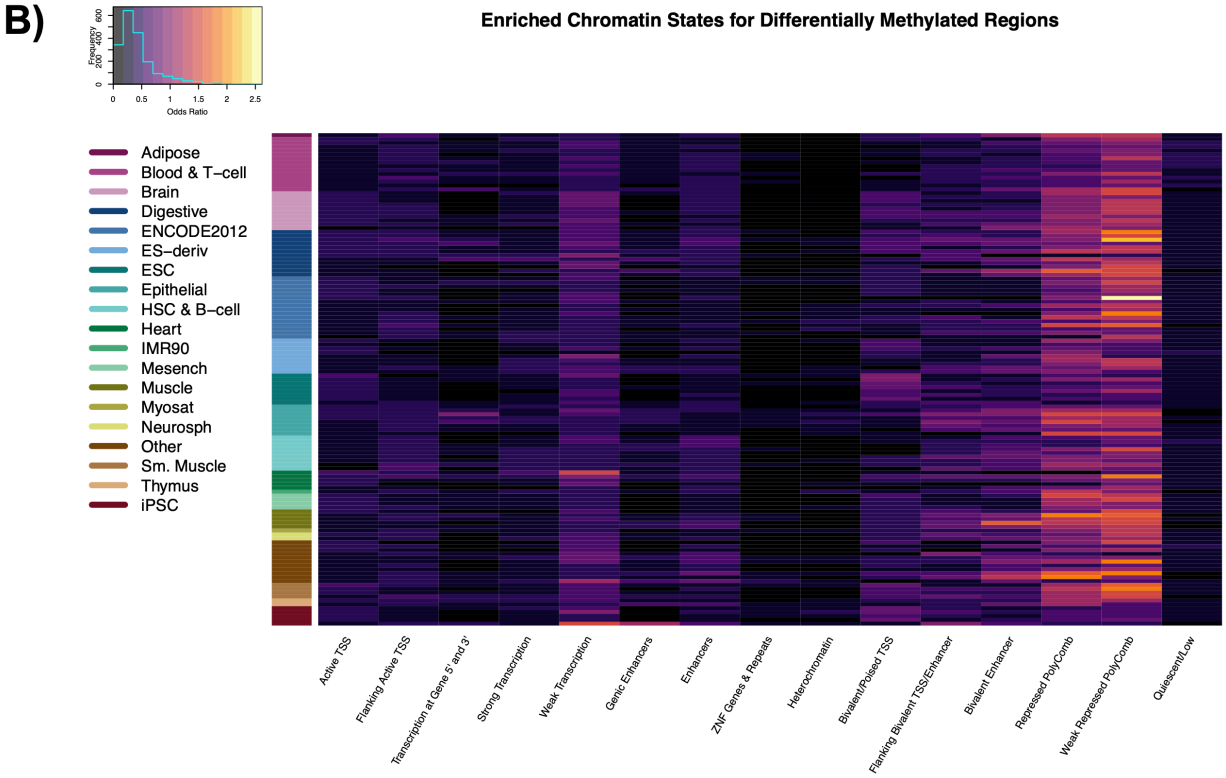


Supplemental Figure 2.8: Venn diagrams of male and female cfDNA ASD DMR gene lists's overlap with developmentally differentially methylated genes (DDMGs) as identified by the dDMPs in Spiers et al. 2015. Only genes appearing in the possible background of the DMRs and DDMGs included in analysis. Both overlaps determined significant compared to conserved background region overlap via Fisher's exact test ($p = 2.6 \times 10^{-13}$ for males and $p = 2.2 \times 10^{-10}$ for females).

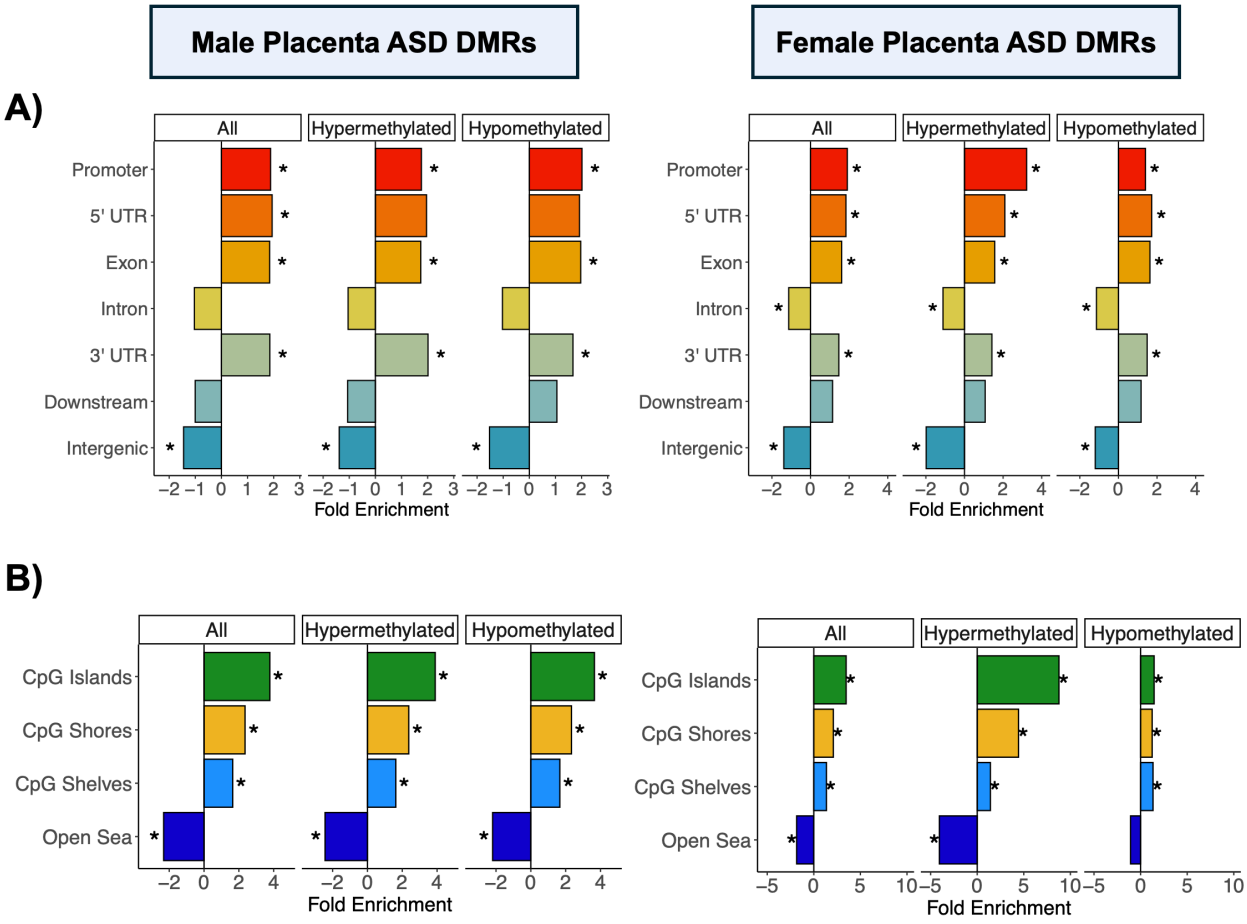
A)


Enriched Chromatin States for Differentially Methylated Regions
Frequency
Odds Ratio
Adipose
Blood & T−cell
Brain
Digestive
ENCODE2012
ES−deriv
ESC
Epithelial
HSC & B−cell
Heart
IMR90
Mesench
Muscle
Myosat
Neurosph
Other
Sm. Muscle
Thymus
iPSC
Active TSS
Flanking Active TSS
Transcription at Gene 5' and 3'
Strong Transcription
Weak Transcription
Genic Enhancers
Enhancers
ZNF Genes & Repeats
Heterochromatin
Bivalent/Poised TSS
Flanking Bivalent TSS/Enhancer
Bivalent Enhancer
Repressed PolyComb
Weak Repressed PolyComb
Quiescent/Low

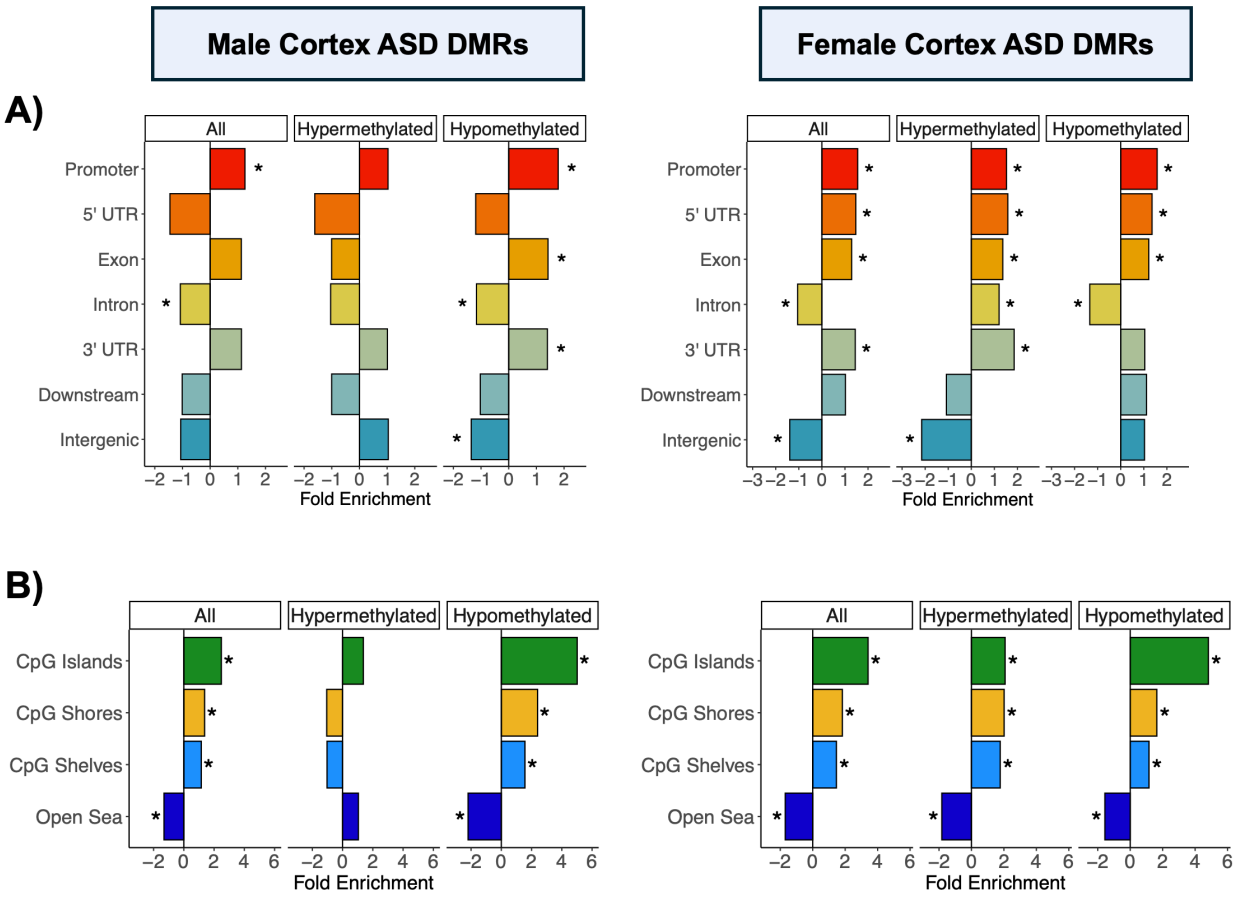
B)


Enriched Chromatin States for Differentially Methylated Regions
Frequency
Odds Ratio
Adipose
Blood & T−cell
Brain
Digestive
ENCODE2012
ES−deriv
ESC
Epithelial
HSC & B−cell
Heart
IMR90
Mesench
Muscle
Myosat
Neurosph
Other
Sm. Muscle
Thymus
iPSC
Active TSS
Flanking Active TSS
Transcription at Gene 5' and 3'
Strong Transcription
Weak Transcription
Genic Enhancers
Enhancers
ZNF Genes & Repeats
Heterochromatin
Bivalent/Poised TSS
Flanking Bivalent TSS/Enhancer
Bivalent Enhancer
Repressed PolyComb
Weak Repressed PolyComb
Quiescent/Low

Supplemental Figure 2.9: The results of region epigenome enrichment analysis of **A)** male and **B)** female ASD cfDNA DMRs using the ChromHMM Epigenomics Roadmap as a reference. The intensity of the heatmap's tiles correspond to the magnitude of a given enrichment, as quantified by odds ratio.

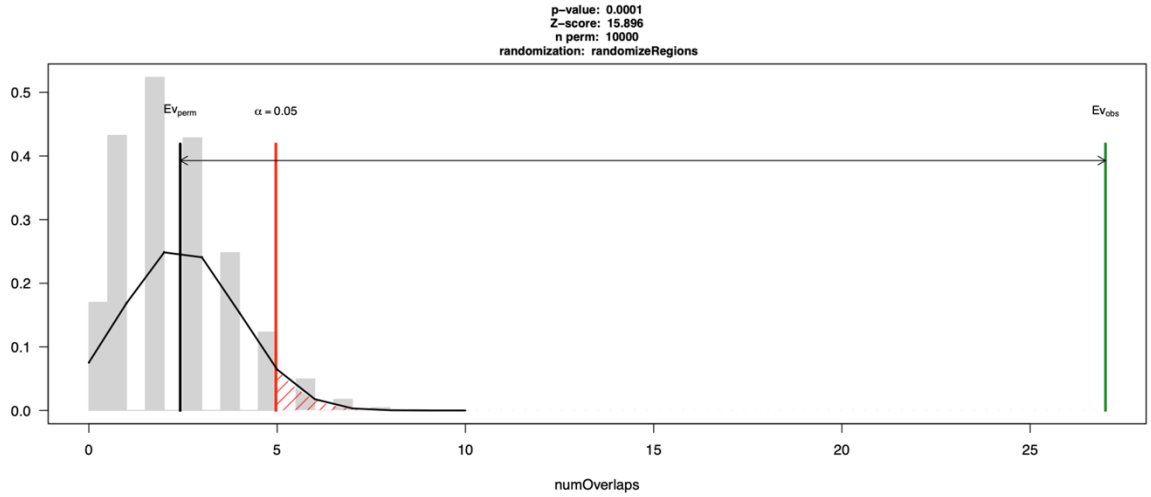


Supplemental Figure 2.10: Enrichment analyses of male and female placenta ASD DMRs (permutation p-value <0.05) for both **A)** genic annotations and **B)** CpG annotations as performed and plotted by DMRichR. DMRs were compared to background regions for each comparison, with significance determined by Fisher's test with FDR correction (* = q-value < 0.05).

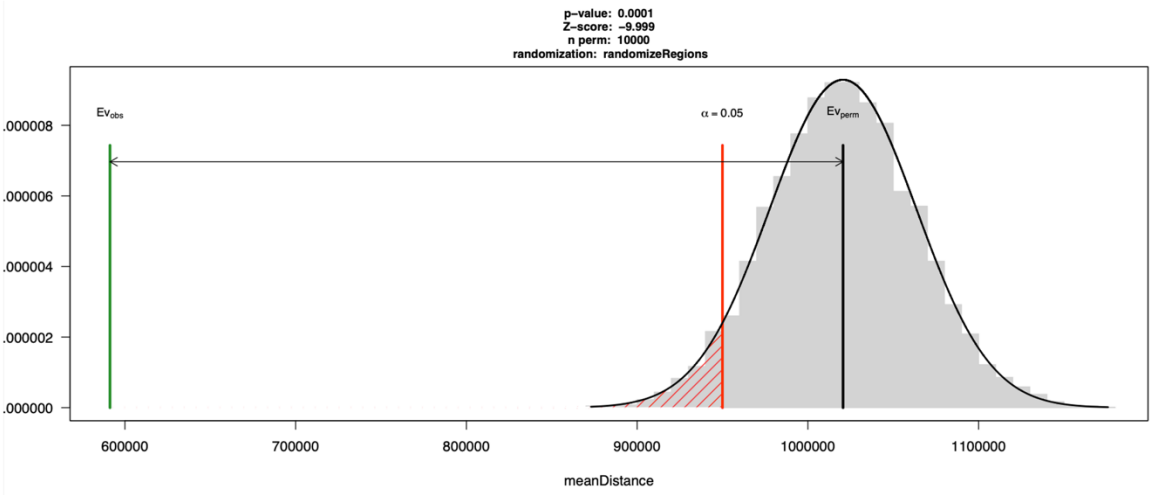


Supplemental Figure 2.11: Enrichment analyses of male and female Cortex ASD DMRs (permutation p-value <0.05) for both **A)** genic annotations and **B)** CpG annotations as performed and plotted by DMRichR. DMRs were compared to background regions for each comparison, with significance determined by Fisher's test with FDR correction (* = q-value < 0.05).

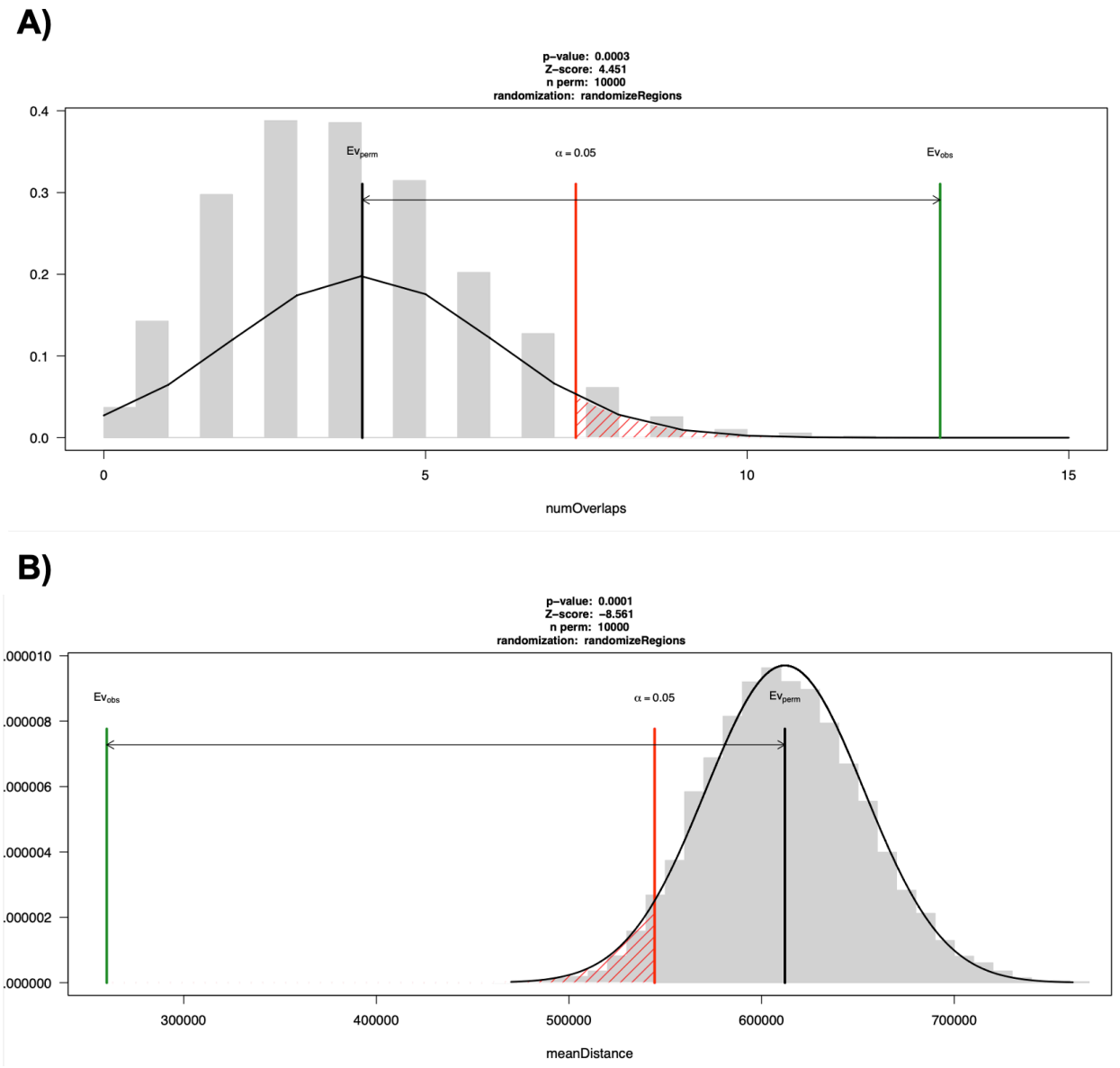
A)



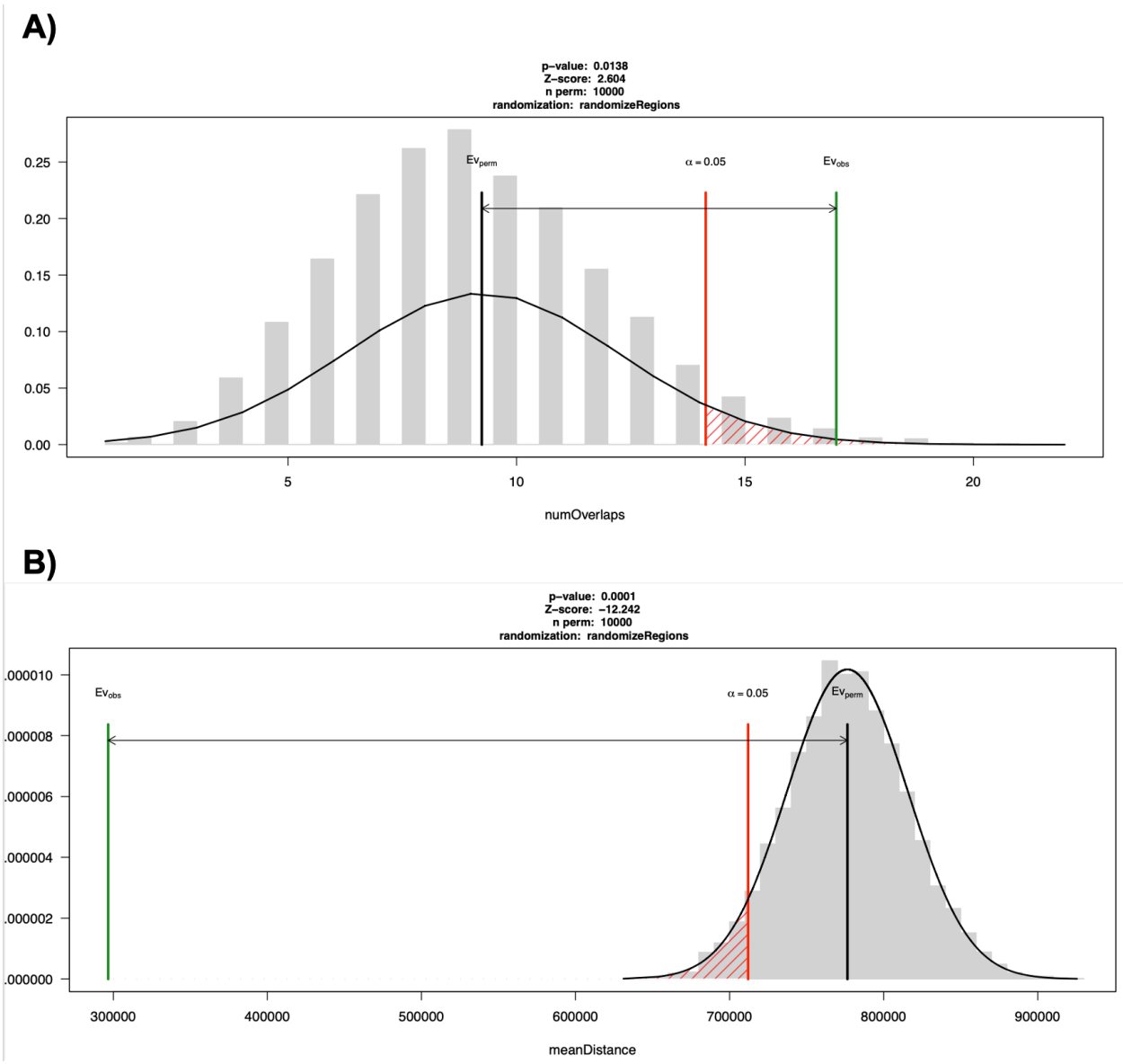
B)



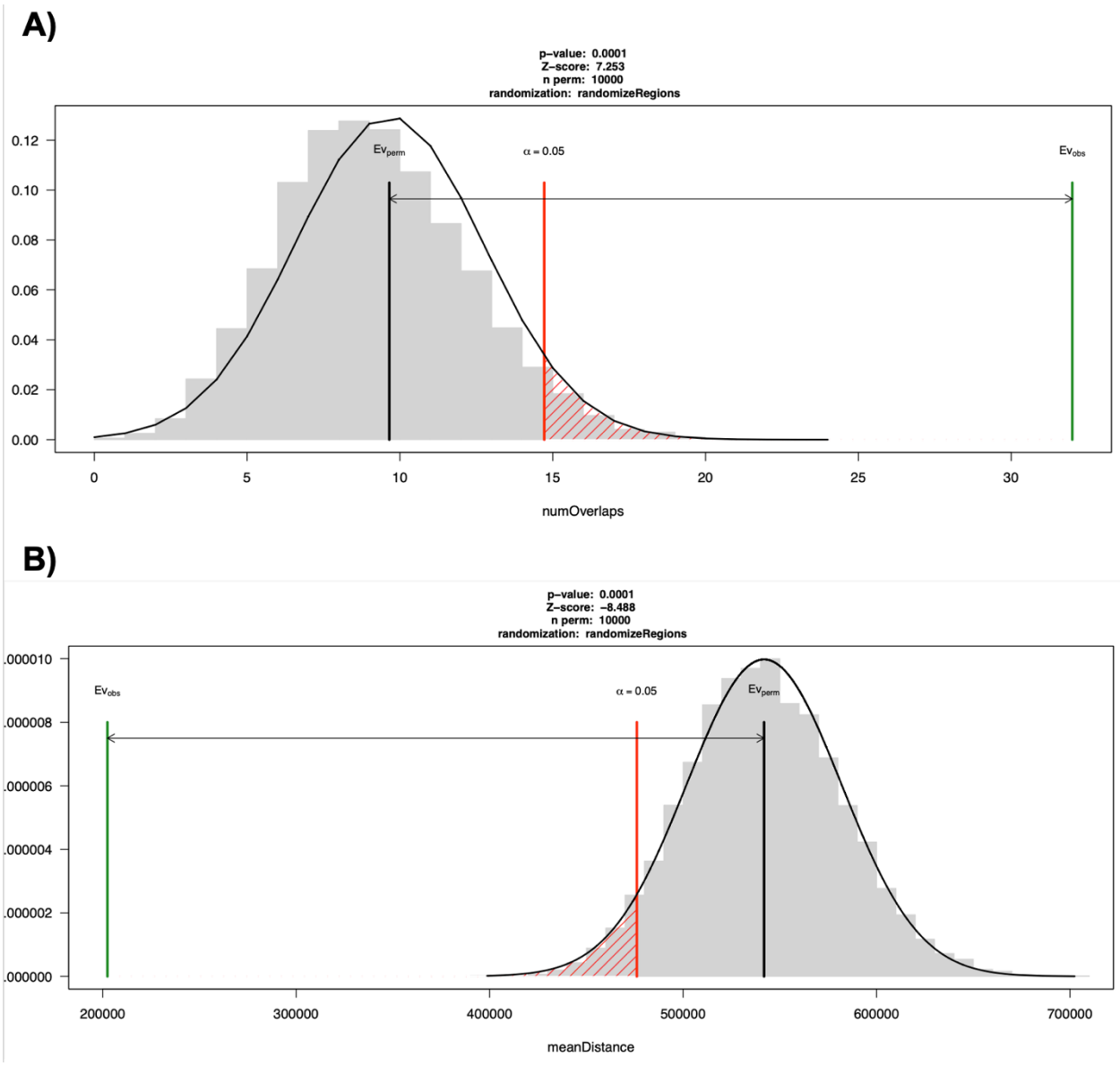
Supplemental Figure 2.12: Plots of the significance of region level overlap between Male cfDNA ASD DMRs and Male Placenta ASD DMRs as determined by permutations testing with respect to **A)** the number of overlaps between the two DMR sets and **B)** the mean distance between the DMRs in those two sets. Y-axis is probability density on both plots.



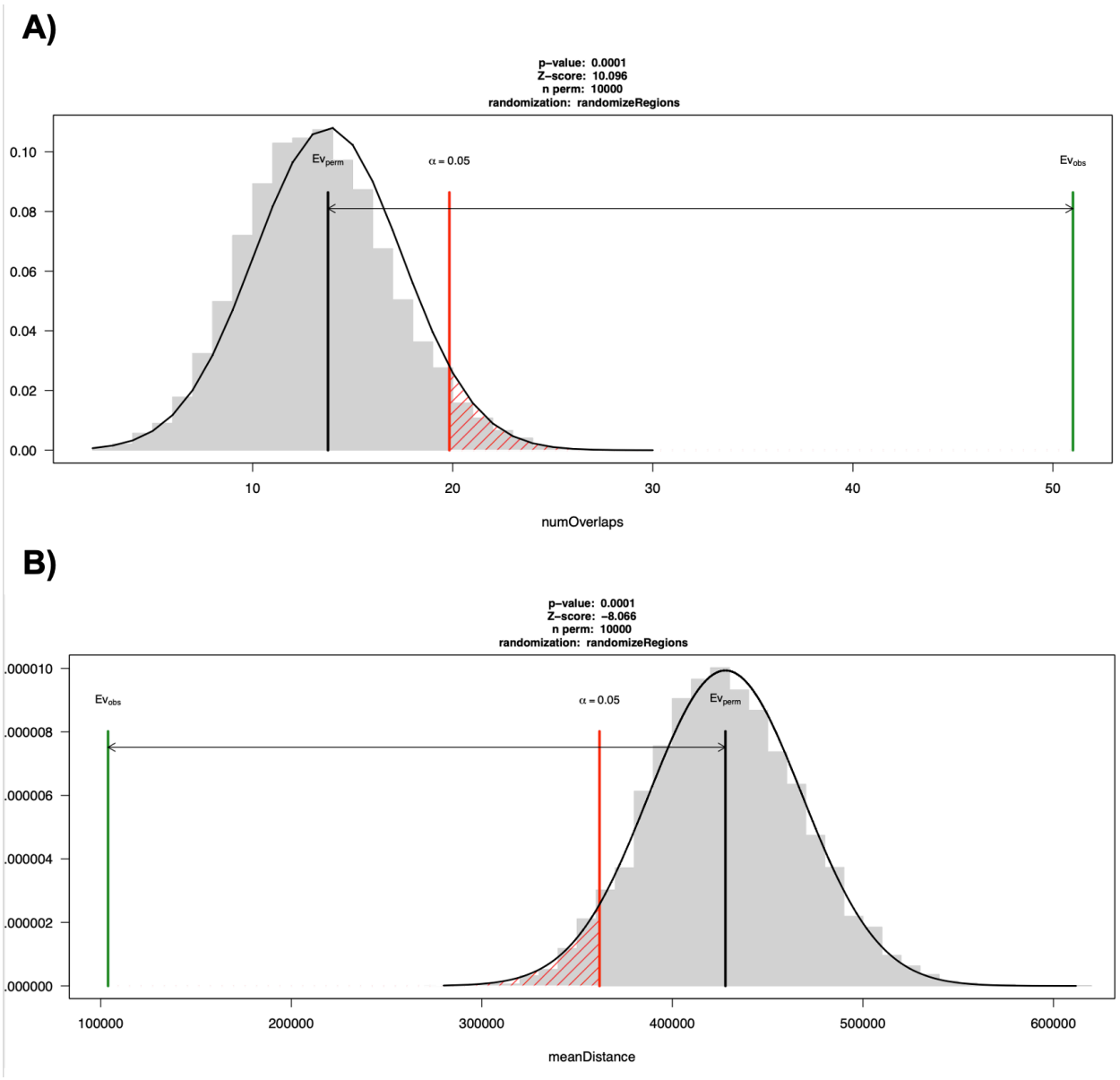
Supplemental Figure 2.13: Plots of the significance of region level overlap between Male cfDNA ASD DMRs and Male Cortex ASD DMRs as determined by permutations testing with respect to **A)** the number of overlaps between the two DMR sets and **B)** the mean distance between the DMRs in those two sets. Y-axis is probability density on both plots.



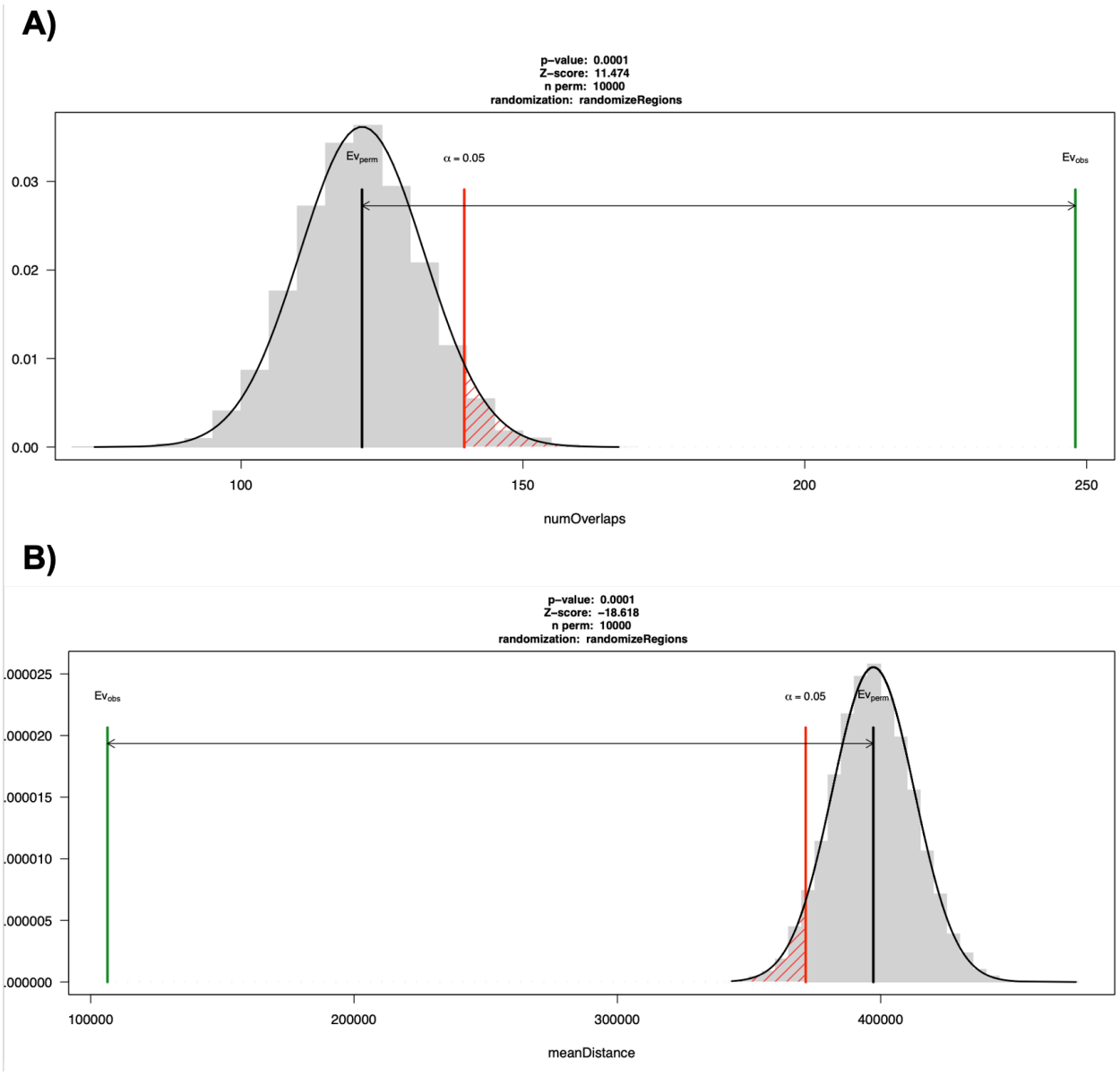
Supplemental Figure 2.14: Plots of the significance of region level overlap between Male Placenta ASD DMRs and Male Cortex ASD DMRs as determined by permutations testing with respect to **A)** the number of overlaps between the two DMR sets and **B)** the mean distance between the DMRs in those two sets. Y-axis is probability density on both plots.



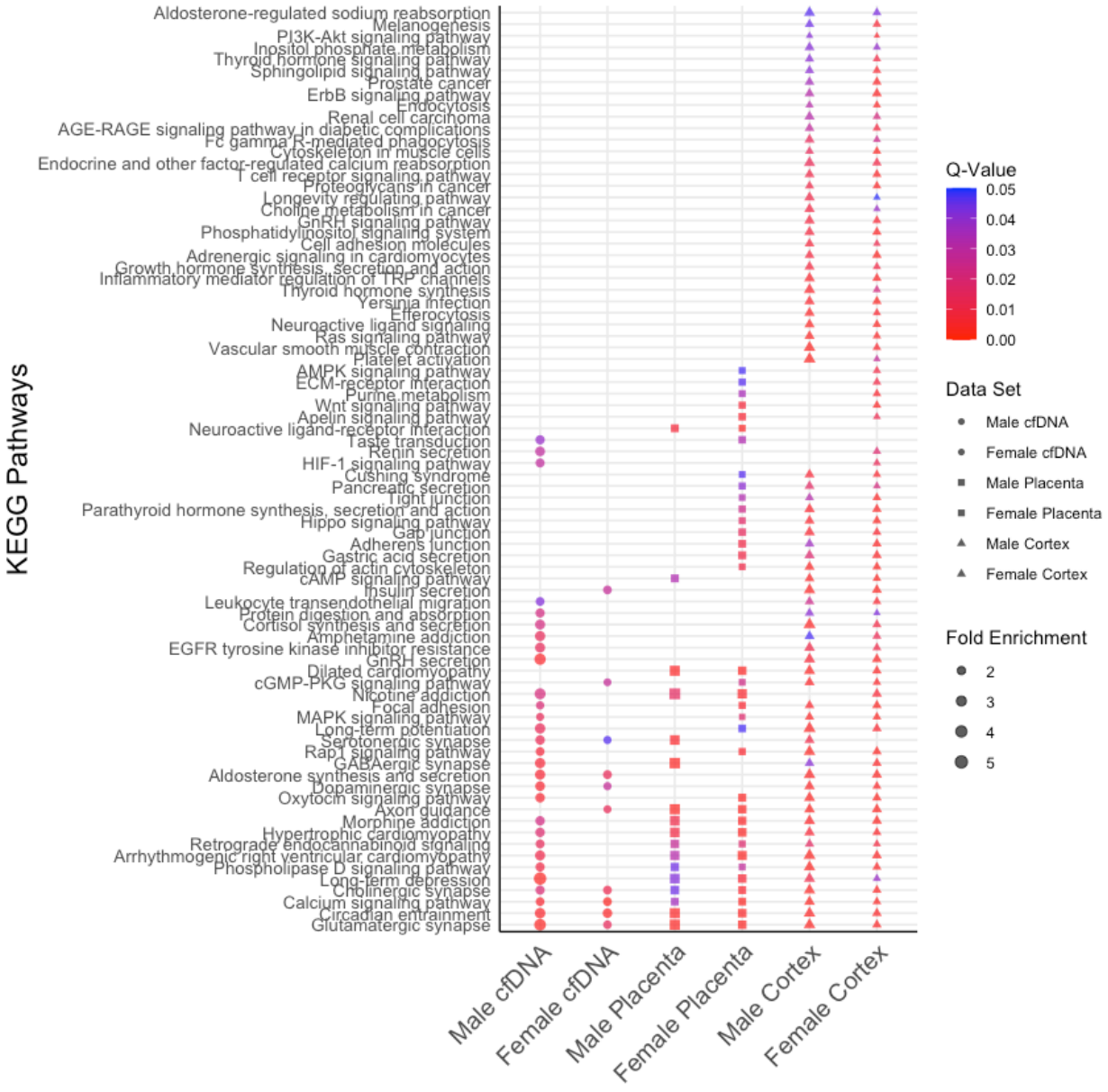
Supplemental Figure 2.15: Plots of the significance of region level overlap between Female cfDNA ASD DMRs and Female Placenta ASD DMRs as determined by permutations testing with respect to **A)** the number of overlaps between the two DMR sets and **B)** the mean distance between the DMRs in those two sets. Y-axis is probability density on both plots.



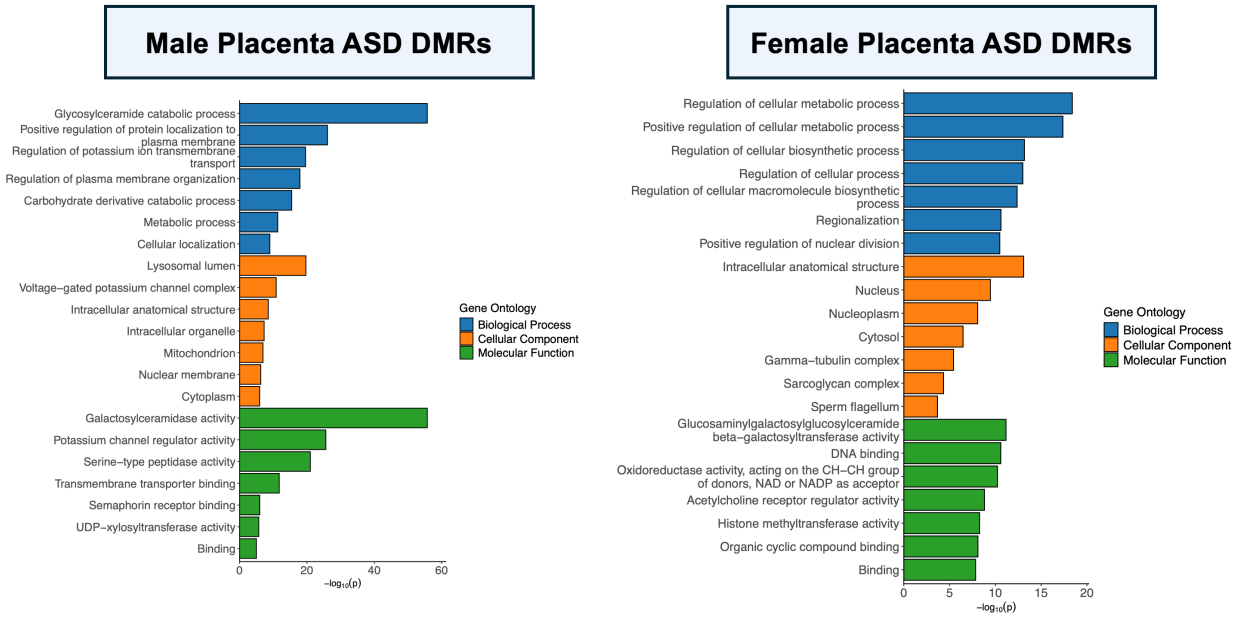
Supplemental Figure 2.16: Plots of the significance of region level overlap between Female cfDNA ASD DMRs and Female Cortex ASD DMRs as determined by permutations testing with respect to **A)** the number of overlaps between the two DMR sets and **B)** the mean distance between the DMRs in those two sets. Y-axis is probability density on both plots.



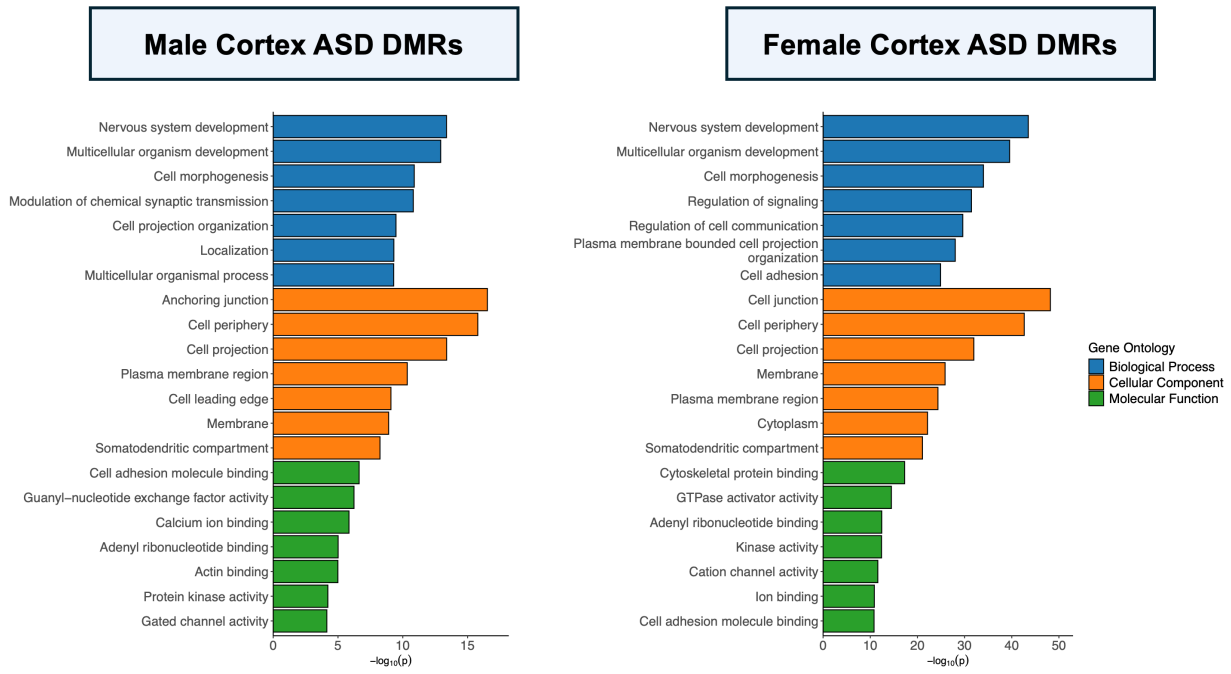
Supplemental Figure 2.17: Plots of the significance of region level overlap between Female Placenta ASD DMRs and Female Cortex ASD DMRs as determined by permutations testing with respect to **A)** the number of overlaps between the two DMR sets and **B)** the mean distance between the DMRs in those two sets. Y-axis is probability density on both plots.



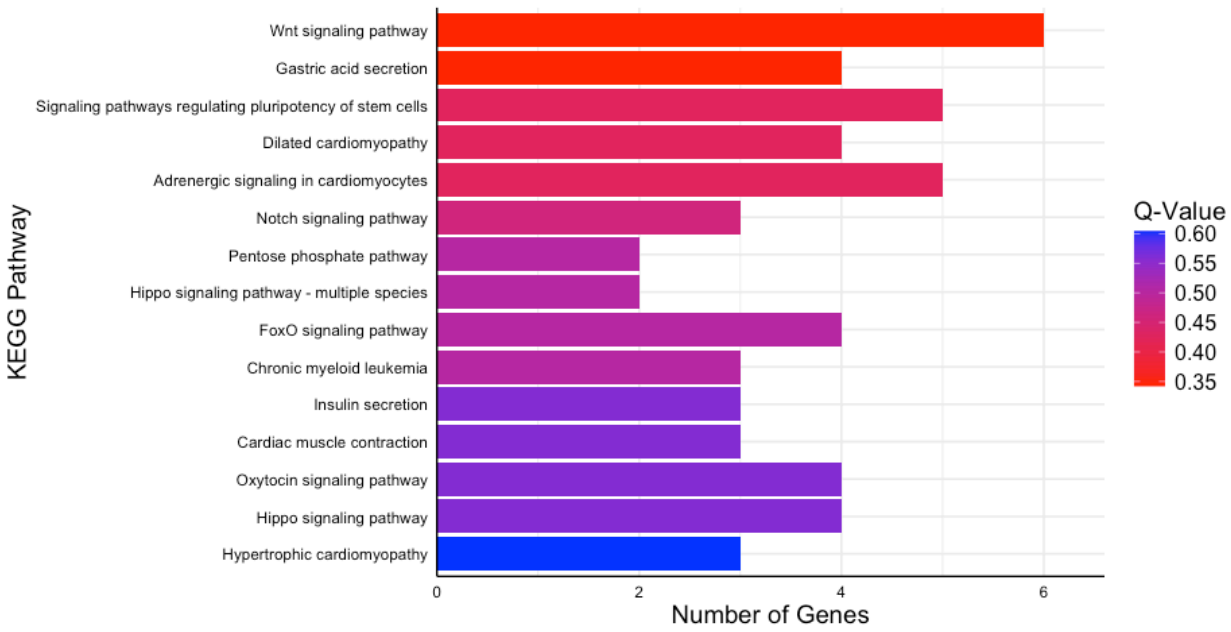
Supplemental Figure 2.18: The results of KEGG pathway enrichment analyses for all six ASD DMR gene lists, sex-stratified. Terms are ordered bottom to top on the y-axis by the number of DMR gene lists they are significantly enriched in. Significance determined by Fisher's Exact Test with BH correction.



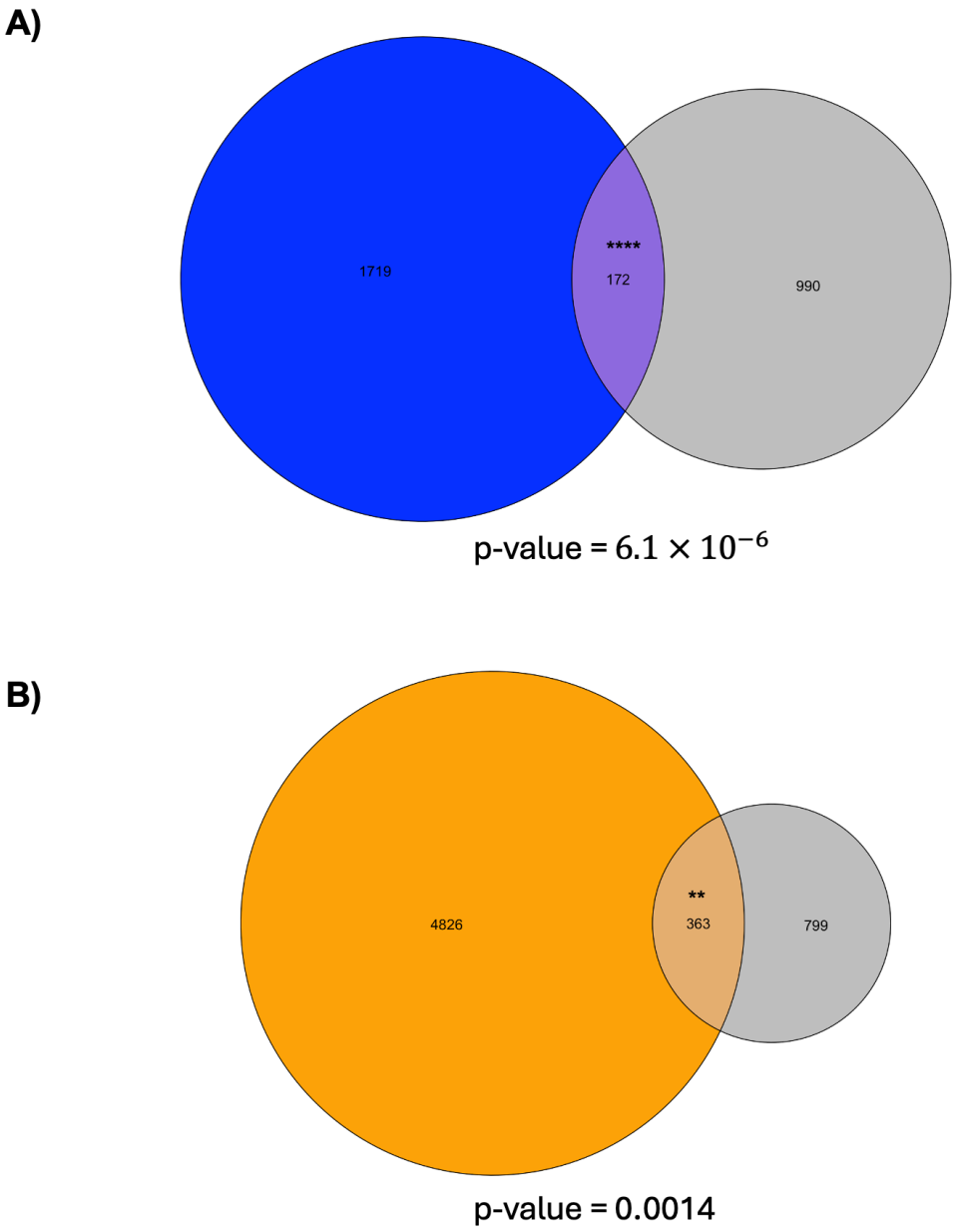
Supplemental Figure 2.19: The results of Gene ontology (GO) term enrichment analyses for male and female placenta ASD DMR gene lists, as performed by GREAT. The top seven most significantly enriched terms for each of the three gene ontologies are shown.



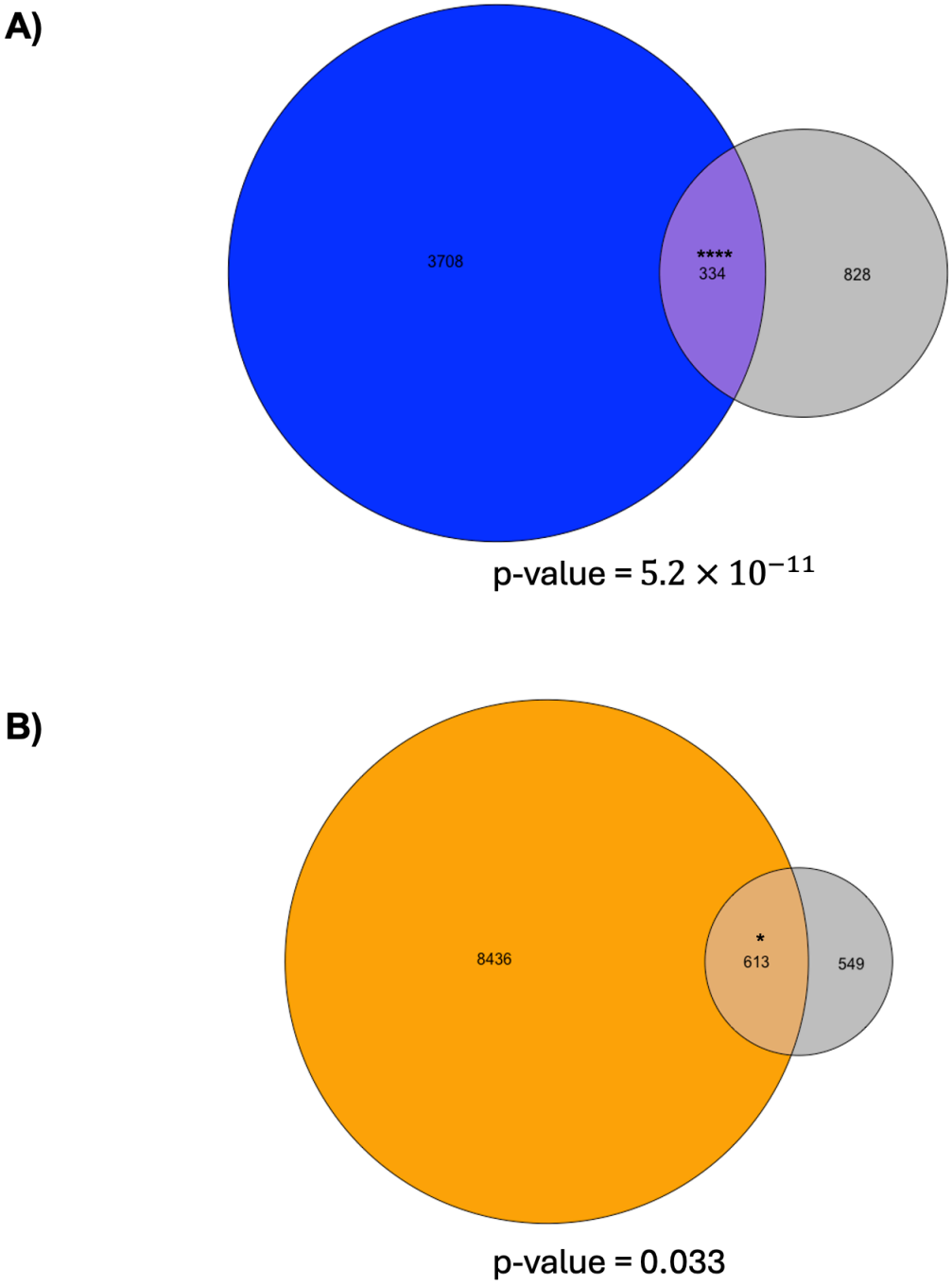
Supplemental Figure 2.20: The results of Gene ontology (GO) term enrichment analyses for male and female cortex ASD DMR gene lists, as performed by GREAT. The top seven most significantly enriched terms for each of the three gene ontologies are shown.



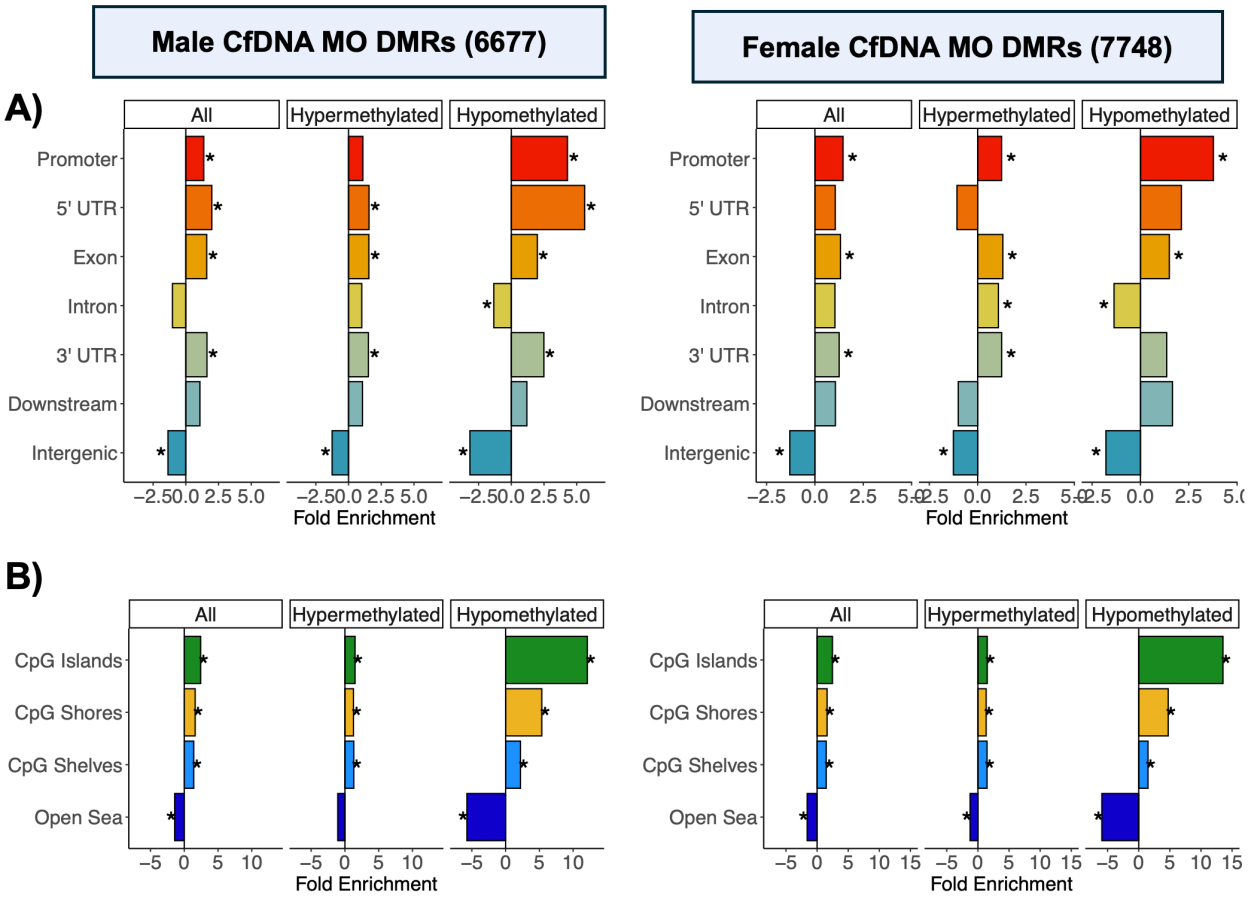
Supplemental Figure 2.21: Barplot of the top 15 most significantly enriched for KEGG pathways in the list of 227 genes whose overlap is specific to female cfDNA, placenta, and cortex ASD DMRs. No pathway enrichment passed a significance threshold of $q < 0.05$.



Supplemental Figure 2.22: Venn diagrams of the overlapping genes between the SFARI gene list and **A)** male placenta ASD DMRs and **B)** female placenta ASD DMRs.

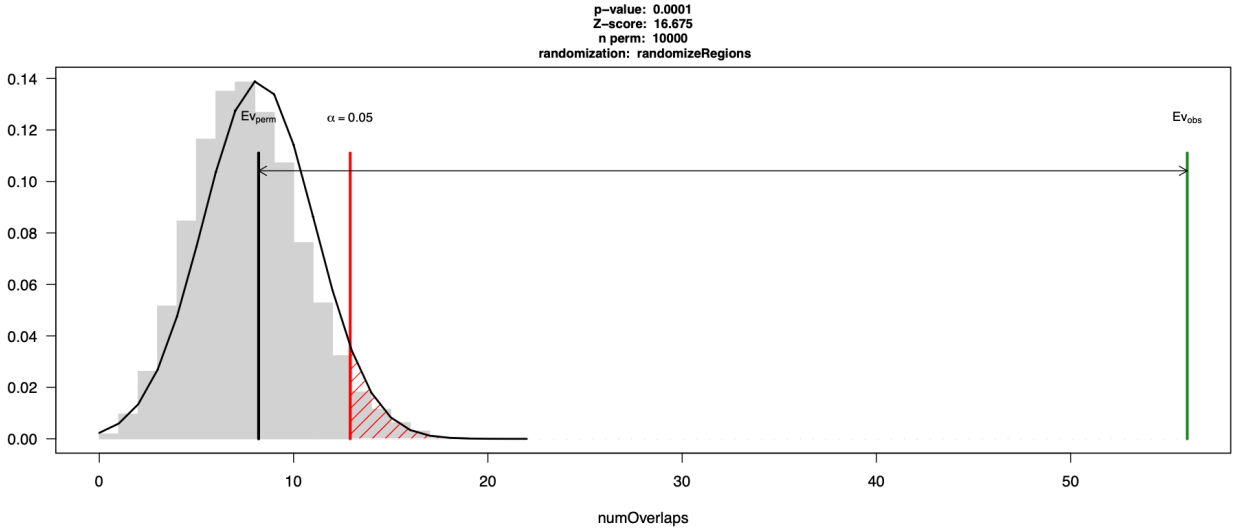


Supplemental Figure 2.23: Venn diagrams of the overlapping genes between the SFARI gene list and **A)** male cortex ASD DMRs and **B)** female cortex ASD DMRs.

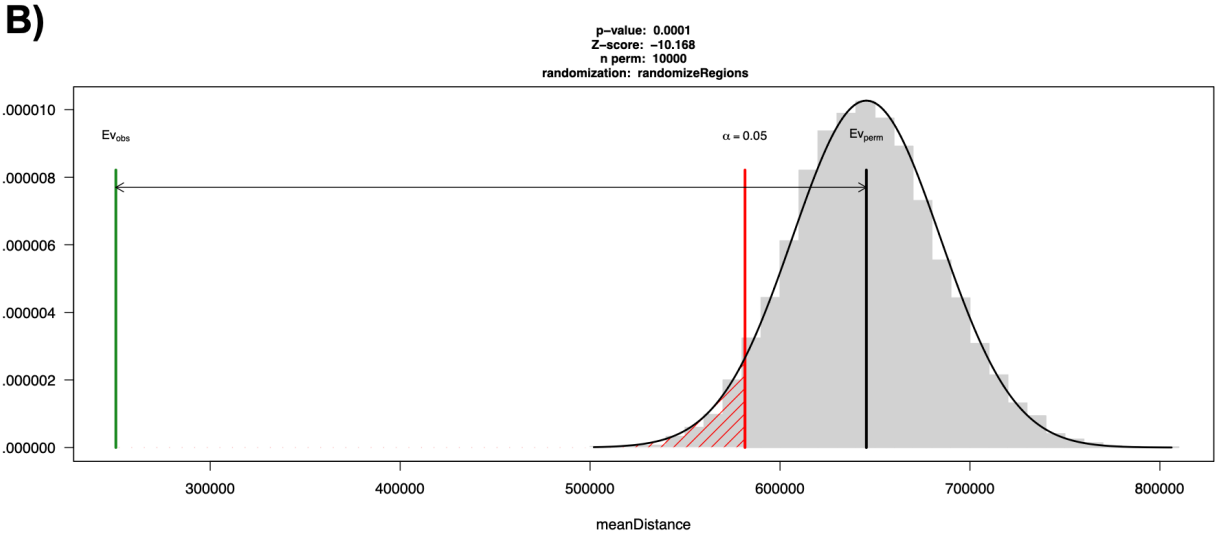


Supplemental Figure 2.24: Enrichment analyses of male and female cfDNA MO DMRs (permutation p-value < 0.05) for both **A)** genic annotations and **B)** CpG annotations as performed and plotted by DMRichR. DMRs were compared to background regions for each comparison, with significance determined by Fisher's test with FDR correction (* = q-value < 0.05).

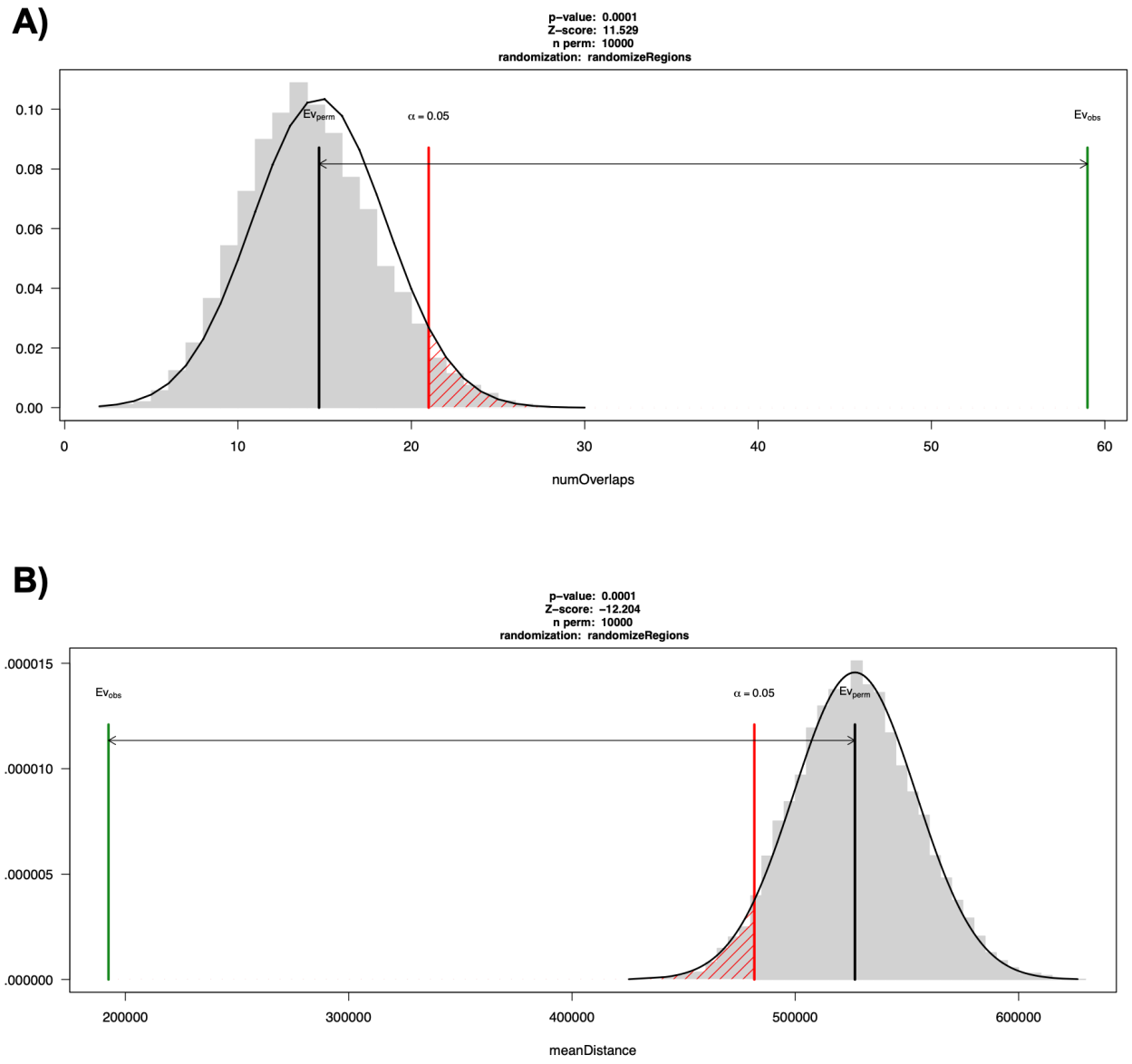
A)



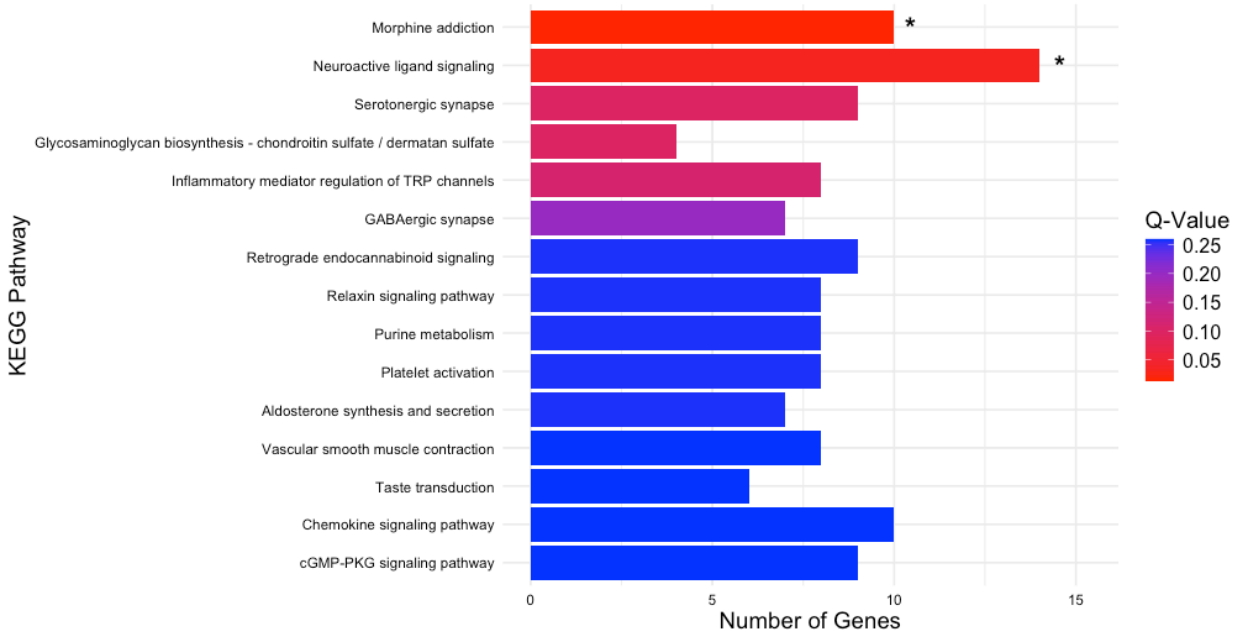
B)



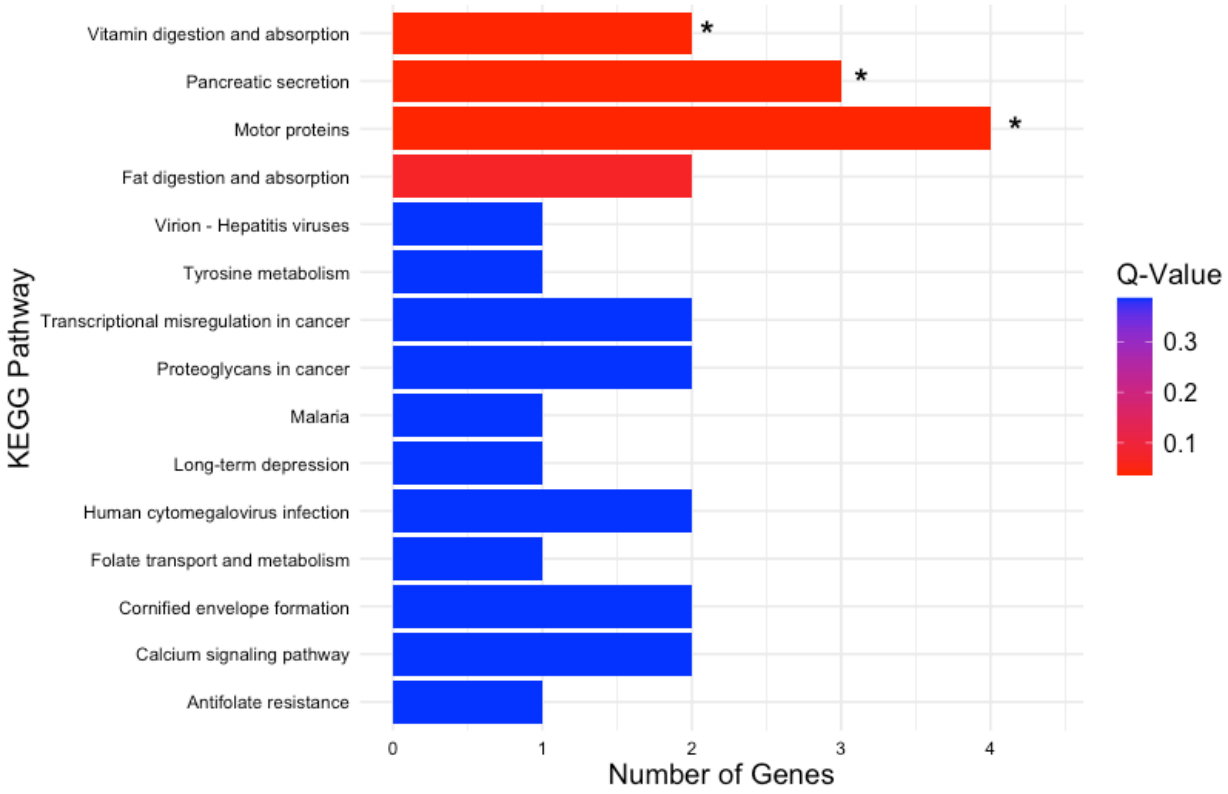
Supplemental Figure 2.25: Plots of the significance of region level overlap between Male cfDNA ASD and MO DMRs as determined by permutations testing with respect to **A)** the number of overlaps between the two DMR sets and **B)** the mean distance between the DMRs in those two sets. Y-axis is probability density on both plots.



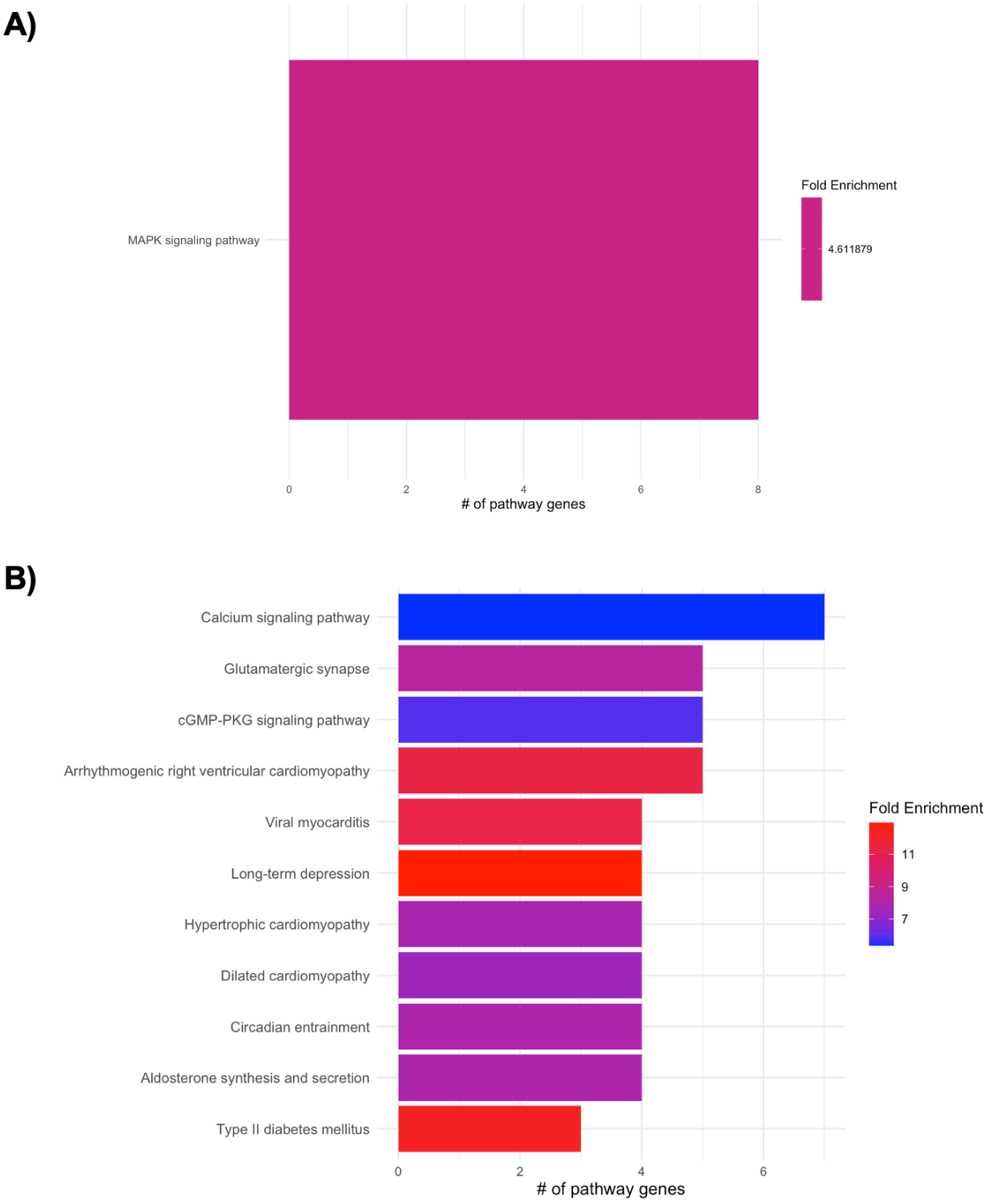
Supplemental Figure 2.26: Plots of the significance of region level overlap between Female cfDNA ASD and MO DMRs as determined by permutations testing with respect to **A)** the number of overlaps between the two DMR sets and **B)** the mean distance between the DMRs in those two sets. Y-axis is probability density on both plots.



Supplemental Figure 2.27: Bar plot of the top 15 most significantly enriched for KEGG pathways in the list of 922 genes whose overlap is specific to male and female MO DMRs and not intersecting with any cfDNA ASD DMRs. Significance determined by Fisher's Exact Test (* $q < 0.05$).

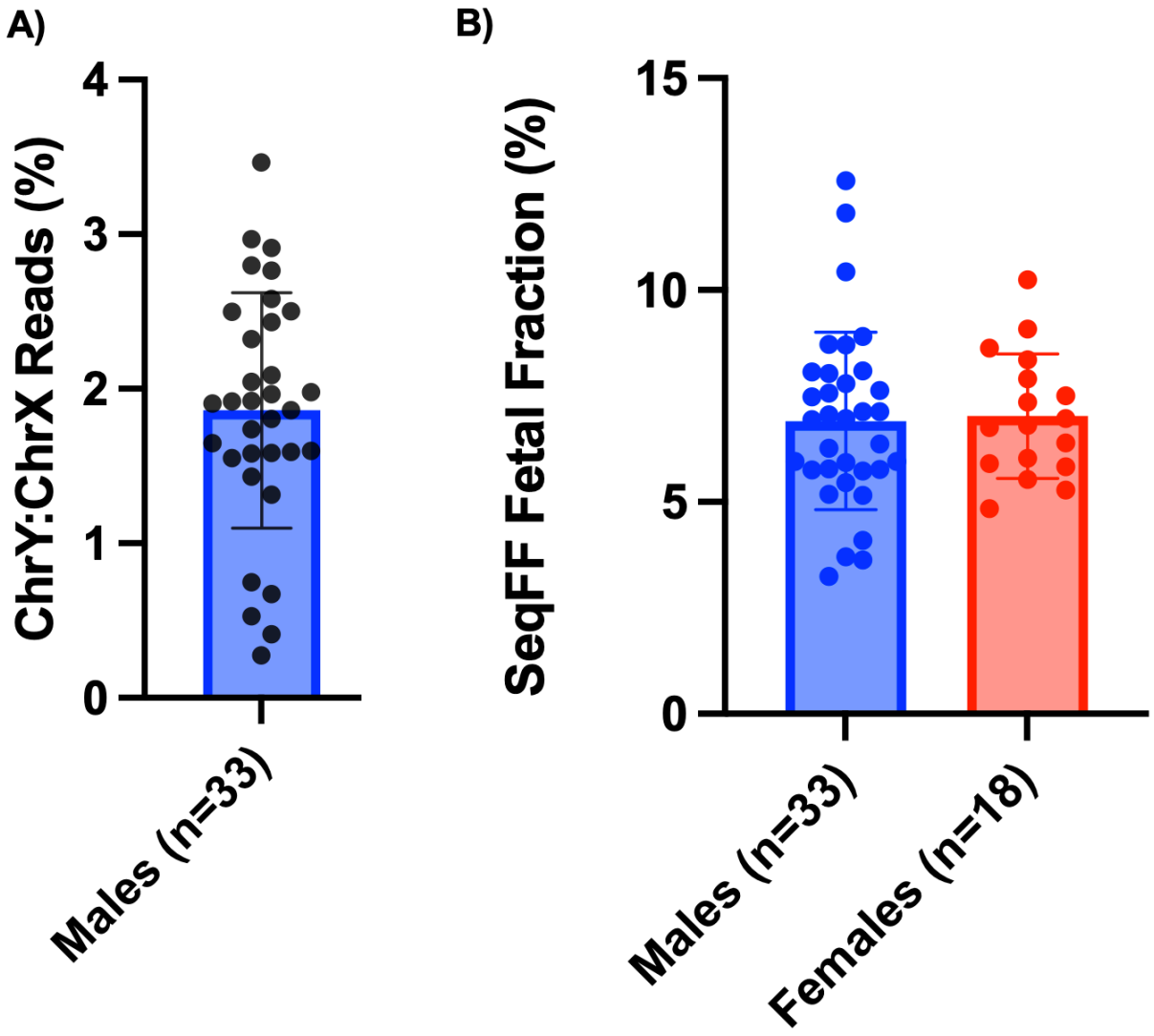


Supplemental Figure 2.28: Bar plot of the top 15 most significantly enriched for KEGG pathways in the list of 70 genes whose overlap is specific to male and female cfDNA ASD DMRs and not intersecting with MO DMR genes. Significance determined by Fisher's Exact Test (* $q < 0.05$).

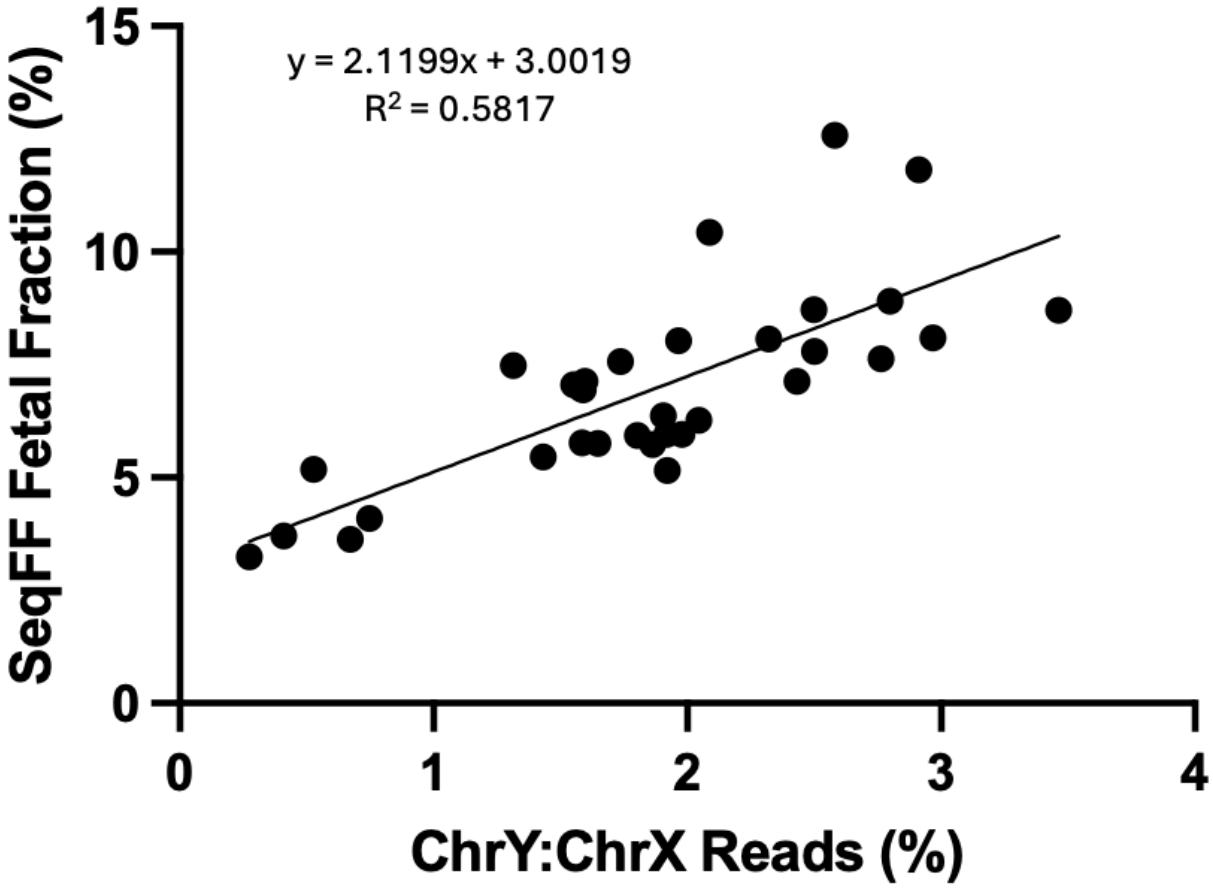


Supplemental Figure 2.29: Bar plot of all significantly enriched for KEGG pathways in the subset of cfDNA ASD DMR genes shared between male and females with **A)**

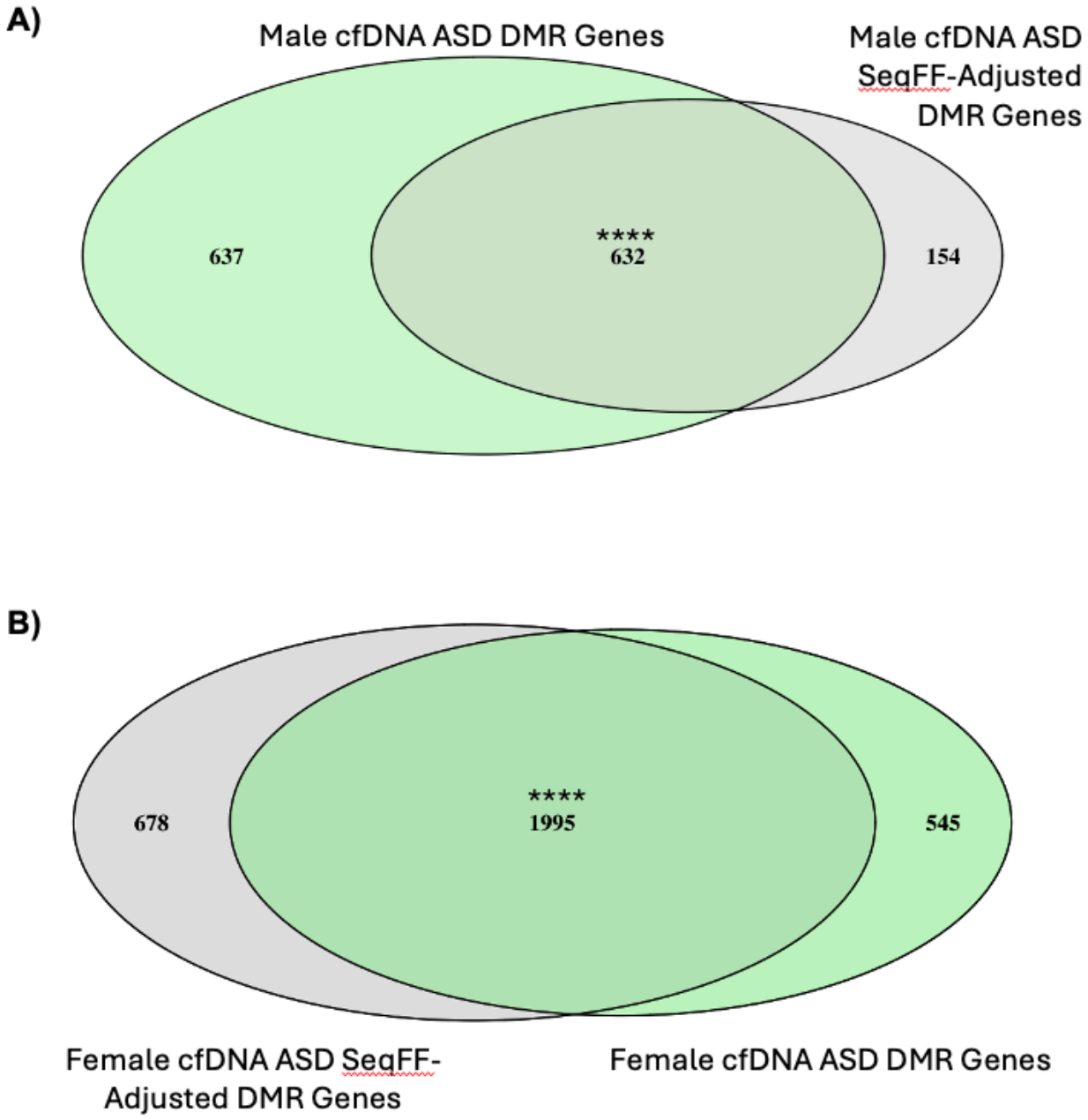
diverging methylation between sexes and **B)** converging methylation between sexes**.** Significance determined by Fisher's Exact Test (* q < 0.05), and all pathways shown in these plots meet significance standard.



Supplemental Figure 2.30: Graphs depicting the fraction of cfDNA calculated to be of fetal origin as quantified by **A)** ChrY:ChrX ratios in the fetal male samples and **B)** SeqFF in all samples.

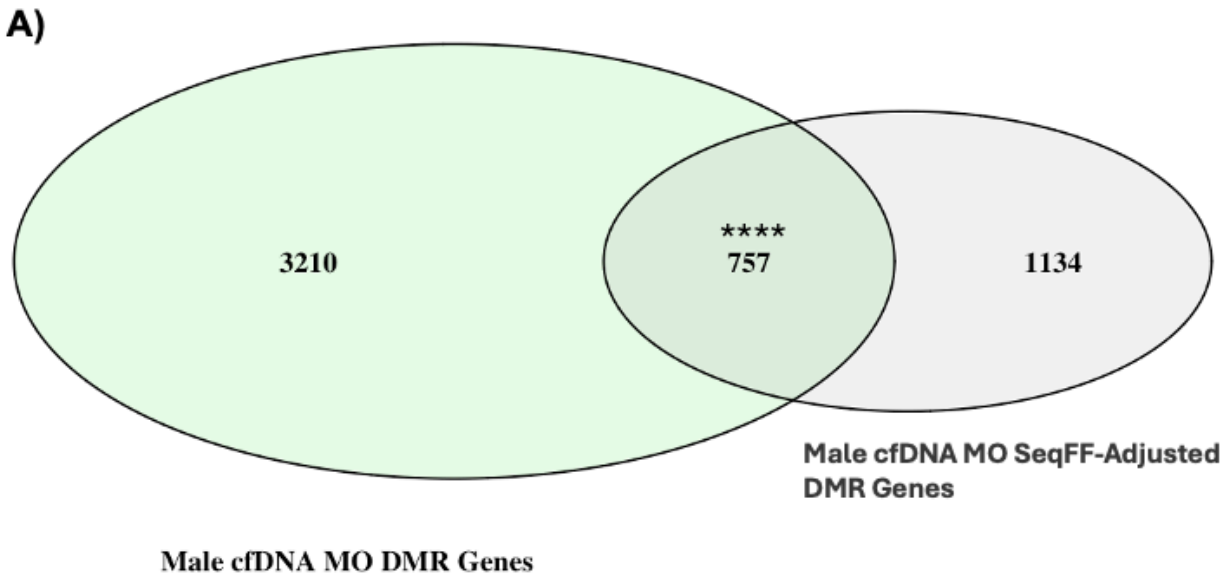


Supplemental Figure 2.31: Simple linear regression of ChrY:ChrX read fraction vs. SeqFF-estimated fetal fraction in males (n = 33). Equation of the regression provided.



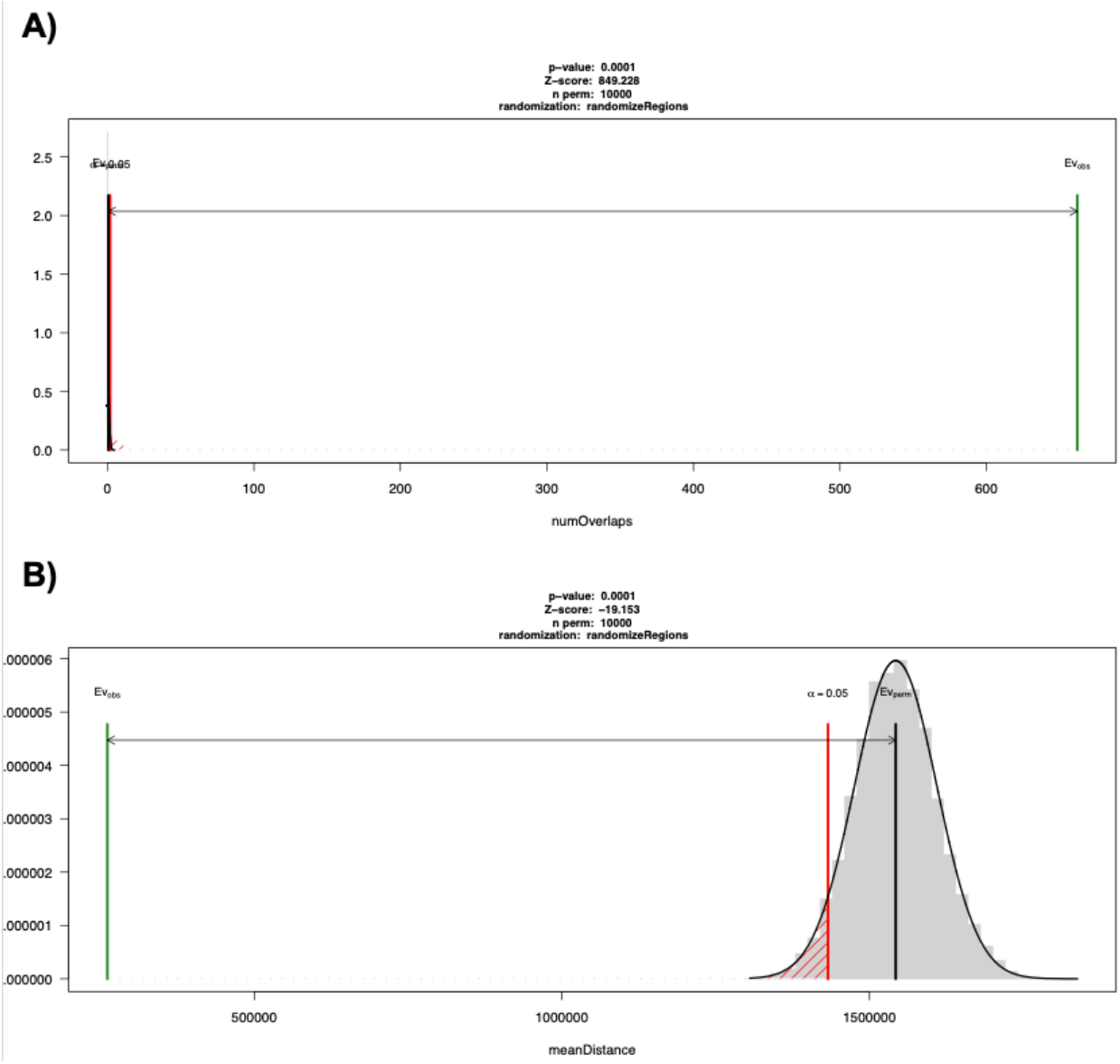
Supplemental Figure 2.32: Venn diagrams showing gene-level overlap of the genes conserved between reported cfDNA DMRs and cfDNA DMRs generated with adjustment for SeqFF-estimated fetal fraction. Significance of gene lists overlaps relative to the universe of background regions denoted with asterisks (****). Significant overlaps

observed for **A)** Male ASD DMRs (p = 0, 632 intersecting genes) and **B)** Female ASD DMRs (p = 0, 1995 intersecting genes).

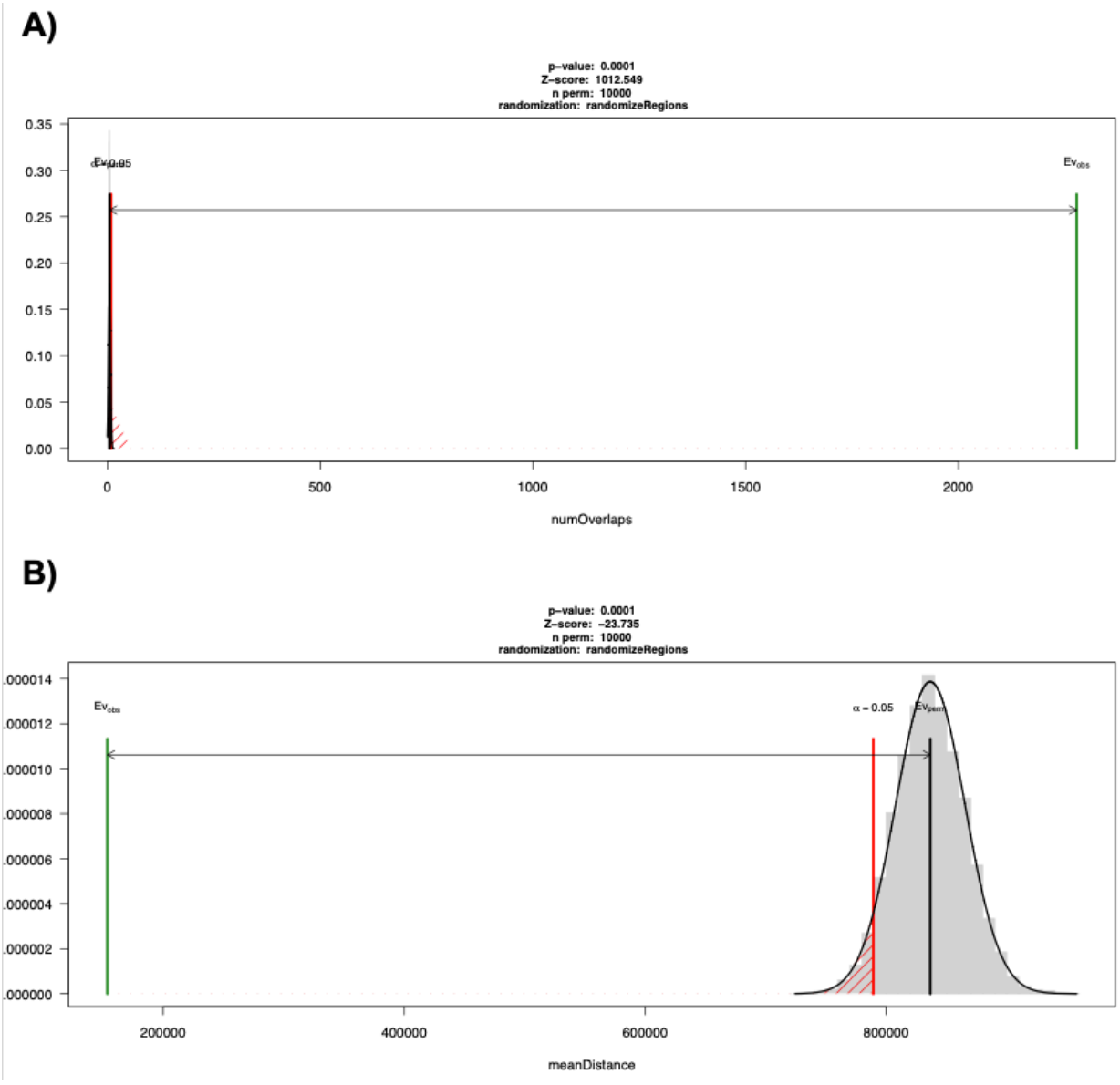


Supplemental Figure 2.33: Venn diagrams showing gene-level overlap of the genes conserved between reported cfDNA DMRs and cfDNA DMRs generated with adjustment

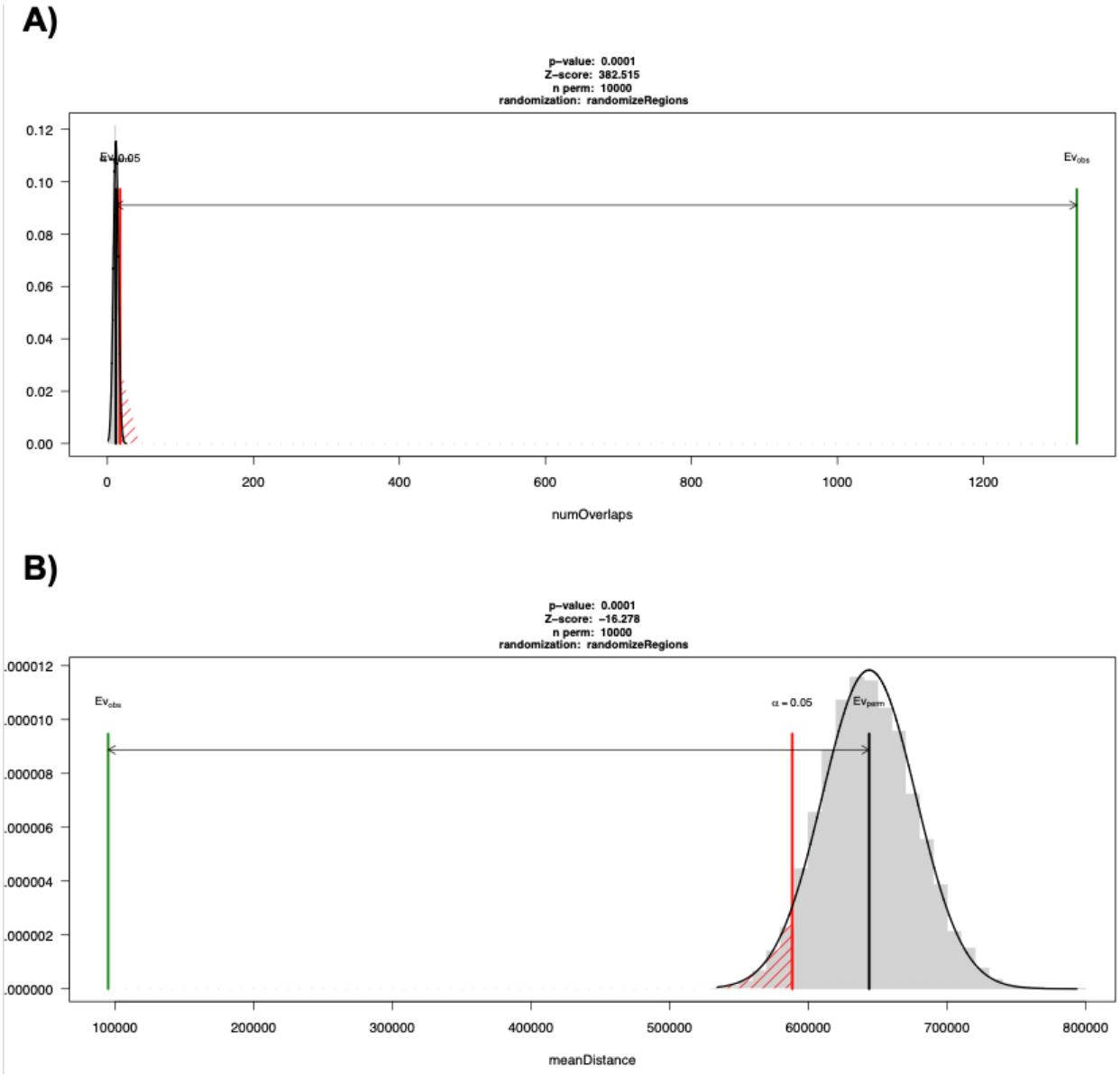
for SeqFF-estimated fetal fraction. Significance of gene lists overlaps relative to the universe of background regions denoted with asterisks (****). Significant overlaps observed for **A)** Male MO DMRs (p = 5.8e-75, 757 intersecting genes), and **B)** Female MO DMRs (p = 4.8e-125, 1933 intersecting genes).



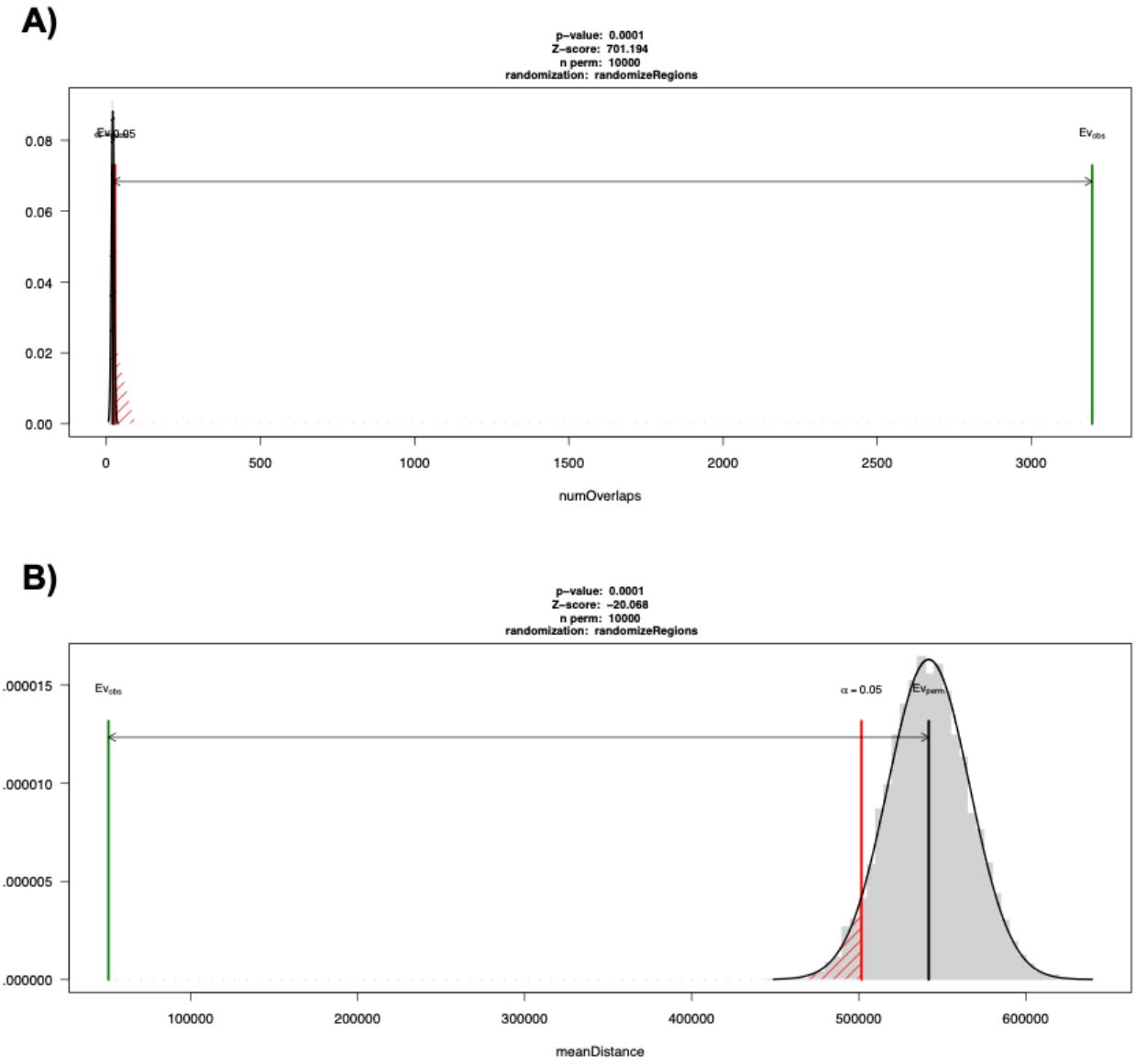
Supplemental Figure 2.34: Plots of the significance of region level overlap between Male CfDNA ASD DMRs and Male cfDNA ASD SeqFF-adjusted DMRs as determined by permutations testing with respect to **A)** the number of overlaps between the two DMR sets and **B)** the mean distance between the DMRs in those two sets. Y-axis is probability density on both plots.



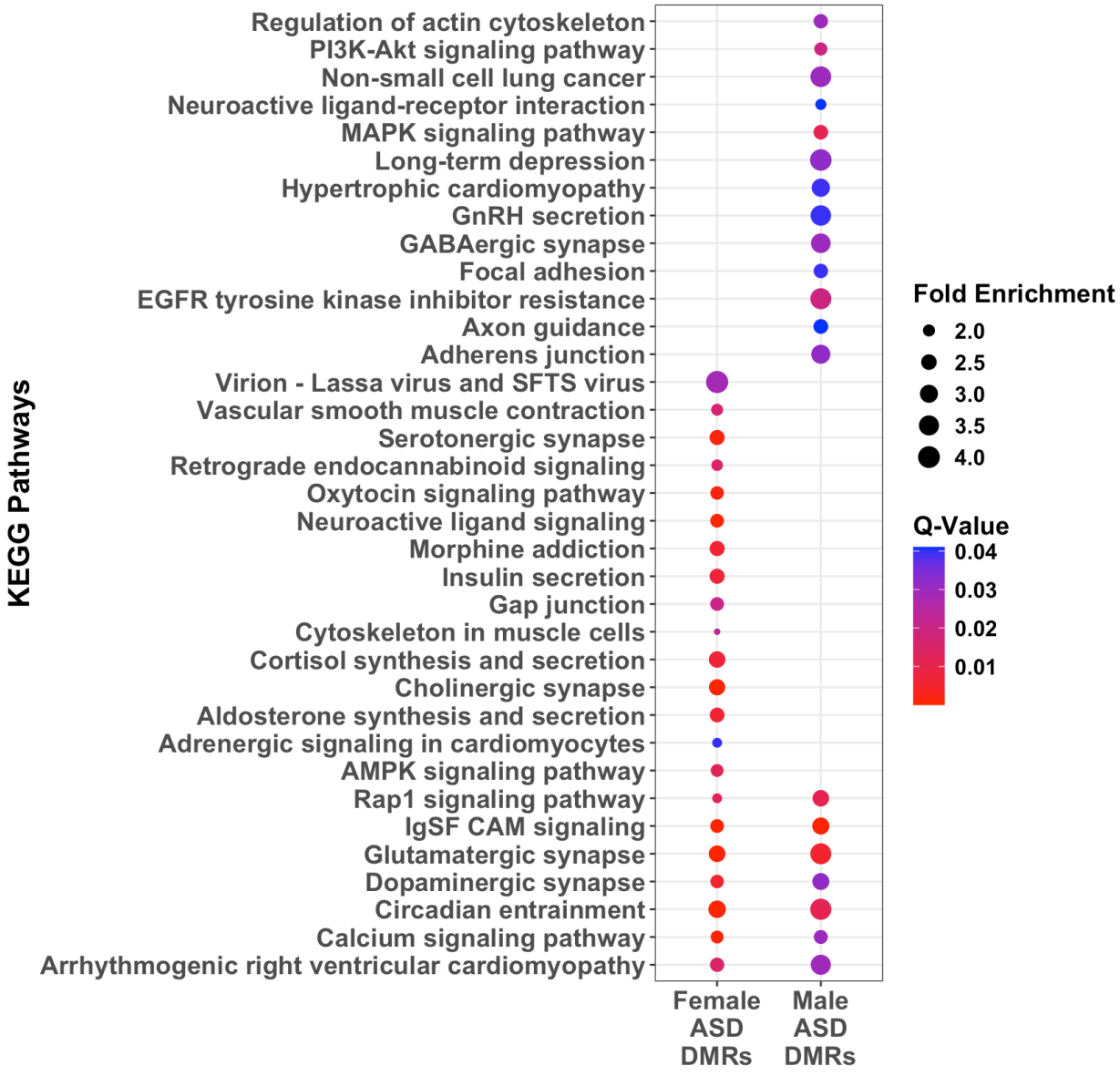
Supplemental Figure 2.35: Plots of the significance of region level overlap between Female CfDNA ASD DMRs and Female cfDNA ASD SeqFF-adjusted DMRs as determined by permutations testing with respect to **A)** the number of overlaps between the two DMR sets and **B)** the mean distance between the DMRs in those two sets. Y-axis is probability density on both plots.



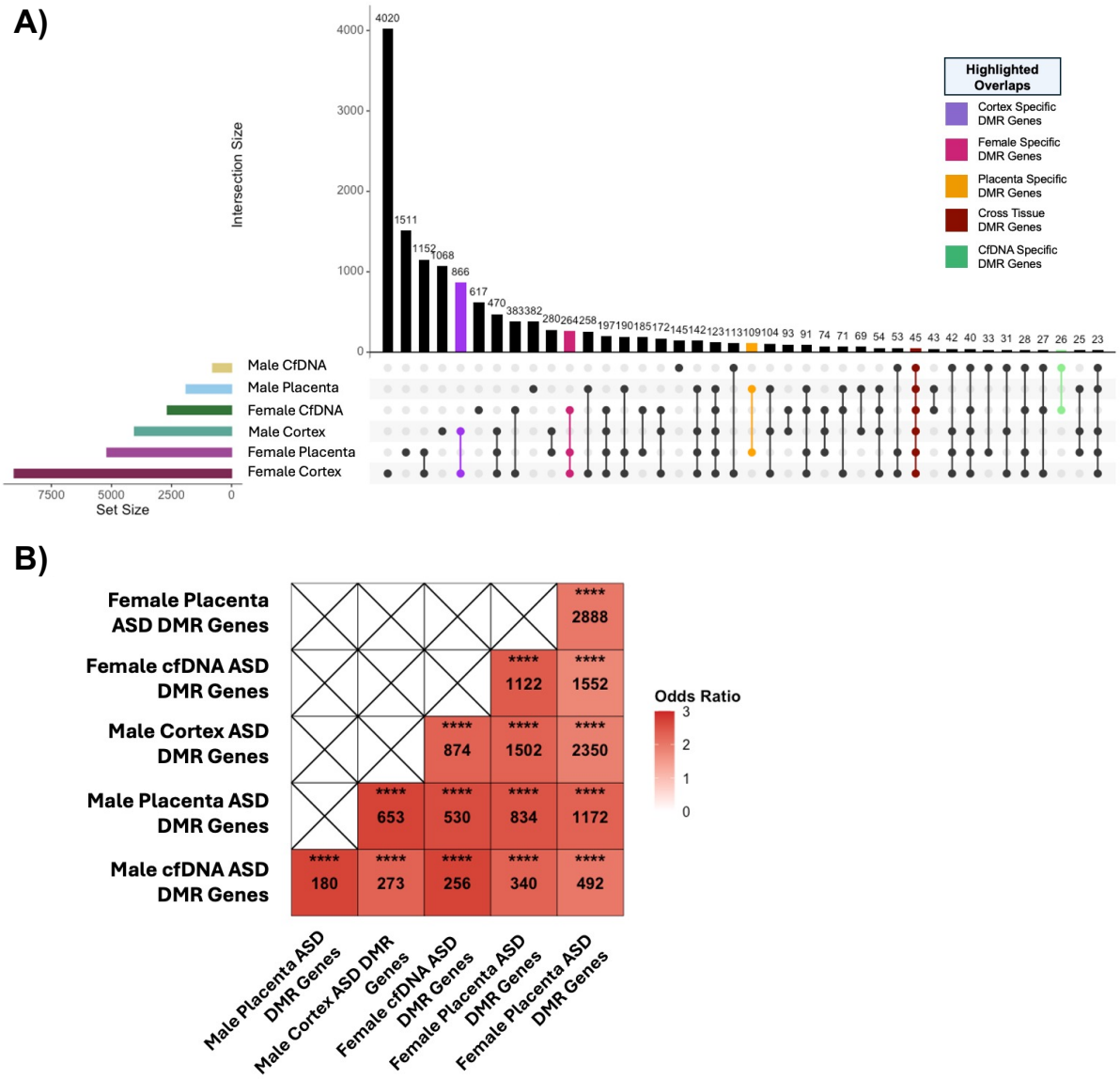
Supplemental Figure 2.36: Plots of the significance of region level overlap between Male CfDNA MO DMRs and Male cfDNA MO SeqFF-adjusted DMRs as determined by permutations testing with respect to **A)** the number of overlaps between the two DMR sets and **B)** the mean distance between the DMRs in those two sets. Y-axis is probability density on both plots.



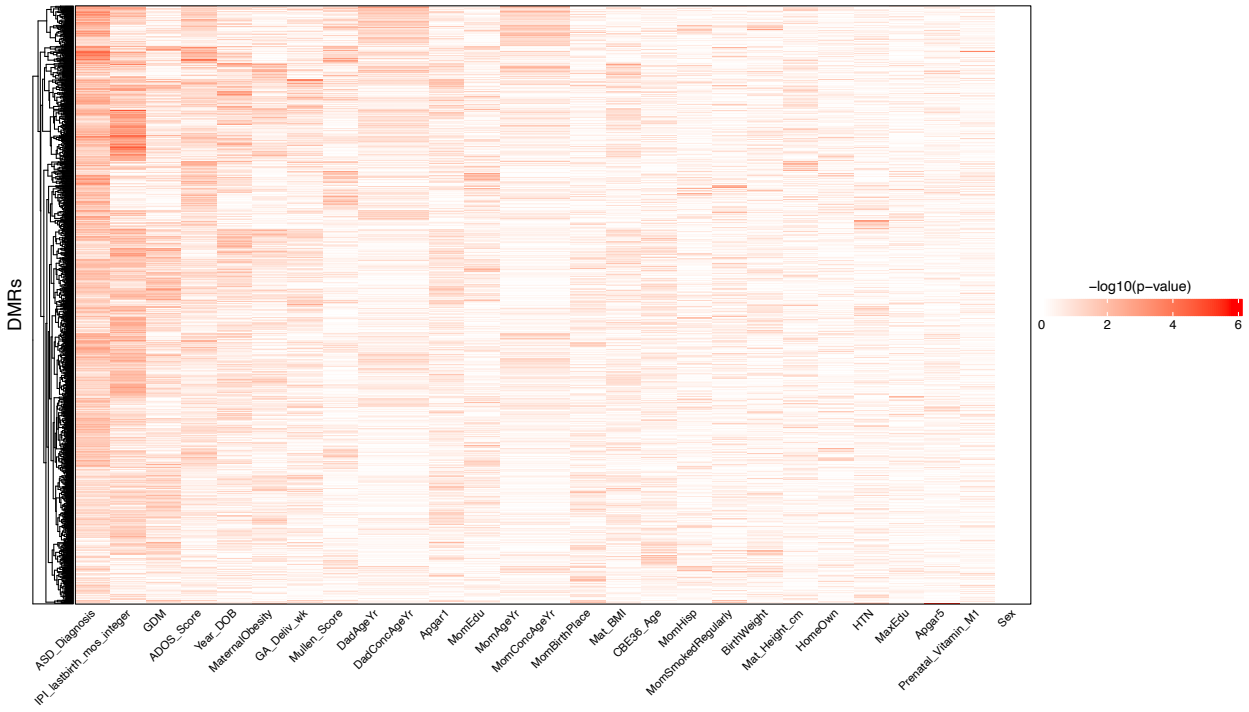
Supplemental Figure 2.37: Plots of the significance of region level overlap between Female CfDNA MO DMRs and Female cfDNA MO SeqFF-adjusted DMRs as determined by permutations testing with respect to **A)** the number of overlaps between the two DMR sets and **B)** the mean distance between the DMRs in those two sets. Y-axis is probability density on both plots.



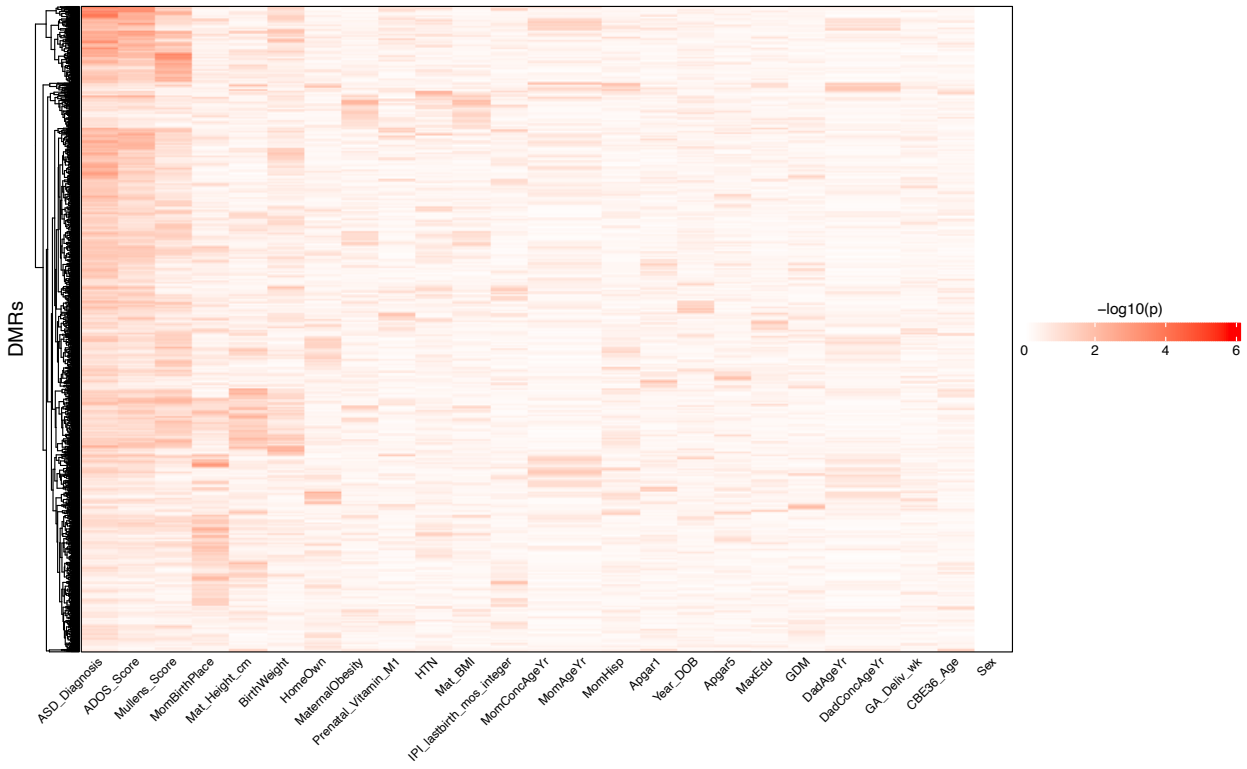
Supplemental Figure 2.38: All significant KEGG pathway enrichments for male and female cfDNA ASD SeqFF-adjusted DMRs. Seven pathways were significantly enriched in both males and females, clustering around synapse development and cell signaling. Four of the seven pathways significantly enriched in both sexes were also significantly enriched in both sexes of the original, non-SeqFF-adjusted DMRs.



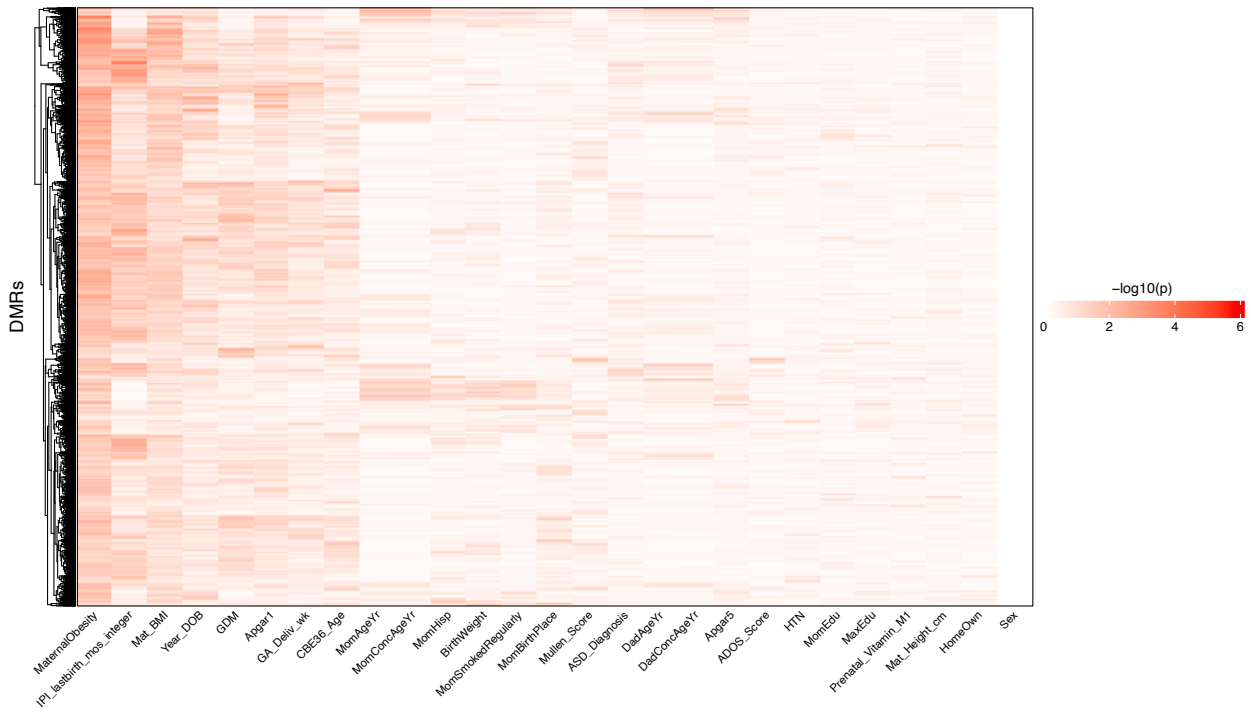
Supplemental Figure 2.39: A) All gene level overlaps between SeqFF-adjusted cfDNA ASD DMRs, placenta DMRs, and cortex DMRs. **B)** Significance of each the overlap between all possible combinations of DMR gene lists, including the SeqFF-adjusted cfDNA ASD DMRs in males and females. Significance determined by Fisher's Exact Test. The numbers shown on each tile correspond to the number of genes overlapping the two gene lists in question. Asterisks denote p-value as follows: **** $p < 0.0001$



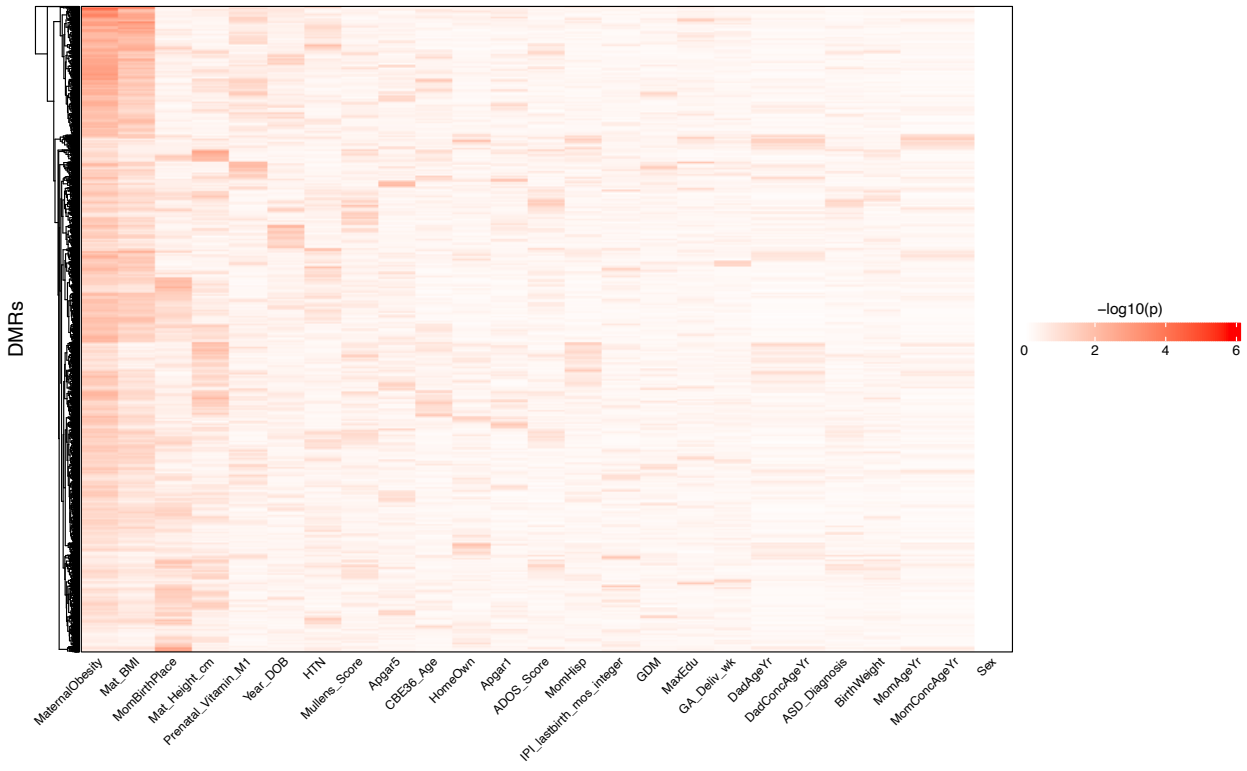
Supplemental Figure 2.40: Heatmap of significance of association between each male cfDNA ASD DMR (y-axis) and each sample covariate (x-axis). Significance determined by t-test of the regression coefficient and quantified as a permutation p-value. Sample covariates ordered on the x-axis by total number of significant (p-value < 0.05) associations with the DMRs, descending from left to right.



Supplemental Figure 2.41: Heatmap of significance of association between each female cfDNA ASD DMR (y-axis) and each sample covariate (x-axis). Significance determined by t-test of the regression coefficient and quantified as a permutation p-value. Sample covariates ordered on the x-axis by total number of significant (p-value < 0.05) associations with the DMRs, descending from left to right.



Supplemental Figure 2.42: Heatmap of significance of association between each male cfDNA MO DMR (y-axis) and each sample covariate (x-axis). Significance determined by t-test of the regression coefficient and quantified as a permutation p-value. Sample covariates ordered on the x-axis by total number of significant (p-value < 0.05) associations with the DMRs, descending from left to right.



Supplemental Figure 2.43: Heatmap of significance of association between each female cfDNA MO DMR (y-axis) and each sample covariate (x-axis). Significance determined by t-test of the regression coefficient and quantified as a permutation p-value. Sample covariates ordered on the x-axis by total number of significant (p-value < 0.05) associations with the DMRs, descending from left to right.

2.9.2 Supplemental Tables

While the supplemental tables referenced throughout this chapter are too large to include in print, you can find them in full at the following Box directory: (https://ucdavis.box.com/s/7sw9ipmu7194tfy4e6xg9p0u6fdy5g42).

If this directory has become inaccessible since time of writing, the supplemental tables can likely be found attached to an online publication describing these results. As a last resort, contact Dr. Janine LaSalle at jmlasalle@health.ucdavis.edu to inquire about accessing these supplemental tables.

Chapter 3: Placental DNA methylation gene networks associate with wildfire particulate matter exposure and child neurodevelopmental outcomes.

3.1 Preface

This chapter contains original research that is currently unpublished and is intended for use in a future publication.

3.2 Authorship

I isolated DNA from placenta samples and prepared them for WGBS. Matthew Kramer and I preformed bioinformatic analysis. Amanda Goodrich and Elizabeth Angel provided data on MARBLES and B-SAFE participants. Sean Raffuse provided air pollution estimates. Meghan Miller oversaw all behavioral assessments of MARBLES participants used in this manuscript's analyses. Irva Hertz-Picciotto conceived of the MARBLES study itself. Cheryl K. Walker led the recruitment of MARBLES participant mothers and the drawing of blood plasma samples. Rebecca J. Schmidt, Janine M. LaSalle, and I conceived of the experiments and analyses described in this manuscript.

3.3 Abstract

Wildfire-associated particulate matter represents an increasingly prominent prenatal air pollution exposure in the western United States, particularly in regions afflicted with longer and more intense wildfire seasons. However, the epigenetic impacts of these exposures

during gestation on the placenta remains poorly characterized. We investigated whether source specific preconception and pregnancy exposure to fine particulate matter ($PM_{2.5}$), from wildfire events associate with coordinated alterations in placental DNA methylation networks. We further examined whether the wildfire-associated $PM_{2.5}$ DNA methylation alterations overlapped with those linked to ambient air pollution and neurodevelopmental outcomes. We performed whole-genome bisulfite sequencing (WGBS) on 221 placentae, then performed comethylation network analysis to identify modules of correlated DNA methylation associated with wildfire $PM_{2.5}$ exposures, as well as other factors including ambient $PM_{2.5}$ exposures and neurodevelopmental outcomes. We identified 85 placental comethylation modules, 22 of which were significantly associated with prenatal air pollution exposures. Multiple modules were found to exclusively associate with only wildfire-derived or ambient $PM_{2.5}$ exposures. Modules significantly associated with wildfire-derived $PM_{2.5}$ exposures exclusively contained genes involved in neurodevelopment and cell signaling, enrichments distinct from those identified from modules associated exclusively with ambient $PM_{2.5}$ exposures. Pregnancy air pollution preferentially correlated with modules annotated to semaphorin signaling and cytoskeletal remodeling pathways, while preconception exposures were enriched for modules proximal to transcriptional regulators. Ten exposure-associated modules correlated with child neurodevelopmental measures, including ASD diagnosis. These modules contained neurodevelopmentally relevant genes, including *NHIP, AUTS2*, and *EBF3,* and were enriched for synaptic and cell-cell signaling pathways. Prenatal wildfire air pollution exposures associate with temporally and source-specific placental methylation networks enriched for signaling pathways relevant to placental function and neurodevelopment.

These findings support the placenta as an epigenetic interface linking air pollution exposures to altered developmental trajectories.

3.4 Introduction

As global temperatures have risen and the climate becomes more arid, the United States has seen a corresponding increase in the length and severity of wildfire seasons, particularly in Western regions (188–192). Consequently, more attention has been focused on the potential contributions of wildfire smoke to air pollution, and the subsequent effects of wildfire smoke exposure. Exposure to high levels of wildfire smoke has been associated with numerous adverse outcomes, including declining respiratory health (193,194), diminished cardiovascular health (195–197), cancer risk (198,199), and worsened cognitive performance (200,201).

Additionally, a growing body of evidence supports associations between air pollution, including wildfire smoke derived air pollution, and sub-optimal child developmental outcomes. Associations between gestational air pollutant exposure and low birth weight and preterm birth outcomes are well-established (202–206), and many publications support the potential neurodevelopmental impacts of prenatal air pollution exposure (20-27). Increased prenatal air pollutant exposure has been inversely correlated with child cognitive test performance (207,208) and positively correlated with behavioral problems (209,210). Emerging evidence points to significant associations between perinatal air pollution exposure and autism spectrum disorder (autism) diagnosis, though debate

persists as to which component of air pollution is most strongly linked to autism (211–214).

A growing body of evidence suggests that air pollution exposure may influence child health outcomes not just during pregnancy, but also in the preconception window (defined as the 3 months prior to conception). The preconception period is an essential development window for both sperm and ova cells, and exposure to high levels of air pollutants during this period could have long-term impacts on fetal development (215–217). Increased preconception exposure to $PM_{2.5}$ was found to associate with increased child BMI at 2 yrs of age (218), and with lower Psychomotor Development Index scores (219). Some studies have shown associations between preconception air pollution exposure and autism diagnosis, though the replicability of these findings remain unclear (220,221).

Furthermore, many of the prior studies examining the potential connection between prenatal air pollution exposure and child neurodevelopment outcomes focus on ambient measurements of components like ultrafine particulate matter ($PM_{2.5}$), ignoring the unique toxicological makeup of wildfire smoke-derived air pollution. Wildfire smoke is often enriched for heavy metals, low molecular weight polycyclic aromatic hydrocarbons, flame retardants, and numerous other compounds absent from ambient air pollution (222). Thus, elucidating the impact of prenatal wildfire smoke-derived air pollution exposure on neurodevelopment requires studying wildfire exposed individuals, not just extrapolating

the findings of ambient air pollution studies onto wildfire-affected populations. Recent studies of wildfire smoke-derived air pollution specifically have identified associations between exposure and autism risk that interplay with factors such as timepoint in the pregnancy and wildfire severity. For example, exposure to wildfire smoke-derived air pollution in 3rd trimester has been found to more strongly associate with autism risk than comparable exposure in other stages of pregnancy (223). Pregnancy exposure to severe wildfire events (defined by $\geq 35 \mu g/m^3$ wildfire-derived particulate concentration) was observed to more strongly associate with autism than total wildfire-derived $PM_{2.5}$ as quantified by percentile (224).

Acting as the interface between genes and the environment, epigenetic markers such as DNA methylation have previously been shown to associate with wildfire smoke exposure (225,226). This raises the possibility of DNA methylation as an epigenetic mediator of the effects of prenatal wildfire smoke exposure on child development, particularly if changes to DNA methylation occur in gene pathways critical to neurodevelopment. The placenta serves as an ideal tissue to interrogate the epigenetic markers of prenatal wildfire smoke exposure, as is acts as the interface between the maternal and fetal circulatory systems and has been shown to have dynamic changes to DNA methylation in response to other sources of air pollution (227–229).

To test the hypothesis that prenatal and/or preconception wildfire $PM_{2.5}$ on exposures associate with epigenetic markers unique from those associated with ambient air

pollution and in gene pathways implicated in neurodevelopment, we performed whole genome bisulfite sequencing (WGBS) on 221 placenta DNA samples and identified comethylation networks associated with estimated air pollutant concentrations throughout the preconception and pregnancy period [Figure 3.1]. Comethylation network analysis was ideal for the investigation of specific components of wildfire versus ambient air pollution particulate matter. As a complementary approach, we also identified differentially methylated regions between pregnancies exposed to any wildfire versus those that were not.

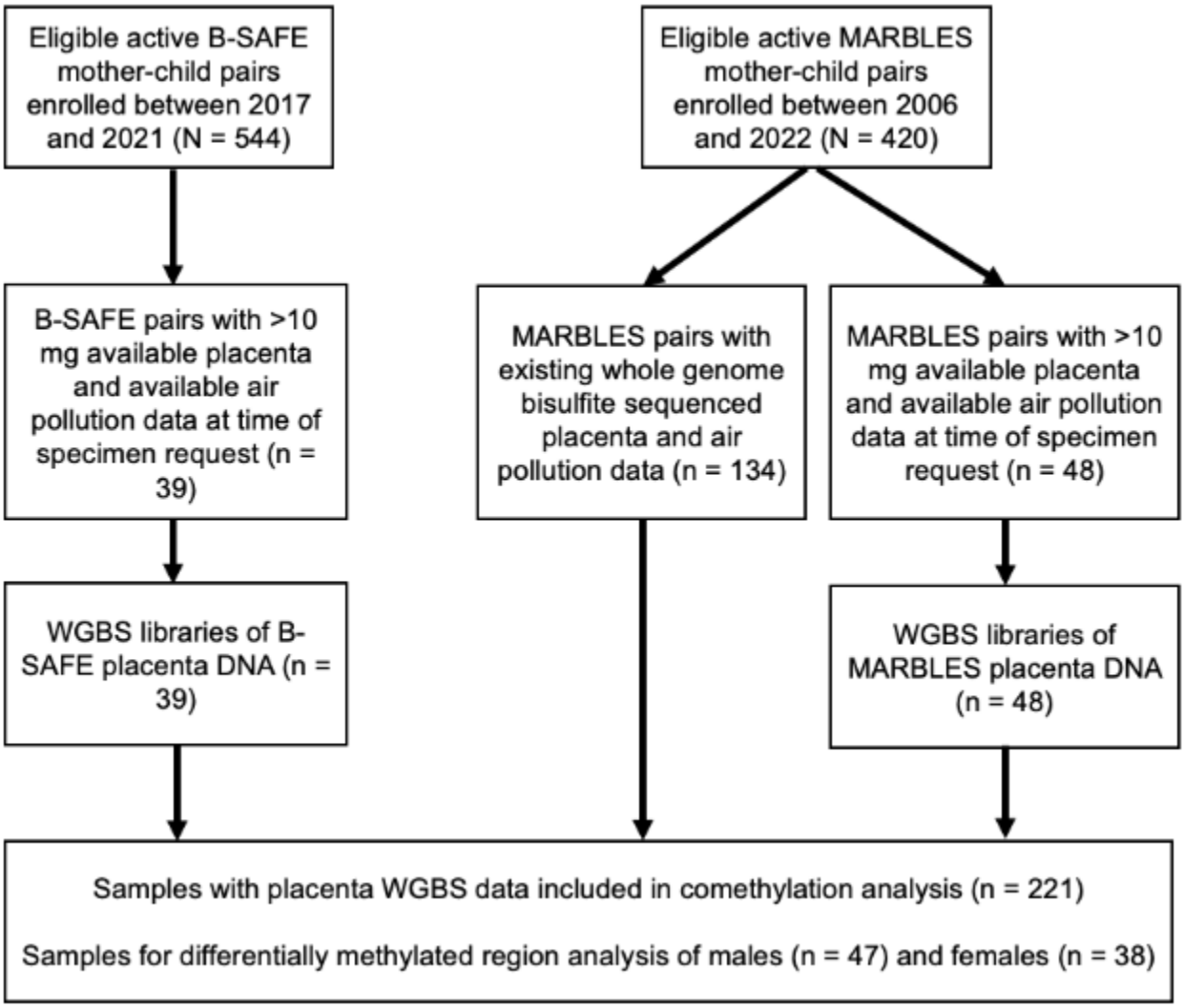


Figure 3.1: A flowchart describing sample inclusion in this study from MARBLES and B-SAFE participants.

3.5 Methods

3.5.1 Study cohort

Our study consisted of participants from both the B-SAFE (Bio-Specimen Assessment of Fire Effects) and MARBLES (Markers of Autism Risk in Babies – Learning Early Signs) cohorts [Supplemental Tables 3.1-3.2]. The B-SAFE study enrolled women pregnant

during or shortly after major wildfire events in California that occurred between 2017 and 2021 and followed up with these participants to collect observations of their health and their children's heath. Participants were required to be at least 18 years of age, be Northern California residents at time of enrollment, and be fluent in either English or Spanish to enroll. Upon enrollment, participants completed questionnaires to provide information on their wildfire exposures, pregnancy outcomes, and demographic factors. A subsection of these participants also provided the B-SAFE study with their placental tissue after delivery, which were stored at -80°C until dissection and DNA isolation was performed. Additionally, 11 B-SAFE participants provided CBCL (Child Behavior Checklist) (230) scores and sub-scores from observation of their children while they were less than six years of age. CBCL scores were calculated by parent-reported responses to questionaries on numerous kinds of child behaviors, with the results of these questionaries summed within prescribed syndromic categories converted into standardized T-scores by age and gender-matched norms. T-scores ≥65 on syndromic scales and ≥60 on broadband scales denote clinical significance.

As previously described, the MARBLES study is a Northern California based prospective longitudinal study of pregnancies at elevated ASD risk (231). Women were enrolled in MARBLES provided they already had a child diagnosed with ASD, were at least 18 years of age, were pregnant or planning to become pregnant, were Northern California residents at time of enrollment, and demonstrated English fluency. In addition to providing information on their pregnancy, health, and demographic factors upon enrollment, the children of MARBLES participants were assessed for autism at or around age 3 years by

a skilled clinician. Other neurodevelopmental assessments, including the ADOS (Autism Diagnostic Observation Schedule) (232), MSEL (Mullen Scales of Early Learning) (233) and CBCL (230) were also performed at this time. The ADOS is a standardized assessment module regimen whereby an examiner assesses a child's communication skills, social interaction, and imaginative use of materials. Children were scored for each module on a scale of 0-30 by severity, then module scores were converted to a final severity score with range of 1-10. The MSEL is another standardized behavioral evaluation that assesses child performance in numerous motor, visual, and language tasks. An early learning composite score (MSLelcStandard) was derived from the sum of a child's T-scores across the four MSEL cognitive subscale as a summary metric of neurodevelopment. Composite scores ranged from 49-140 for study participants, with a score of less than 70 indicating neurodevelopmental delays. Nearly all MARBLES participants provided the study samples of their placenta from the delivery of the child of interest, and these placenta samples were stored at -80°C until dissection and DNA isolation.

Information on participant demographic, pregnancy, and medical information was compiled and traits of interest were extracted [Supplemental Table 3.1]. Traits were coded numerically to facilitate Spearman correlation analysis, and traits with low numbers of observations across cohorts were removed from consideration [Supplemental Table 3.3, Supplemental Figure 3.1].

3.5.2 Wildfire air pollution measurement

Air pollution exposures were estimated with a hybrid modeling approach that predicted both total ambient particulate matter and wildfire-specific contributions. This approach used Random Forest Regression (RFR) to combine outputs from a source-resolved chemical transport model (CTM) with ground-level observations, generating total pollutant concentrations at daily temporal resolution. The CTM simulated the atmospheric transport and chemical transformation of wildfire emissions, facilitating the distinguishing of rural fire contributions from urban fire contributions (234–236). Emissions inputs were calculated using satellite-derived burn area calls under the BlueSky modeling framework (237). Model estimated daily $PM_{2.5}$ coverage was generated at 4 km $\times$ 4 km resolution for most regions in California, though a small subsection of regions could only be resolved at 24 km $\times$ 24km resolution.

To disentangle wildfire contributions to $PM_{2.5}$ from contributions from other sources, source apportionment techniques were applied (236). Using the different size profile and chemical composition of biomass-fueled combustion and wildfire-urban interface (WUI) combustion in comparison to combustion from anthropogenic sources, it is possible to estimate the fraction of total particulate matter of a given size range attributable to wildfire from the total estimated $PM_{2.5}$ for any given day. In contrast to ambient $PM_{2.5}$, biomass-derived particles are enriched for organic compounds and contain reliable tracers such as levoglucosam and potassium (238,239). WUI combustion is distinguished from ambient $PM_{2.5}$ by the abundance of urban material-derived burn byproducts, including polychlorinated biphenyls and heavy metals (240). Biomass-specific and WUI-specific

contributions to total $PM_{2.5}$ were modeled as continuous variables of particle concentration, denoted by Tracer 5 and Tracer 10, respectively.

All estimated $PM_{2.5}$ concentrations were averaged into two time periods: preconception (describing the 3 months prior to the start of the pregnancy) and the duration of the pregnancy. Tracer 5 and Tracer 10 measurements were also summed across these time periods to synthesize a new measurement of total $PM_{2.5}$ contributions from wildfire-specific sources. These summed wildfire-$PM_{2.5}$ were also subtracted from total $PM_{2.5}$ concentrations recorded in that period to model ambient air pollution separate from wildfire contributions. Finally, a binary categorical variable was added to denote whether a pregnancy overlapped for any duration with any one of six major Northen California wildfire periods recorded between 2008 and 2022 to provide a rough metric of pregnancy exposure specifically to major wildfire events [Supplemental Table 3.4].

3.5.3 DNA isolation from placenta and whole genome bisulfite sequencing

Placenta samples were obtained, chilled, and transferred to a central lab for processing within 24 hours of delivery. Full thickness samples (3cm by 3cm) were taken from the midpoint between the cord insertion and periphery, then frozen at -80°C. Aliquots of these larger samples were collected by excising a small portion of the fetal surface, which was then refrozen until time of DNA isolation. The placenta samples used in this study were processed in three batches, the first two of which have previously been described (241). For clarity, these three groups are described here as “Discovery”, “Replication” and

“Expansion”. The batch code for any given sample can be found as the “Sequencing_Group” variable in the supplement [Supplemental Table 3.1].

For the tissues processed the Discovery batch (n = 90), DNA was extracted from placenta using the Gentra Puregene kit (Qiagen, Hilden, Germany), sheared by sonication, bisulfite-converted with the EZ DNA Methylation Lightning kit (Zymo, Irvine, CA, USA), and made into sequencing libraries via the TruSeq DNA Methylation kit (Illumina, San Diego, CA, USA). Libraries were made using indexed PCR primers with 14 cycles of amplification. Completed libraries were pooled and sequenced for 150bp paired end reads on 2 lanes of the Illumina HiSeq X (San Diego, CA, USA) by Novogene (Sacramento, CA, USA).

Tissues processed in the Replication batch (n = 44) were subject to DNA isolation from placenta by application of the Gentra Puregene kit (Qiagen, Hilden, Germany). The resulting DNA was sheared by sonication, bisulfite-converted with the EZ DNA Methylation Lightning kit (Zymo, Irvine, CA, USA) and made into sequencing libraries via the Accel-NGS Methyl-Seq DNA Library kit (Swift Biosciences, Ann Arbor, MI, USA). Libraries were made with indexed PCR primers over 12 cycles of amplification, then pooled and sequenced for 150bp paired end reads on 2 lanes of the Illumina NovaSeq 6000 S4 (San Diego, CA, USA) by the DNA Technologies Core at University of California, Davis (Davis, CA, USA).

Finally, placenta samples in the Expansion batch (n = 87) underwent DNA isolation via the Gentra Puregene kit (Qiagen, Hilden, Germany). DNA was then sheared by sonication, bisulfite-converted with the EZ DNA Methylation Gold kit (Zymo, Irvine, CA, USA) and made into sequencing libraries via the xGen Methyl Seq Library Prep kit (IDT, Coralville, IA, USA). Libraries were made with indexed PCR primers and underwent 7 cycles of amplification before being pooled and sequenced for 150bp paired end reads on 4 lanes of the NovaSeq 6000 S4 (San Diego, CA, USA) by the DNA Technologies Core at the University of California, Davis (Davis, CA, USA).

3.5.4 WGBS alignment and quality control

Post-sequencing, sequencing data from all samples were preprocessed, aligned to hg38, and used to generate cytosine reports with Epigenerator (242). Epigenerator is a WGBS analysis pipeline that writes cytosine reports from fastq files by applying FASTQ_Me and CpG_Me in tandem via a Snakemake-orchestrated system. Merged reads were trimmed of adaptors, corrected for potential methylation bias at the 5' and 3' ends of the reads, and aligned to the hg38 assembly. These aligned reads were then deduplicated, and CpG methylation was extracted to generate cytosine reports for further analysis. FastQC and MultiQC were also applied to check the quality of sequencing for all samples in the pipeline (178,179).

3.5.5 Placental cell type composition estimates

An estimate of placental cell type composition for each of the 221 samples included in this study was generated using the Placental Cell Type Estimation Tool (PLANET) R package v 1.16.0 (243). To accomplish this, CpG level methylation β-values and genomic coordinates were extracted from sample cytosine reports and projected onto their corresponding Illumina EPIC array probe coordinates, a necessary step given the PLANET reference is defined by array probe nomenclature. The overlapping CpGs were then filtered to only include those overlapping the third trimester placental CpG signature panel, and cell type proportions were estimated using the Houseman reference-based projection method as implemented in the minfi v.1.54.1 R package, with the PLANET reference acting as the basis matrix (244). This approach estimates the relative contributions of six major placental cell populations (trophoblasts, stromal cells, Hofbauer cells, endothelial cells, nucleated red blood cells, and syncytiotrophoblast cells) by projecting sample level methylation profiles onto cell type-specific methylation signatures. For ease of plotting and downstream modeling, estimated cell type contributions were normalized on a per-sample basis such that proportions summed to one. The resulting matrix of placental cell-type composition estimates was incorporated into the sample metadata table to facilitate downstream analyses [Supplemental Table 3.1].

3.5.6 Comethylation network generation and annotation

Placenta cytosine reports were used as input for Comethyl v.1.3.0 via R v. 4.4.3 to perform weighted gene comethylation network analysis (245). In short, Comethyl identifies regions of CpGs with consistently correlated methylation profiles across samples, and groups

those regions into modules defined by a representative region referred to as an eigennode. Once grouped into modules, methylation profiles for each sample across modules can be summarized by quantifying that sample's module eigennode value, which correlates with hypermethylation or hypomethylation of the corresponding module network for that sample. Individual sample eigennode values can then be regressed against other sample traits to identify potential correlations between participant data and a broader methylation network. This approach affords comethylation network analysis a robustness not found in conventional methylation analysis of individual CpGs, as regions defined by correlated methylation profiles are less subject to stochastic variation in methylation than individual CpGs.

To generate a comethylation network, Bismark cytosine reports from the 221 participants were read into a Bsseq object and filtered to only consider CpGs with ≥3X coverage in ≥75% of all samples (20,881,192 CpGs) [Supplemental Figure 3.2]. These filtered CpGs were then clustered into regions, defined as units of ≥3 CpGs within 150bp of each other, and these regions were once again filtered to only include elements with ≥14X coverage and ≥5% methylation standard deviation (418,989 regions) [Supplemental Table 3.5, Supplemental Figures 3.3-3.6]. Methylation over these regions was then adjusted for 33 surrogate variables while protecting variation correlated with neurodevelopmental/behavioral outcomes and air pollution (246).

Adjusted methylation was used to assess scale-free topology of the network with Pearson correlations. Raising correlations to a soft power of 14 was identified as producing a network of optimal fit and connectivity (Fit = 0.91, Mean Connectivity = 40.8) for downstream analysis. Using these soft power raised correlations, modules in the comethylation network were identified using a two-step clustering technique. First, regions were assembled into 12 large blocks using K-means clustering, with cluster centers being calculated from the first principal component and distances between clusters based on Pearson correlation [Supplemental Figure 7, Supplemental Tables 6 and 7]. After this step, adjacency matrices were calculated within each block, with interconnectedness assessed using topographic overlap. Modules were called based on hierarchical clustering followed by adaptive branch pruning, with highly correlated modules across different blocks being merged. Modules were given arbitrary names corresponding to color names available in R. Regions included in the analysis that were not assigned to a module at the end of this process were assigned to the grey 'catch all' module. Of the 418,989 total regions passed to network identification, 3,058 (0.73%) were assigned to modules while the remaining 415,931 (99.27%) regions were assigned into the grey module as a catch-all for regions not assigned to a correlated cluster [Supplemental Table 3.8].

After module assignment, regions included in the completed module were mapped to genes using the Genomic Regions Enrichment of Annotations Tool (GREAT) (247). Biomart provided additional gene information for the annotated region genes and annotatr provided gene context and CpG context (248,249). Module regions were assessed for

enrichment in functional chromatin states from multiple tissue types described in by the Roadmap Epigenomics Project (139,250).

3.5.7 Correlating comethylation module eigennodes with sample traits

Module eigennode values were correlated with one another via biweight midcorrelation (Bicor) in to identify highly correlated modules without being heavily weighted by outliers [Supplemental Figure 3.8] (251). A module dissimilarity dendrogram was also generated to identify potentially correlated modules post-merging [Supplemental Figure 3.9]. Module eigennode values were then correlated with participant traits via Bicor, with p-values for each comparison calculated using Fisher's transformation.

3.5.8 Differentially methylated region detection

To complement holistic comethylation network analysis, differentially methylated region (DMR) identification across prenatal wildfire exposure was performed with DMRichR v 1.7.1 (252). Combining dmrseq and bsseq tools, DMRichR supports the inference of DMRs based on user-supplied variables of interest, in this case the "PregFire_Any" variable denoting whether a given pregnancy overlapped with a major Northern California wildfire event [Supplemental Tables 3.1,3.2, and 3.4]. The dmrseq algorithm pools differences in CpG methylation between case (wildfire exposed) and control (non-wildfire exposed) groups and performs smoothing to assemble background regions. Possible regions were defined as sections of the genome with a minimum of 5 CpGs with a maximum gap of 1000 bp between them. CpGs considered for region identification also

needed to have at least 3X coverage in 75% of our sample group across all sub-group categories adjusted for during covariate adjustment. In this case, two covariates were adjusted for during DMR calls: gestational age at time of delivery and cohort group (participant membership in either MARBLES or B-SAFE). DMR analysis was limited to only samples from the “Expansion” sequencing group due to significant observed differenced in global methylation between sequencing groups [Supplemental Figure 3.10]. Once background regions were identified, a statistic of methylation for each possible region was estimated through generalized least squares regression, and permutation tests were used to identify regions with significantly different methylation between case and control groups. A methylation difference of 5% was used as the minimum threshold for magnitude of difference between regions to be considered significant as a DMR.

Wildfire exposure DMRs were identified in fetal sex-stratified groups, as prior investigations have shown sex-specific DNA methylation signatures in perinatal tissues (253). One sample, SW055, was excluded from consideration because of abnormally high mean methylation, which may be indicative of excessive maternal blood contaminant in the placenta sample. The two wildfire exposure sample sets were adjusted for gestational age and sequencing group. DMR analysis was limited to only samples from the “Expansion” sequencing group due to significant observed differences in global methylation between sequencing groups [Supplemental Figure 3.10]. All DMRs were called with the default variable specifications with the exception that the maximum number of permutations tested was increased to 47 for the males and 39 for the females

to improve statistical rigor. After filtering for coverage thresholds across covariate groups, 12,303,096 and 15,207,473 CpGs were left in consideration for the male set and female set respectively. This resulted in the identification of 43,366 (male set) and 43,026 (female set) background regions for testing as DMRs [Supplemental Tables 3.9 and 3.10]. Significant DMRs were defined as those with a permutation p-value of < 0.05. DMRs were annotated to their nearest gene via the application of the “one closest” rule of the Genomic Regions Enrichment and Annotations Tool (GREAT) (247). These DMR gene lists were used in enrichment analyses.

3.5.9 Global methylation averages

Per sample global averaged methylation values per CpG were calculated for all samples with the “globalStats” function from the DMRichR package. Samples were grouped by select covariates and plotted with Prism v10.3.0. Significance of the differences between these groups were calculated by independent two tailed t-test with Welsch correction, Brown-Forscythe ANOVA, or simple linear regression depending on covariate data characteristics.

3.5.10 DMR enrichment analysis

Enrichment of DMR sets for genic and CpG annotations was performed with the “DMRichGenic” and “DMRichCpG” functions from the DMRichR package, respectively. In both cases a Fisher’s exact test was used to determine significant overrepresentation (q < 0.05) of a given genic of CpG annotation in the DMR set, with the background universe

set as possible regions assessed for differential methylation within a given sample set. The resulting enrichments were then plotted with “DMRichPlot” from the DMRichR package.

Enrichments of DMR sets for gene ontology was performed with the “submitGreatJob” function from the rGREAT package v. 4.0.4 using the one closest rule to assign genes to regions and slimmed with the “slimGO” function from DMRichR. A binomial distribution is assumed, and the input region set was tested for overrepresentation of any ontologies relative to background regions. GREAT enrichments were plotted with “ggplot” from ggplot2.

3.5.11 Gene list overlap analysis, SFARI enrichment analysis, and DMR region overlap analysis

Intersections between male and female wildfire exposure DMR gene lists were tested for significance via the GeneOverlap package v.1.44.0. All SFARI Gene database enrichments tests were also performed with tools from the GeneOverlap package. The SFARI Gene list used for these enrichments tests was the 2023 Q4 release. First, the “newGeneOverlap” function was applied to all combinations of the three gene lists in question. Genome size was defined the intersection of gene names from elements which may have been identified as significant in the query set based on background definition parameters. Next, the “testGeneOverlap” function performed Fisher’s exact tests to determine whether a given input gene list coincided with another gene list more frequently

than expected by chance. Intersections between male and female DMRs themselves were tested for significance via the permTest function of the regioneR package. DMRs were converted into Granges objects and tested for both their number of overlaps and the mean distance between regions relative to intersections between randomly generated sets of regions with comparable length from hg38. This comparison was performed with 10,000 permutations of random regions.

3.5.12 Chromatin state enrichment analysis

Chromatin state enrichment analysis was performed using the ChromHMM 15-state model for hg38 from the Roadmap Epigenomics Project via the LOLA framework (139,187). Significant module regions were submitted with the “runLOLA” function of the LOLA R package v1.38.0 with a reference database of ChromHMM segmentations across multiple tissue and cell types. Chromatin state enrichment p-values were computed using Fisher’s exact test. Chromatin states were annotated with human-readable labels, and infinite values were replaced with the highest finite odds ratio to enable plotting. Heatmaps of enriched states across tissues were generated with the “heatmap.2” function of the ggplots R package v3.2.0.

3.6 Results

3.6.1 Comethylation networks were identified in placenta and displayed expected topologic features

Participant methylation profiles of the 418,989 genomic regions passing the filtration standards were adjusted for the 33 identified surrogate variables for to reduce the influence of batch effects on the resulting network [Supplemental Figure 3.11]. As expected, the identified surrogate variables correlated most substantially and with sex, sequencing platform, sequencing batch, project of origin, and estimated placental cell type composition [Supplemental Figure 3.12]. The correlations between adjusted region methylation statistics were then modeled after transformation with multiple different soft powers, allowing the identification of 14 as the ideal soft power to raise region correlations by to achieve sufficient scale-free fit while maintaining network connectivity (Figure 3.2A). The resulting placenta comethylation network was composed of 85 modules of comethylated regions, with the constituent regions of each module being predominantly clustered to linear stretches of a single given chromosome (Figure 3.2B). This regional clustering is consistent with previously identified placental comethylation networks (254), and is distinct from the interchromosomal region clustering seen in networks derived from related tissues like cord blood (245). Modules exhibited substantial variation in the number of regions assigned to them, ranging from 154 to 10. (Figure 3.2C).

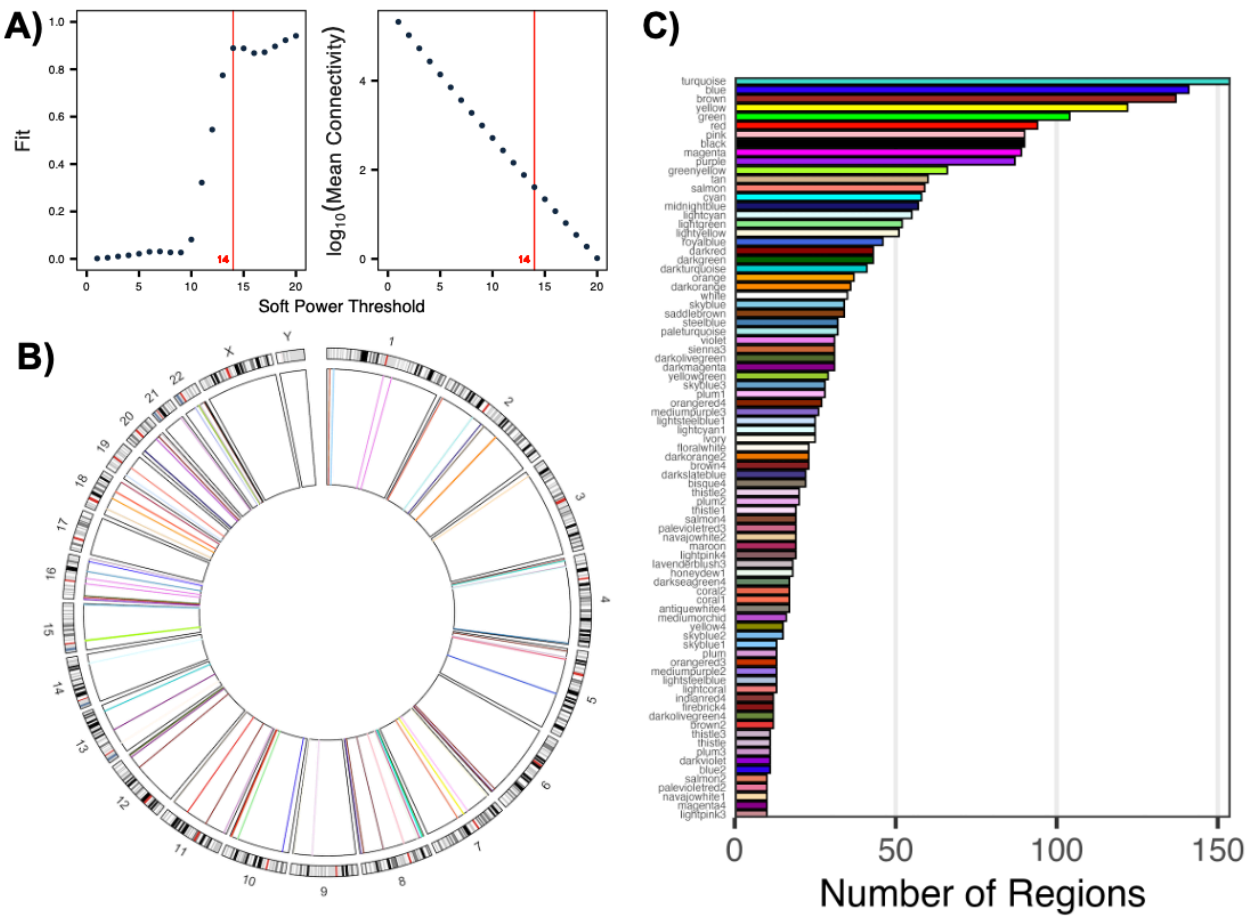


Figure 3.2: A comethylation network analysis was performed using SVA-adjusted region methylation statistics. **A)** The scale-free topology fit and connectivity of potential networks were assessed at numerous soft power thresholds. A soft power of 14 (Fit = 0.91 | Mean Connectivity = 40.8) was selected for final network construction. **B)** Circos plot of non-grey regions mapped to hg38. Network architecture is defined by continuous intrachromosomal regions assembled into modules, in contrast to the more intrachromosomal architecture of other tissues**. C)** The numbers of regions assigned to each non-grey module ranged from 154 to 10.

Module regions were then annotated for genic features (i.e. promoter, exon, intron, UTR, enhancer, and intergenic) and CpG context (i.e. island, shore, shelf, and open sea) using annotatr and tested for enrichment relative to the background of all filtered regions passed into network generation [Supplemental Table 3.12]. We identified regions assigned to modules to be significantly enriched for exons and introns, while also being significantly depleted of promoters and intergenic elements [Supplemental Figure 3.13]. Module regions also were shown to be significantly enriched for CpG open sea and significantly depleted of CpG shore [Supplemental Figure 3.14]. To assess whether module region were concentrated in specific chromatin states, we referenced our module regions against the predicted chromatin profiles of multiple tissues provided by the RoadMap Epigenomics Project (139). Comethylated regions were significantly enriched for chromatin states of predicted heterochromatin, zinc finger gene and repeat regions, and bivalent/poised transcription start sites [Supplemental Figure 3.15, Supplemental Table 3.13]. We identified three pairs of modules as strongly correlated with one another via Bicor: salmon and darkseagreen4 (Bicor = 0.78), brown and violet (Bicor = 0.70), and plum3 and sienna3 (Bicor = 0.67) [Supplemental Table 3.14]. While strongly correlated, these pairs of modules did not pass the 0.90 correlation threshold required for module merging.

3.6.2 Wildfire air pollution is correlated with modules of placenta comethylation in patterns distinct from non-wildfire derived air pollution

To investigate whether placenta comethylation networks also associated air pollution and neurodevelopment outcomes, sample level module eigennode values were correlated

with numerous sample traits using Bicor, with significance of all possible module-trait combinations determined by Fisher's transformation [Supplemental Table 3.15]. A total of 122 significant (p-value < 0.05) module-trait correlations were identified, including 45 correlations between air pollution exposures and comethylation modules [Figure 3.3].

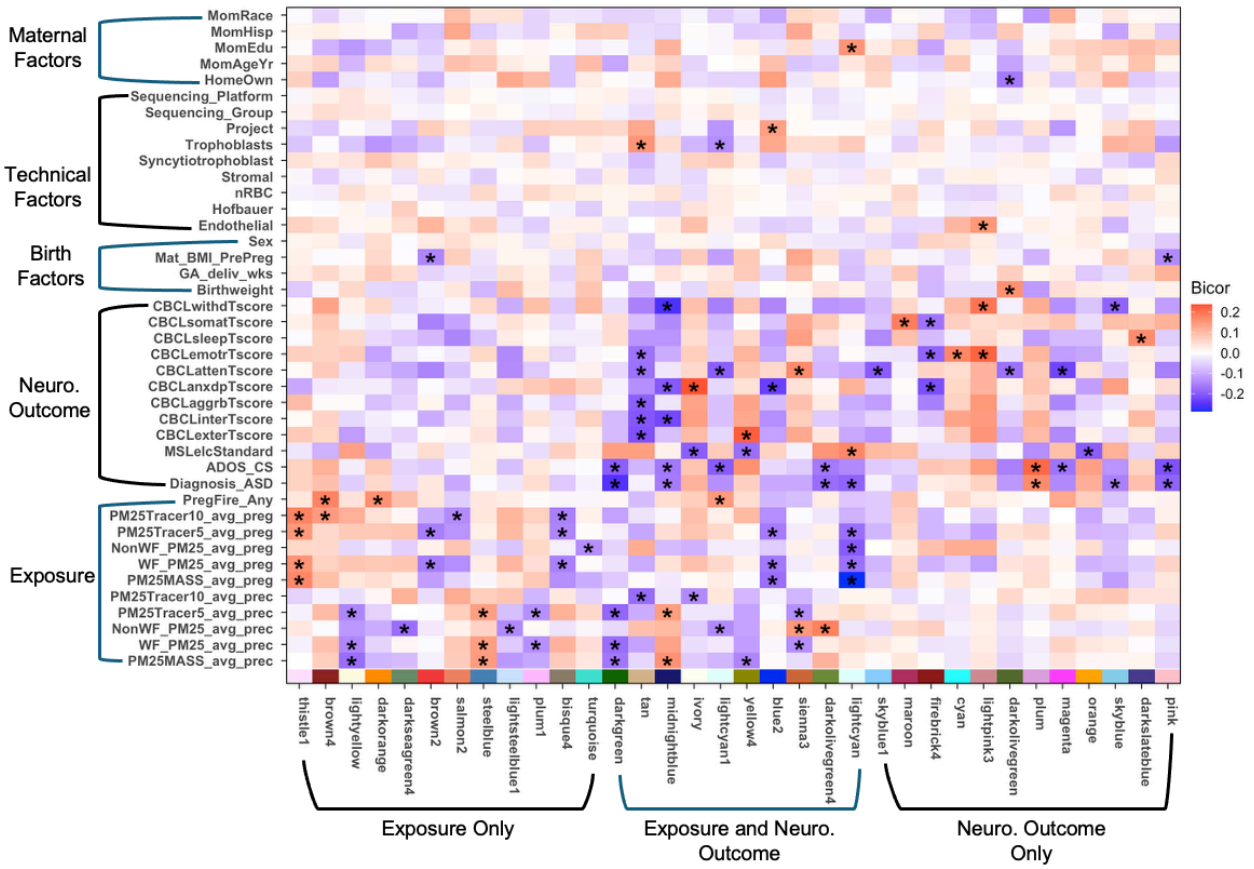


Figure 3.3: A heatmap depicting biweight midcorrelations (Bicor) for all combinations of sample data (y-axis) and comethylation module eigennode values (x-axis). Significant correlations (p-value < 0.05) as determined by Fisher's transformation are annotated with a star. Sample data are sorted into five groups: Exposure (describing all variables which track types of $PM_{2.5}$ pollution or proximity to wildfires during pregnancy generally), Outcome (describing all assessments of child developmental benchmarks and neurodevelopmental outcomes where available), Birth Factors (describing biological variables on record ascribed to either the child or the mother), Technical Factors (describing covariates relating to sequencing or sample processing batches and estimated placental cell type composition in the sample as determined by PLANET) and Maternal Factors (describing non-biological covariates on record which relate to the

mother). Modules are sorted into three groups on the x-axis as determined by their correlations with the Exposure and Outcome traits. ‘Exposure Only’ traits are significantly associated with at least one Exposure trait but are not significantly associated with any Outcome trait, ‘Exposure and Outcome’ modules are significantly associated with at least one Exposure trait and at least one Outcome trait, and ‘Outcome Only’ modules are significantly associated with at least one Outcome trait but are not significantly associated with any Exposure trait. Remaining 50 modules not shown.

Of the 85 modules assessed, 22 were significantly correlated with at least one prenatal air pollution exposure. Significant correlations between these modules and the various air pollution exposures are diversified in the direction of methylation, with 15/45 (33.33%) of the significant correlations showing hypermethylation in association with exposure, and 30/45 (66.66%) significant correlations showing hypomethylation in association with exposure. Significant correlations were seen with exposure in both the preconception (n = 23/45, 51.11%) and pregnancy duration (n = 22/45, 48.89%) time periods. Regions assigned to modules significantly associated with the preconception air pollution exposure variables exhibited similar genic and CpG annotation to regions assigned to modules significantly associated with pregnancy duration air pollution exposure [Supplemental Figure 3.16]. Most of the identified modules did not associate with estimated placental cell type proportion or other technical variables, which appear to have been significant contributors to variation as quantified by principal components [Supplemental Figure 3.11].

An asymmetry in module associations emerged when stratifying modules into groups based on association with wildfire-derived and ambient components of air pollution [Supplemental Table 3.16]. Most air pollution associated modules (14/22) were significantly associated with wildfire-derived exposure variables but not ambient variables. In contrast, only 5 modules uniquely associated with ambient exposures, and 2 modules (lightcyan and sienna3) showed associations with both wildfire-derived and ambient variables. A single module (yellow4) associated exclusively with total $PM_{2.5}$ exposure, and not with and wildfire-derived or ambient $PM_{2.5}$ variables.

One of the two modules significantly associated with both wildfire-derived and ambient exposures, lightcyan, presented a unifying correlation between both varieties of air pollution exposure and module methylation, as both wildfire-derived and ambient $PM_{2.5}$ exposure during pregnancy were shown to associate with module hypomethylation [Supplemental Table 3.15]. The component regions of lightcyan annotated to *GALC*, a gene that encodes the enzyme galactosylceramidase, a functional component of myelin coating (255). The other module that significantly associated with both wildfire-derived and ambient exposures, sienna3, is unique in that its correlations with air pollution exposure have differing directions depending on whether the exposure is wildfire-derived or ambient. Specifically, the sienna3 module eigennode values negatively correlate with wildfire-derived $PM_{2.5}$ exposure during preconception ($p = 0.0443$) and biomass-derived $PM_{2.5}$ exposure during preconception ($p = 0.0467$), but positively correlate with ambient $PM_{2.5}$ exposure during preconception ($p = 0.0295$) as well [Figures 3.4A-3.4C]. The genomic regions of sienna3 annotate to proximal to the *NPHP4*, which a protein coding

gene involved in renal tubular development and downregulation of Wnt/β-catenin signaling pathways (256).

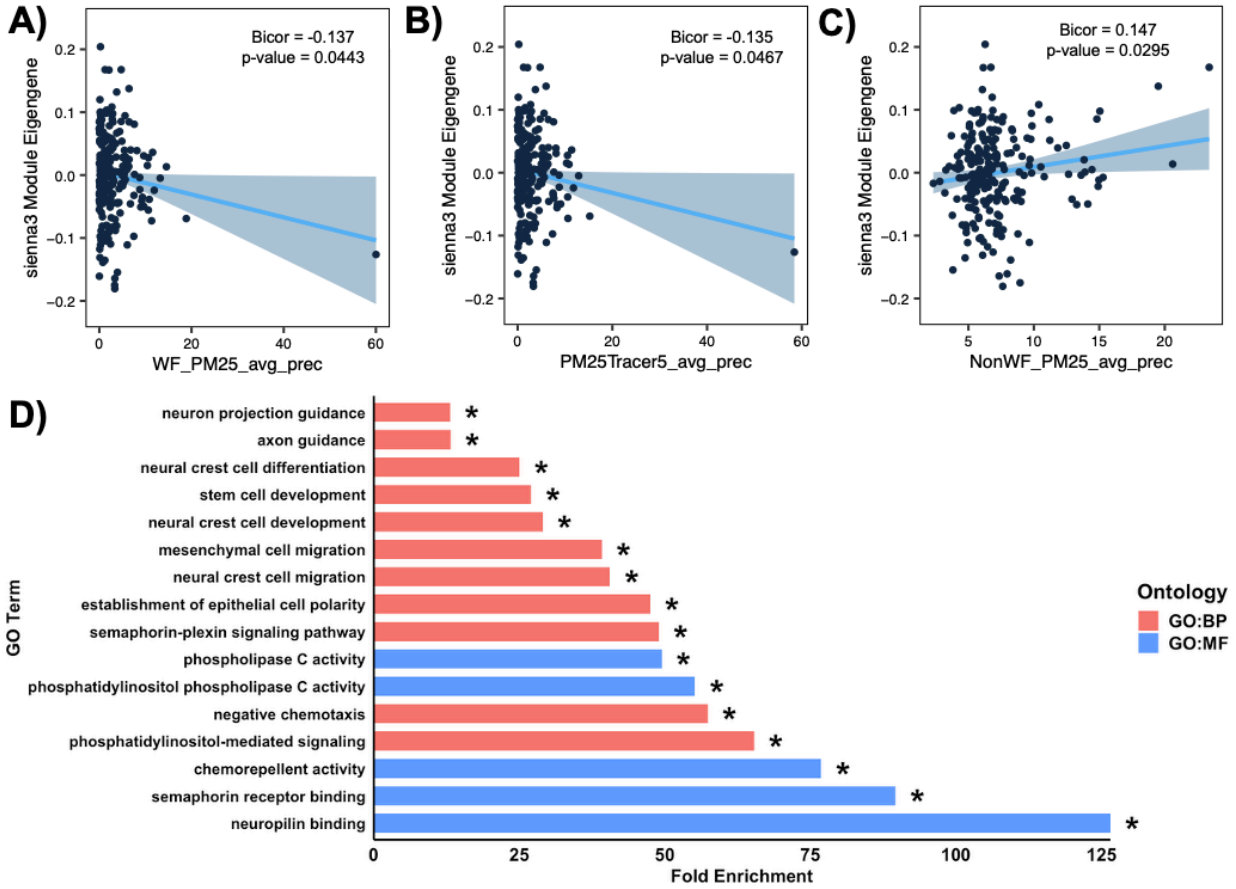


Figure 3.4: Scatterplots and dot plot of the associations between sienna3 module eigennode values and **A)** wildfire-derived $PM_{2.5}$ exposure during preconception (WF_PM25_avg_prec), **B)** biomass-derived $PM_{2.5}$ exposure during preconception (PM25Tracer5_avg_prec), **C)** non-wildfire derived $PM_{2.5}$ exposure during preconception (NonWF_PM25_avg_prec). **D)** All significantly enriched Gene Ontologies for the genes from the 14 modules significantly correlated with at least one perinatal wildfire-derived air pollution exposure and none of the non-wildfire derived air pollution exposures.

Significant associations ($q < 0.05$) are denoted with a star. Enrichments separated by ontology: BP = Biological Process, MP = Molecular Function.

To investigate the biological relevance of comethylation modules exclusively associated with wildfire-derived or ambient air pollution, we performed GO Gene Ontology pathway enrichment analysis on the gene sets assigned to the relevant modules. Genes from wildfire-derived exposure associated modules (n=14) were significantly enriched for 16 GO terms, primarily reflecting processes related to neurodevelopment and cell signaling (Figure 3.4D). This included semaphorin receptor binding (GO:0030215), negative chemotaxis (GO:0050919), neural crest cell migration (GO:0001755), and axon guidance (GO:0007411). In contrast, ambient exposure associated modules were significantly enriched only for the term “ciliary membrane” (GO: 0060170), suggesting a more restricted functional profile related to cellular sensing structures.

3.6.3 Placenta comethylation networks correlate differently with preconception versus pregnancy wildfire-informed particulate exposures

While many of the 22 modules significantly associated with air pollution displayed associations with multiple air pollution variables, a subset of these modules exhibited more specific behaviors. This includes the salmon2 module, the methylation of which negative correlated ($p = 0.0483$) only with WUI-derived $PM_{2.5}$ exposure during pregnancy [Figure 3.5A]. The regions of salmon2 were annotated to the *SEMA3A* gene, a secreted extracellular signaling protein implicated as repressive of angiogenesis and axonal

guidance (257,258). *CRMP1,* the downstream intracellular mediator of *SEMA3A* (259), is present in the turquoise module, whose methylation was negative correlated (p = 0.0496) with non-wildfire derived $PM_{2.5}$ exposure during pregnancy [Figure 3.4B]. Methylation of the *RND3*-containing darkorange module positively correlated (p = 0.0182) with exposure to a major wildfire event during a participant's pregnancy. *RND3* is part the Rho family of small GTPases, which function in conjunction with semaphorin proteins to facilitate cytoskeletal rearrangements (260). All three of these modules (salmon2, turquoise, and darkorange) did not correlate with any preconception air pollution exposures.

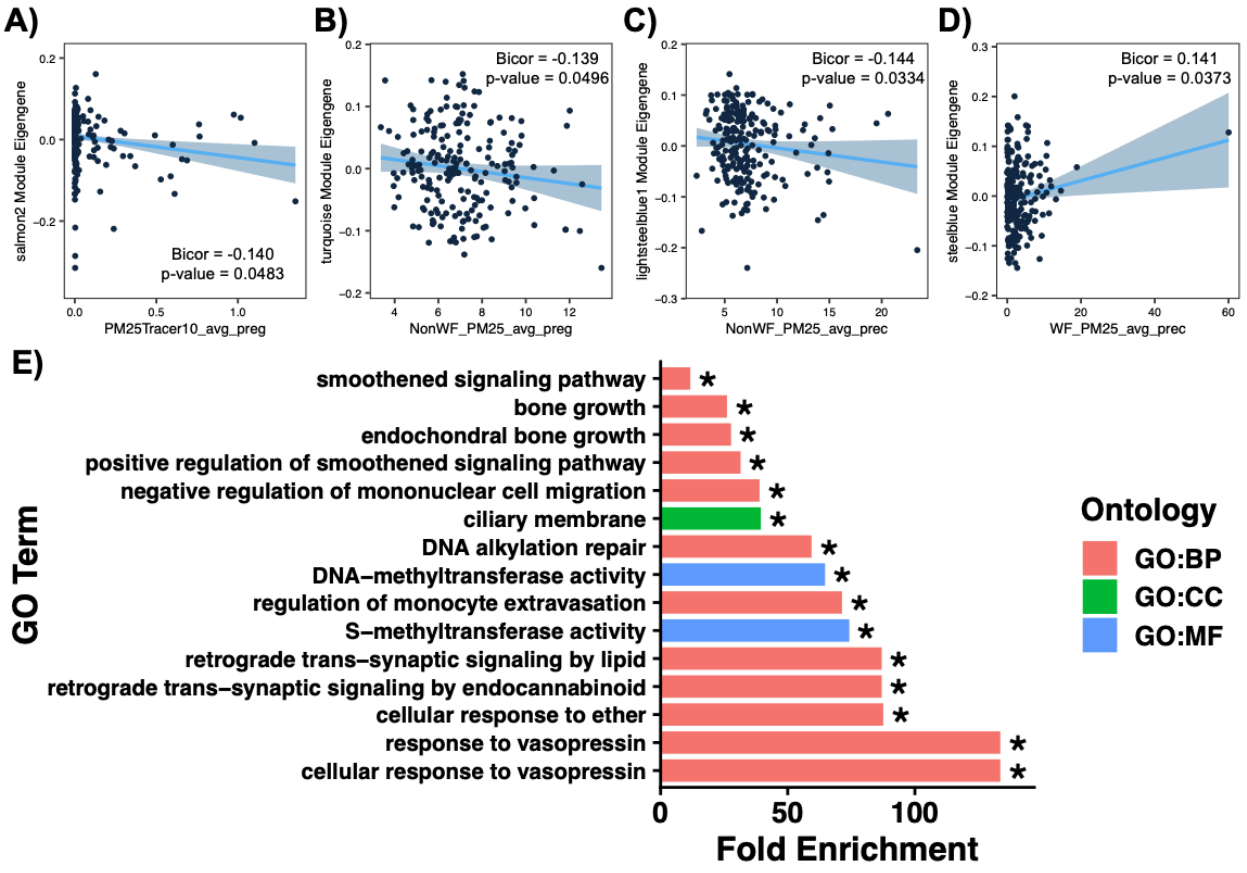


Figure 5: Scatterplots and dot plot of the associations between A) salmon2 module eigennode values and WUI-derived $PM_{2.5}$ exposure during pregnancy (PM25Tracer10_avg_preg), B) turquoise module eigennode values and non-wildfire

derived $PM_{2.5}$ exposure during pregnancy (NonWF_PM25_avg_prec), C) lightsteelblue1 module eigennode values and non-wildfire derived $PM_{2.5}$ exposure during preconception (NonWF_PM25_avg_prec), and D) steelblue module eigennode values and total wildfire derived $PM_{2.5}$ exposure during preconception (WF_PM25_avg_prec). E) The top 15 most significantly enriched Gene Ontologies for the genes from the 22 modules significantly correlated with at least one prenatal air pollution exposure. Significant associations ($q < 0.05$) are denoted with a star. Enrichments separated by ontology: BP = Biological Process, CC = Cellular Component, MP = Molecular Function.

Conversely, comethylation modules that correlated with only preconception air pollution exposures did not coalesce around a unified molecular signaling pathway, presenting a broader spectrum of gene annotations. For instance, the lightsteelblue1 module negatively correlated ($p = 0.0334$) with non-wildfire derived $PM_{2.5}$ exposure during preconception, and was annotated to the *MBD3L1* gene, best characterized for its role in transcriptional repression in testis (261,262) [Figure 3.5C]. The steelblue module presented negative associations with total $PM_{2.5}$ exposure during preconception ($p = 0.0335$), wildfire-derived $PM_{2.5}$ exposure during preconception ($p = 0.0373$), and biomass-derived $PM_{2.5}$ exposure during preconception ($p = 0.0368$) [Figure 3.5D]. This module's regions reside adjacent to the *FAT1* gene, a protocadherin involved in numerous signaling pathways related to cell proliferation and migration, including Wnt/β-cadherin and MAPK/ERK (263). Functional enrichment of genes in air pollution associated modules reinforce the centrality of signal transduction pathways to this module grouping, as seen by the significant enrichment of terms such as "cellular response to vasopressin"

and “regulation of monocyte extravasation” Gene Ontology enrichment analysis [Figure 3.5E].

Notably, only a single module was identified that displayed significant correlations with both a preconception air pollution exposure and a pregnancy air pollution exposure: lightcyan1. Lightcyan1 negatively associated with non-wildfire derived $PM_{2.5}$ exposure during preconception ($p = 0.0371$), positively associated with exposure to a major wildfire event during a participant’s pregnancy ($p = 0.0298$), and negatively associated with ADOS Severity Scores ($p = 0.0153$). The module annotates to the *SLIT2* gene, which encodes a secreted glycoprotein that binds to the Robo family of immunoglobulin receptors initially characterized for their role in axonal guidance (264). However, recent studies have shown *SLIT2* signaling to repress IL-6 expression in the placenta (265), and its expression has been observed in syncytiotrophoblast cells, highlighting a potential role for *SLIT2* in placental angiogenesis (266).

3.6.4 Comethylation modules associated with air pollution and child developmental outcomes contain multiple genes previously tied to autism etiology.

Of the 22 modules associated with air pollution exposures, 10 also significantly correlated with child developmental outcomes: darkgreen, tan, midnightblue, ivory, lightcyan1, yellow4, blue2, sienna3, darkolivegreen4, and lightcyan [Supplemental Figure 16]. One of these modules, darkgreen, mapped proximal to *NHIP*, a recently discovered ASD-implicated gene (267). The darkgreen module negatively correlated with ASD Diagnosis

(p = 7.72E-03), ADOS Score (p = 0.0164), total $PM_{2.5}$ exposure during preconception (p = 0.0141), biomass-derived $PM_{2.5}$ (p = 0.00564) exposure during preconception, and cumulative wildfire-derived $PM_{2.5}$ exposure during preconception (p = 0.00827) [Figures 3.6A-3.6C]. Collectively, these associations illustrate a pattern of decreased placental methylation in regions proximal to *NHIP* associating with preconception $PM_{2.5}$ exposure and increased ASD severity. *NHIP* expression has been observed to increase in response to neuronal differentiation as well as hypoxia, and heightened exposure to $PM_{2.5}$ has been hypothesized to be induce maternal and fetal hypoxia (268).

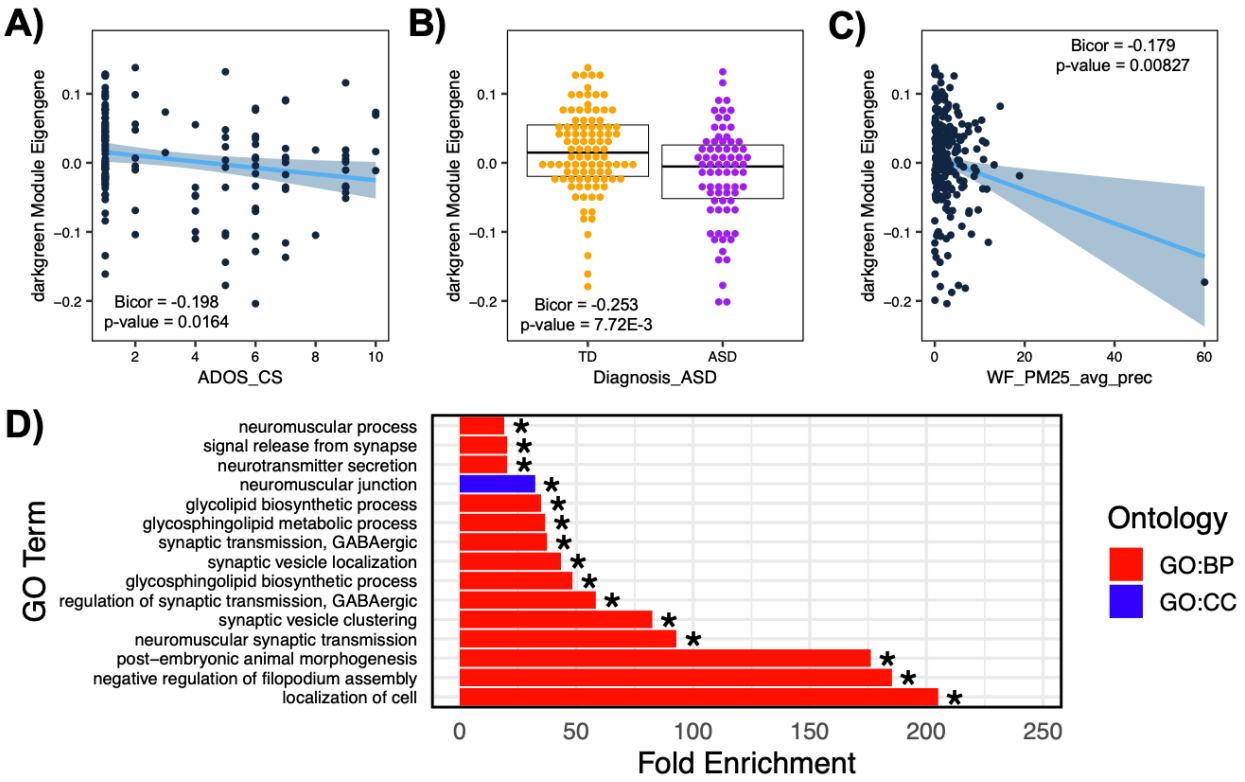


Figure 3.6: Scatterplots and dot plot of the associations between darkgreen module eigennode values and **A)** ADOS Severity Score (ADOS_CS), **B)** ASD Diagnosis (Diagnosis_ASD), **C)** and preconception wildfire-derived $PM_{2.5}$ exposure (WF_PM25_avg_prec). **D)** The top 15 most significantly enriched Gene Ontologies for

the genes from the 10 modules significantly correlated with at least one prenatal air pollution exposure and at least one child development outcome. Significant associations ($q < 0.05$) are denoted with a star. Enrichments separated by ontology: BP = Biological Process, CC = Cellular Component.

The previously discussed lightcyan module demonstrated broad negative correlations with multiple air pollution exposures during pregnancy ($p < 0.05$) and ASD diagnosis ($p = 0.0114$), as well as a positive correlation with Mullen Early Learning Composite Score (0.0351). Lightcyan is distinguished from the other 10 modules significantly associated with both a child neurodevelopmental outcome and an exposure by the breadth of its correlations with air pollution. Lightcyan is the only module to consistency associate with both total $PM_{2.5}$, wildfire-derived $PM_{2.5}$, and ambient $PM_{2.5}$ with the same methylation direction, as hypomethylation of the module's regions correlates with increased exposure in all cases [Supplemental Figure 3.17]. Annotated to the *GALC* gene, which encodes the galactosylceramidase enzyme essential for myelin sheath maintenance (269), the hypomethylation of the lightcyan module represents one of the most consistent epigenetic patterns associated with air pollution exposure broadly and child neurodevelopment outcomes.

Beyond *NHIP* and *GALC*, three ASD-implicated genes as defined by the Simons Foundation Autism Research Initiative (SFARI) gene list were present amongst the 10 module set previously described: *AUTS2*, *EBF3*, and *PLCB1* [Supplemental Figure 3.18]

(270–273). The *AUTS2*-containing yellow4 module negatively correlated with Mullen Early Learning Composite Score ($p = 0.0291$) and total $PM_{2.5}$ exposure during preconception ($p = 0.0286$) but positively correlated with externalizing problems as measured by CBCL ($p = 0.00781$). Interestingly, CpG regions annotated to *AUTS2* can also be found in the yellow module, which did not display any significant associations with any Exposure or Outcome variables. Compared to regions assigned to the yellow module, the regions assigned to yellow4 are fewer in number, and closer to the *AUTS2* gene body. *AUTS2* encodes a component of a PRC1 complex that facilitates transcriptional activation (274), and variants in the *AUTS2* locus have been tied to numerous neurological conditions beyond ASD, including intellectual disability, developmental delay, and bipolar disorder (275). The tan module, annotated to *EBF3*, associated with WUI-derived $PM_{2.5}$ exposure during preconception ($p = 0.00751$) and multiple CBCL summary T-scores for child externalizing behavior ($p = 0.0108$), internalizing behavior ($p = 0.0132$), aggressive behavior ($p = 0.0184$), attentional behavior ($p = 0.0361$), and emotional behavior ($p = 0.0394$). This represents the single greatest number of significant associations with child developmental outcome traits of any modules in the comethylation network. A protein-coding gene, *EBF3* is expressed as a transcription factor in the early B-cell family, a group of transcription factors implicated in B-cell differentiation and neurogenesis (276,277). Finally, the midnightblue module contains *PLCB1*, and is associated with total $PM_{2.5}$ exposure during preconception ($p = 0.0206$), biomass-derived $PM_{2.5}$ exposure during preconception ($p = 0.0362$), ASD diagnosis ($p = 0.0357$), ADOS Severity Score ($p = 0.0475$), and CBCL summary T-scores for child internalizing behavior ($p = 0.00666$), anxiety/depression behavior ($p = 0.0134$), and withdrawn behavior ($p = 0.00184$). Gene

ontology analysis of genes annotated to the 10 modules associated with both air pollution and child development outcomes share exhibit greater specificity for synaptic transmission pathways than the general enrichment for cell signaling seen amongst all air pollution associated module genes [Figure 3.6D].

3.6.5 Sex-stratified placental methylomes reveal wildfire exposure associated differentially methylated regions enriched in neurodevelopmental pathways

To complement the findings of the comethylation network's association with various air pollution variables, differentially methylated regions (DMRs) in placenta between wildfire-exposed pregnancies and control pregnancies were identified in a sex-stratified manner with adjustment for gestational age and sequencing group covariates. This revealed 116 DMRs in the male pregnancies and 536 DMRs in the female pregnancies [Figure 3.6A, Supplemental Tables 3.15 and 3.16]. While a greater number of DMRs were identified within the female sample set, no significant difference in DMR magnitude was observed between sexes [Supplemental Figure 3.18]. Methylation directionality was extremely consistent between sexes, with the vast majority of both male and female DMRs skewing towards hypomethylation. This pattern of DMR methylation replicates the global pattern of CpG methylation, which also associated hypomethylation with wildfire exposure in both sex-combined and sex-stratified analyses [Supplemental Figures 3.10 and 3.20]. Both male and female DMRs show enrichment for the less characterized CpG open sea compared to loci tightly clustered in CpG islands [Supplemental Figure 3.21]. With regards to genic annotations, the male DMRs displayed significant depletion for promoters and enrichment for intergenic elements, while the female DMRs exhibited

significant enrichment for exons [Supplemental Figure 3.21]. Sex-combined DMR identification with adjustment for sex, gestational age, and sequencing group was also performed, though this analysis identified only 16 DMRs from 1,111 background regions [Supplemental Tables 3.19 and 3.20].

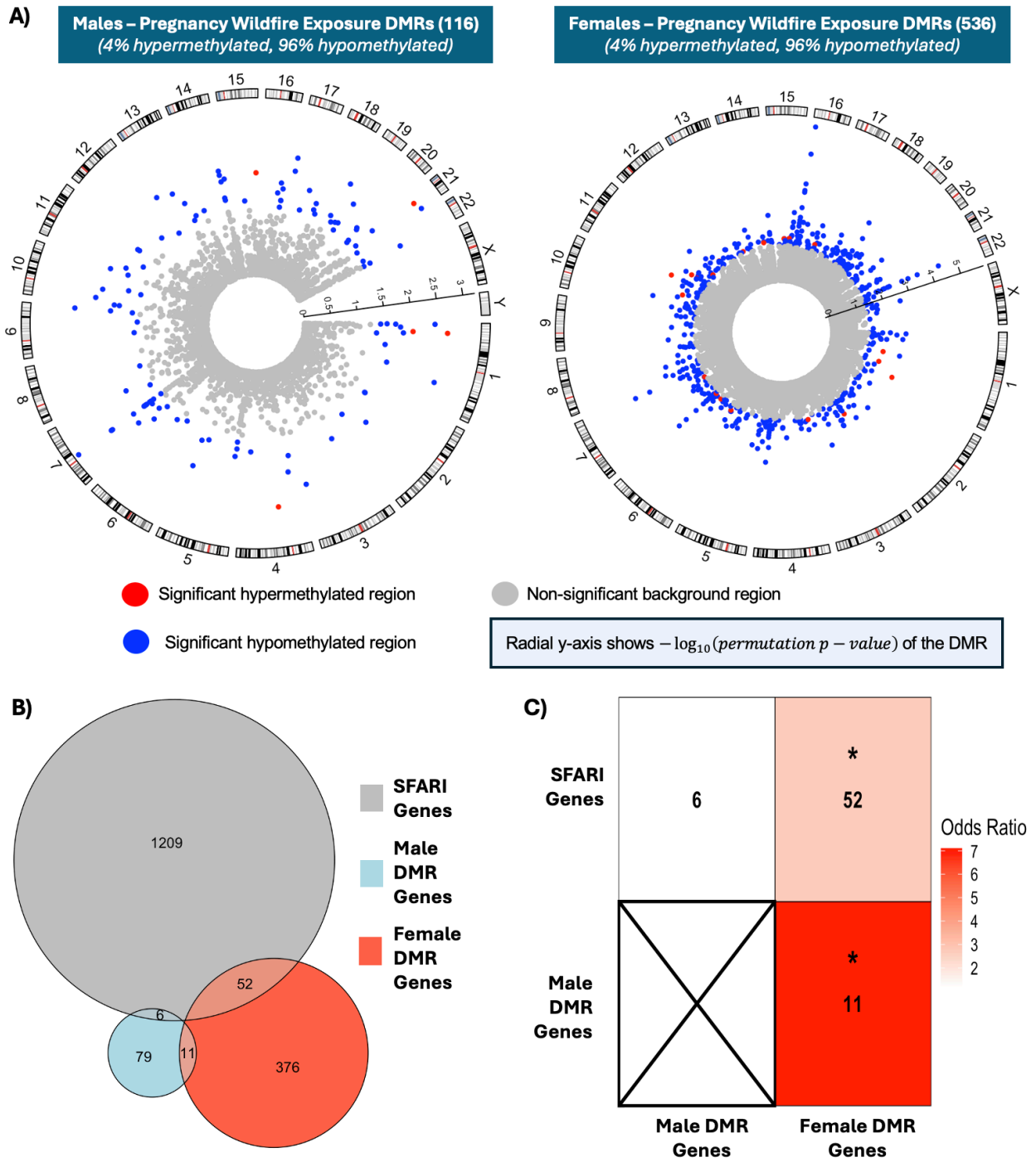


Figure 3.7: Circos plots of the genomic coordinates of the identified wildfire exposure DMRs in placenta from **A)** male (n = 132) and female (n = 88) sample sets. DMR directionality with respect to wildfire exposure is denoted by dot color, with red indicating hypermethylation and blue indicating hypomethylation in the wildfire exposed samples. Grey dots denote non-significant background regions. Significance of a DMR is shown by its placement on the radial y-axis. **B)** Venn diagram showing the number of overlapping genes both sets of DMRs and the SFARI Gene List. **C)** Heatmap displaying the significance of gene overlaps between both sets of DMRs and the SGARI gene list. The number in each tile corresponds to the number of overlapping genes in each comparison, while the color of the tile corresponds to the odds ratio of the genes in each comparison overlapping as opposed to not overlapping. An asterisk denotes a p-values < 0.05 of a Fisher's Exact Test.

Larger blocks of differential methylation were identified in both male and female sample sets [Supplemental Table 3.21]. In the males, three differentially methylated blocks (DMBs) were found to associate with wildfire exposure. These DMBs included a 234 kb hypermethylated element annotated to *SEMA5A,* a 360 kb hypomethylated block at uncharacterized LOC730100, and a 157 kb hypomethylated sequence proximal to the *CSMD1* gene [Supplemental Figure 3.22]. For the females, DMBs were identified in a 154 kb hypomethylated element at uncharacterized LOC105371070, a 326 kb hypermethylated range in uncharacterized LOC105374511, and a 117 kb hypomethylated sequence annotated to the *SGSM1* gene [Supplemental Figure 3.23].

Wildfire exposure DMR sets were assessed for functional relevance via gene ontology (GO) enrichment analysis of their component genes as implemented by GREAT [Supplemental Figure 3.24, Supplemental Tables 3.22 and 3.23]. Following false discovery rate (FDR) correction, the male DMR gene list demonstrated significant enrichment for 186 GO terms and the female DMR gene list showed significant enrichment for 111 GO terms. In males, DMR genes were robustly enriched for GO terms related to neurodevelopmental patterning, cytoskeletal regulation, and vascular development. This includes numerous terms centered on axon guidance and synapse organization, including negative regulation of axon extension involved in axon guidance (GO:0048843), axonal fasciculation (GO:0007413), and regulation of synaptic maturation (GO:0090128). These enrichments were accompanied by overrepresentation of actin filament construction pathways (GO:0030836, GO:0030832, GO:0032970) and multiple angiogenic signaling pathways (GO:0002043, GO:0002040 GO:0001935 . Collectively, these enrichments for cytoskeletal organization, neuronal development, and vascular development terms mirror the implication of the same pathways in multiple comethylated modules associated with both air pollution exposures and child development outcomes. Female DMR genes exhibited a truncated enrichment profile also dominated by terms related to cytoskeletal dynamics (GO:0016327, GO:0030833, GO:0008201) and neurodevelopmental patterning (GO:0021966, GO:0021966, GO:0048846), but differentiate themselves from the male DMR enrichments with a unique overabundance of chemokine and immune migration terms. Some of the most significant enrichments include negative regulation of chemokine-mediated signaling pathway (GO:0002042),

negative regulation of neutrophil chemotaxis (GO:0090024), and negative regulation of response to cytokine stimulus (GO:0060761), all of which promote negative regulation of inflammatory recruitment.

Despite differences in GO enrichments, male and female wildfire exposure DMR genes were found to significantly overlap ($p = 5.3 \times 10^{-52}$, Fisher's exact test), highlighting convergent impacts on shared gene pathways between the two groups (Figure 3.7B and 3.7C). The two DMR sets also demonstrated significantly greater overlap ($p = 0.0001$, permutation test) than would be expected from randomly generated genomic regions of comparable length [Supplemental Figure 3.25]. Both male ($p = 7.5 \times 10^{-9}$, Fisher's exact test) and female ($p = 6.7 \times 10^{-8}$, Fisher's exact test) wildfire DMR gene lists also demonstrated significant enrichment for the SFARI ASD risk gene list, providing evidence for the impact of wildfire exposure during pregnancy on ASD-implicated genes specifically [Supplemental Table 3.24].

3.7 Discussion

Utilizing WGBS of placenta samples from pregnancies with varied exposure to prenatal air pollutants, we have identified epigenetic markers of prenatal air pollution exposure with chronological and source-specific specificity. A collection of 22 comethylation modules were discovered to bear significant associations with prenatal air pollution, with those associations often being distinct to a particular time period or pollutant category. Annotation of the genomic regions that comprise these modules implicate different

biological pathways in the placental response to air pollution dependent upon the source of the pollution and the time of exposure.

The results of this study provide evidence for differential methylomic response to wildfire-derived air pollution versus ambient air pollution. While air pollution measurements taken at the same pregnancy timepoint reliably correlated with one another regardless of the origin of that pollution, numerous comethylation modules exhibited divergent correlations with wildfire-derived and ambient air pollution [Supplemental Table 3.3]. While the sienna3 module exemplified this divergence in region methylation in response to wildfire-derived versus ambient air pollution exposure, this pattern is present to varying extents among other modules significantly associated with air pollution metrics of any kind [Supplemental Table 3.25]. Furthermore, comparison of functional enrichment analysis of modules associated exclusively with wildfire-derived air pollution versus ambient air pollution implicates contrasting biological pathways. The exclusively wildfire-associated module region genes show a noticeable clustering in neurodevelopment and cell signaling pathways driven by the inclusion of multiple semaphorin and adhesion-related genes (*SEMA3A, SEMA3E, CNTN5, FAT1*). In contrast, the exclusively ambient air pollution associated module gene list was smaller and more functionally heterogenous, displaying significant enrichment only for involvement in ciliary membrane structures. However, this is a potential byproduct of wildfire-derived air pollution being quantified by more variables than ambient air pollution and may not represent a difference in magnitude of epigenetic response to wildfire-derived air pollution. Nevertheless, these contrasting comethylation modules in association with wildfire-derived and ambient air pollution exposures provide

evidence for divergent placental DNA methylation patterns at specific loci in association with different air pollution sources. While our module comparisons hint at wildfire-derived air pollution exposure impacting placental DNA methylation in more neurodevelopmentally relevant genes than ambient air pollution exposure, additional sequencing of placentae from heavily wildfire-impacted pregnancies is necessary to clarify any potential difference in epigenetic effect.

Many of the modules associated with air pollution exposures during pregnancy (including darkorange, salmon2, and turquoise) annotated to genes involved in semaphorin-mediated signaling pathways and cytoskeletal remodeling [Supplemental Table 3.10]. Initially characterized as an essential component of axon guidance, semaphorin signaling plays a critical role in the regulation of cell-cell communication and cytoskeletal structure during placental development, and is essential for proper trophoblast invasion and the establishment of the maternal-fetal interface (258,278–280). The enrichment of these pathways among pregnancy air pollution exposures to a much greater extent than that seen in preconception air pollution exposure-associated modules suggests a temporally specific response of the placental epigenome to *in utero* environmental conditions. Cytoskeletal remodeling and guidance signaling pathways are highly responsive to oxidative stress and inflammatory cues (281,282), both of which are well-characterized consequences of air pollution exposure (283,284), providing a plausible mechanistic link between maternal air pollution exposures during pregnancy and altered placental regulatory programming. Together, these findings support the interpretation that air pollution exposure during pregnancy may perturb epigenetic regulation of the

developmental signaling pathways in the placenta, with implications for downstream fetal development.

In contrast, comethylation modules associated with preconception air pollution exposure appeared to reside in more top-level gene regulation pathways. While cytoskeletal regulation wasn't completely absent, namely through the existence of the *FAT1*-containing steelblue module, this set of modules was more enriched for genes involved in transcriptional and epigenetic regulation. Differential methylation of genes including *FOXK1*, *ZFP42*, *ZNF716*, and *MBD3L1* in association with preconception air pollution exposure raises the possibility of systemic differences in chromatin accessibility for the genes regulated by these factors. Such changes may reflect an epigenetic priming process, whereby environmental exposures occurring prior to conception alter the responsiveness of gene regulatory networks later engaged during placenta development. Consistent with this hypothesis, prenatal exposures to environmental stressors have previously been hypothesized to influence transcription factor activity (285), and prenatal exposure to nitrogen dioxide and ozone has previously associated with altered methylation of other zinc finger proteins, including *ZNF442* (286).

Perhaps most interesting among the identified comethylation modules are the subset of 10 which associate both with prenatal air pollution exposure and child developmental outcomes, annotated to a set of genes that converge on pathways related to cell-cell signaling, neurodevelopmental patterning, and transcriptional regulation. Multiple genes

in these modules (*SLIT2, PLCB1, PLCB4, ADGRD1,* and *FRMD4A*) participate in signaling pathways that regulate cellular guidance, polarity, and intracellular calcium dynamics (287–290). These processes are essential components of both placental and neuronal development, representing a potential underlying epigenetic dysregulation of the hypothesized placenta-brain axis (67,291). Simultaneously, the presence of genes implicated in cellular stress response and genome maintenance (*MGMT*, *TMX4*, and *UBAC1*) suggests a role for DNA damage response and protein quality control pathways, which are known to be sensitive to the oxidative and inflammatory stressors that accompany air pollution exposure (292,293). Notably, several genes in this set have established roles in neurodevelopment (*GALC*, *SLIT2*) (294,295), or are directly associated with ASD (*AUTS2*, *EBF3*, *PLCB*) (273), identifying specific loci which may represent a mechanistic interface through which prenatal air pollution contributes to altered neurodevelopmental trajectories. Together, these findings support a model in which air pollution-associated epigenetic variation in the placenta converges on signaling and regulatory pathways that are relevant to both placental function and fetal development outcomes.

Alongside shifts in comethylation networks, sex-stratified DMR analysis revealed several placenta genomic regions whose methylation correlates with major wildfire smoke exposure during pregnancy. Functional enrichment analysis of the DMRs reinforce a sexually dimorphic yet convergent biological impact of wildfire exposure on the placental methylome. Male DMR genes were robustly enriched for chromatin modifying processes, small GTPase signaling, and neuronal morphogenesis. These enrichments mirror

pathways implicated in our comethylation modules and position wildfire exposure within a regulatory axis linking chromatin remodeling to cytoskeletal dynamics and neurodevelopmental patterning. In contrast, female DMR genes were enriched for apicolateral membrane components and extracellular matrix architecture. Thus, while both sexes demonstrate enrichment for cytoskeletal-related components, the context of these enrichments differ from one another. In males, cytoskeletal pathways are embedded within chromatin-regulatory and neuronal ontologies while in females they are a part of spatial ontologies, especially the functions of epithelial polarity and barrier structure that are core determinants of placental exchange performance (298,299).

Despite these differences, male and female DMR gene sets significantly overlapped, indicating shared pathway vulnerability to wildfire exposure. Notably, only the female DMR genes list demonstrated significant enrichment for the SFARI gene list. This finding provides evidence that wildfire exposure during gestation may intersect with ASD-relevant gene networks via placental methylation, representing a potential mechanistic link between air pollution and neurodevelopment outcomes previously described (211–214). While the male DMRs showed broader enrichment for neurodevelopmental ontologies, the female-specific overrepresentation of SFARI genes suggests that the placental response to wildfire exposure may have sex-specific effects on ASD-linked loci. Together, these data support a model in which prenatal wildfire exposure induces sexually dimorphic yet convergent epigenomic remodeling in placenta, targeting regulatory networks that bridge chromatin architecture, cytoskeletal organization, and neurodevelopmental gene programs.

Our study has limitations. Replication is necessary to determine whether the comethylation modules and DMRs identified in this study are broadly applicable to pregnancies with exposure to California wildfires. While the set of air pollution associated module genes did significantly overlap with genes identified as being differentially methylated in the nasal epithelium of Rhesus macaques with early-life exposure to California wildfires [Supplemental Figure 3.26] (300), further replication in human placenta will strengthen the validity of the identified module regions as signals of prenatal air pollution exposure. Additionally, the association of any single module eigennode with a trait of interest reported in this study should be replicated in other populations, as the definition of significant module associations by the passing of an empirical permutation p-value threshold (while in alignment with prior studies) holds the potential for Type 1 errors (254,267,301). Furthermore, the lack of longitudinal placental DNA methylation data narrows our findings to a single timepoint, thus making us unable to determine whether the methylation profiles associated with air pollution exposure persist in earlier periods of pregnancy. Future studies could make use of placenta-derived cell-free fetal DNA for longitudinal sampling of placenta methylation throughout pregnancy (302).

3.8 Conclusion

In summary, our findings provide evidence that prenatal air pollution exposure is associated with coordinated methylation networks in placenta, which converge on regulatory pathways that bridge chromatin architecture, cytoskeletal organization, and

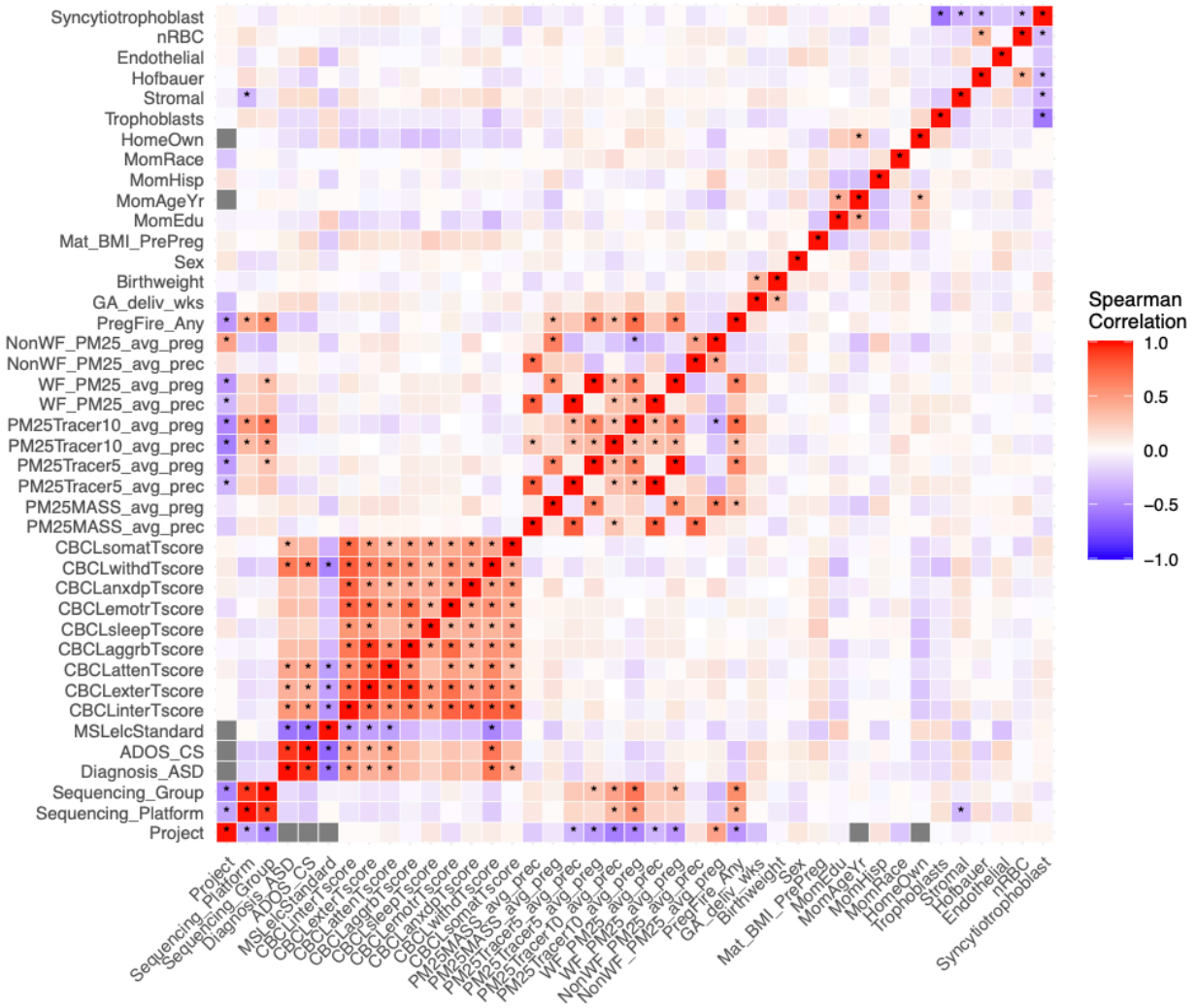
neurodevelopmental signaling. Through WGBS and comethylation network analysis, we identify temporally distinct epigenetic signatures of preconception versus *in utero* air pollution exposure, as well as source-specific differences between wildfire-derived and ambient particulate matter. While replication in independent wildfire-impacted cohorts and longitudinal profiling will be essential to establish the persistence of these signals and potential causality, these data support a model in which wildfire smoke exposure during critical windows of development alters the placental epigenome at regulatory domains relevant to fetal neurodevelopment. As wildfire seasons intensify and lengthen, elucidating these molecular signatures is critical for understanding how wildfire smoke exposures may shape health trajectories.

3.9 Data and code availability

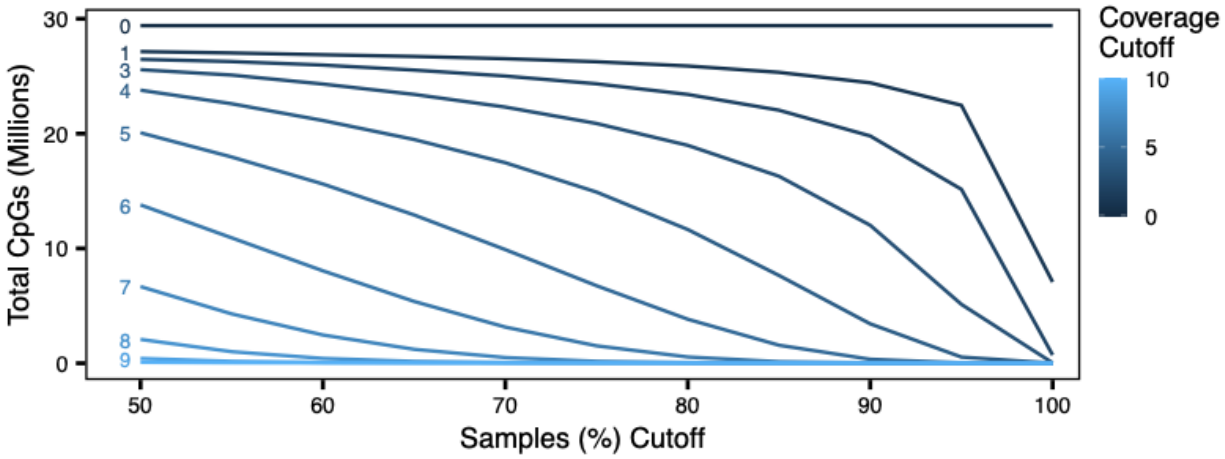
The sequencing data generated by this study from all subjects that provided consent (n=85) have been deposited in the GEO database under accession code GSE324959. During review, you can access this data by providing the following token: wvevwiechrgtdix. Previously reported placenta sequencing data used in analysis for this study can be found on GEO under accession code GSE178206. All original code has been deposited on GitHub (https://github.com/lwilliams27/PlacentaMethylome_AirPollutionExposure) .

3.10 Supplemental Material

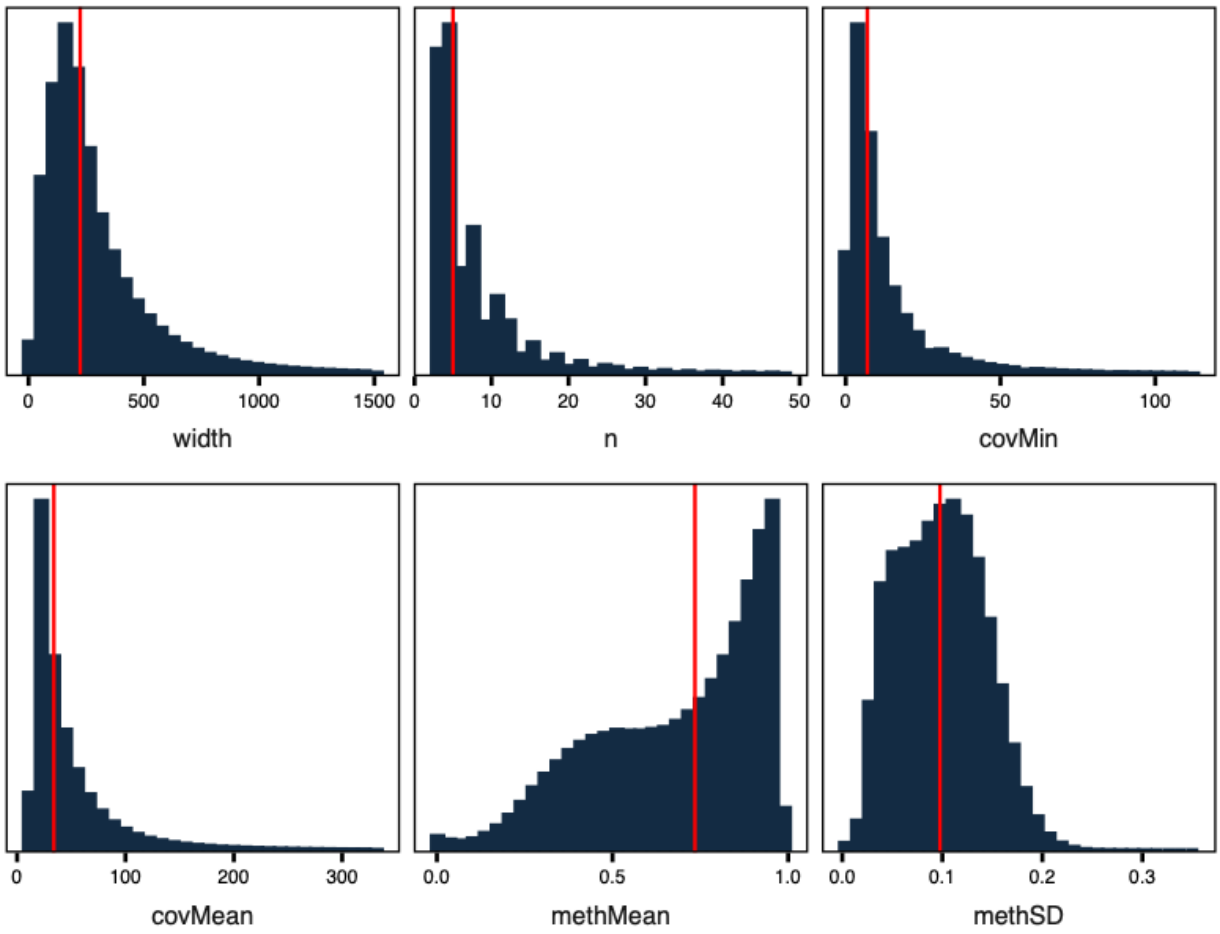
3.10.1 Supplemental Figures



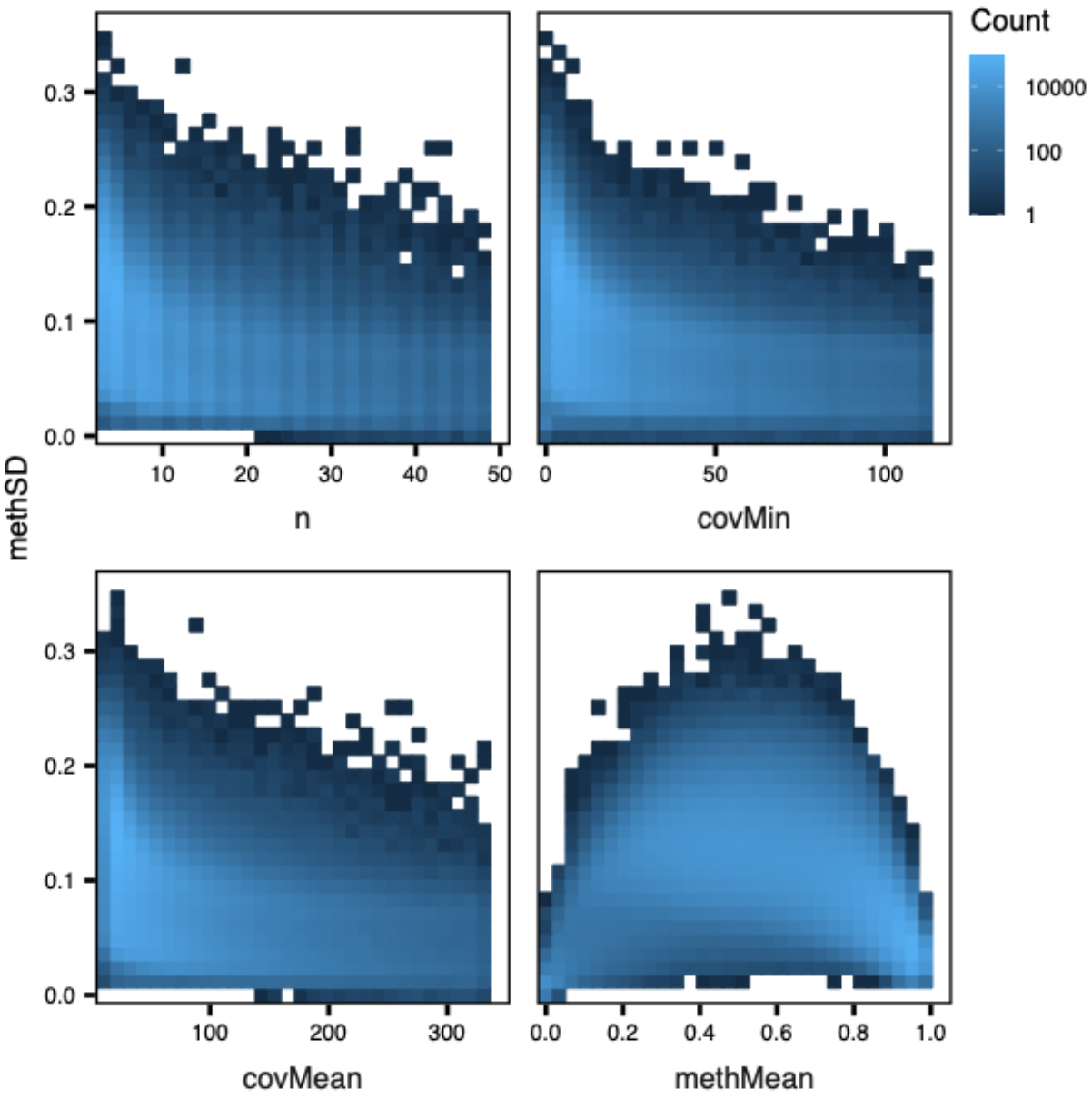
Supplemental Figure 3.1: Heatmap displaying Spearman correlation values of all sample traits included in the comethylation network analysis, with significant associations (FDR < 0.05) denoted by an asterisk. Most significant associations are between related neurodevelopmental traits and between air pollution metrics. Spearman correlation was used to lessen the impact of outliers.



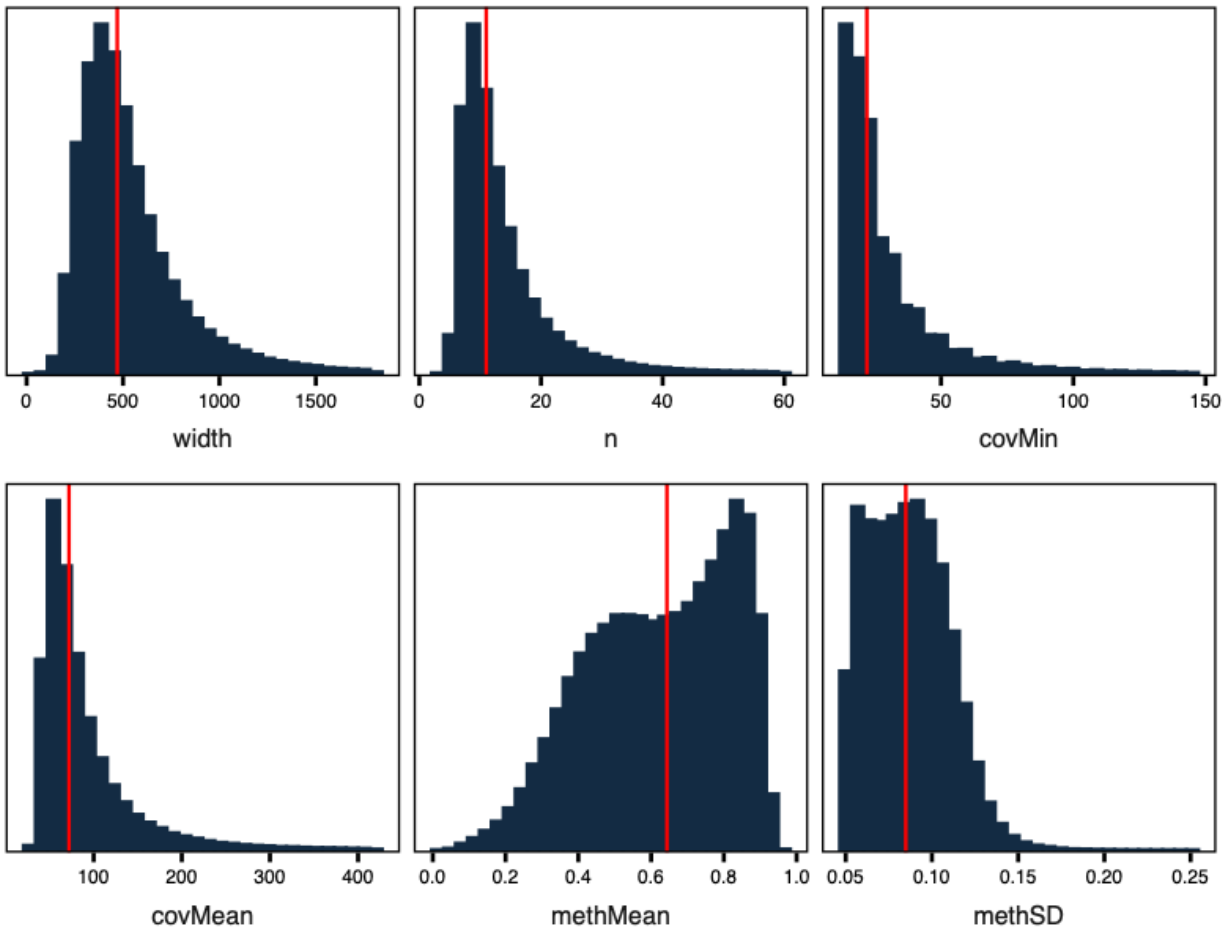
Supplemental Figure 3.2: Plot displaying how the total number of CpG loci considered in region identification is dependent upon specified coverage and sample perentage parameters. For the analysis described in this study, thresholds of ≥3X coverage in ≥75% of all samples were applied, resulting in the selection of 20,881,192 CpGs for region identification.



Supplemental Figure 3.3: Frequency plots of unfiltered region statistics. The x-axes denote various parameters of relevance to the unfiltered region sets, including width (number of base pairs within a given region), n (number of CpGs within a given region), covMin (minimum coverage of that region), covMean (mean coverage of that region), methMean (mean methylation across a region), and methSD (methylation standard deviationa cross samples for a given region). The y-axes display normalized frequencies of regions with those parameters. Red lines denote medians.

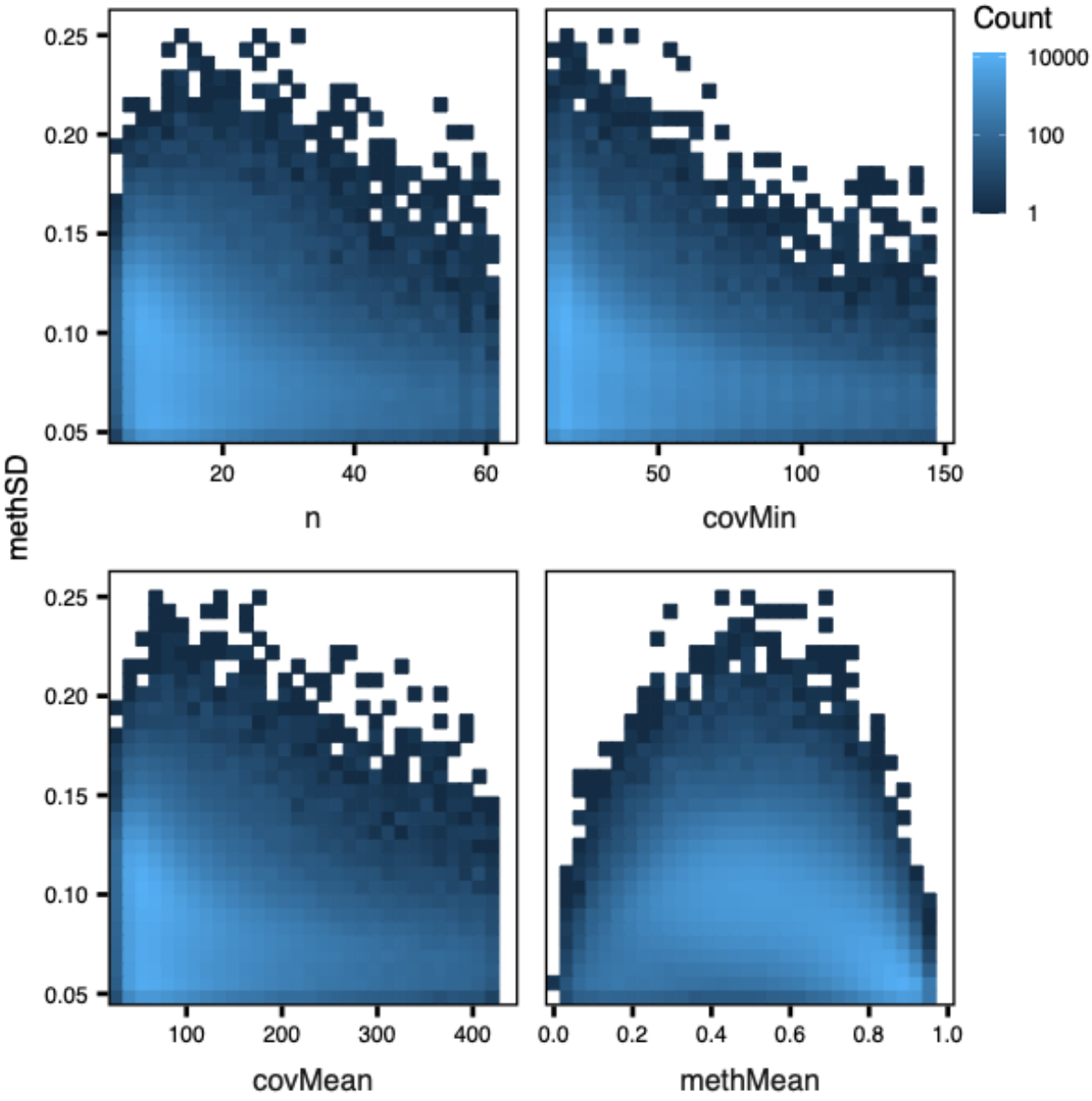


Supplemental Figure 3.4: Heatmaps displaying the number of unfiltered regions with various combinations of standard deviation in methylation across samples (methSD) and four other metrics of note. These metrics are denoted on the x-axes as n (number of CpGs in each region), covMin (minimum coverage of a given region), covMean (mean coverage of a given region) and methMean (mean methylation of a given region).



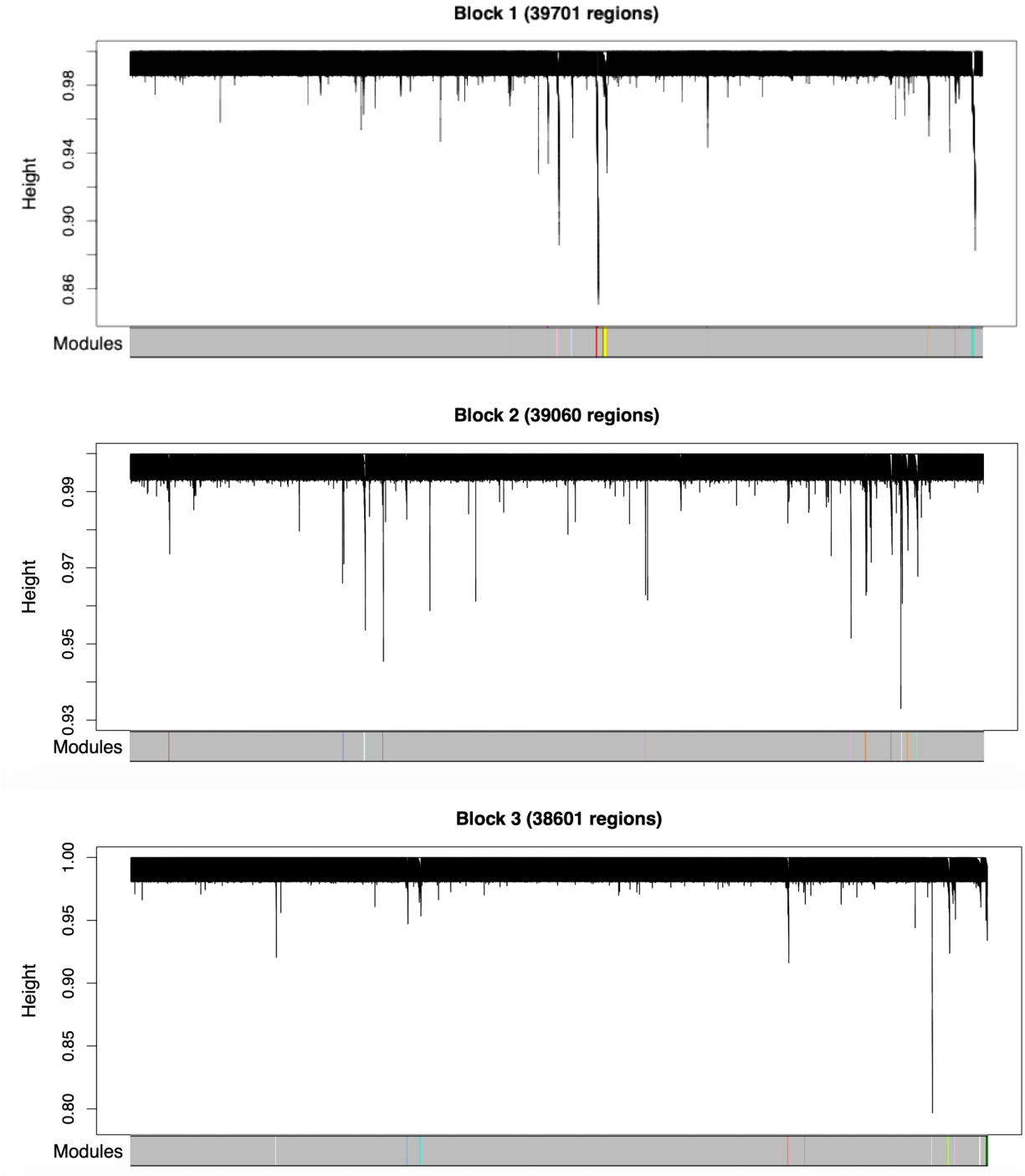
Supplemental Figure 3.5: Frequency plots of filtered region statistics. The x-axes denote various parameters of relevance to the unfiltered region sets, including width (number of base pairs within a given region), n (number of CpGs within a given region), covMin (minimum coverage of that region), covMean (mean coverage of that region), methMean (mean methylation across a region), and methSD (methylation standard deviation across samples for a given region). The y-axes display normalized frequencies of regions with those parameters. Red lines denote medians. In contrast to

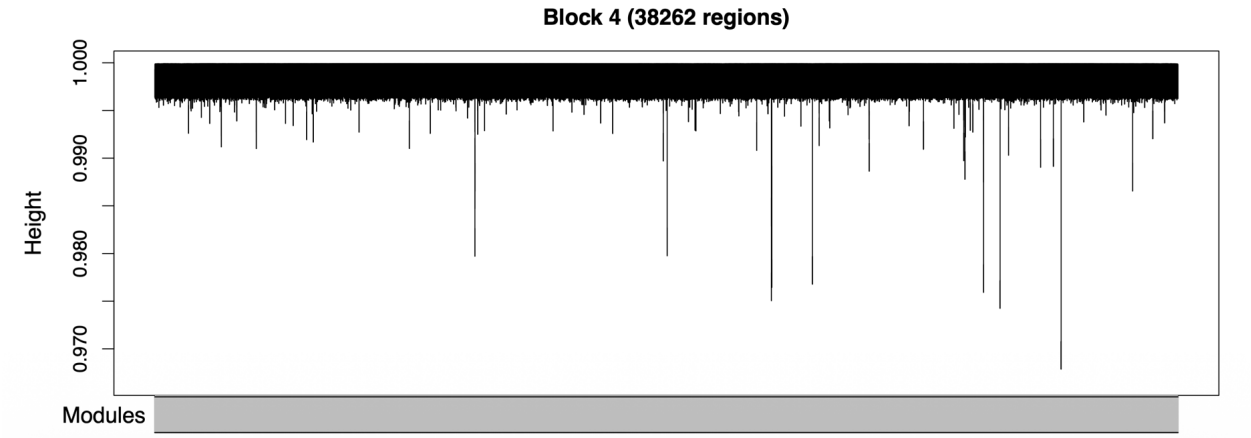
the unfiltered regions, the filtered regions display higher coverage, reduced mean methylation, and comparable methylation standard deviation.

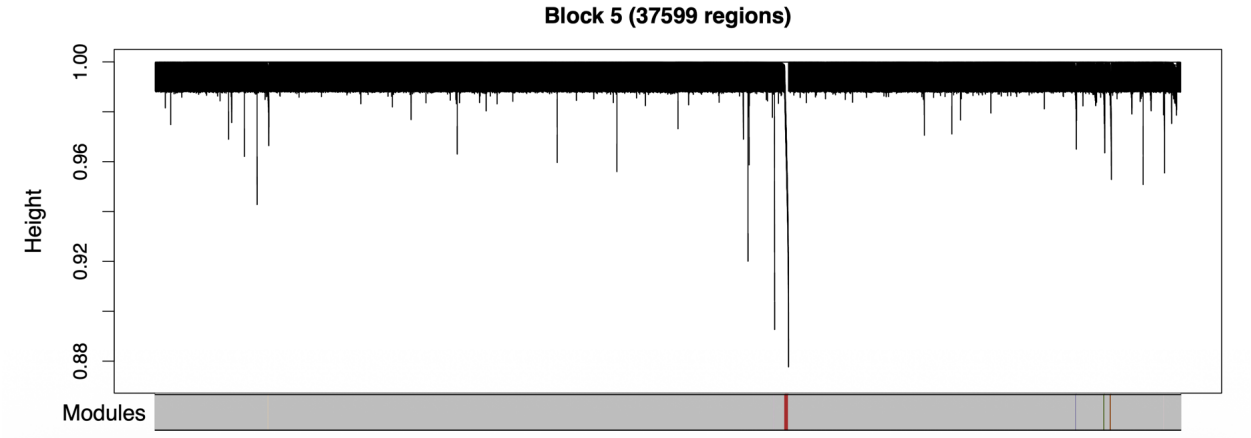


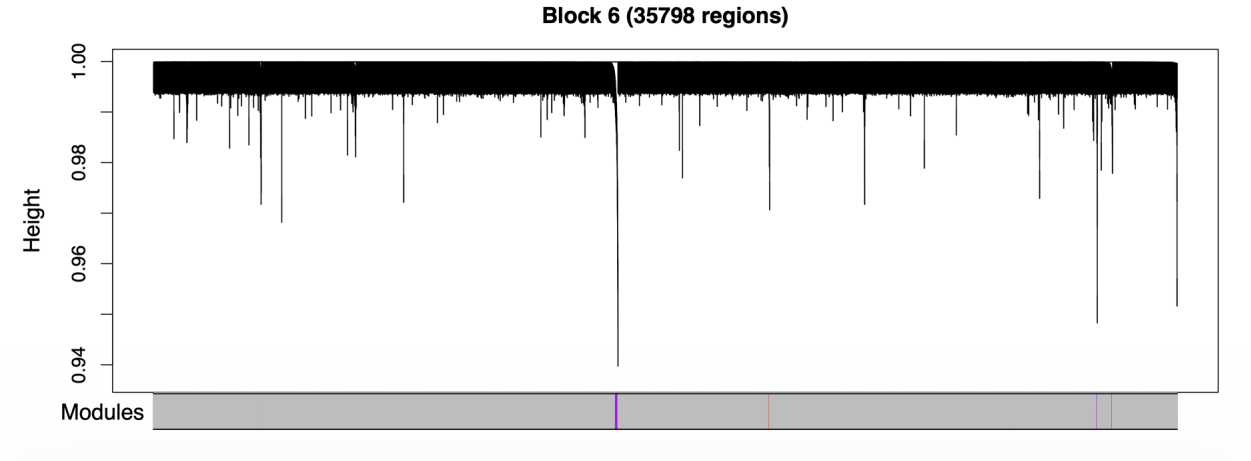
Supplemental Figure 3.6: Heatmaps displaying the number of filtered regions with various combinations of standard deviation in methylation across samples (methSD)

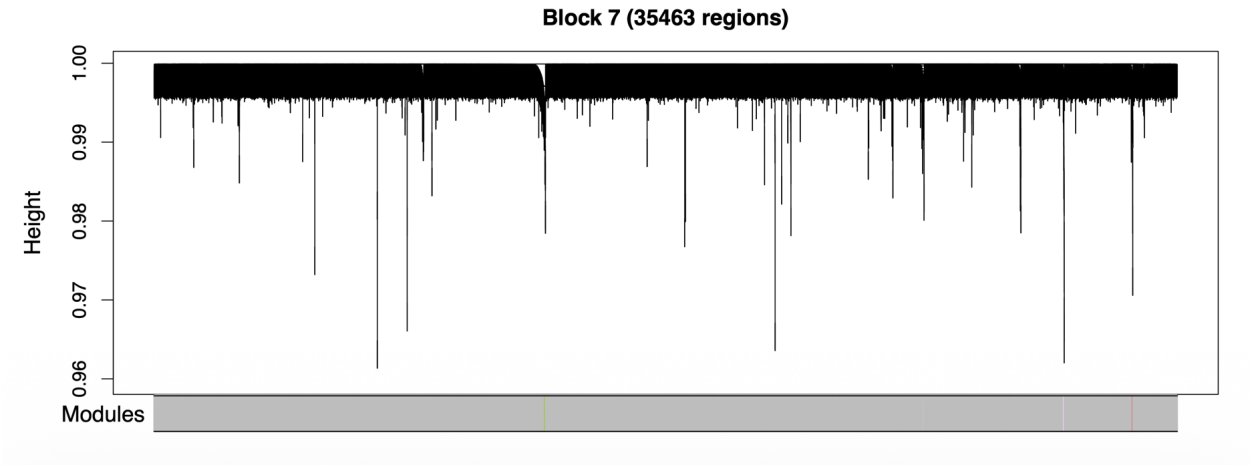
and four other metrics of note. These metrics are denoted on the x-axes as n (number of CpGs in each region), covMin (minimum coverage of a given region), covMean (mean coverage of a given region) and methMean (mean methylation of a given region).

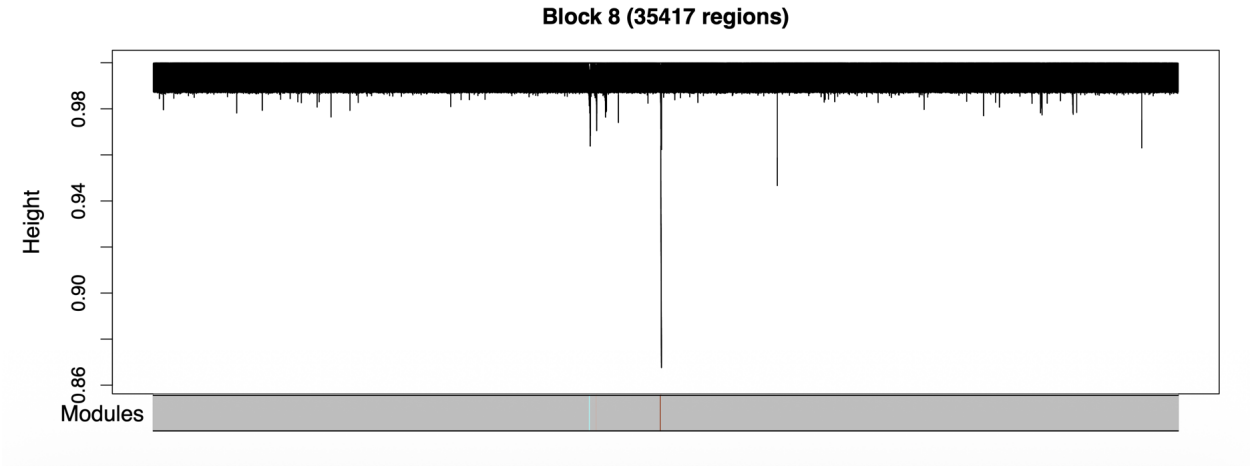

Block 1 (39701 regions)
Height
0.98
0.94
0.90
0.86
Modules
Block 2 (39060 regions)
Height
0.99
0.97
0.95
0.93
Modules
Block 3 (38601 regions)
Height
1.00
0.95
0.90
0.85
0.80
Modules

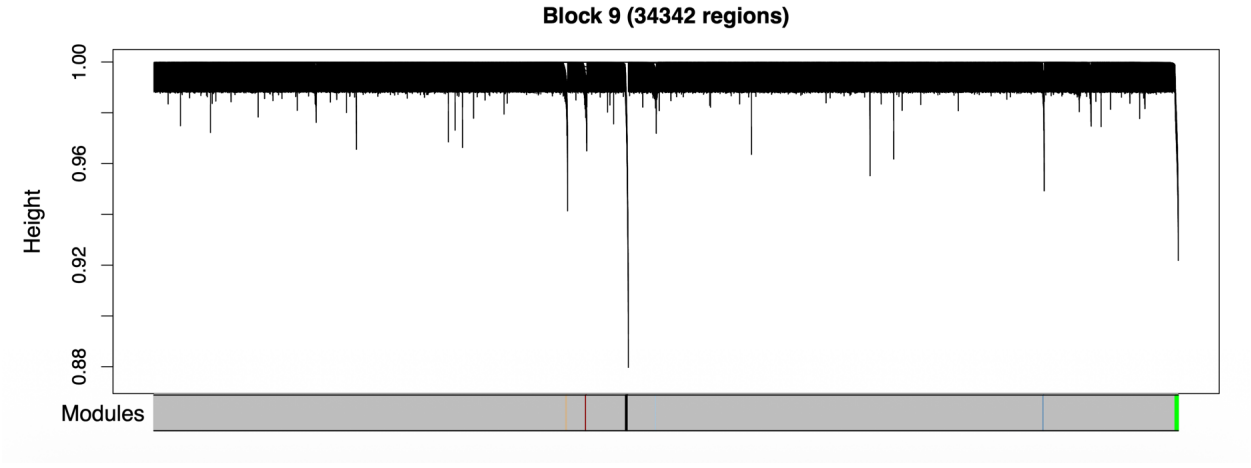

Block 4 (38262 regions)
Height
1.000
0.990
0.980
0.970
Modules

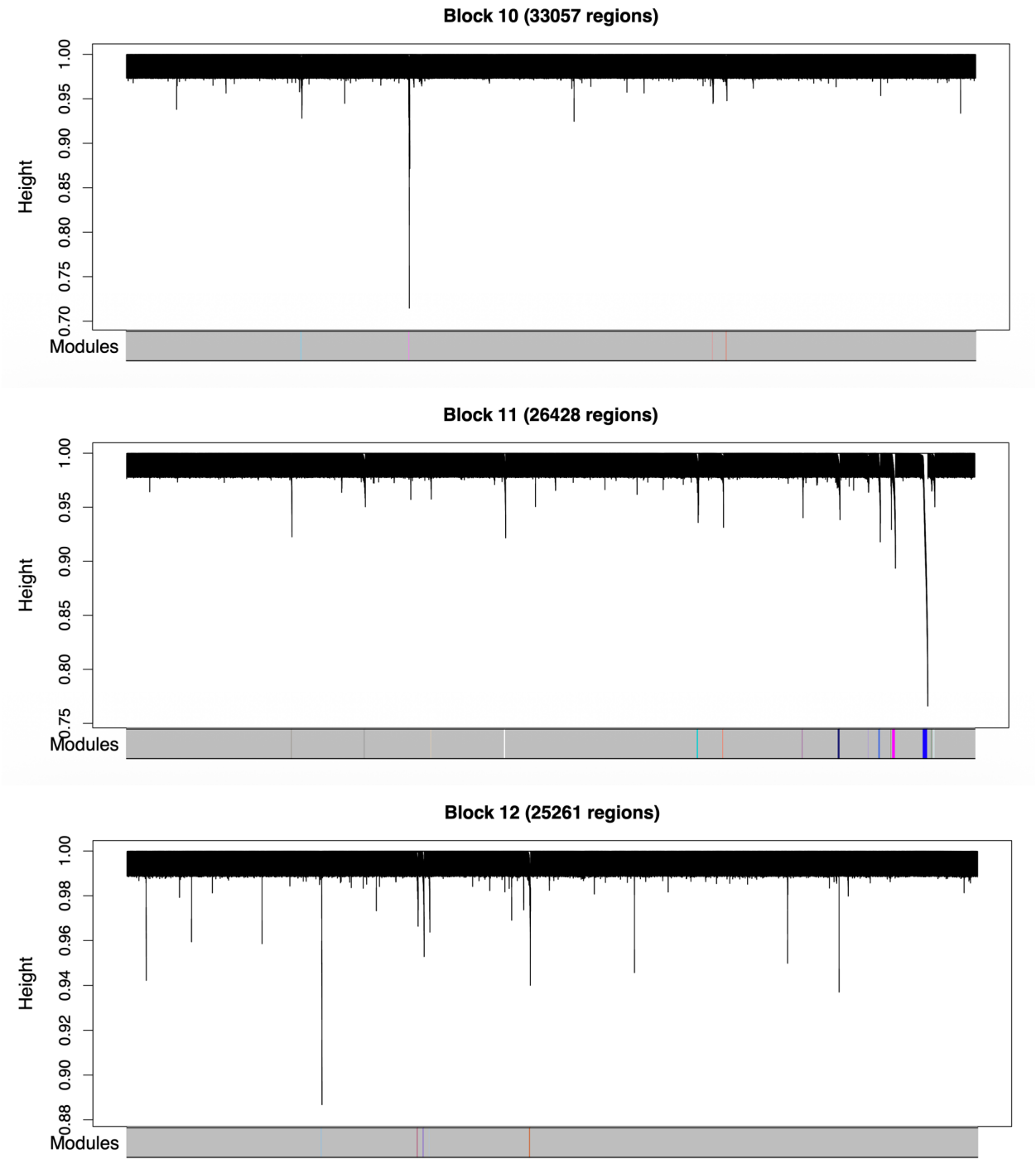

Block 5 (37599 regions)
Height
1.00
0.96
0.92
0.88
Modules


Block 6 (35798 regions)
Height
1.00
0.98
0.96
0.94
Modules


Block 7 (35463 regions)
Height
1.00
0.99
0.98
0.97
0.96
Modules

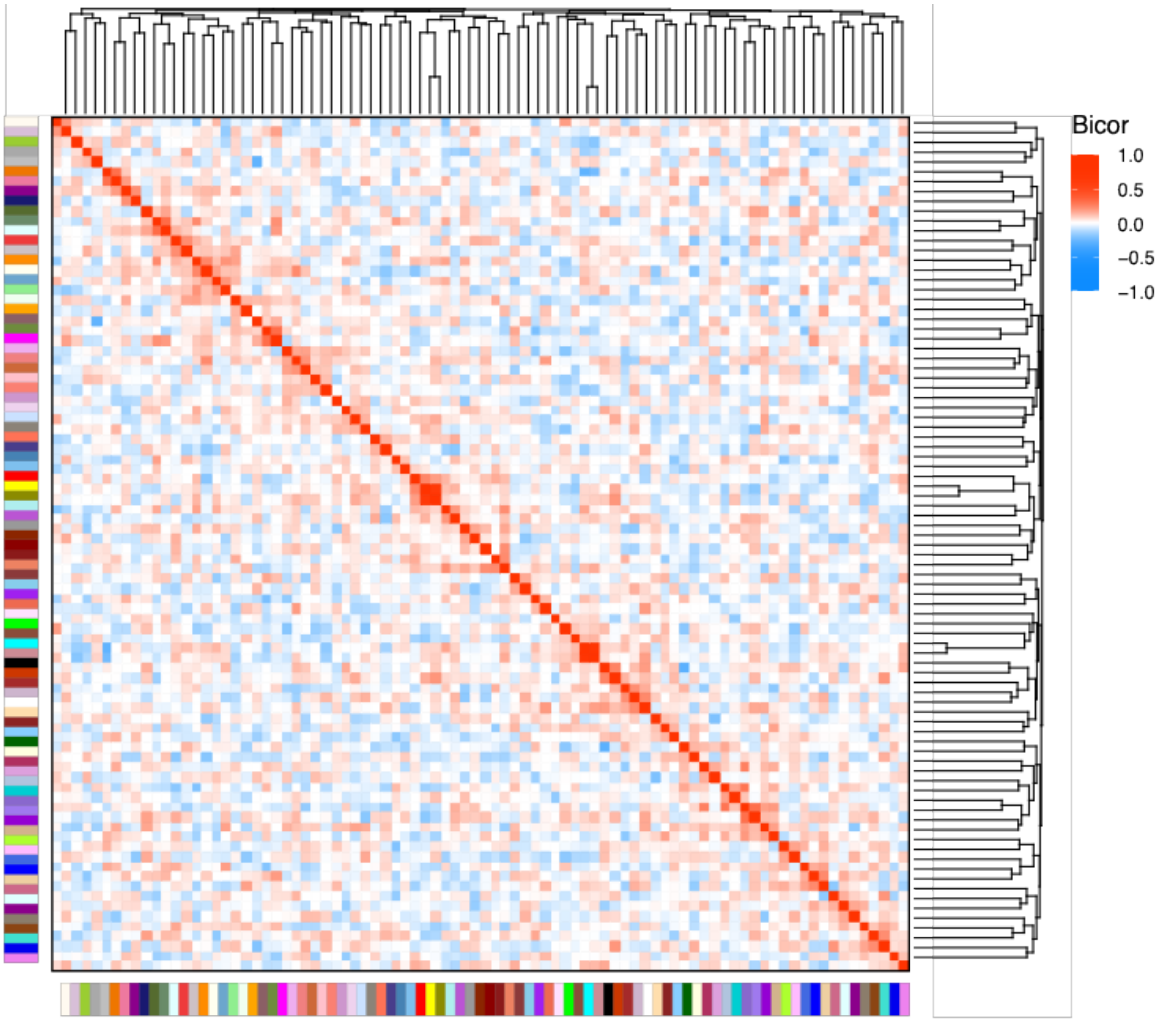

Block 8 (35417 regions)
Height
0.98
0.94
0.90
0.86
Modules


Block 9 (34342 regions)
Height
1.00
0.96
0.92
0.88
Modules

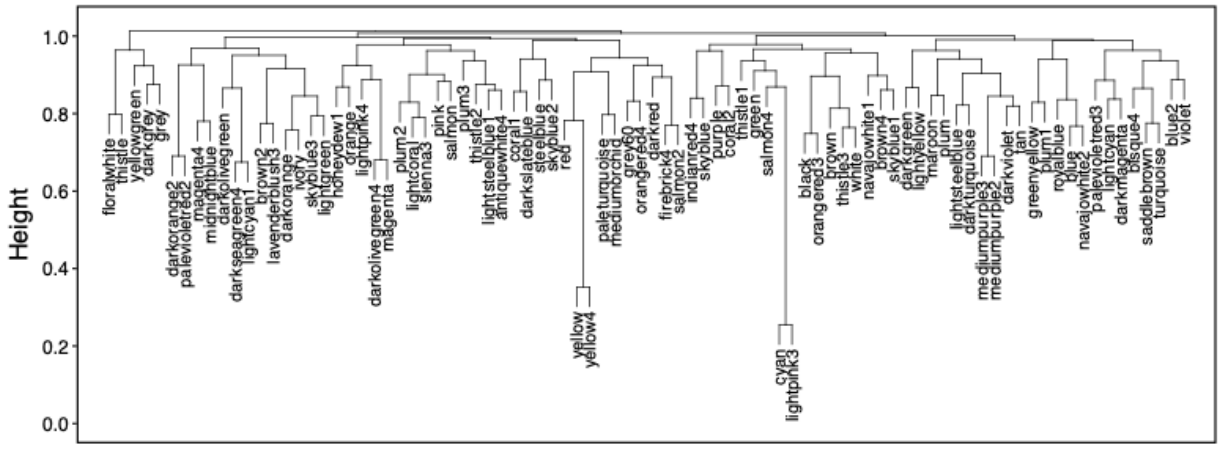


Supplemental Figure 3.7: Region dendrograms for the 12 blocks used during comethylation network generation. Regions were assigned into blocks of ~40,000 regions and subjected to full network analysis to assign regions to modules. Modules

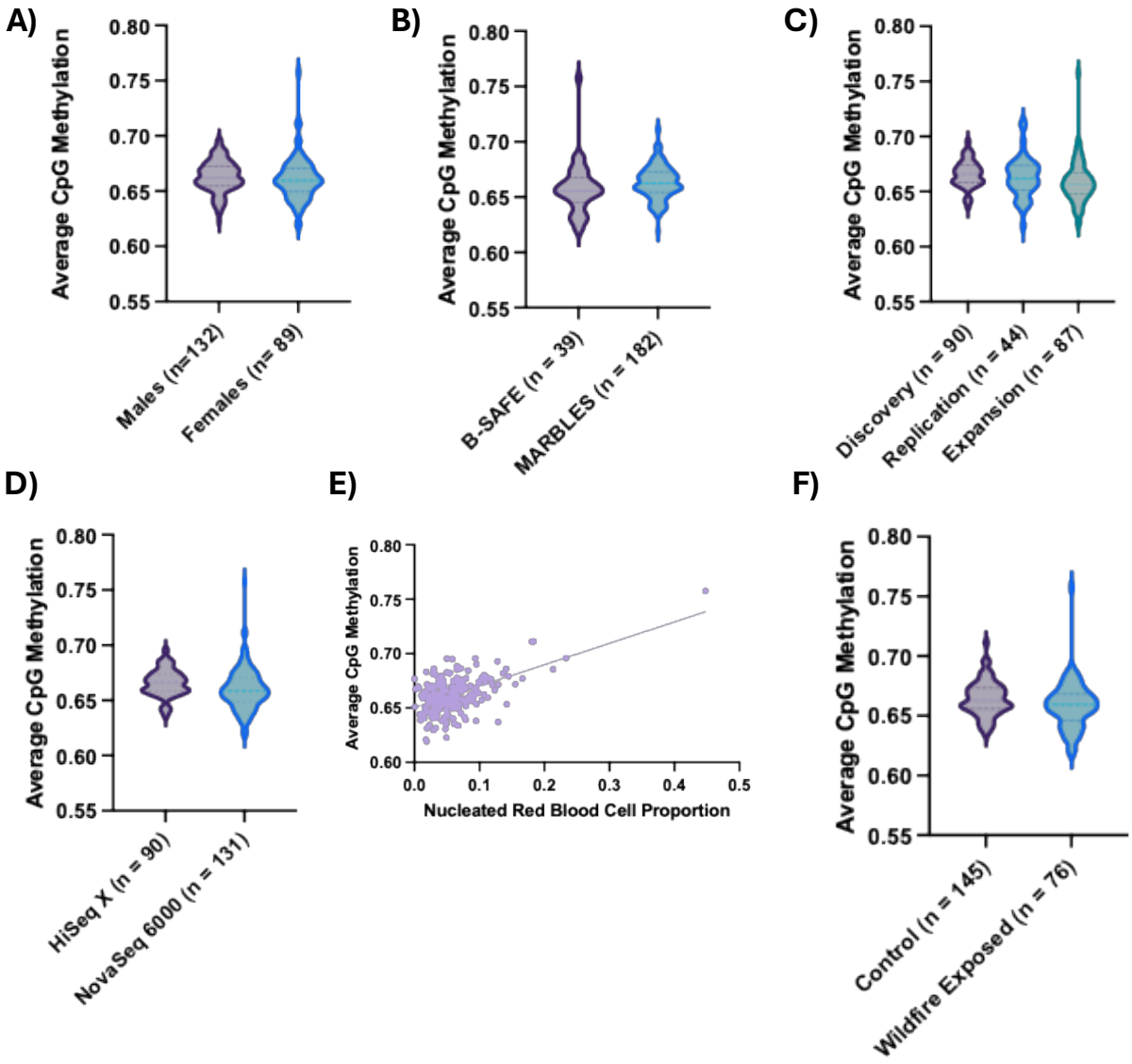
with highly correlated module eigennode values (r < 0.90) across different blocks were merged. Regions were clustered by dissimilarity.



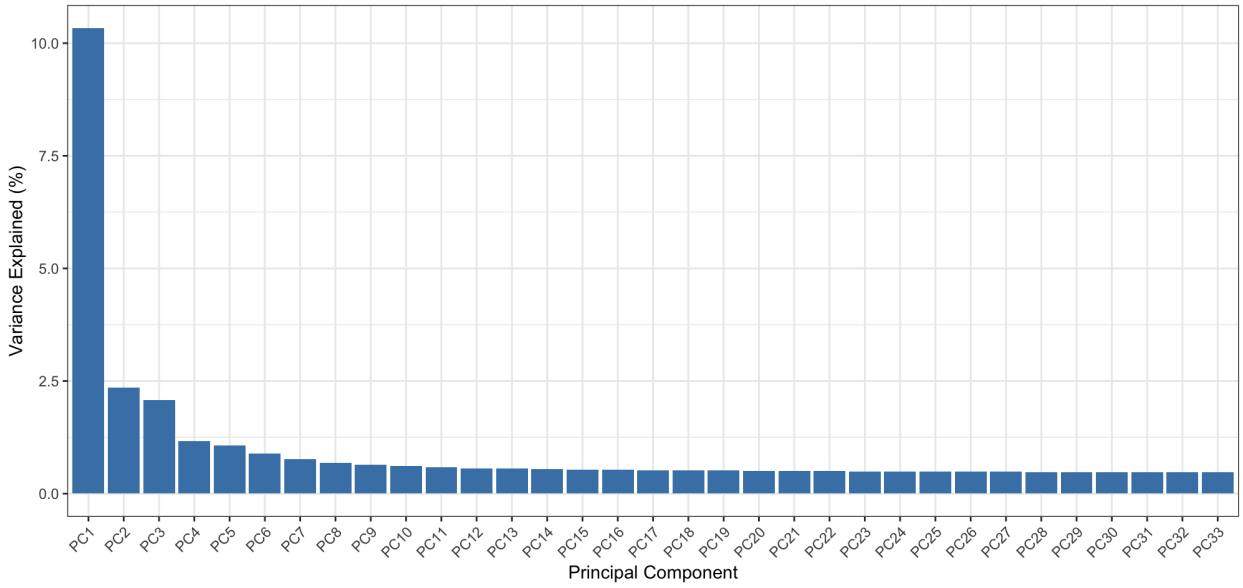
Supplemental Figure 3.8: Heatmap of comethylation module correlations with one another, as quantified by Bicor. Module identity shown by color on the x and y axes.



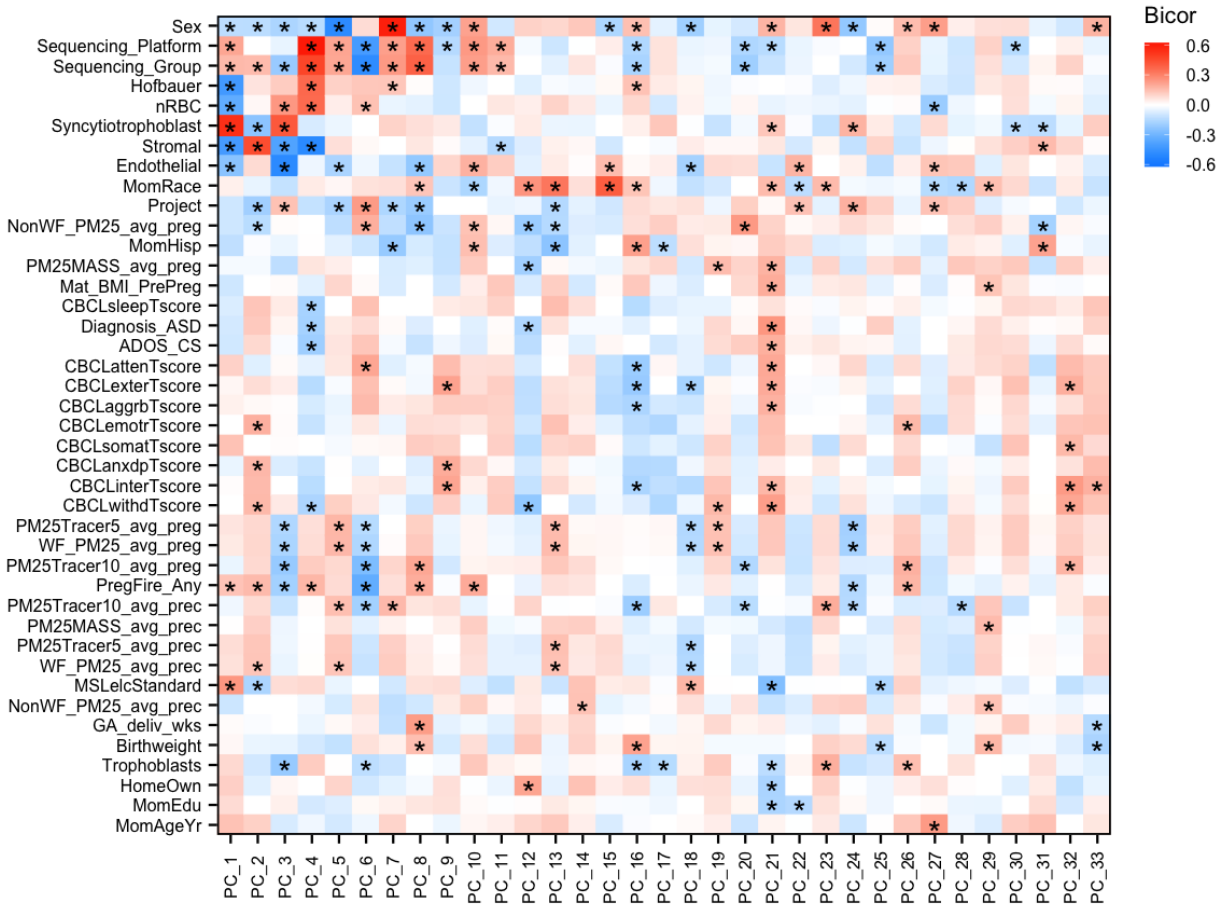
Supplemental Figure 3.9: Dendrogram of modules clustered by dissimilarity of eigennode values. Only two pairs of modules appear highly similar: cyan and lightpink3, and yellow and yellow4.



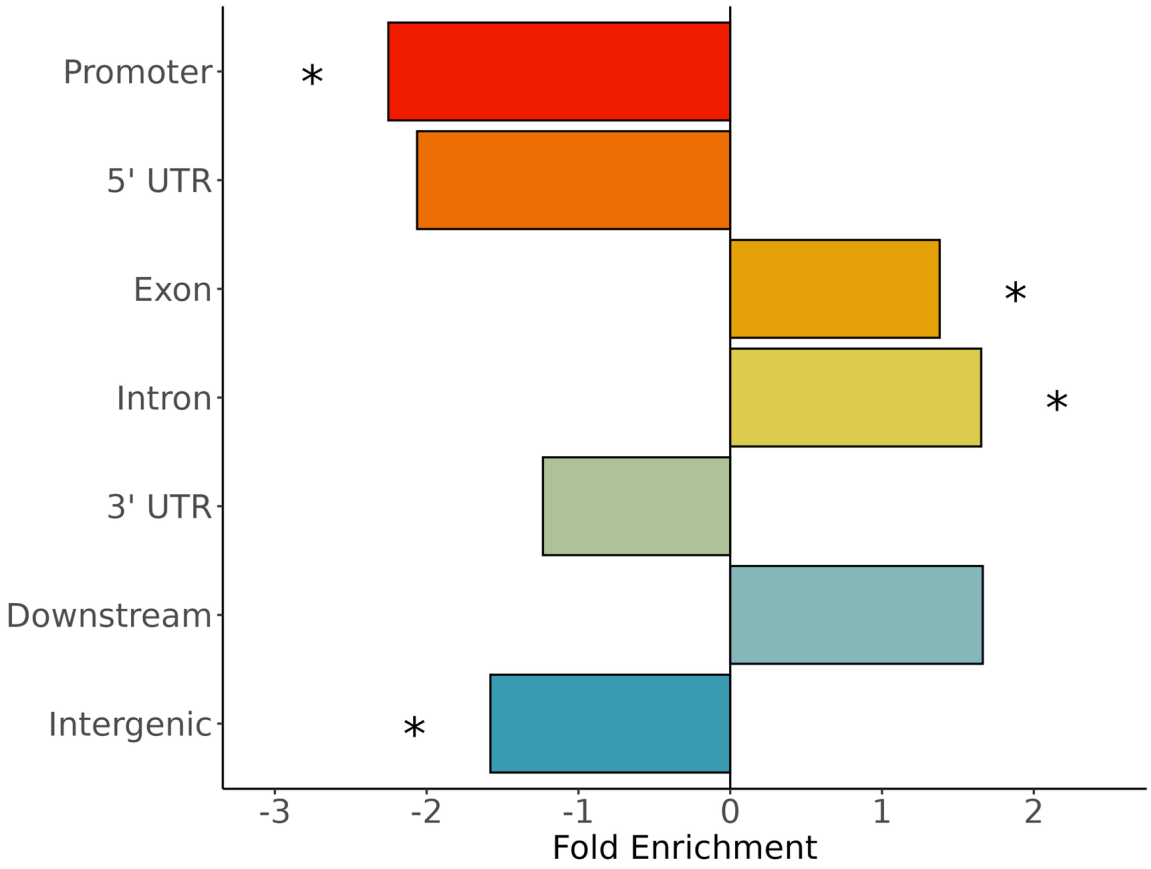
Supplemental Figure 3.10: Global methylation differences between different groups as quantified by proportion of methylated CpGs, including groups A) sexes (p = 0.37, Student's t-test), B) project group (p = 0.17, Student's t-test), C) sequencing groups (p = 0.018, Brown-Forsythe ANOVA), D) sequencing platform (p = 0.0060, Student's t-test), E) proportion of estimated placenta sample from nucleated red blood cells (Slope = 0.021, R^2 = 0.2828, simple linear regression), and F) wildfire exposure during pregnancy (p = 0.0243, Student's t-test). Images made with GraphPad Prism 10.



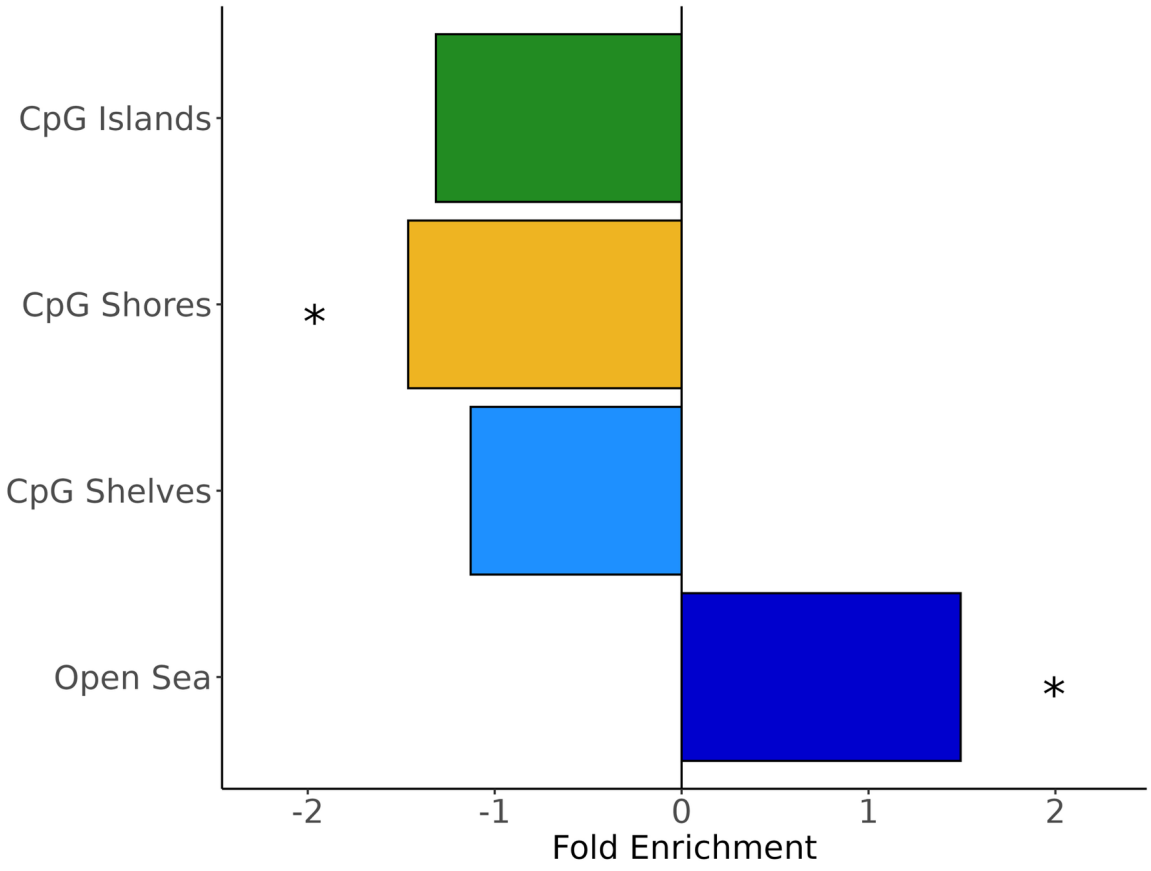
Supplemental Figure 3.11: Bar plot showing the calculated variance of each of the 33 top principal components identified from filtered region methylation prior to soft power thresholding.



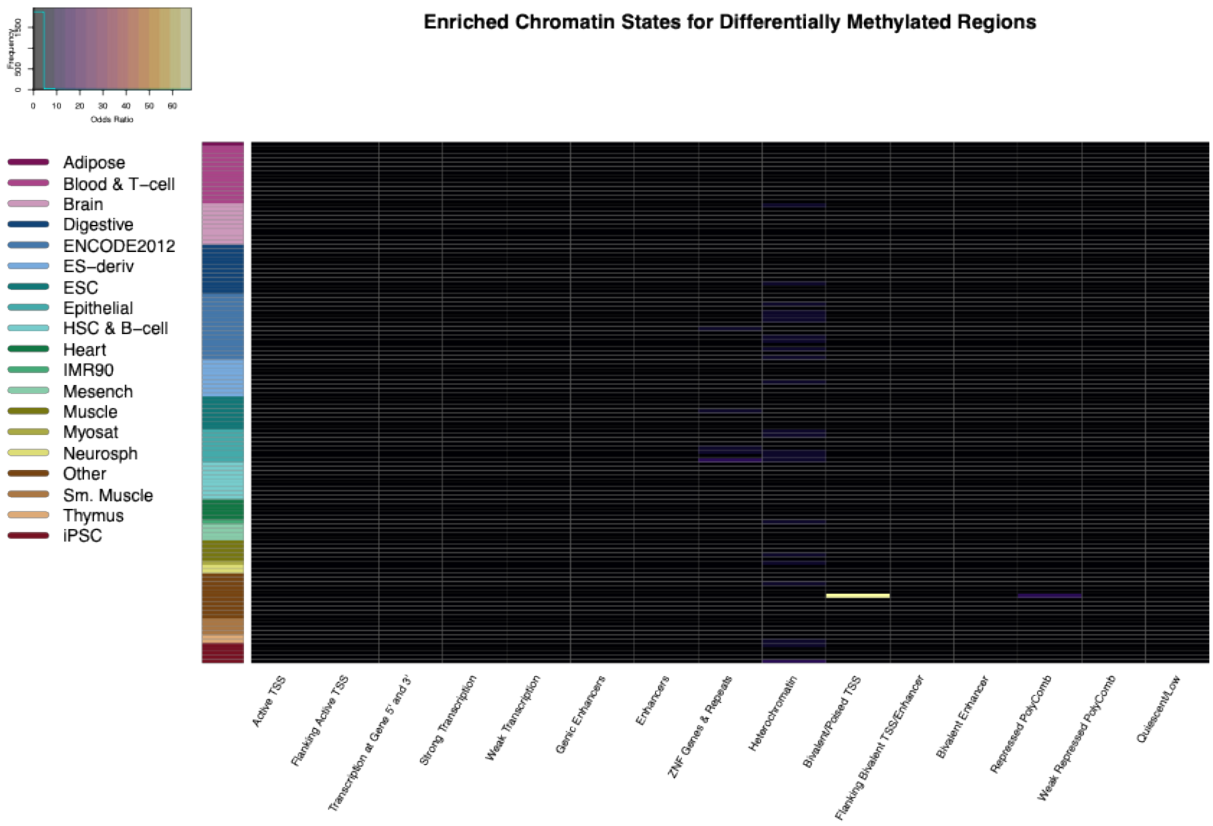
Supplemental Figure 3.12: Heatmap showing biweight midcorrelation (Bicor) between the 33 calculate prinicipal component values for each included sample (x-axis) and all sample traits clustered by similarity dendrogram (y-axis). Significant associations as determined by Fisher's transformation are denoted with a star.



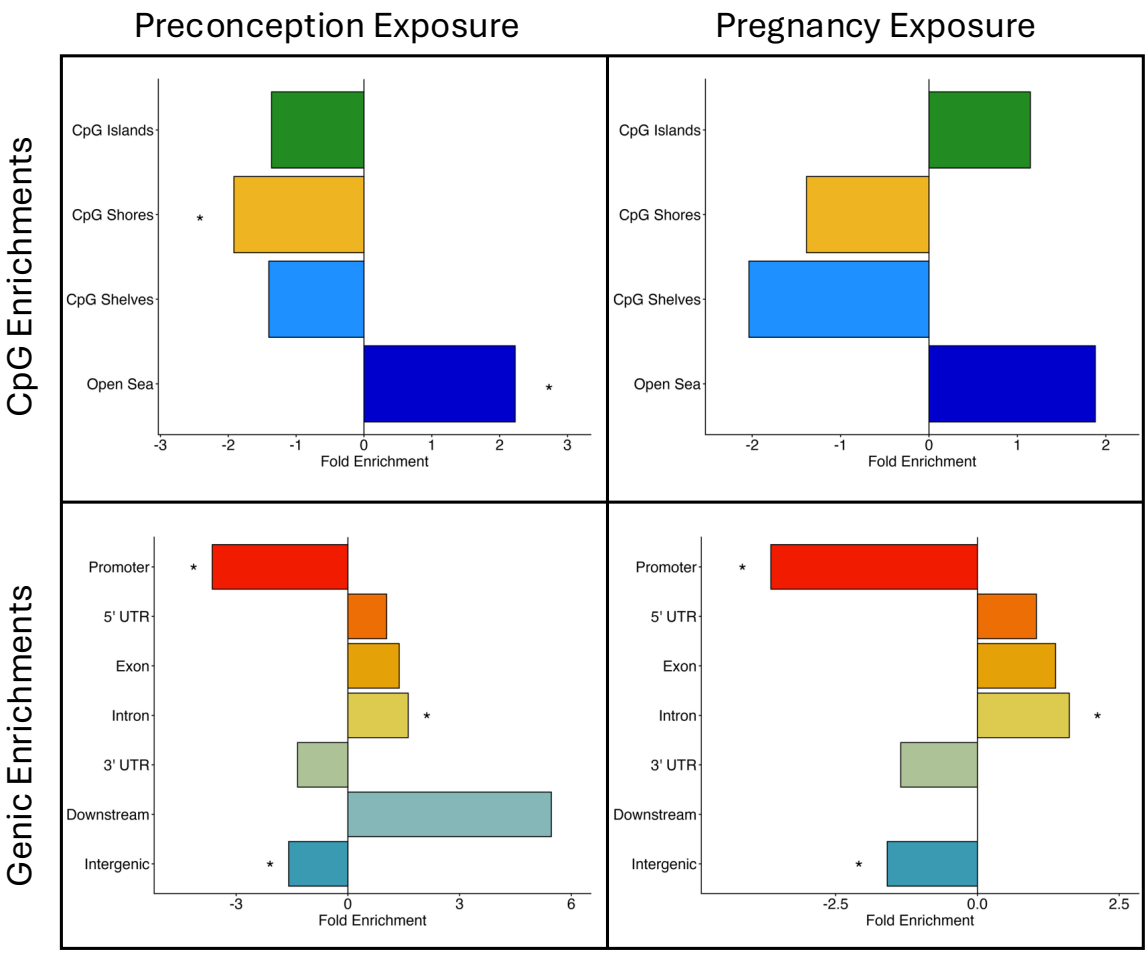
Supplemental Figure 3.13: Bar plot of Fold Enrichment of genic elements in regions assigned to modules relative to all regions considered in comethylation network generation. * denotes significant (adj.p < 0.05) enrichment or depletion as defined by Fisher's Exact Test with FDR (Benjamini and Hochberg) correction.



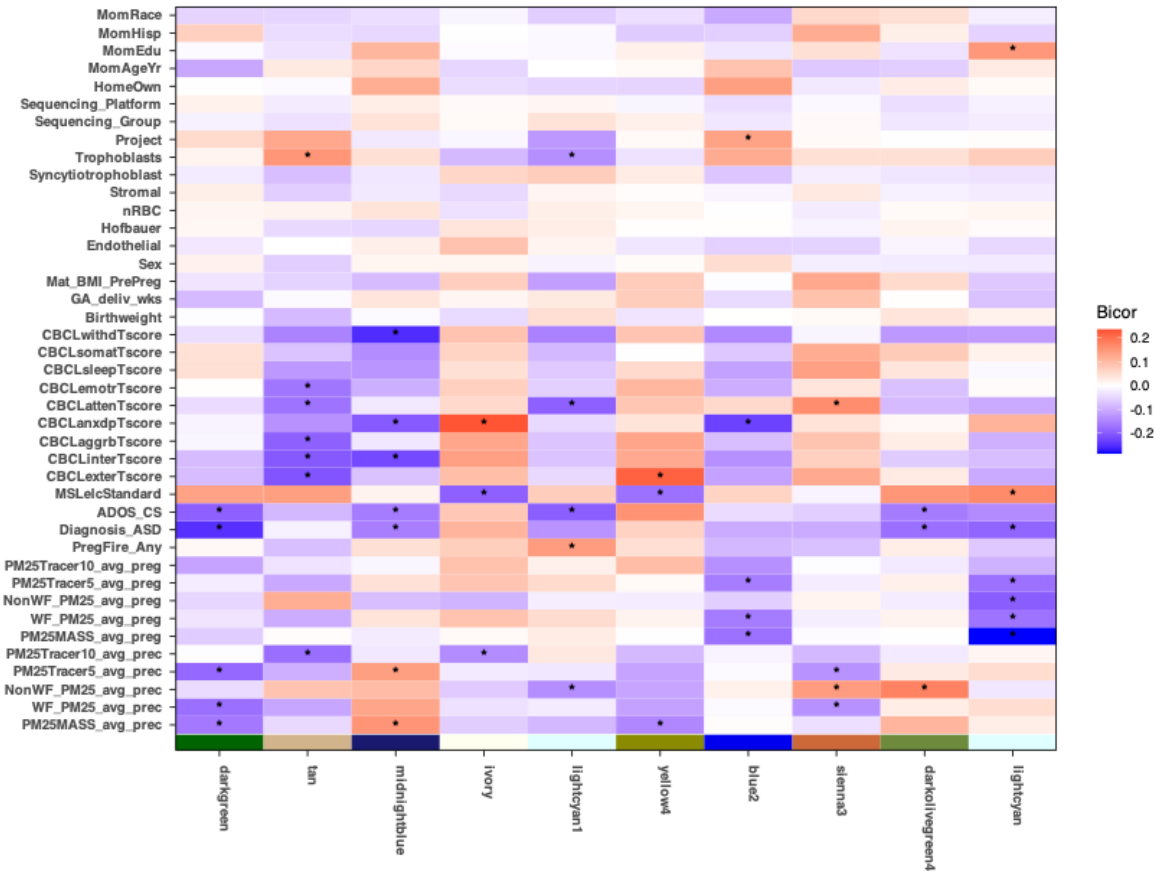
Supplemental Figure 3.14: Bar plot of Fold Enrichment of CpG context in regions assigned to modules relative to all regions considered in comethylation network generation. * denotes significant (adj.p < 0.05) enrichment or depletion as defined by Fisher's Exact Test with FDR (Benjamini and Hochberg) correction.



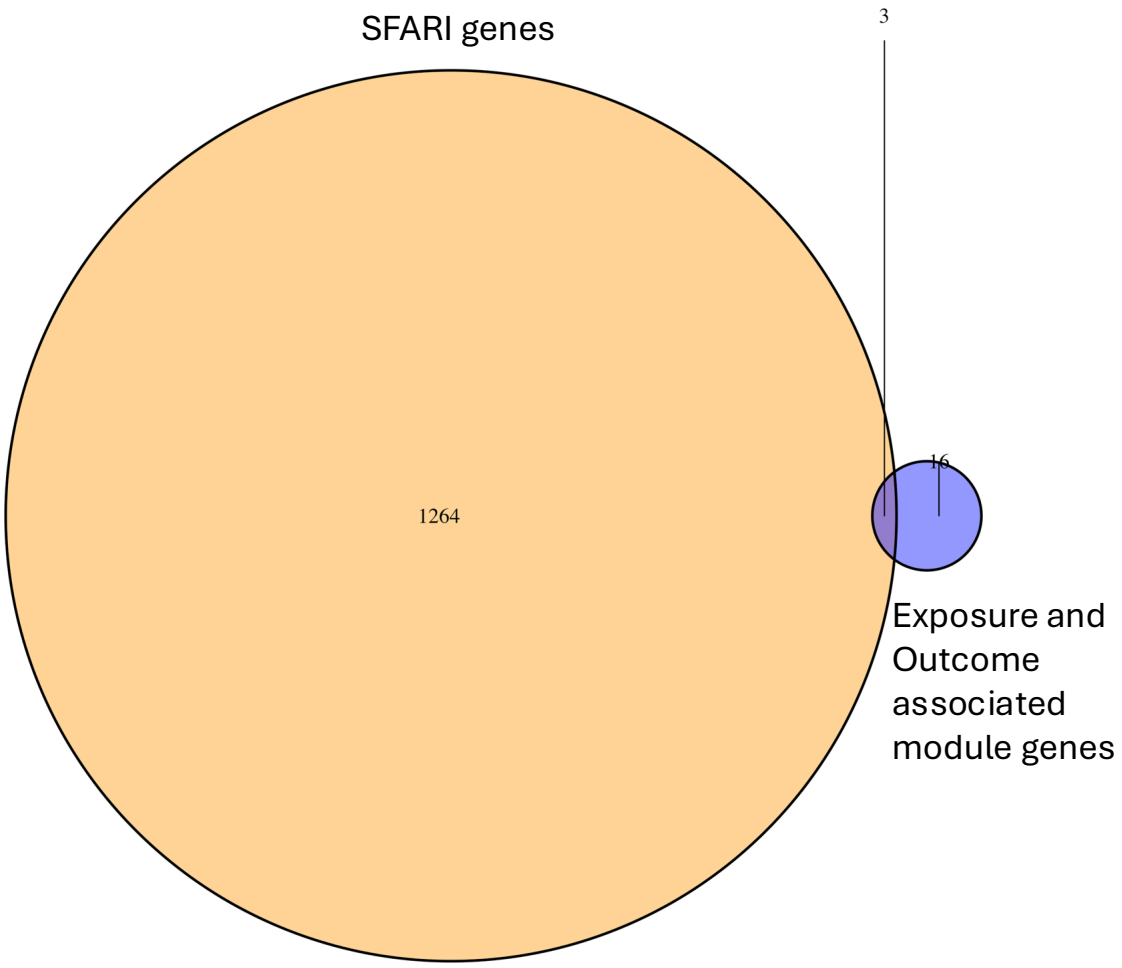
Supplemental Figure 3.15: Heatmap displaying the Odds Ratio for calculated enrichment of all module regions relative to all filtered regions included in network analysis, using the predicted chromatin states from multiple tissues provided by the Roadmap Epigenomics Project. Enrichment determined by Fisher's Exact Test as executed by the LOLA R package.



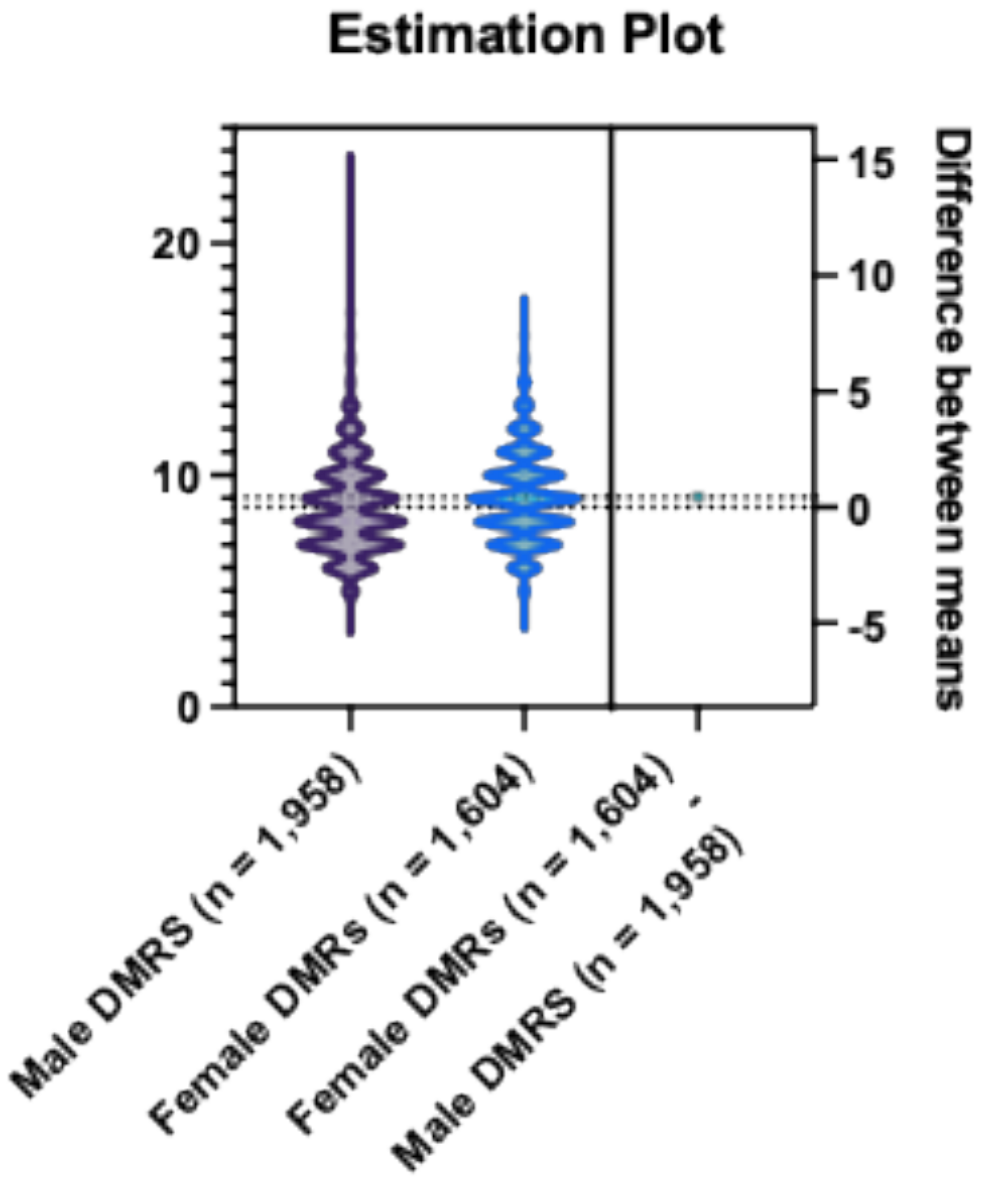
Supplemental Figure 3.16: Comparison of the significant enrichments of the regions assigned to modules significantly associated with at least one preconceptional air pollution exposure trait and regions assigned to modules significantly associated with at least one pregnancy air pollution exposure trait. * denotes significant (adj.p < 0.05) enrichment or depletion as defined by Fisher's Exact Test with FDR (Benjamini and Hochberg) correction. No significant differences between preconceptional and pregnancy air pollution exposure-associated module regions are observed.



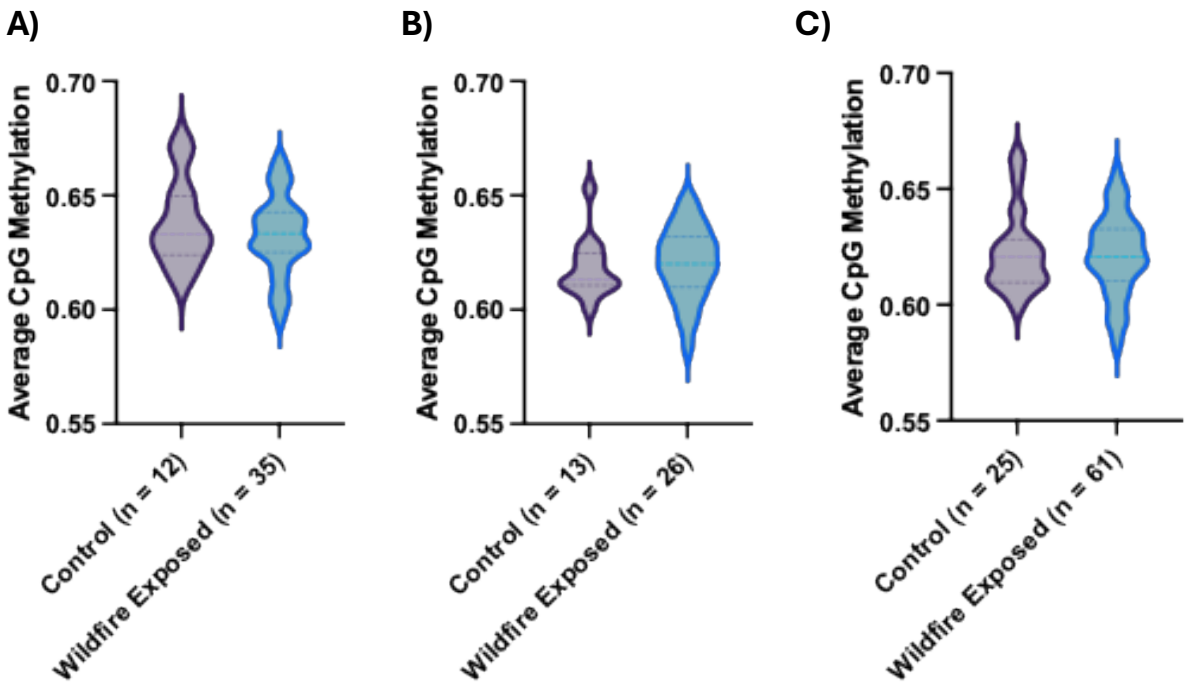
Supplemental Figure 3.17: Heatmap showing Bicor correlations of all sample traits included in network analysis with 10 of the 85 identified modules. The 10 modules shown are those with a significant ($p < 0.05$) association with at least one ‘Exposure’ and at least one ’Outcome’ variable. Significant associations (as determined by Fisher’s transformation) are denoted with a star.



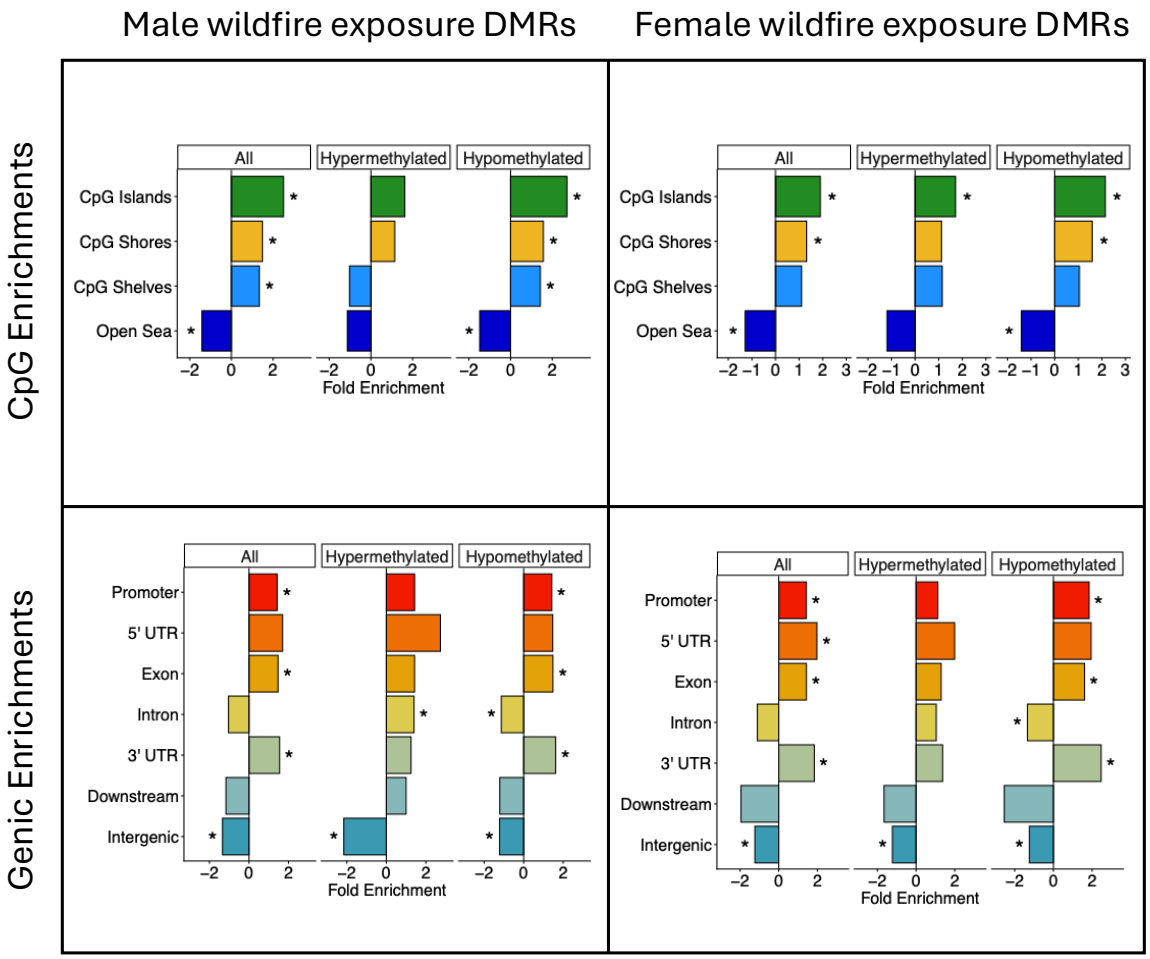
Supplemental Figure 3.18: Venn diagram displaying the overlap between genes annotated to human placenta comethylation modules associated with at least one air pollution variables and at least one child developmental outcome variable and genes in the SFARI gene database. A non-significant overlap of 3 genes was observed, with significance determined by Fisher's Exact Test ($p = 0.15$), and a background universe of genes annotated to all modules considered in network construction.



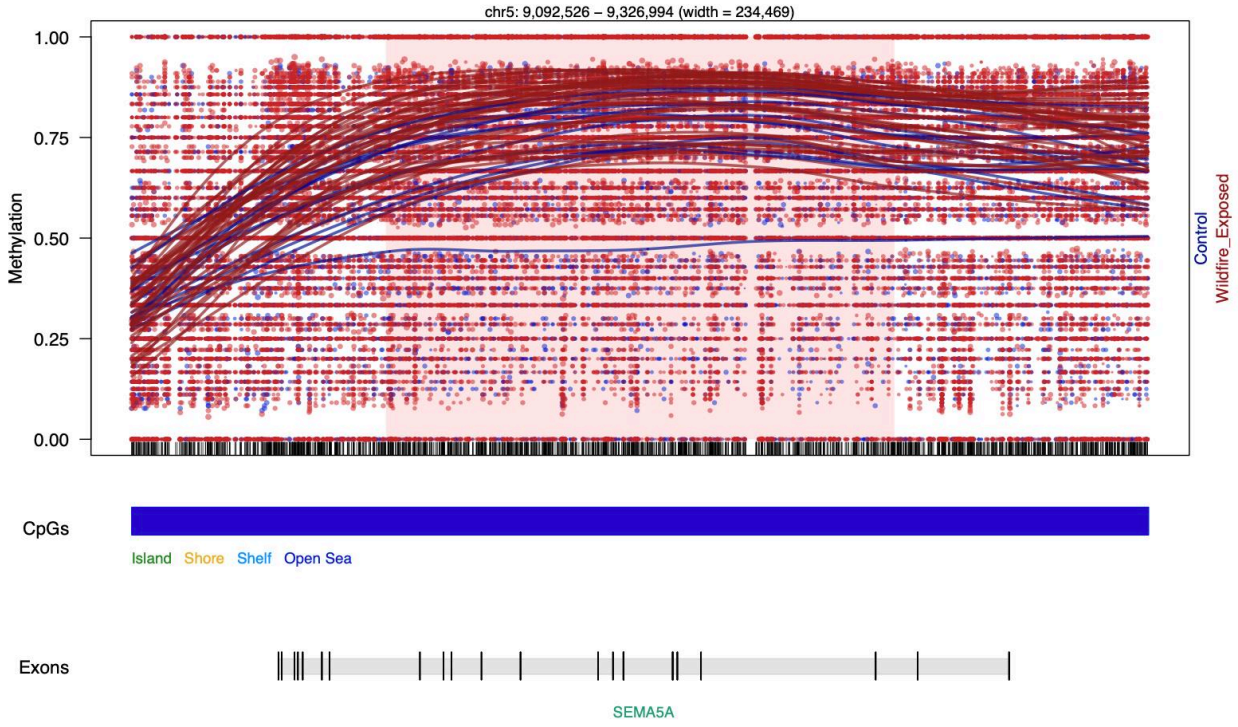
Supplemental Figure 3.19: Estimation plot of difference between average DMR magnitude (defined as the absolute value of % difference in methylation between wildfire exposed and control samples) between sexes. A significant difference was observed between males and females ($p < 0.0001$, Student's t-test), with the average magnitude of the female DMRs (9.065%) being significantly greater than the average magnitude of the male DMRs (8.616%). Plot created with GraphPad Prism 10.

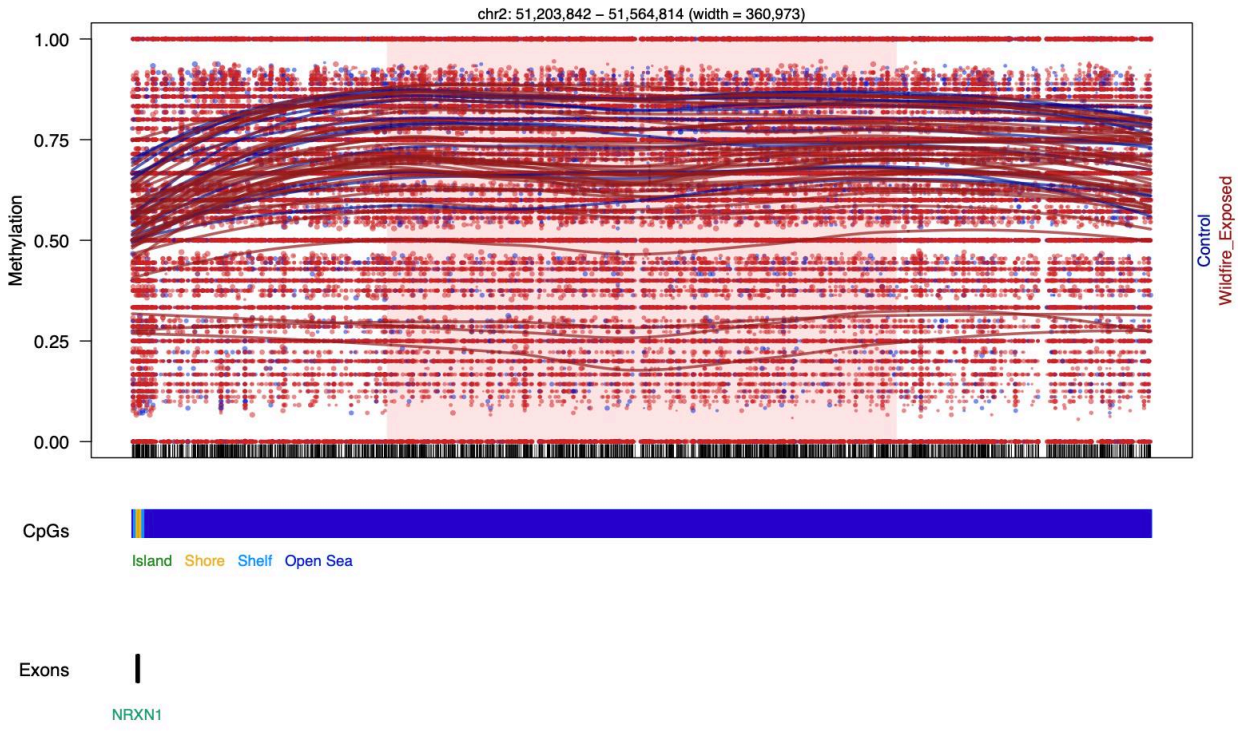


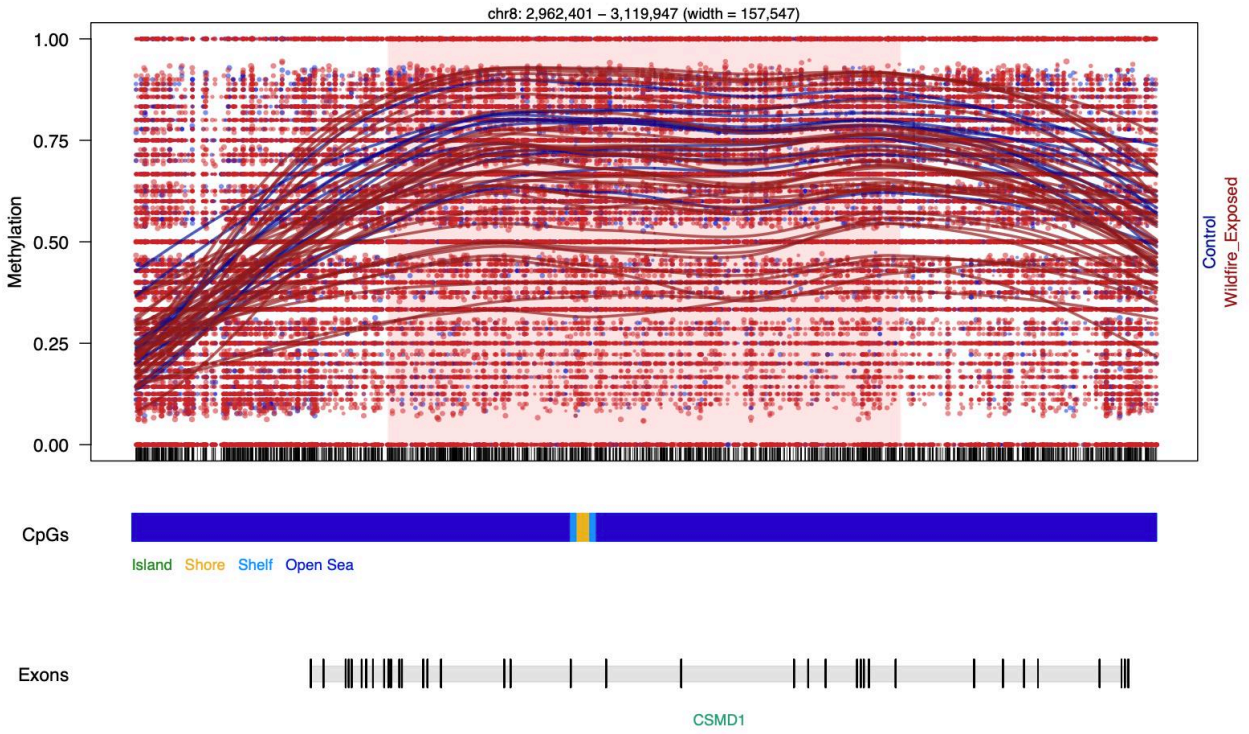
Supplemental Figure 3.20: Global methylation differences between wildfire exposure groups in the Expansion sequencing group as quantified by proportion of methylated CpGs in the **A)** males-only sample set (p = 0.384, Student's t-test), **B)** females only sample set (p = 0.649, Student's t-test), and **C**) all Expansion samples (p = 0.758, Student's t-test). Images made with GraphPad Prism 10.



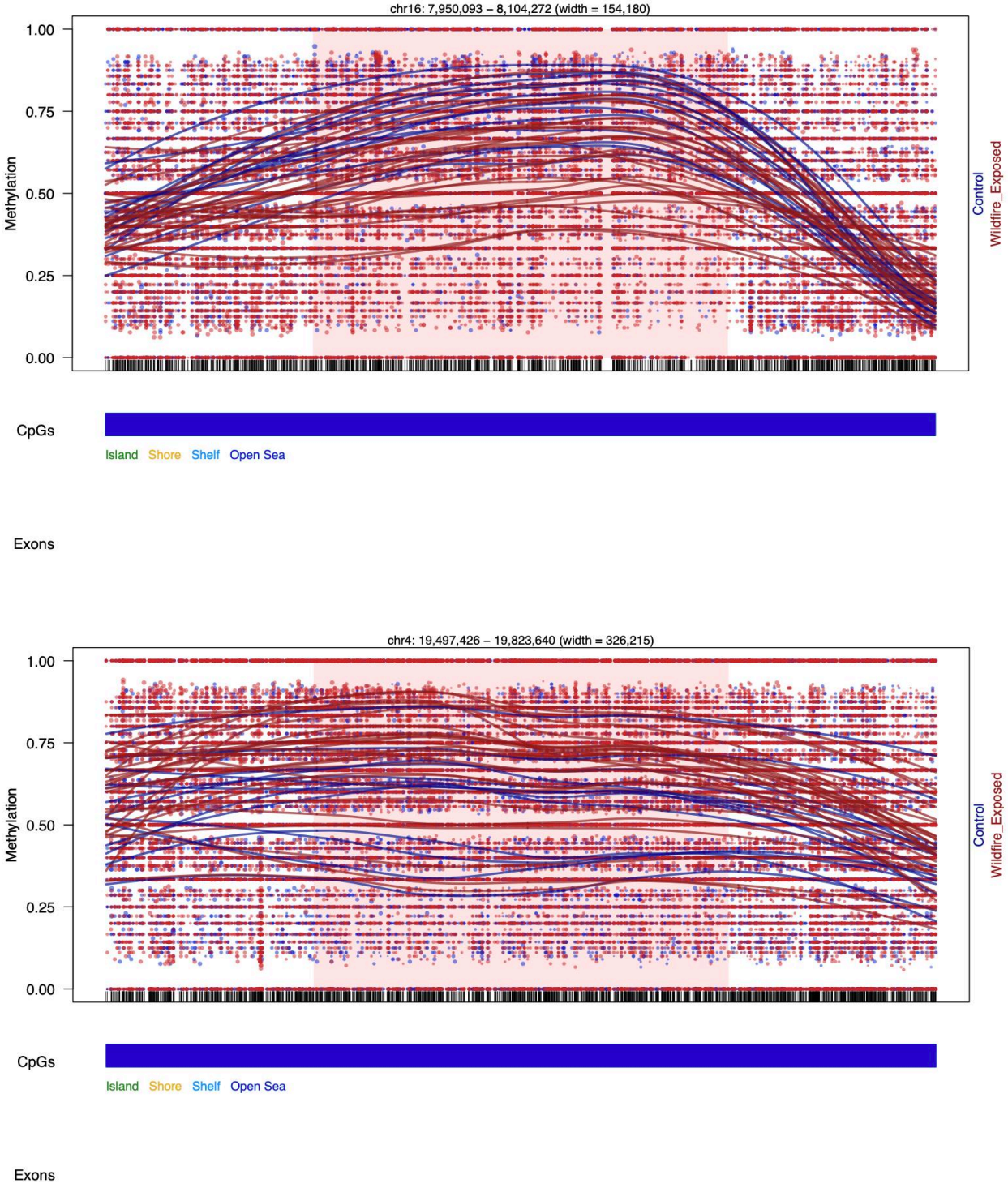
Supplemental Figure 3.21: Comparison of the significant enrichments of the male and female wildfire exposure DMRs regions with respect to annotated CpG topography and genic elements. * denotes significant (adj.p < 0.05) enrichment or depletion as defined by Fisher's Exact Test with FDR (Benjamini and Hochberg) correction. Plots generated by DMRichR.

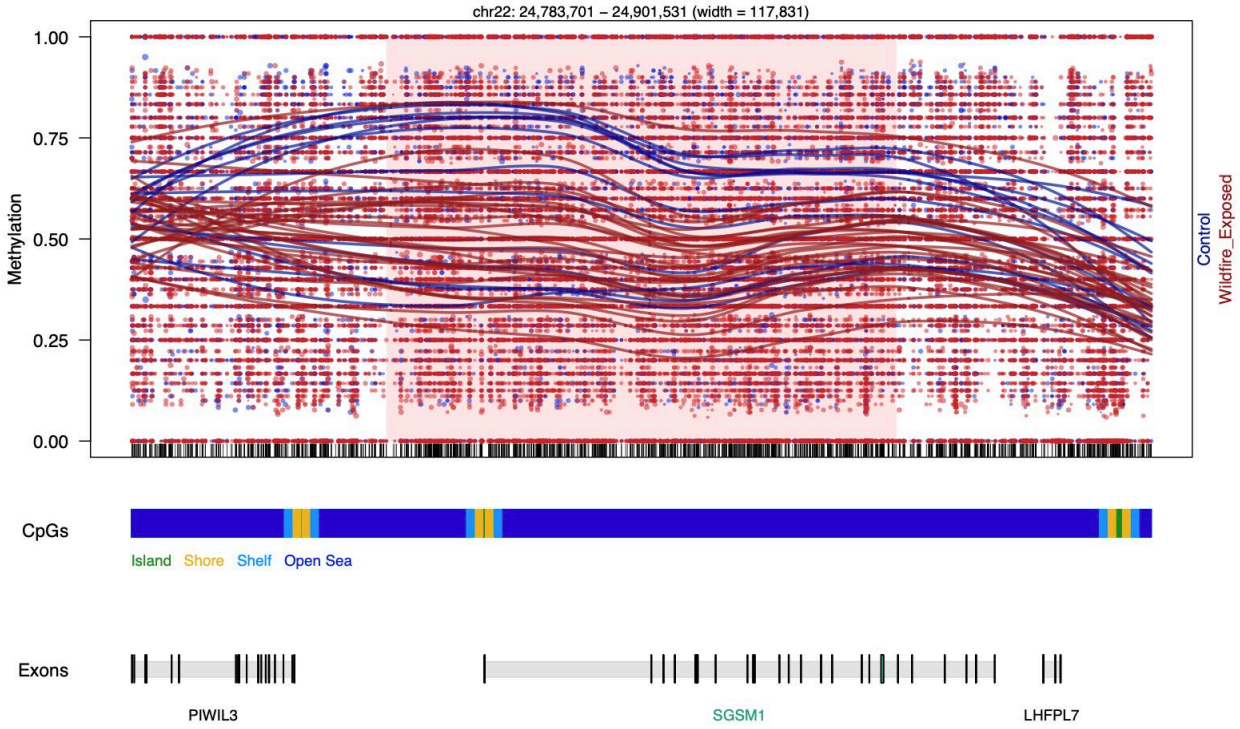

chr5: 9,092,526 – 9,326,994 (width = 234,469)
1.00
0.75
0.50
0.25
0.00
Methylation
Control
Wildfire_Exposed
CpGs
Island
Shore
Shelf
Open Sea
Exons
SEMA5A


chr2: 51,203,842 – 51,564,814 (width = 360,973)
1.00
0.75
0.50
0.25
0.00
Methylation
Control
Wildfire_Exposed
CpGs
Island
Shore
Shelf
Open Sea
Exons
NRXN1

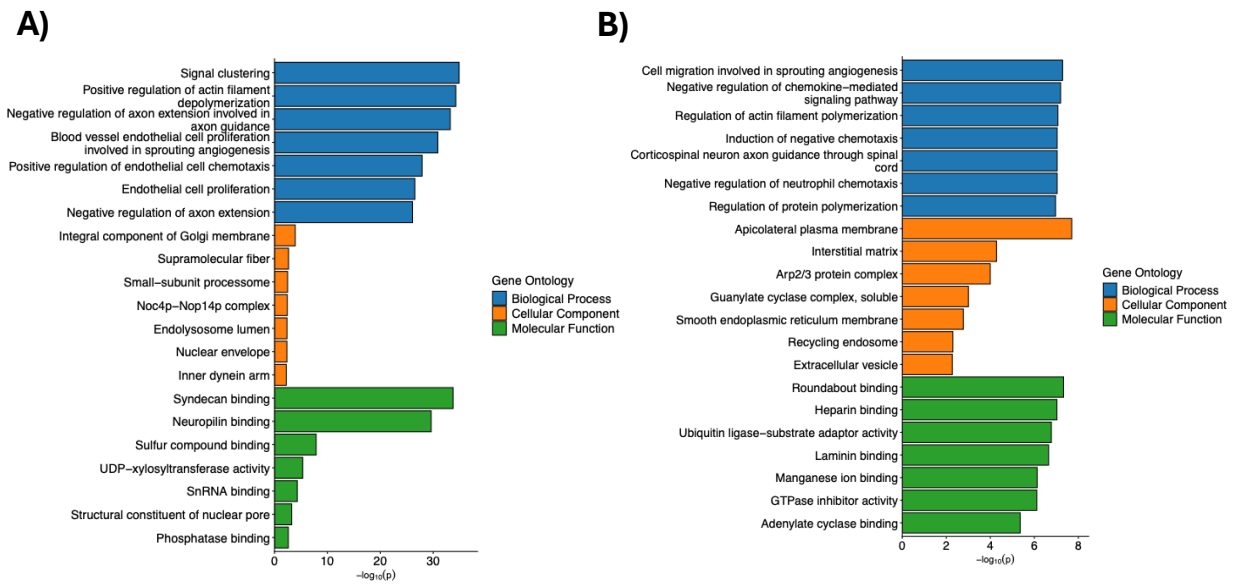


Supplemental Figure 3.22: Plot of the differentially methylated blocks detected by DMRichR in the males-only Expansion sample set. Blue points depict control (non-wildfire exposed) samples, and red dots depict wildfire exposed samples. Smoothed methylation for each sample shown as lines.

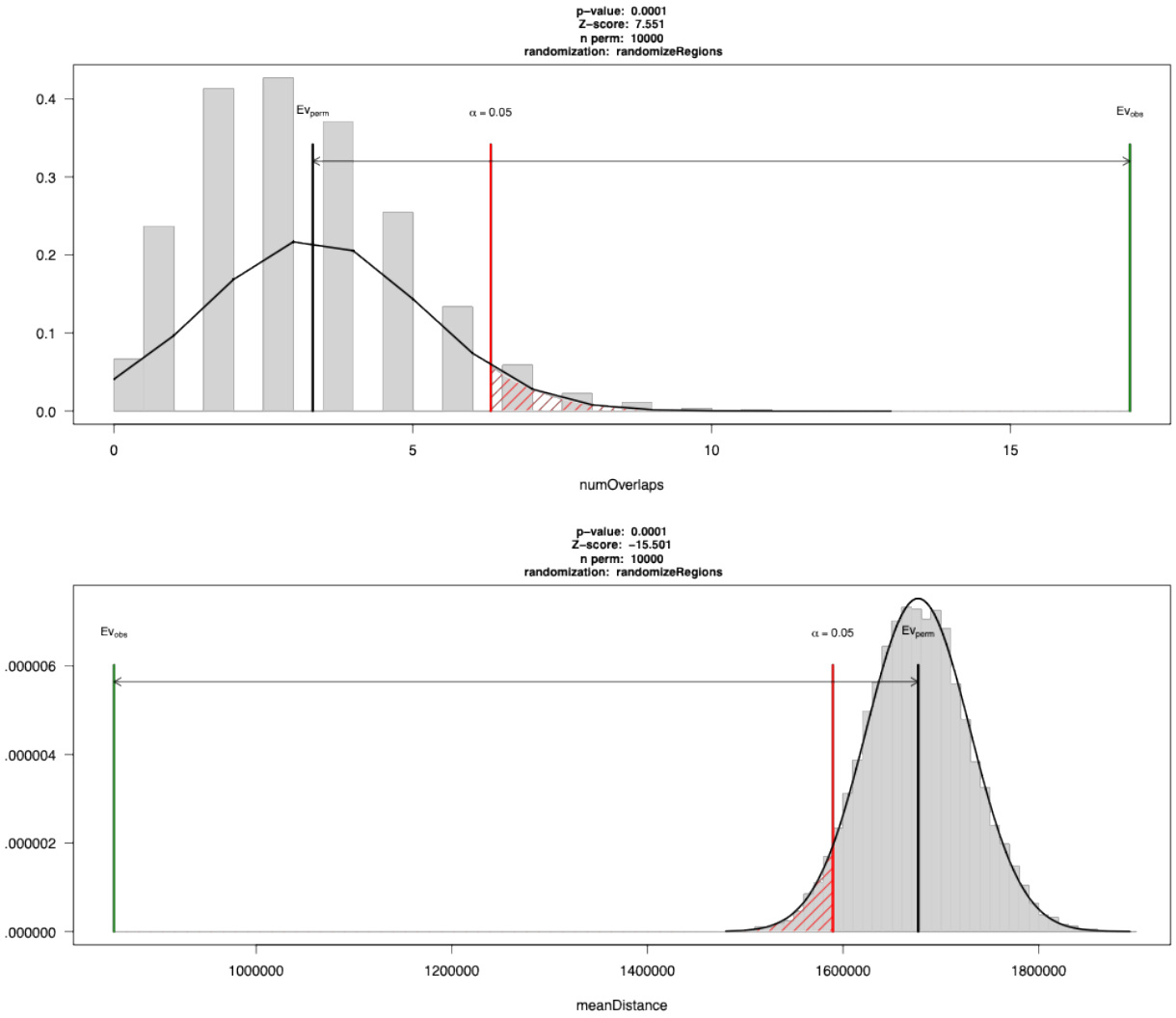

chr16: 7,950,093 – 8,104,272 (width = 154,180)
1.00
0.75
0.50
0.25
0.00
Methylation
Control
Wildfire_Exposed
CpGs
Island
Shore
Shelf
Open Sea
Exons
chr4: 19,497,426 – 19,823,640 (width = 326,215)
1.00
0.75
0.50
0.25
0.00
Methylation
Control
Wildfire_Exposed
CpGs
Island
Shore
Shelf
Open Sea
Exons



Supplemental Figure 3.23: Plot of the differentially methylated blocks detected by DMRichR in the females-only Expansion sample set. Blue points depict control (non-wildfire exposed) samples, and red dots depict wildfire exposed samples. Smoothed methylation for each sample shown as lines.

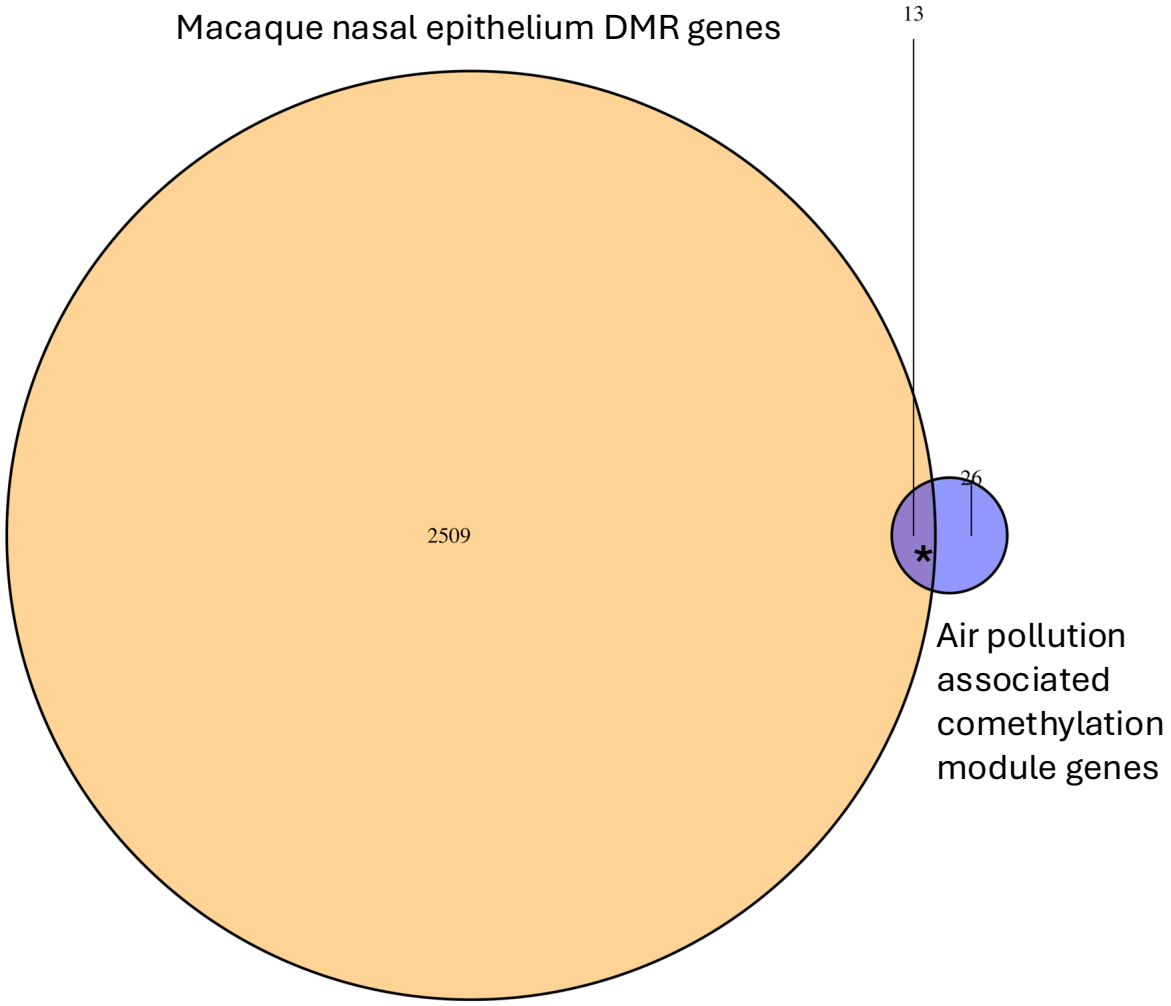


Supplemental Figure 3.24: Top 7 gene ontology enrichments per category for **A)** male and **B)** female DMR gene lists as assessed by rGREAT. Y-axis denotes names of the ontology terms, x-axis shows the –log(permutation p-value) for each enrichment tested. Ontology categories color-coded, as identified in the legend.



Supplemental Figure 3.25: Significance of the intersection of genomic ranges defined by Expansion male wildfire exposure DMRs and Expansion female wildfire exposure DMRs, as defined by number of overlaps between the two sets and mean distance between the DMRs in the two sets. Permutations test preformed with the permTest function in the regioneR R package. Observed number of overlaps and distance compared to a 10,000 permutations of randomized genomic regions of comparable length created with the randomizeRegions function. The observed number of overlaps

in the data set was 17, and the observed mean distance between DMRs was 854,695bp.



Supplemental Figure 3.26: Venn diagram displaying the overlap between genes annotated to human placenta comethylation modules associated with $PM_{2.5}$ air pollution variables and genes annotated to Macaque nasal epithelium differentially methylated regions associated with early life wildfire smoke exposure in California. A significant overlap of 13 genes was observed, with significance determined by Fisher's Exact Test

(p = 3.73E-03), and a background universe of genes annotated to all modules considered in network construction.

3.10.2 Supplemental Tables

While the supplemental tables referenced throughout this chapter are too large to include in print, you can find them in full at the following Box directory: (https://ucdavis.box.com/s/7sw9ipmu7194tfy4e6xg9p0u6fdy5g42). If this directory has become inaccessible since time of writing, the supplemental tables can likely be found attached to an online publication describing these results. As a last resort, contact Dr. Janine LaSalle at jmlasalle@health.ucdavis.edu to inquire about accessing these supplemental tables.

Chapter 4: Conclusion

4.1 Summary of Work

This dissertation presents a characterization of epigenetic markers of ASD associated with prenatal exposure to two well-characterized environmental risk factors: maternal obesity and air pollution. Chapter 2 describes the results of WGBS on cell-free DNA (cfDNA) and subsequently identifies differentially methylated regions (DMRs) associated with both prospective ASD diagnosis and MO. The identified cfDNA ASD DMRs are shown to intersect with ASD DMRs from placenta and cortex, as well as known ASD risk genes. Furthermore, ASD and MO DMRs are shown to overlap with one another, and both display enrichments for genes implicated in synapse development, providing a plausibly convergent molecular pathway of epigenetic dysregulation that may tie MO to increased ASD likelihood. Chapter 3 details placenta comethylation networks that associate with wildfire-informed air pollution metrics and child neurodevelopmental outcomes, including ASD. Preconceptional and pregnancy air pollution exposures present unique associations with placenta comethylation networks, and it has been observed that multiple comethylation modules associated with both air pollution and child developmental outcomes reside in known ASD risk genes. Comethylation modules associated with air pollution and child neurodevelopmental outcomes present sizable enrichments for gene ontologies involved in cell signaling and cell guidance, the disruption of which may be implicated in the association between air pollution and ASD outcomes. In tandem, these two chapters provide new, comprehensive analyses of the epigenetic profiles associated with two well-characterized environmental risk factors of

ASD, illuminating the molecular etiologies that may underlie environmentally-mediated ASD development and providing ample groundwork for further investigation.

4.2 Future Directions

4.2.1 Longitudinal analysis of the cfDNA methylome in relation to ASD

Having successfully piloted methylome analysis of delivery cfDNA from maternal plasma, future studies could focus on preforming longitudinal analysis to identify trimester-specific epigenetic markers associated with ASD development. The development of the fetal central nervous system is dynamic and segmented (303), corresponding to the dynamic changes in fetal brain and placenta methylation observed throughout pregnancy (138,304). Therefore, we hypothesize that cfDNA methylation in ASD pregnancies may also change throughout pregnancy, implicating differential methylation of gene networks critical to the developmental processes occurring time of assessment. To test this hypothesis, we could perform WGBS of cfDNA collected at multiple timepoints (such as each of the three trimesters) from additional individuals in the MARBLES cohort. Subsequent DMRichR analysis within longitudinal groups between ASD and Non-ASD participants would identify ASD-associated DMRs at each timepoint, which could then be compared between timepoints to determine whether a signal was chronologically specific or applicable throughout fetal development. A study of this sort would not only act as a replication test of the 3rd trimester cfDNA DMRs identified near delivery in Chapter 2 but would also provide a rich new dataset of ASD-associated loci across pregnancy duration to interrogate in further studies.

4.2.2 Identifying markers of smoke exposure in adult blood plasma, with a focus on cancer risk assessment

Building off the identified markers of air pollution exposure observed in placenta described in Chapter 3, future investigations into the epigenetic effects of air pollution exposure will involve WGBS of cfDNA from individuals directly exposed to wildfires on a regular basis: firefighters. Pivoting from our previous focus on the developmental impacts of prenatal exposure to air pollutants, this study will instead assess methylomic signatures associated with smoke exposure by preforming WGBS of blood plasma-derived cfDNA from California firefighters sampled before and after a 3-month intensive training regimen where firefighter trainees and instructors are exposed to smoke regularly in live fire trainings. Comethylation network analysis or DMRichR analysis of the resulting data is projected to identify thousands of significant differences in DNA methylation between pre-exposure and post-exposure samples, which can be further screened for their overlap with known cancer-sensitive loci to identify epigenetically responsive markers of cancer risk detectable from a simple blood draw. This study will draw on our existing experience in quantifying differential air pollution exposures and apply them to a more controlled experimental context, with the aim of producing a short-list of wildfire exposure associated regions of differential methylation that may have utility in early cancer risk screening.

4.2.3 Future prospects for epigenetics in Autism Spectrum Disorder

Beyond theorizing on how the results of the two principal studies described in this manuscript may be expanded upon in the future, it is worthwhile to discuss potential future applications of epigenetics in the study of ASD more generally.

The heterogeneity of symptomatic presentation in ASD poses a challenge to both researchers and clinical practitioners. While all ASD cases are broadly diagnosed by the presence of impairments in social behavior, language, and repetitive behavioral patterns, the manifestations and severity of these symptoms can vary substantially between individuals. Furthermore, the potential for common comorbid psychopathologies produces great difficulty in attempting to generalize studies of ASD individuals to the broader population (305,306). In response to this problem, clinicians and scientists have often attempted to stratify ASD individuals into subgroups for the purpose of studying more distinct manifestations of ASD, such as those with or without intellectual disability. The identification of reliable, consistent subtypes of ASD reflective of psychological and biological phenomena has transformative potential, as it would enable more highly targeted studies of specific pathways involved in the manifestation of sub-phenotypes. Such an approach may also highlight subtype-specific treatment outcomes from behavioral intervention therapy with ASD youth (307,308).

Unfortunately, review of an assortment of subtype stratification studies reports that many identified ASD subtypes are insufficiently verified by more than two strategies (309). Furthermore, many employed substratification methods have been found to be over reliant on symptom scores and cognitive measures, with few adequately including sensory processing and biological variables (310).

The incorporation of ASD-associated methylation patterns into substratification criteria, in combination with other data such as transcriptomics or metabolomics, has the potential to enhance the biological considerations of substratification criteria substantially. This is especially true with regards to discerning subtypes of idiopathic ASD, defined as cases of ASD arising from unknown causes (311). In contrast to occurrences of ASD where a specific cause can be identified (known as syndromic ASD), idiopathic ASD describes the ~85% of ASD cases arising from an unknown combination of genetic and environmental factors. Epigenetic analyses are uniquely well-suited to uncover the mechanics of gene-environment interactions, and have been highlighted in reviews of neurodevelopmental conditions like ADHD and anxiety disorders as a likely origin of condition risk that cannot be directly explained by genetic variation (312,313).

While few studies have attempted to incorporate epigenetic data into ASD substratification, preliminary investigations of the epigenetic profiles associated with phenotypic ASD subtypes offer support for an epigenetic component in substratification criteria. Lee and Hu (2020) compared methylation profiles across three phenotypically

distinct subtypes (severe language impairment, intermediate, and mild) of ASD lymphoblastoid cell lines, and observed that a greater number of significant DMRs were detected when comparing control cell lines to a specific phenotype subtype than were detected when comparing control cell lines to all pooled ASD samples (314). Furthermore, functional analysis of subtype-specific DMRs revealed those DMRs to be enriched for subtype-specific biological pathways. For example, severe language impairment ASD DMRs have been shown to be highly enriched for neuritogenesis genes, while the intermediate ASD DMRs are heavily populated with neuroinflammation genes and the mild ASD DMRs included genes involved in sensory system development. Epigenetic investigation of ASD subtyping holds the potential to uncover subtype-specific insights into ASD etiology that will enable researchers and clinicians alike to better understand the molecular dynamics of ASD's various manifestations and etiologies (Figure 4.1). In reducing the heterogeneity of ASD, these approaches may also empower large scale ASD differential methylation analyses of peripheral tissue to uncover subtype-specific DMRs even in the absence of more generalizable ASD DMRs (61,63).

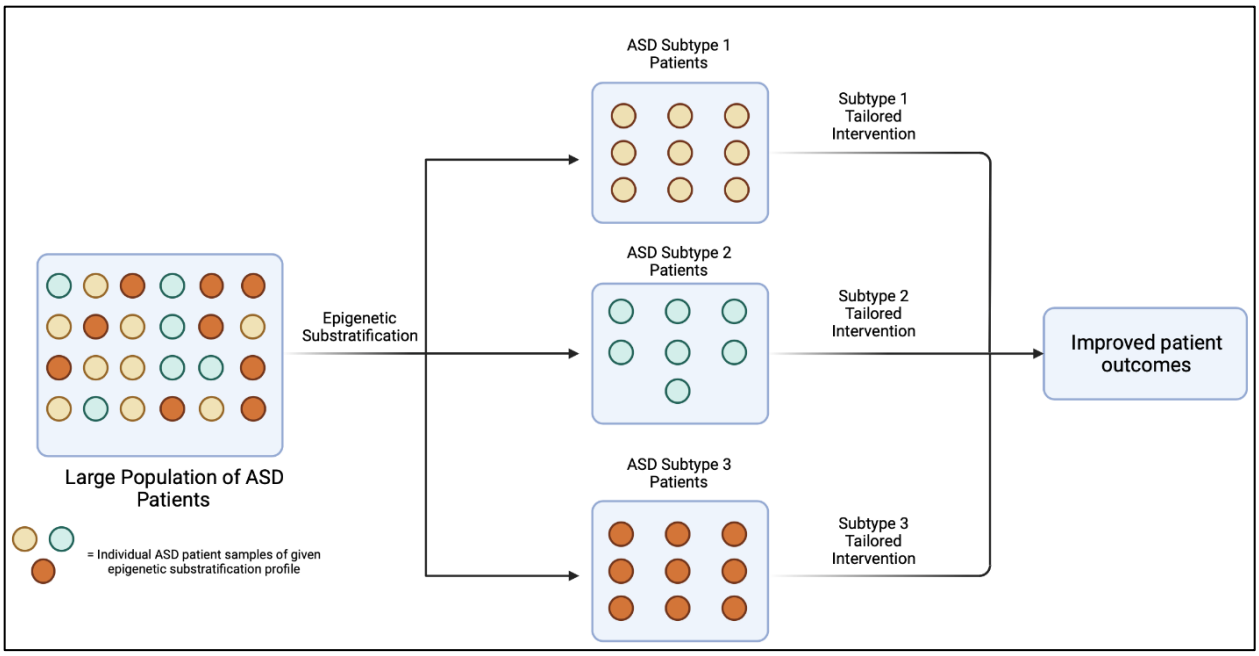


Figure 4.1: A hypothetical example showing how epigenetic substratification of ASD patients could facilitate subtype specific interventions and improve patient outcomes. *ASD* autism spectrum disorder

ASD's heterogeneity of presentation can also contribute to difficulties in diagnosis and treatment, especially for younger children. The average age of clinical diagnosis has been found to be 4-5 years old (315,316), though it is fairly common for youth with ASD with poor access to health care services to remain undiagnosed until early adolescence (317). This is particularly concerning given the body of evidence indicating early behavioral interventions can confer substantial improvements to ASD children's social, vocal, and adaptive skills that translate into increased thriving later in life (318–320). Such interventions have already been proven to reduce symptom severity, and sometimes even diagnosis rates, when administered at ~12 months of age (321,322).

One strategy to lessen the consequences of delayed ASD diagnosis is to identify ASD biomarkers that are predictive of risk for ASD prior to diagnosis. Infants at a higher risk could be offered behavioral intervention, followed up with behaviorally-based ASD diagnoses at 3-5 years of age, a time when diagnosis is more informative (Figure 3). Extensive studies in this field have identified a broad spectrum of ASD biomarkers across various sample types, but have generally failed to identify a consistent set of genetic differences collectively associated with ASD diagnosis (323–325). In light of this “missing heritability problem” (326), epigenetic biomarkers of ASD have been investigated as alternative predictive features for ASD diagnosis. Studies focusing on biomarkers detectable before the typical ASD diagnosis window hold particularly high value for potential ASD intervention, and some early investigations have shown success in this field.

Reports of significant ASD-associated methylation biomarkers detected early in development from accessible peripheral tissues including buccal swabs (327) and placenta (56,59) could be implemented in ASD risk factor calculations, thereby giving clinicians additional levels of evidence when attempting to make an early ASD diagnosis. Furthermore, the development of methods for assessing ASD biomarkers prenatally through the assessment of cell-free fetal DNA (cffDNA) would provide a window of opportunity for in utero interventions. CffDNA is derived from the placenta, representing circulating fetal genetic material deposited in the maternal bloodstream throughout gestation (328,329). This potential value is highlighted in a preprint by Laufer et. al (2021)

describing how longitudinal cffDNA DMRs in a macaque model of maternal obesity was associated with behavioral measures and brain methylation patterns of offspring (330). Additionally, these cffDNA and brain DMRs associated with maternal obesity were found to significantly overlap with DMRs in human ASD brain and placenta, a result that aligns with established knowledge of maternal obesity as an ASD risk factor (27,331). Larger studies searching for prenatal cffDNA epigenetic biomarkers of ASD in humans may likewise identify consistent signals associated with likelihood of ASD development. Working in combination with established postnatal ASD biomarkers, these new tools would empower earlier and more accurate ASD diagnosis, and in turn allow clinicians to begin administering behavioral intervention therapies in the developmental window where they are proven to be most effective (Figure 4.2).

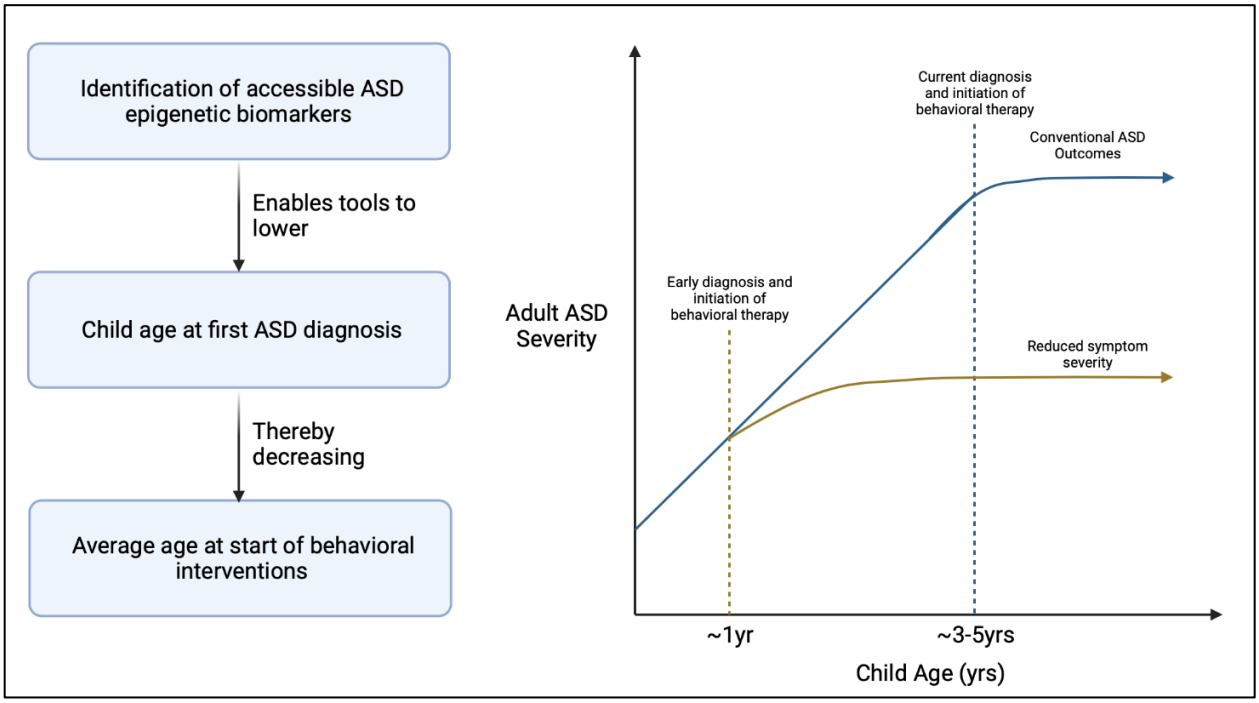


Figure 4.2: Hypothetical example of how epigenetic ASD biomarkers can result in earlier ASD behavioral therapy interventions, and the potential reductions to ASD severity resulting from earlier therapy administration. *ASD* autism spectrum disorder, *yrs* years

While additional investigations of existing associations between epigenetics and ASD will provide actionable results that support clinical practices like substratification and biomarker development, they are fundamentally limited in the extent to which these correlative findings can uncover the direct mechanisms by which epigenetic alterations influence ASD phenotype. By their very nature, association studies of epigenetic alterations and ASD can only report differential epigenetic layers that associate with ASD phenotype. Even more direct interventions, such as knockout of chromatin-modifying enzymes (332,333), are complicated due to the broad range of non-explicitly epigenetic functionality observed in such proteins (334–336). Thus, these studies are capable of identifying loci whose epigenetics *may* play a role in ASD development, but are incapable of identifying true causality (337).

However, the rapid proliferation of epigenetic editing technologies has begun to make casual studies between epigenetic alterations and phenotypes feasible (338–340). Many labs have generated fusion proteins where a given deactivated DNA targeting protein such as dCas9 is ligated to an effector domain capable of making chromatin or DNA methylation modifications. These fusion proteins are then introduced to a given organism, such as a mouse model or human cell line model, and researchers directly observe how

the engineered modifications result in changes to organism phenotype (341). Rather than being merely associative, these investigations using direct epigenetic editing of a locus make possible observations of causality.

Applied to ASD, these methods can prove helpful in narrowing the scope of epigenetic investigations to loci shown to have direct phenotypic impacts in other models. While human epigenetic editing of loci implicated in ASD remains clinically difficult (342) and ethically dubious (343,344), epigenetic mechanism experiments in non-human models of ASD can provide preliminary indications on whether a given locus's chromatin conformation contributes to broader neurodevelopmental phenotypes. Considering the growing list of epigenetically divergent loci associated with ASD, filtering for proven high-impact epigenetic variants will enable researchers to focus their studies on regions whose epigenetic profile is likely to be most impactful in endeavors like substratification and biomarker discovery.

For example, a plethora of preclinical mouse models of rare genetic syndromic forms of ASD have been generated that display novel social, communicative, and behavioral symptoms (345). While investigations of ASD epigenetic mechanism in these models have been undertaken using enzymatic inhibition (346–348), an additional degree of mechanistic certainty of the role a particular epigenetic mark plays in ASD development could be acquired by making precise epigenetic edits to loci of interest and observing downstream effects on both the molecular and phenotypic level. Lu et. al (2020) describe

an early example of dCas9-based epigenetic investigation, with the authors reporting targeted methylation of the *MECP2* transcription start site in mice induced deficits in social behavior (349). These tools could also be employed in developed ASD mouse models to study potential for phenotypic rescue. Furthermore, one could imagine a study applying the CRISPRoff tool designed by Nuñez et. al (2021) to selectively repress loci of interest in the *Myt1l*$^{+/-}$ mouse model of ASD developed by Chen et. al (2021) (339,350). The *Myt1l*$^{+/-}$ mouse model was shown to replicate ASD-related social impairments in males, and also had greater chromatin accessibility in some regions of cortex than WT mice. By using an epigenetic editor like CRISPRoff to target some of these more accessible regions in the *Myt1l*$^{+/-}$ mouse model and observing any changes in ASD-related trait severity, direct hypotheses as to whether the action of the *MYT1L* gene in mouse ASD-like pathways is explicitly epigenetic could be tested. Such conclusions could then inform future human studies.

Unfortunately, the heterogeneous origins of idiopathic ASD make them a more challenging target for direct model generation and subsequent mechanistic investigations. Nonetheless, some attempts to generate non-syndromic rodent ASD models have been mildly successful at reproducing ASD phenotypes (351–353). These non-syndromic models exhibit a wide range of neurodevelopmental impacts caused by environmental exposures and accumulation of numerus mutations implicated in altered neurodevelopment. These multifactorial etiologies mirror the etiologies of many idiopathic cases of ASD in the US. While limited in their direct translation to humans, non-syndromic

ASD rodent models could offer a valuable tool for refinement for epigenetic variants of interest in future studies (Figure 4.3).

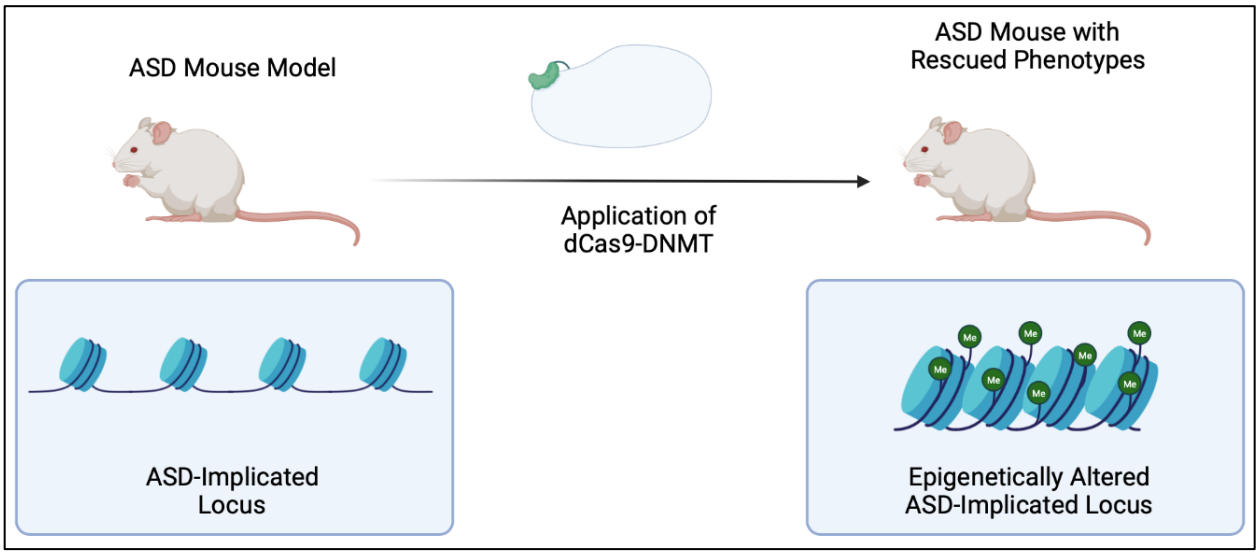


Figure 4.3: Hypothetical experiment investigating epigenetic mechanisms of ASD through phenotype rescue attempt using dCas9 fused to a DNA methyltransferase (DNMT). *ASD* autism spectrum disorder, *dCas9-DNMT* deactivated CRISPR associated protein 9 – deoxyribose nucleic acid methyltransferase, *Me* methyl functional group.

4.3 Conclusion

In conclusion, this dissertation demonstrates the utility of WGBS of prenatal tissues in identifying epigenetic markers at the intersection of environmental exposures and ASD outcomes. In so doing, it raises the epigenetic dysregulation of synaptic development, cell signaling, and cell guidance gene pathways as a possible contributing factor to the etiology of ASD in the context of environmental exposures. While focused on the impacts of MO and air pollution, the principles underlying these studies could be extrapolated to

numerous other known ASD risk factors, acting as the basis for future research that establishes a more comprehensive profile of the genomic loci most impacted by environmental exposures and observed with differential methylation in ASD children. Through the pursuit of collaborative research at the intersection of genetics, bioinformatics, and epidemiology, we can make novel discoveries even in the context of a highly heterogenous neurodevelopmental condition, discoveries that hold the potential to both strengthen our knowledge of basic ASD etiology and lay the groundwork for the application of that knowledge to improve the lives of people with ASD around the world.

References

1. American Psychiatric Association. Diagnostic and Statistical Manual of Mental Disorders [Internet]. Fifth Edition. American Psychiatric Association; 2013 [cited 2022 Mar 23]. Available from: https://psychiatryonline.org/doi/book/10.1176/appi.books.9780890425596 doi:10.1176/appi.books.9780890425596

2. Eugen B. Dementia Praecox oder Gruppe der Schizophrenien. Leipzig, Germany: Deuticke; 1911. (Handbuch der Psychiatrie).

3. American Psychiatric Association, editor. Diagnostic and statistical manual of mental disorders: DSM-IV ; includes ICD-9-CM codes effective 1. Oct. 96. 4. ed., 7. print. Washington, DC; 1998. 886 p.

4. Scandurra V, Emberti Gialloreti L, Barbanera F, Scordo MR, Pierini A, Canitano R. Neurodevelopmental Disorders and Adaptive Functions: A Study of Children With Autism Spectrum Disorders (ASD) and/or Attention Deficit and Hyperactivity Disorder (ADHD). Front Psychiatry. 2019;10:673. doi:10.3389/fpsyt.2019.00673 PubMed PMID: 31551839; PubMed Central PMCID: PMC6737073.

5. Shaw KA, Williams S, Patrick ME, Valencia-Prado M, Durkin MS, Howerton EM, et al. Prevalence and Early Identification of Autism Spectrum Disorder Among Children Aged 4 and 8 Years — Autism and Developmental Disabilities Monitoring Network, 16 Sites, United States, 2022. MMWR Surveill Summ. 2025 Apr 17;74(2):1–22. doi:10.15585/mmwr.ss7402a1

6. Autism and Developmental Disabilities Monitoring Network Surveillance Year 2000 Principal Investigators, Centers for Disease Control and Prevention. Prevalence of autism spectrum disorders--autism and developmental disabilities monitoring network, six sites, United States, 2000. Morb Mortal Wkly Rep Surveill Summ. 2007 Feb 9;56(1):1–11. PubMed PMID: 17287714.

7. Zeidan J, Fombonne E, Scorah J, Ibrahim A, Durkin MS, Saxena S, et al. Global prevalence of autism: A systematic review update. Autism Res. 2022 May;15(5):778–90. doi:10.1002/aur.2696

8. Modabbernia A, Velthorst E, Reichenberg A. Environmental risk factors for autism: an evidence-based review of systematic reviews and meta-analyses. Mol Autism. 2017;8:13. doi:10.1186/s13229-017-0121-4 PubMed PMID: 28331572; PubMed Central PMCID: PMC5356236.

9. Russell G, Stapley S, Newlove-Delgado T, Salmon A, White R, Warren F, et al. Time trends in autism diagnosis over 20 years: a UK population-based cohort study. J Child Psychol Psychiatry. 2022 Jun;63(6):674–82. doi:10.1111/jcpp.13505

10. Forbes G, Kent R, Charman T, Baird G, Pickles A, Simonoff E. How do autistic people fare in adult life and can we predict it from childhood? Autism Res Off J Int Soc Autism Res. 2023 Feb;16(2):458–73. doi:10.1002/aur.2868 PubMed PMID: 36519265; PubMed Central PMCID: PMC10947100.

11. Roux AM, Shattuck PT, Cooper BP, Anderson KA, Wagner M, Narendorf SC. Postsecondary employment experiences among young adults with an autism spectrum disorder. J Am Acad Child Adolesc Psychiatry. 2013 Sep;52(9):931–9. doi:10.1016/j.jaac.2013.05.019 PubMed PMID: 23972695; PubMed Central PMCID: PMC3753691.

12. Magiati I, Tay XW, Howlin P. Cognitive, language, social and behavioural outcomes in adults with autism spectrum disorders: A systematic review of longitudinal follow-up studies in adulthood. Clin Psychol Rev. 2014 Feb;34(1):73–86. doi:10.1016/j.cpr.2013.11.002

13. Eaves LC, Ho HH. Young adult outcome of autism spectrum disorders. J Autism Dev Disord. 2008 Apr;38(4):739–47. doi:10.1007/s10803-007-0441-x PubMed PMID: 17764027.

14. Curnow E, Rutherford M, Maciver D, Johnston L, Prior S, Boilson M, et al. Mental health in autistic adults: A rapid review of prevalence of psychiatric disorders and umbrella review of the effectiveness of interventions within a neurodiversity informed perspective. PloS One. 2023;18(7):e0288275. doi:10.1371/journal.pone.0288275 PubMed PMID: 37440543; PubMed Central PMCID: PMC10343158.

15. Daniolou S, Pandis N, Znoj H. The Efficacy of Early Interventions for Children with Autism Spectrum Disorders: A Systematic Review and Meta-Analysis. J Clin Med. 2022 Aug 30;11(17):5100. doi:10.3390/jcm11175100 PubMed PMID: 36079029; PubMed Central PMCID: PMC9457367.

16. Hus Y, Segal O. Challenges Surrounding the Diagnosis of Autism in Children. Neuropsychiatr Dis Treat. 2021 Dec;Volume 17:3509–29. doi:10.2147/NDT.S282569

17. Genovese A, Butler MG. Clinical Assessment, Genetics, and Treatment Approaches in Autism Spectrum Disorder (ASD). Int J Mol Sci. 2020 Jul 2;21(13):4726. doi:10.3390/ijms21134726

18. Hallmayer J. Genetic Heritability and Shared Environmental Factors Among Twin Pairs With Autism. Arch Gen Psychiatry. 2011 Nov 1;68(11):1095. doi:10.1001/archgenpsychiatry.2011.76

19. Pizzo L, Jensen M, Polyak A, Rosenfeld JA, Mannik K, Krishnan A, et al. Rare variants in the genetic background modulate cognitive and developmental phenotypes in individuals carrying disease-associated variants. Genet Med. 2019 Apr;21(4):816–25. doi:10.1038/s41436-018-0266-3

20. Myers SM, Challman TD, Bernier R, Bourgeron T, Chung WK, Constantino JN, et al. Insufficient Evidence for “Autism-Specific” Genes. Am J Hum Genet. 2020 May;106(5):587–95. doi:10.1016/j.ajhg.2020.04.004

21. Srivastava S, Love-Nichols JA, Dies KA, Ledbetter DH, Martin CL, Chung WK, et al. Meta-analysis and multidisciplinary consensus statement: exome sequencing is a first-tier clinical diagnostic test for individuals with neurodevelopmental disorders. Genet Med. 2019 Nov;21(11):2413–21. doi:10.1038/s41436-019-0554-6

22. Ramaswami G, Geschwind DH. Genetics of autism spectrum disorder. In: Handbook of Clinical Neurology [Internet]. Elsevier; 2018 [cited 2022 Mar 23]. p. 321–9. Available from: saxena doi:10.1016/B978-0-444-63233-3.00021-X

23. Robert C, Pasquier L, Cohen D, Fradin M, Canitano R, Damaj L, et al. Role of Genetics in the Etiology of Autistic Spectrum Disorder: Towards a Hierarchical Diagnostic Strategy. Int J Mol Sci. 2017 Mar 12;18(3):618. doi:10.3390/ijms18030618 PubMed PMID: 28287497; PubMed Central PMCID: PMC5372633.

24. Sandin S, Lichtenstein P, Kuja-Halkola R, Hultman C, Larsson H, Reichenberg A. The Heritability of Autism Spectrum Disorder. JAMA. 2017 Sep 26;318(12):1182. doi:10.1001/jama.2017.12141

25. Gaugler T, Klei L, Sanders SJ, Bodea CA, Goldberg AP, Lee AB, et al. Most genetic risk for autism resides with common variation. Nat Genet. 2014 Aug;46(8):881–5. doi:10.1038/ng.3039 PubMed PMID: 25038753; PubMed Central PMCID: PMC4137411.

26. Saxena R, Babadi M, Namvarhaghighi H, Roullet FI. Role of environmental factors and epigenetics in autism spectrum disorders. In: Progress in Molecular Biology and Translational Science [Internet]. Elsevier; 2020 [cited 2022 Jun 27]. p. 35–60. Available from: https://linkinghub.elsevier.com/retrieve/pii/S1877117320300697 doi:10.1016/bs.pmbts.2020.05.002

27. Sanchez CE, Barry C, Sabhlok A, Russell K, Majors A, Kollins SH, et al. Maternal pre-pregnancy obesity and child neurodevelopmental outcomes: a meta-analysis. Obes Rev Off J Int Assoc Study Obes. 2018 Apr;19(4):464–84. doi:10.1111/obr.12643 PubMed PMID: 29164765; PubMed Central PMCID: PMC6059608.

28. Wan H, Zhang C, Li H, Luan S, Liu C. Association of maternal diabetes with autism spectrum disorders in offspring: A systemic review and meta-analysis. Medicine (Baltimore). 2018 Jan;97(2):e9438. doi:10.1097/MD.0000000000009438

29. Maher GM, O’Keeffe GW, Kearney PM, Kenny LC, Dinan TG, Mattsson M, et al. Association of Hypertensive Disorders of Pregnancy With Risk of Neurodevelopmental Disorders in Offspring: A Systematic Review and Meta-analysis. JAMA Psychiatry. 2018 Aug 1;75(8):809. doi:10.1001/jamapsychiatry.2018.0854

30. Costa LG, Cole TB, Dao K, Chang YC, Garrick JM. Developmental impact of air pollution on brain function. Neurochem Int. 2019 Dec;131:104580. doi:10.1016/j.neuint.2019.104580

31. Bennett DH, Busgang SA, Kannan K, Parsons PJ, Takazawa M, Palmer CD, et al. Environmental exposures to pesticides, phthalates, phenols and trace elements are associated with neurodevelopment in the CHARGE study. Environ Int. 2022 Mar;161:107075. doi:10.1016/j.envint.2021.107075 PubMed PMID: 35085933.

32. Gerges P, Bitar T, Hawat M, Alameddine A, Soufia M, Andres CR, et al. Risk and Protective Factors in Autism Spectrum Disorders: A Case Control Study in the Lebanese Population. Int J Environ Res Public Health. 2020 Aug 31;17(17):6323. doi:10.3390/ijerph17176323

33. Levine SZ, Kodesh A, Viktorin A, Smith L, Uher R, Reichenberg A, et al. Association of Maternal Use of Folic Acid and Multivitamin Supplements in the Periods Before and During Pregnancy With the Risk of Autism Spectrum Disorder in Offspring. JAMA Psychiatry. 2018 Feb 1;75(2):176. doi:10.1001/jamapsychiatry.2017.4050

34. Sharp GC, Salas LA, Monnereau C, Allard C, Yousefi P, Everson TM, et al. Maternal BMI at the start of pregnancy and offspring epigenome-wide DNA methylation: findings from the pregnancy and childhood epigenetics (PACE) consortium. Hum Mol Genet. 2017 Oct 15;26(20):4067–85. doi:10.1093/hmg/ddx290

35. Ornoy A, Reece EA, Pavlinkova G, Kappen C, Miller RK. Effect of maternal diabetes on the embryo, fetus, and children: Congenital anomalies, genetic and epigenetic changes and developmental outcomes: Maternal Diabetes and Pregnancy Outcome. Birth Defects Res Part C Embryo Today Rev. 2015 Mar;105(1):53–72. doi:10.1002/bdrc.21090

36. Wang C, Geng H, Liu W, Zhang G. Prenatal, perinatal, and postnatal factors associated with autism: A meta-analysis. Medicine (Baltimore). 2017 May;96(18):e6696. doi:10.1097/MD.0000000000006696

37. Raghavan R, Riley AW, Volk H, Caruso D, Hironaka L, Sices L, et al. Maternal Multivitamin Intake, Plasma Folate and Vitamin B_{12} Levels and Autism Spectrum Disorder Risk in Offspring. Paediatr Perinat Epidemiol. 2018 Jan;32(1):100–11. doi:10.1111/ppe.12414

38. Lintas C. Linking genetics to epigenetics: The role of folate and folate-related pathways in neurodevelopmental disorders. Clin Genet. 2019 Feb;95(2):241–52. doi:10.1111/cge.13421

39. Bibikova M, Barnes B, Tsan C, Ho V, Klotzle B, Le JM, et al. High density DNA methylation array with single CpG site resolution. Genomics. 2011 Oct;98(4):288–95. doi:10.1016/j.ygeno.2011.07.007

40. Bruchhage MMK, Bucci MP, Becker EBE. Cerebellar involvement in autism and ADHD. In: Handbook of Clinical Neurology [Internet]. Elsevier; 2018 [cited 2022 Apr 18]. p. 61–72. Available from: https://linkinghub.elsevier.com/retrieve/pii/B9780444641892000044 doi:10.1016/B978-0-444-64189-2.00004-4

41. Wong CCY, Smith RG, Hannon E, Ramaswami G, Parikshak NN, Assary E, et al. Genome-wide DNA methylation profiling identifies convergent molecular signatures associated with idiopathic and syndromic autism in post-mortem human brain tissue. Hum Mol Genet. 2019 Jul 1;28(13):2201–11. doi:10.1093/hmg/ddz052

42. Ramaswami G, Won H, Gandal MJ, Haney J, Wang JC, Wong CCY, et al. Integrative genomics identifies a convergent molecular subtype that links epigenomic with transcriptomic differences in autism. Nat Commun. 2020 Dec;11(1):4873. doi:10.1038/s41467-020-18526-1

43. Corley MJ, Vargas-Maya N, Pang APS, Lum-Jones A, Li D, Khadka V, et al. Epigenetic Delay in the Neurodevelopmental Trajectory of DNA Methylation States in Autism Spectrum Disorders. Front Genet. 2019 Oct 1;10:907. doi:10.3389/fgene.2019.00907

44. Fetit R, Hillary RF, Price DJ, Lawrie SM. The neuropathology of autism: A systematic review of post-mortem studies of autism and related disorders. Neurosci Biobehav Rev. 2021 Oct;129:35–62. doi:10.1016/j.neubiorev.2021.07.014

45. Gilbert J, Man HY. Fundamental Elements in Autism: From Neurogenesis and Neurite Growth to Synaptic Plasticity. Front Cell Neurosci. 2017 Nov 20;11:359. doi:10.3389/fncel.2017.00359

46. Meltzer A, Van de Water J. The Role of the Immune System in Autism Spectrum Disorder. Neuropsychopharmacology. 2017 Jan;42(1):284–98. doi:10.1038/npp.2016.158

47. Vogel Ciernia A, Laufer BI, Hwang H, Dunaway KW, Mordaunt CE, Coulson RL, et al. Epigenomic Convergence of Neural-Immune Risk Factors in Neurodevelopmental Disorder Cortex. Cereb Cortex. 2020 Mar 21;30(2):640–55. doi:10.1093/cercor/bhz115

48. Ladd-Acosta C, Hansen KD, Briem E, Fallin MD, Kaufmann WE, Feinberg AP. Common DNA methylation alterations in multiple brain regions in autism. Mol Psychiatry. 2014 Aug;19(8):862–71. doi:10.1038/mp.2013.114

49. Nardone S, Sharan Sams D, Reuveni E, Getselter D, Oron O, Karpuj M, et al. DNA methylation analysis of the autistic brain reveals multiple dysregulated biological pathways. Transl Psychiatry. 2014 Sep;4(9):e433–e433. doi:10.1038/tp.2014.70

50. Nardone S, Sams DS, Zito A, Reuveni E, Elliott E. Dysregulation of Cortical Neuron DNA Methylation Profile in Autism Spectrum Disorder. Cereb Cortex. 2017 Dec 1;27(12):5739–54. doi:10.1093/cercor/bhx250

51. James SJ, Shpyleva S, Melnyk S, Pavliv O, Pogribny IP. Complex epigenetic regulation of Engrailed-2 (EN-2) homeobox gene in the autism cerebellum. Transl Psychiatry. 2013 Feb;3(2):e232–e232. doi:10.1038/tp.2013.8

52. Rustad SR, Papale LA, Alisch RS. DNA Methylation and Hydroxymethylation and Behavior. In. Berlin, Heidelberg: Springer Berlin Heidelberg; 2019 [cited 2022 Apr 21]. (Current Topics in Behavioral Neurosciences). Available from: http://link.springer.com/10.1007/7854_2019_104 doi:10.1007/7854_2019_104

53. Cheng Y, Li Z, Manupipatpong S, Lin L, Li X, Xu T, et al. 5-Hydroxymethylcytosine alterations in the human postmortem brains of autism spectrum disorder. Hum Mol Genet. 2018 Sep 1;27(17):2955–64. doi:10.1093/hmg/ddy193

54. Tylee DS, Kawaguchi DM, Glatt SJ. On the outside, looking in: A review and evaluation of the comparability of blood and brain "-omes." Am J Med Genet B Neuropsychiatr Genet. 2013 Oct;162(7):595–603. doi:10.1002/ajmg.b.32150

55. Lin D, Chen J, Perrone-Bizzozero N, Bustillo JR, Du Y, Calhoun VD, et al. Characterization of cross-tissue genetic-epigenetic effects and their patterns in schizophrenia. Genome Med. 2018 Dec;10(1):13. doi:10.1186/s13073-018-0519-4

56. Zhu Y, Mordaunt CE, Yasui DH, Marathe R, Coulson RL, Dunaway KW, et al. Placental DNA methylation levels at CYP2E1 and IRS2 are associated with child outcome in a prospective autism study. Hum Mol Genet. 2019 Aug 15;28(16):2659–74. doi:10.1093/hmg/ddz084

57. Bahado-Singh RO, Vishweswaraiah S, Aydas B, Radhakrishna U. Placental DNA methylation changes and the early prediction of autism in full-term newborns. Kumar A, editor. PLOS ONE. 2021 Jul 14;16(7):e0253340. doi:10.1371/journal.pone.0253340

58. Bakulski KM, Dou JF, Feinberg JI, Aung MT, Ladd-Acosta C, Volk HE, et al. Autism-Associated DNA Methylation at Birth From Multiple Tissues Is Enriched for Autism Genes in the Early Autism Risk Longitudinal Investigation. Front Mol Neurosci. 2021 Nov 25;14:775390. doi:10.3389/fnmol.2021.775390

59. Zhu Y, Gomez JA, Laufer BI, Mordaunt CE, Mouat JS, Soto DC, et al. Placental methylome reveals a 22q13.33 brain regulatory gene locus associated with autism. Genome Biol. 2022 Dec;23(1):46. doi:10.1186/s13059-022-02613-1

60. James SJ, Cutler P, Melnyk S, Jernigan S, Janak L, Gaylor DW, et al. Metabolic biomarkers of increased oxidative stress and impaired methylation capacity in children with autism. Am J Clin Nutr. 2004 Dec 1;80(6):1611–7. doi:10.1093/ajcn/80.6.1611

61. Andrews SV, Sheppard B, Windham GC, Schieve LA, Schendel DE, Croen LA, et al. Case-control meta-analysis of blood DNA methylation and autism spectrum disorder. Mol Autism. 2018 Dec;9(1):40. doi:10.1186/s13229-018-0224-6

62. Hannon E, Lunnon K, Schalkwyk L, Mill J. Interindividual methylomic variation across blood, cortex, and cerebellum: implications for epigenetic studies of neurological and neuropsychiatric phenotypes. Epigenetics. 2015 Nov 2;10(11):1024–32. doi:10.1080/15592294.2015.1100786

63. Hannon E, Schendel D, Ladd-Acosta C, Grove J, Agerbo E, Als TD, et al. Elevated polygenic burden for autism is associated with differential DNA methylation at birth. Genome Med. 2018 Mar 28;10(1):19. doi:10.1186/s13073-018-0527-4

64. Wong CCY, Meaburn EL, Ronald A, Price TS, Jeffries AR, Schalkwyk LC, et al. Methylomic analysis of monozygotic twins discordant for autism spectrum disorder and related behavioural traits. Mol Psychiatry. 2014 Apr;19(4):495–503. doi:10.1038/mp.2013.41

65. Pidsley R, Zotenko E, Peters TJ, Lawrence MG, Risbridger GP, Molloy P, et al. Critical evaluation of the Illumina MethylationEPIC BeadChip microarray for whole-genome DNA methylation profiling. Genome Biol. 2016 Dec;17(1):208. doi:10.1186/s13059-016-1066-1

66. Mir IN, Leon R, Chalak LF. Placental origins of neonatal diseases: toward a precision medicine approach. Pediatr Res. 2021 Jan;89(2):377–83. doi:10.1038/s41390-020-01293-6

67. Rosenfeld CS. The placenta-brain-axis. J Neurosci Res. 2021 Jan;99(1):271–83. doi:10.1002/jnr.24603

68. Mordaunt CE, Jianu JM, Laufer BI, Zhu Y, Hwang H, Dunaway KW, et al. Cord blood DNA methylome in newborns later diagnosed with autism spectrum disorder reflects early dysregulation of neurodevelopmental and X-linked genes. Genome Med. 2020 Dec;12(1):88. doi:10.1186/s13073-020-00785-8

69. Bakulski KM, Halladay A, Hu VW, Mill J, Fallin MD. Epigenetic Research in Neuropsychiatric Disorders: the “Tissue Issue.” Curr Behav Neurosci Rep. 2016 Sep;3(3):264–74. doi:10.1007/s40473-016-0083-4

70. Zhou L, Ng HK, Drautz-Moses DI, Schuster SC, Beck S, Kim C, et al. Systematic evaluation of library preparation methods and sequencing platforms for high-throughput whole genome bisulfite sequencing. Sci Rep. 2019 Dec;9(1):10383. doi:10.1038/s41598-019-46875-5

71. Gunasekara CJ, Scott CA, Laritsky E, Baker MS, MacKay H, Duryea JD, et al. A genomic atlas of systemic interindividual epigenetic variation in humans. Genome Biol. 2019 Jun 3;20(1):105. doi:10.1186/s13059-019-1708-1

72. Autism and Developmental Disabilities Monitoring Network Surveillance Year 2002 Principal Investigators, Centers for Disease Control and Prevention. Prevalence of autism spectrum disorders--autism and developmental disabilities monitoring network, 14 sites, United States, 2002. Morb Mortal Wkly Rep Surveill Summ Wash DC 2002. 2007 Feb 9;56(1):12–28. PubMed PMID: 17287715.

73. American Psychiatric Association. Diagnostic and Statistical Manual of Mental Disorders [Internet]. Fifth Edition. American Psychiatric Association; 2013 [cited 2025 Feb 18]. Available from: https://psychiatryonline.org/doi/book/10.1176/appi.books.9780890425596 doi:10.1176/appi.books.9780890425596

74. Posar A. Long-term outcome of autism spectrum disorder. Türk Pediatri Arş. 2019. doi:10.14744/TurkPediatriArs.2019.16768

75. Allen G. Attention function and dysfunction in autism. Front Biosci. 2001;6(1):d105. doi:10.2741/allen

76. O'Nions E, Brown J, Buckman JEJ, Charlton R, Cooper C, El Baou C, et al. Diagnosis of common health conditions among autistic adults in the UK: evidence from a matched cohort study. Lancet Reg Health Eur. 2024 Jun;41:100907. doi:10.1016/j.lanepe.2024.100907 PubMed PMID: 39119101; PubMed Central PMCID: PMC11306212.

77. Sammels O, Karjalainen L, Dahlgren J, Wentz E. Autism Spectrum Disorder and Obesity in Children: A Systematic Review and Meta-Analysis. Obes Facts. 2022;15(3):305–20. doi:10.1159/000523943

78. Reilly C, Atkinson P, Das KB, Chin RFMC, Aylett SE, Burch V, et al. Neurobehavioral Comorbidities in Children With Active Epilepsy: A Population-Based Study. Pediatrics. 2014 Jun 1;133(6):e1586–93. doi:10.1542/peds.2013-3787

79. Vasa RA, Mazurek MO. An update on anxiety in youth with autism spectrum disorders. Curr Opin Psychiatry. 2015 Mar;28(2):83–90. doi:10.1097/YCO.0000000000000133 PubMed PMID: 25602249; PubMed Central PMCID: PMC5764108.

80. Lever AG, Geurts HM. Psychiatric Co-occurring Symptoms and Disorders in Young, Middle-Aged, and Older Adults with Autism Spectrum Disorder. J Autism Dev Disord. 2016 Jun;46(6):1916–30. doi:10.1007/s10803-016-2722-8

81. Fuller EA, Kaiser AP. The Effects of Early Intervention on Social Communication Outcomes for Children with Autism Spectrum Disorder: A Meta-analysis. J Autism Dev Disord. 2020 May;50(5):1683–700. doi:10.1007/s10803-019-03927-z PubMed PMID: 30805766; PubMed Central PMCID: PMC7350882.

82. Bent S, Wahlberg J, Chen Y, Widjaja F, McDonald MG, Hendren RL. Quality of Life Among School-Age Children With Autism: The Oak Hill School Outcomes Study.

Semin Pediatr Neurol. 2020 Jul;34:100808. doi:10.1016/j.spen.2020.100808 PubMed PMID: 32446439.

83. Leaf JB, Cihon JH, Ferguson JL. The Relationship of Early Intensive Behavioral Intervention and Adulthood for Autistics/Individuals Diagnosed with Autism Spectrum Disorder. In: Leaf JB, Cihon JH, Ferguson JL, Gerhardt PF, editors. Handbook of Quality of Life for Individuals with Autism Spectrum Disorder [Internet]. Cham: Springer International Publishing; 2022 [cited 2025 Feb 24]. p. 253–65. (Autism and Child Psychopathology Series). Available from: https://link.springer.com/10.1007/978-3-030-98507-3_15 doi:10.1007/978-3-030-98507-3_15

84. Okoye C, Obialo-Ibeawuchi CM, Obajeun OA, Sarwar S, Tawfik C, Waleed MS, et al. Early Diagnosis of Autism Spectrum Disorder: A Review and Analysis of the Risks and Benefits. Cureus. 2023 Aug 9. doi:10.7759/cureus.43226

85. Zablotsky B, Colpe LJ, Pringle BA, Kogan MD, Rice C, Blumberg SJ. Age of Parental Concern, Diagnosis, and Service Initiation Among Children With Autism Spectrum Disorder. Am J Intellect Dev Disabil. 2017 Jan;122(1):49–61. doi:10.1352/1944-7558-122.1.49 PubMed PMID: 28095057; PubMed Central PMCID: PMC5568529.

86. Sauer AK, Stanton JE, Hans S, Grabrucker AM. Autism Spectrum Disorders: Etiology and Pathology. In: Department of Biological Sciences, University of Limerick, Limerick, Ireland, Grabrucker AM, editors. Autism Spectrum Disorders [Internet]. Exon Publications; 2021 [cited 2025 Feb 24]. p. 1–16. Available from: https://exonpublications.com/index.php/exon/article/view/autism-spectrum-disorders-etiology-pathology doi:10.36255/exonpublications.autismspectrumdisorders.2021.etiology

87. Horecka-Lewitowicz A, Lewitowicz W, Wawszczak-Kasza M, Lim H, Lewitowicz P. Autism Spectrum Disorder Pathogenesis-A Cross-Sectional Literature Review Emphasizing Molecular Aspects. Int J Mol Sci. 2024 Oct 20;25(20):11283. doi:10.3390/ijms252011283 PubMed PMID: 39457068; PubMed Central PMCID: PMC11508848.

88. Carroll L, Braeutigam S, Dawes JM, Krsnik Z, Kostovic I, Coutinho E, et al. Autism Spectrum Disorders: Multiple Routes to, and Multiple Consequences of, Abnormal Synaptic Function and Connectivity. Neurosci Rev J Bringing Neurobiol Neurol Psychiatry. 2021 Feb;27(1):10–29. doi:10.1177/1073858420921378 PubMed PMID: 32441222; PubMed Central PMCID: PMC7804368.

89. Betancur C. Etiological heterogeneity in autism spectrum disorders: more than 100 genetic and genomic disorders and still counting. Brain Res. 2011 Mar 22;1380:42–77. doi:10.1016/j.brainres.2010.11.078 PubMed PMID: 21129364.

90. Genovese A, Butler MG. Clinical Assessment, Genetics, and Treatment Approaches in Autism Spectrum Disorder (ASD). Int J Mol Sci. 2020 Jul 2;21(13):4726. doi:10.3390/ijms21134726

91. Ramaswami G, Geschwind DH. Genetics of autism spectrum disorder. In: Handbook of Clinical Neurology [Internet]. Elsevier; 2018 [cited 2025 Feb 18]. p. 321–9. Available from: https://linkinghub.elsevier.com/retrieve/pii/B978044463233300021X doi:10.1016/B978-0-444-63233-3.00021-X

92. Bölte S, Girdler S, Marschik PB. The contribution of environmental exposure to the etiology of autism spectrum disorder. Cell Mol Life Sci CMLS. 2019 Apr;76(7):1275–97. doi:10.1007/s00018-018-2988-4 PubMed PMID: 30570672; PubMed Central PMCID: PMC6420889.

93. Deputy NP, Dub B, Sharma AJ. Prevalence and Trends in Prepregnancy Normal Weight — 48 States, New York City, and District of Columbia, 2011–2015. MMWR Morb Mortal Wkly Rep. 2018 Jan 5;66(5152):1402–7. doi:10.15585/mmwr.mm665152a3

94. Driscoll AK, Gregory ECW. Increases in prepregnancy obesity: United States, 2016–2019. NCHS Data Brief. 2020 Nov 25;(no 392).

95. Duko B, Mengistu TS, Stacey D, Moran LJ, Tessema G, Pereira G, et al. Associations between maternal preconception and pregnancy adiposity and neuropsychiatric and behavioral outcomes in the offspring: A systematic review and meta-analysis. Psychiatry Res. 2024 Dec;342:116149. doi:10.1016/j.psychres.2024.116149

96. Windham GC, Anderson M, Lyall K, Daniels JL, Kral TVE, Croen LA, et al. Maternal Pre-pregnancy Body Mass Index and Gestational Weight Gain in Relation to Autism Spectrum Disorder and other Developmental Disorders in Offspring. Autism Res Off J Int Soc Autism Res. 2019 Feb;12(2):316–27. doi:10.1002/aur.2057 PubMed PMID: 30575327; PubMed Central PMCID: PMC7778460.

97. Getz KD, Anderka MT, Werler MM, Jick SS. Maternal Pre-pregnancy Body Mass Index and Autism Spectrum Disorder among Offspring: A Population-Based Case–Control Study. Paediatr Perinat Epidemiol. 2016 Sep;30(5):479–87. doi:10.1111/ppe.12306

98. Li M, Fallin MD, Riley A, Landa R, Walker SO, Silverstein M, et al. The Association of Maternal Obesity and Diabetes With Autism and Other Developmental Disabilities. Pediatrics. 2016 Feb 1;137(2):e20152206. doi:10.1542/peds.2015-2206

99. Wang Y, Tang S, Xu S, Weng S, Liu Z. Maternal Body Mass Index and Risk of Autism Spectrum Disorders in Offspring: A Meta-analysis. Sci Rep. 2016 Sep 30;6(1):34248. doi:10.1038/srep34248

100. Han VX, Patel S, Jones HF, Nielsen TC, Mohammad SS, Hofer MJ, et al. Maternal acute and chronic inflammation in pregnancy is associated with common neurodevelopmental disorders: a systematic review. Transl Psychiatry. 2021 Jan 21;11(1):71. doi:10.1038/s41398-021-01198-w

101. van der Burg JW, Sen S, Chomitz VR, Seidell JC, Leviton A, Dammann O. The role of systemic inflammation linking maternal BMI to neurodevelopment in children.

Pediatr Res. 2016 Jan;79(1–1):3–12. doi:10.1038/pr.2015.179 PubMed PMID: 26375474; PubMed Central PMCID: PMC4888781.

102. Kim YS, Choi J, Yoon BE. Neuron-Glia Interactions in Neurodevelopmental Disorders. Cells. 2020 Sep 27;9(10):2176. doi:10.3390/cells9102176

103. Radford-Smith DE, Anthony DC. Mechanisms of Maternal Diet-Induced Obesity Affecting the Offspring Brain and Development of Affective Disorders. Metabolites. 2023 Mar 20;13(3):455. doi:10.3390/metabo13030455

104. Nardone S, Elliott E. The Interaction between the Immune System and Epigenetics in the Etiology of Autism Spectrum Disorders. Front Neurosci. 2016 Jul 12;10. doi:10.3389/fnins.2016.00329

105. Vogel Ciernia A, Laufer BI, Hwang H, Dunaway KW, Mordaunt CE, Coulson RL, et al. Epigenomic Convergence of Neural-Immune Risk Factors in Neurodevelopmental Disorder Cortex. Cereb Cortex. 2020 Mar 21;30(2):640–55. doi:10.1093/cercor/bhz115

106. Ravaei A, Emanuele M, Nazzaro G, Fadiga L, Rubini M. Placental DNA methylation profile as predicting marker for autism spectrum disorder (ASD). Mol Med. 2023 Jan 16;29(1):8. doi:10.1186/s10020-022-00593-3

107. Mouat JS, Li X, Neier K, Zhu Y, Mordaunt CE, La Merrill MA, et al. Networks of placental DNA methylation correlate with maternal serum PCB concentrations and child neurodevelopment. Environ Res. 2023 Mar;220:115227. doi:10.1016/j.envres.2023.115227

108. Mordaunt CE, Jianu JM, Laufer BI, Zhu Y, Hwang H, Dunaway KW, et al. Cord blood DNA methylome in newborns later diagnosed with autism spectrum disorder reflects early dysregulation of neurodevelopmental and X-linked genes. Genome Med. 2020 Dec;12(1). doi:10.1186/s13073-020-00785-8

109. Mouat JS, Krigbaum NY, Hakam S, Thrall E, Kuodza GE, Mellis J, et al. Sex-specific DNA methylation signatures of autism spectrum disorder from whole genome bisulfite sequencing of newborn blood. Biol Sex Differ. 2025 Apr 30;16(1). doi:10.1186/s13293-025-00712-9

110. Bakulski KM, Dou JF, Feinberg JI, Aung MT, Ladd-Acosta C, Volk HE, et al. Autism-Associated DNA Methylation at Birth From Multiple Tissues Is Enriched for Autism Genes in the Early Autism Risk Longitudinal Investigation. Front Mol Neurosci. 2021 Nov 25;14. doi:10.3389/fnmol.2021.775390

111. Laufer BI, Hasegawa Y, Zhang Z, Hogrefe CE, Del Rosso LA, Haapanen L, et al. Multi-omic brain and behavioral correlates of cell-free fetal DNA methylation in macaque maternal obesity models. Nat Commun. 2022 Sep 21;13(1):5538. doi:10.1038/s41467-022-33162-7

112. McKee SE, Zhang S, Chen L, Rabinowitz JD, Reyes TM. Perinatal high fat diet and early life methyl donor supplementation alter one carbon metabolism and DNA methylation in the brain. J Neurochem. 2018 Jun;145(5):362–73. doi:10.1111/jnc.14319

113. Urbonaite G, Knyzeliene A, Bunn FS, Smalskys A, Neniskyte U. The impact of maternal high-fat diet on offspring neurodevelopment. Front Neurosci. 2022 Jul 22;16:909762. doi:10.3389/fnins.2022.909762

114. Bonnet-Brilhault F, Rajerison TA, Paillet C, Guimard-Brunault M, Saby A, Ponson L, et al. Autism is a prenatal disorder: Evidence from late gestation brain overgrowth. Autism Res. 2018 Dec;11(12):1635–42. doi:10.1002/aur.2036

115. Courchesne E, Gazestani VH, Lewis NE. Prenatal Origins of ASD: The When, What, and How of ASD Development. Trends Neurosci. 2020 May;43(5):326–42. doi:10.1016/j.tins.2020.03.005

116. Parikshak NN, Luo R, Zhang A, Won H, Lowe JK, Chandran V, et al. Integrative Functional Genomic Analyses Implicate Specific Molecular Pathways and Circuits in Autism. Cell. 2013 Nov;155(5):1008–21. doi:10.1016/j.cell.2013.10.031

117. Willsey AJ, Sanders SJ, Li M, Dong S, Tebbenkamp AT, Muhle RA, et al. Coexpression Networks Implicate Human Midfetal Deep Cortical Projection Neurons in the Pathogenesis of Autism. Cell. 2013 Nov;155(5):997–1007. doi:10.1016/j.cell.2013.10.020

118. Everett TR, Chitty LS. Cell-free fetal DNA: the new tool in fetal medicine. Ultrasound Obstet Gynecol. 2015 May;45(5):499–507. doi:10.1002/uog.14746

119. Lo YMD, Corbetta N, Chamberlain PF, Rai V, Sargent IL, Redman CW, et al. Presence of fetal DNA in maternal plasma and serum. The Lancet. 1997 Aug;350(9076):485–7. doi:10.1016/S0140-6736(97)02174-0

120. Tjoa ML, Cindrova-Davies T, Spasic-Boskovic O, Bianchi DW, Burton GJ. Trophoblastic Oxidative Stress and the Release of Cell-Free Feto-Placental DNA. Am J Pathol. 2006 Aug;169(2):400–4. doi:10.2353/ajpath.2006.060161

121. Chan KCA, Zhang J, Hui ABY, Wong N, Lau TK, Leung TN, et al. Size Distributions of Maternal and Fetal DNA in Maternal Plasma. Clin Chem. 2004 Jan 1;50(1):88–92. doi:10.1373/clinchem.2003.024893

122. Flori E. Circulating cell-free fetal DNA in maternal serum appears to originate from cyto- and syncytio-trophoblastic cells. Case report. Hum Reprod. 2004 Jan 29;19(3):723–4. doi:10.1093/humrep/deh117

123. Alberry M, Maddocks D, Jones M, Abdel Hadi M, Abdel-Fattah S, Avent N, et al. Free fetal DNA in maternal plasma in anembryonic pregnancies: confirmation that the

origin is the trophoblast. Prenat Diagn. 2007 May;27(5):415–8. doi:10.1002/pd.1700 PubMed PMID: 17286310.

124. Masuzaki H. Detection of cell free placental DNA in maternal plasma: direct evidence from three cases of confined placental mosaicism. J Med Genet. 2004 Apr 1;41(4):289–92. doi:10.1136/jmg.2003.015784

125. Chen C, Cram DS, Xie F, Wang P, Xu X, Li H, et al. A pregnancy with discordant fetal and placental chromosome 18 aneuploidies revealed by invasive and noninvasive prenatal diagnosis. Reprod Biomed Online. 2014 Jul;29(1):136–9. doi:10.1016/j.rbmo.2014.03.017

126. Lui YYN, Chik KW, Chiu RWK, Ho CY, Lam CWK, Lo YMD. Predominant hematopoietic origin of cell-free DNA in plasma and serum after sex-mismatched bone marrow transplantation. Clin Chem. 2002 Mar;48(3):421–7. PubMed PMID: 11861434.

127. Haghiac M, Vora NL, Basu S, Johnson KL, Presley L, Bianchi DW, et al. Increased Death of Adipose Cells, a Path to Release Cell-Free DNA Into Systemic Circulation of Obese Women. Obesity. 2012 Nov;20(11):2213–9. doi:10.1038/oby.2012.138

128. Sun K, Jiang P, Chan KCA, Wong J, Cheng YKY, Liang RHS, et al. Plasma DNA tissue mapping by genome-wide methylation sequencing for noninvasive prenatal, cancer, and transplantation assessments. Proc Natl Acad Sci U S A. 2015 Oct 6;112(40):E5503-5512. doi:10.1073/pnas.1508736112 PubMed PMID: 26392541; PubMed Central PMCID: PMC4603482.

129. Lun FMF, Chiu RWK, Sun K, Leung TY, Jiang P, Chan KCA, et al. Noninvasive prenatal methylomic analysis by genomewide bisulfite sequencing of maternal plasma DNA. Clin Chem. 2013 Nov;59(11):1583–94. doi:10.1373/clinchem.2013.212274 PubMed PMID: 23857673.

130. Deger T, Boers RG, De Weerd V, Angus L, Van Der Put MMJ, Boers JB, et al. High-throughput and affordable genome-wide methylation profiling of circulating cell-free DNA by methylated DNA sequencing (MeD-seq) of LpnPI digested fragments. Clin Epigenetics. 2021 Dec;13(1):196. doi:10.1186/s13148-021-01177-4

131. De Borre M, Che H, Yu Q, Lannoo L, De Ridder K, Vancoillie L, et al. Cell-free DNA methylome analysis for early preeclampsia prediction. Nat Med. 2023 Sep;29(9):2206–15. doi:10.1038/s41591-023-02510-5

132. Jensen TJ, Kim SK, Zhu Z, Chin C, Gebhard C, Lu T, et al. Whole genome bisulfite sequencing of cell-free DNA and its cellular contributors uncovers placenta hypomethylated domains. Genome Biol. 2015 Dec;16(1):78. doi:10.1186/s13059-015-0645-x

133. Hertz-Picciotto I, Schmidt RJ, Walker CK, Bennett DH, Oliver M, Shedd-Wise KM, et al. A Prospective Study of Environmental Exposures and Early Biomarkers in Autism

Spectrum Disorder: Design, Protocols, and Preliminary Data from the MARBLES Study. Environ Health Perspect. 2018 Nov;126(11):117004. doi:10.1289/EHP535

134. Mordaunt CE, Jianu JM, Laufer BI, Zhu Y, Hwang H, Dunaway KW, et al. Cord blood DNA methylome in newborns later diagnosed with autism spectrum disorder reflects early dysregulation of neurodevelopmental and X-linked genes. Genome Med. 2020 Dec;12(1):88. doi:10.1186/s13073-020-00785-8

135. Kawano S, Baba M, Fukushima H, Miura D, Hashimoto H, Nakazawa T. Autism-associated ANK2 regulates embryonic neurodevelopment. Biochem Biophys Res Commun. 2022 May;605:45–50. doi:10.1016/j.bbrc.2022.03.058

136. Buddell T, Friedman V, Drozd CJ, Quinn CC. An autism-causing calcium channel variant functions with selective autophagy to alter axon targeting and behavior. Frankel WN, editor. PLOS Genet. 2019 Dec 5;15(12):e1008488. doi:10.1371/journal.pgen.1008488

137. Sabo SL, Lahr JM, Offer M, Weekes AL, Sceniak MP. GRIN2B-related neurodevelopmental disorder: current understanding of pathophysiological mechanisms. Front Synaptic Neurosci. 2023 Jan 10;14:1090865. doi:10.3389/fnsyn.2022.1090865

138. Spiers H, Hannon E, Schalkwyk LC, Smith R, Wong CCY, O'Donovan MC, et al. Methylomic trajectories across human fetal brain development. Genome Res. 2015 Mar;25(3):338–52. doi:10.1101/gr.180273.114

139. Roadmap Epigenomics Consortium, Kundaje A, Meuleman W, Ernst J, Bilenky M, Yen A, et al. Integrative analysis of 111 reference human epigenomes. Nature. 2015 Feb 19;518(7539):317–30. doi:10.1038/nature14248 PubMed PMID: 25693563; PubMed Central PMCID: PMC4530010.

140. Ernst J, Kellis M. Chromatin-state discovery and genome annotation with ChromHMM. Nat Protoc. 2017 Dec;12(12):2478–92. doi:10.1038/nprot.2017.124 PubMed PMID: 29120462; PubMed Central PMCID: PMC5945550.

141. Gao Z, Lee P, Stafford JM, von Schimmelmann M, Schaefer A, Reinberg D. An AUTS2-Polycomb complex activates gene expression in the CNS. Nature. 2014 Dec 18;516(7531):349–54. doi:10.1038/nature13921 PubMed PMID: 25519132; PubMed Central PMCID: PMC4323097.

142. Liu S, Aldinger KA, Cheng CV, Kiyama T, Dave M, McNamara HK, et al. NRF1 association with AUTS2-Polycomb mediates specific gene activation in the brain. Mol Cell. 2021 Nov;81(22):4663-4676.e8. doi:10.1016/j.molcel.2021.09.020

143. Doi M, Usui N, Shimada S. Prenatal Environment and Neurodevelopmental Disorders. Front Endocrinol. 2022;13:860110. doi:10.3389/fendo.2022.860110 PubMed PMID: 35370942; PubMed Central PMCID: PMC8964779.

144. Jeste SS, Geschwind DH. Disentangling the heterogeneity of autism spectrum disorder through genetic findings. Nat Rev Neurol. 2014 Feb;10(2):74–81. doi:10.1038/nrneurol.2013.278 PubMed PMID: 24468882; PubMed Central PMCID: PMC4125617.

145. Ramaswami G, Won H, Gandal MJ, Haney J, Wang JC, Wong CCY, et al. Integrative genomics identifies a convergent molecular subtype that links epigenomic with transcriptomic differences in autism. Nat Commun. 2020 Sep 25;11(1):4873. doi:10.1038/s41467-020-18526-1

146. LaSalle JM. Epigenomic signatures reveal mechanistic clues and predictive markers for autism spectrum disorder. Mol Psychiatry. 2023 May;28(5):1890–901. doi:10.1038/s41380-022-01917-9 PubMed PMID: 36650278; PubMed Central PMCID: PMC10560404.

147. Gandal MJ, Haney JR, Wamsley B, Yap CX, Parhami S, Emani PS, et al. Broad transcriptomic dysregulation occurs across the cerebral cortex in ASD. Nature. 2022 Nov 17;611(7936):532–9. doi:10.1038/s41586-022-05377-7

148. Bale TL. The placenta and neurodevelopment: sex differences in prenatal vulnerability. Dialogues Clin Neurosci. 2016 Dec 31;18(4):459–64. doi:10.31887/DCNS.2016.18.4/tbale

149. Clifton VL. Review: Sex and the Human Placenta: Mediating Differential Strategies of Fetal Growth and Survival. Placenta. 2010 Mar;31:S33–9. doi:10.1016/j.placenta.2009.11.010

150. de Paula RM, Lamb TM, Bennett L, Bell-Pedersen D. A connection between MAPK pathways and circadian clocks. Cell Cycle Georget Tex. 2008 Sep 1;7(17):2630–4. doi:10.4161/cc.7.17.6516 PubMed PMID: 18728391; PubMed Central PMCID: PMC2577295.

151. Van Drunen R, Eckel-Mahan K. Circadian rhythms as modulators of brain health during development and throughout aging. Front Neural Circuits. 2022;16:1059229. doi:10.3389/fncir.2022.1059229 PubMed PMID: 36741032; PubMed Central PMCID: PMC9893507.

152. Duffy JF, Cain SW, Chang AM, Phillips AJK, Münch MY, Gronfier C, et al. Sex difference in the near-24-hour intrinsic period of the human circadian timing system. Proc Natl Acad Sci U S A. 2011 Sep 13;108 Suppl 3(Suppl 3):15602–8. doi:10.1073/pnas.1010666108 PubMed PMID: 21536890; PubMed Central PMCID: PMC3176605.

153. Sheppard PAS, Puri TA, Galea LAM. Sex Differences and Estradiol Effects in MAPK and Akt Cell Signaling across Subregions of the Hippocampus. Neuroendocrinology. 2022;112(7):621–35. doi:10.1159/000519072 PubMed PMID: 34407537.

154. Buonocore F, Suntharalingham JP, Ogunbiyi OK, Jones A, Moreno N, Niola P, et al. Transcriptomic sex differences in early human fetal brain development. Commun Biol. 2025 Apr 25;8(1):664. doi:10.1038/s42003-025-08070-3

155. Wheelock MD, Hect JL, Hernandez-Andrade E, Hassan SS, Romero R, Eggebrecht AT, et al. Sex differences in functional connectivity during fetal brain development. Dev Cogn Neurosci. 2019 Apr;36:100632. doi:10.1016/j.dcn.2019.100632

156. Toledo VHCD, Feltrin AS, Barbosa AR, Tahira AC, Brentani H. Sex differences in gene regulatory networks during mid-gestational brain development. Front Hum Neurosci. 2022 Aug 17;16:955607. doi:10.3389/fnhum.2022.955607

157. Xiang AH, Wang X, Martinez MP, Walthall JC, Curry ES, Page K, et al. Association of Maternal Diabetes With Autism in Offspring. JAMA. 2015 Apr 14;313(14):1425. doi:10.1001/jama.2015.2707

158. Wang C, Geng H, Liu W, Zhang G. Prenatal, perinatal, and postnatal factors associated with autism: A meta-analysis. Medicine (Baltimore). 2017 May;96(18):e6696. doi:10.1097/MD.0000000000006696

159. Xu RT, Chang QX, Wang QQ, Zhang J, Xia LX, Zhong N, et al. Association between hypertensive disorders of pregnancy and risk of autism in offspring: a systematic review and meta-analysis of observational studies. Oncotarget. 2018 Jan 2;9(1):1291–301. doi:10.18632/oncotarget.23030

160. Kodesh A, Levine SZ, Khachadourian V, Rahman R, Schlessinger A, O'Reilly PF, et al. Maternal health around pregnancy and autism risk: a diagnosis-wide, population-based study. Psychol Med. 2022 Dec;52(16):4076–84. doi:10.1017/S0033291721001021

161. Fernandez-Jimenez N, Fore R, Cilleros-Portet A, Lepeule J, Perron P, Kvist T, et al. A meta-analysis of pre-pregnancy maternal body mass index and placental DNA methylation identifies 27 CpG sites with implications for mother-child health. Commun Biol. 2022 Nov 30;5(1):1313. doi:10.1038/s42003-022-04267-y PubMed PMID: 36446949; PubMed Central PMCID: PMC9709064.

162. Nogues P, Dos Santos E, Jammes H, Berveiller P, Arnould L, Vialard F, et al. Maternal obesity influences expression and DNA methylation of the adiponectin and leptin systems in human third-trimester placenta. Clin Epigenetics. 2019 Dec;11(1). doi:10.1186/s13148-019-0612-6

163. Rivell A, Mattson MP. Intergenerational Metabolic Syndrome and Neuronal Network Hyperexcitability in Autism. Trends Neurosci. 2019 Oct;42(10):709–26. doi:10.1016/j.tins.2019.08.006 PubMed PMID: 31495451; PubMed Central PMCID: PMC6779523.

164. Urbonaite G, Knyzeliene A, Bunn FS, Smalskys A, Neniskyte U. The impact of maternal high-fat diet on offspring neurodevelopment. Front Neurosci. 2022 Jul 22;16. doi:10.3389/fnins.2022.909762

165. Maldonado-Ruiz R, Garza-Ocañas L, Camacho A. Inflammatory domains modulate autism spectrum disorder susceptibility during maternal nutritional programming. Neurochem Int. 2019 Jun;126:109–17. doi:10.1016/j.neuint.2019.03.009

166. Liu J, Dai L, Wang Q, Li C, Liu Z, Gong T, et al. Multimodal analysis of cfDNA methylomes for early detecting esophageal squamous cell carcinoma and precancerous lesions. Nat Commun. 2024 May 2;15(1):3700. doi:10.1038/s41467-024-47886-1

167. McNamara ME, Jain SS, Oza K, Muralidaran V, Kiliti AJ, Patrick McDeed A, et al. Circulating cell-free DNA methylation patterns indicate cellular sources of allograft injury after liver transplant. Nat Commun. 2025 Jun 17;16(1):5310. doi:10.1038/s41467-025-60507-9

168. Li SJ, Gao X, Wang ZH, Li J, Zeng LT, Dang YM, et al. Cell-free DNA methylation patterns in aging and their association with inflamm-aging. Epigenomics. 2024;16(10):715–31. doi:10.1080/17501911.2024.2340958 PubMed PMID: 38869474; PubMed Central PMCID: PMC11318736.

169. Lyall K, Schmidt RJ, Hertz-Picciotto I. Maternal lifestyle and environmental risk factors for autism spectrum disorders. Int J Epidemiol. 2014 Apr;43(2):443–64. doi:10.1093/ije/dyt282

170. Martin E, Smeester L, Bommarito PA, Grace MR, Boggess K, Kuban K, et al. Sexual epigenetic dimorphism in the human placenta: implications for susceptibility during the prenatal period. Epigenomics. 2017 Mar;9(3):267–78. doi:10.2217/epi-2016-0132 PubMed PMID: 28234023; PubMed Central PMCID: PMC5331919.

171. Tekola-Ayele F, Biedrzycki RJ, Habtewold TD, Wijesiriwardhana P, Burt A, Marsit CJ, et al. Sex-differentiated placental methylation and gene expression regulation has implications for neonatal traits and adult diseases. Nat Commun. 2025 May 1;16(1):4004. doi:10.1038/s41467-025-58128-3

172. Mouat JS, Krigbaum NY, Hakam S, Thrall E, Kuodza GE, Mellis J, et al. Sex-specific DNA methylation signatures of autism spectrum disorder from whole genome bisulfite sequencing of newborn blood. Biol Sex Differ. 2025 Apr 30;16(1):30. doi:10.1186/s13293-025-00712-9

173. Ozonoff S, Young GS, Belding A, Hill M, Hill A, Hutman T, et al. The broader autism phenotype in infancy: when does it emerge? J Am Acad Child Adolesc Psychiatry. 2014 Apr;53(4):398-407.e2. doi:10.1016/j.jaac.2013.12.020 PubMed PMID: 24655649; PubMed Central PMCID: PMC3989934.

174. Chiu RWK, Lo YMD. Cell-free fetal DNA coming in all sizes and shapes. Prenat Diagn. 2021 Sep;41(10):1193–201. doi:10.1002/pd.5952 PubMed PMID: 33882153; PubMed Central PMCID: PMC8518878.

175. Haghani V. Epigenerator: A Practical Workflow for Whole Genome Bisulfite Sequencing (WGBS) Analysis [Shell] [Internet]. 2025 [cited 2025 Mar 5]. Available from: https://github.com/vhaghani26/epigenerator

176. Laufer B. FASTQ_Me [Shell] [Internet]. 2020 [cited 2025 Mar 5]. Available from: https://github.com/ben-laufer/FASTQ_Me

177. Laufer B. CpG_Me: A Whole Genome Bisulfite Sequencing (WGBS) Alignment Pipeline [Shell] [Internet]. 2025 [cited 2025 Mar 5]. Available from: https://github.com/ben-laufer/CpG_Me

178. Andrews S. FastQC: A Quality Control tool for High Throughput Sequence Data [Internet]. 2010 [cited 2025 Mar 5]. Available from: https://www.bioinformatics.babraham.ac.uk/projects/fastqc/

179. Ewels P, Magnusson M, Lundin S, Käller M. MultiQC: summarize analysis results for multiple tools and samples in a single report. Bioinformatics. 2016 Oct 1;32(19):3047–8. doi:10.1093/bioinformatics/btw354

180. Hwang H. SexChecker [Python] [Internet]. Available from: https://github.com/hyeyeon-hwang/SexChecker

181. Kim SK, Hannum G, Geis J, Tynan J, Hogg G, Zhao C, et al. Determination of fetal DNA fraction from the plasma of pregnant women using sequence read counts. Prenat Diagn. 2015 Aug;35(8):810–5. doi:10.1002/pd.4615 PubMed PMID: 25967380.

182. Laufer BI, Hwang H, Jianu JM, Mordaunt CE, Korf IF, Hertz-Picciotto I, et al. Low-pass whole genome bisulfite sequencing of neonatal dried blood spots identifies a role for RUNX1 in Down syndrome DNA methylation profiles. Hum Mol Genet. 2021 Jan 6;29(21):3465–76. doi:10.1093/hmg/ddaa218 PubMed PMID: 33001180; PubMed Central PMCID: PMC7788293.

183. Mouat JS, Krigbaum NY, Hakam S, Thrall E, Kuodza GE, Mellis J, et al. Sex-specific DNA methylation signatures of autism spectrum disorder in newborn blood. BioRxiv Prepr Serv Biol. 2024 Dec 2;2024.07.11.603098. doi:10.1101/2024.07.11.603098 PubMed PMID: 39026708; PubMed Central PMCID: PMC11257592.

184. McLean CY, Bristor D, Hiller M, Clarke SL, Schaar BT, Lowe CB, et al. GREAT improves functional interpretation of cis-regulatory regions. Nat Biotechnol. 2010 May;28(5):495–501. doi:10.1038/nbt.1630

185. Lee Y, Choufani S, Weksberg R, Wilson SL, Yuan V, Burt A, et al. Placental epigenetic clocks: estimating gestational age using placental DNA methylation

levels. Aging. 2019 Jun 24;11(12):4238–53. doi:10.18632/aging.102049 PubMed PMID: 31235674; PubMed Central PMCID: PMC6628997.

186. Shireby GL, Davies JP, Francis PT, Burrage J, Walker EM, Neilson GWA, et al. Recalibrating the epigenetic clock: implications for assessing biological age in the human cortex. Brain J Neurol. 2020 Dec 1;143(12):3763–75. doi:10.1093/brain/awaa334 PubMed PMID: 33300551; PubMed Central PMCID: PMC7805794.

187. Sheffield NC, Bock C. LOLA: enrichment analysis for genomic region sets and regulatory elements in R and Bioconductor. Bioinformatics. 2016 Feb 15;32(4):587–9. doi:10.1093/bioinformatics/btv612

188. Jolly WM, Cochrane MA, Freeborn PH, Holden ZA, Brown TJ, Williamson GJ, et al. Climate-induced variations in global wildfire danger from 1979 to 2013. Nat Commun. 2015 Jul 14;6(1):7537. doi:10.1038/ncomms8537

189. Parks SA, Coop JD, Davis KT. Intensifying Fire Season Aridity Portends Ongoing Expansion of Severe Wildfire in Western US Forests. Glob Change Biol. 2025 Aug;31(8):e70429. doi:10.1111/gcb.70429 PubMed PMID: 40831215; PubMed Central PMCID: PMC12365577.

190. Westerling AL, Hidalgo HG, Cayan DR, Swetnam TW. Warming and Earlier Spring Increase Western U.S. Forest Wildfire Activity. Science. 2006 Aug 18;313(5789):940–3. doi:10.1126/science.1128834

191. Diffenbaugh NS, Swain DL, Touma D. Anthropogenic warming has increased drought risk in California. Proc Natl Acad Sci. 2015 Mar 31;112(13):3931–6. doi:10.1073/pnas.1422385112

192. Gould CF, Heft-Neal S, Johnson M, Aguilera J, Burke M, Nadeau K. Health Effects of Wildfire Smoke Exposure. Annu Rev Med. 2024 Jan 29;75(1):277–92. doi:10.1146/annurev-med-052422-020909

193. Reid CE, Brauer M, Johnston FH, Jerrett M, Balmes JR, Elliott CT. Critical Review of Health Impacts of Wildfire Smoke Exposure. Environ Health Perspect. 2016 Sep;124(9):1334–43. doi:10.1289/ehp.1409277 PubMed PMID: 27082891; PubMed Central PMCID: PMC5010409.

194. Aguilera R, Corringham T, Gershunov A, Benmarhnia T. Wildfire smoke impacts respiratory health more than fine particles from other sources: observational evidence from Southern California. Nat Commun. 2021 Mar 5;12(1):1493. doi:10.1038/s41467-021-21708-0

195. Jones CG, Rappold AG, Vargo J, Cascio WE, Kharrazi M, McNally B, et al. Out-of-Hospital Cardiac Arrests and Wildfire-Related Particulate Matter During 2015–2017 California Wildfires. J Am Heart Assoc. 2020 Apr 21;9(8):e014125. doi:10.1161/JAHA.119.014125

196. Chen H, Samet JM, Bromberg PA, Tong H. Cardiovascular health impacts of wildfire smoke exposure. Part Fibre Toxicol. 2021 Jan 7;18(1):2. doi:10.1186/s12989-020-00394-8

197. Magzamen S, Gan RW, Liu J, O'Dell K, Ford B, Berg K, et al. Differential Cardiopulmonary Health Impacts of Local and Long-Range Transport of Wildfire Smoke. GeoHealth. 2021 Mar;5(3):e2020GH000330. doi:10.1029/2020GH000330

198. Navarro KM, Kleinman MT, Mackay CE, Reinhardt TE, Balmes JR, Broyles GA, et al. Wildland firefighter smoke exposure and risk of lung cancer and cardiovascular disease mortality. Environ Res. 2019 Jun;173:462–8. doi:10.1016/j.envres.2019.03.060

199. Gao Y, Huang W, Xu Z, Xu R, Gasevic D, Liu Y, et al. Wildfire-related PM2.5 and cause-specific cancer mortality. Ecotoxicol Environ Saf. 2024 Oct;285:117023. doi:10.1016/j.ecoenv.2024.117023

200. Cleland SE, Wyatt LH, Wei L, Paul N, Serre ML, West JJ, et al. Short-Term Exposure to Wildfire Smoke and PM2.5 and Cognitive Performance in a Brain-Training Game: A Longitudinal Study of U.S. Adults. Environ Health Perspect. 2022 Jun;130(6):067005. doi:10.1289/EHP10498

201. Elser HC, Frankland TB, Tartof SY, Mayeda ER, Manly JJ, Torres JM, et al. Long-Term Wildfire Smoke Exposure and Incident Dementia in a Large California Cohort. Alzheimers Dement. 2024 Dec;20(S7):e086179. doi:10.1002/alz.086179

202. Liu J, Chen Y, Liu D, Ye F, Sun Q, Huang Q, et al. Prenatal exposure to particulate matter and term low birth weight: systematic review and meta-analysis. Environ Sci Pollut Res Int. 2023 May;30(23):63335–46. doi:10.1007/s11356-023-26831-7 PubMed PMID: 37059952; PubMed Central PMCID: PMC10172254.

203. Parasin N, Amnuaylojaroen T, Saokaew S. Prenatal PM2.5 Exposure and Its Association with Low Birth Weight: A Systematic Review and Meta-Analysis. Toxics. 2024 Jun 21;12(7):446. doi:10.3390/toxics12070446 PubMed PMID: 39058098; PubMed Central PMCID: PMC11280910.

204. Bekkar B, Pacheco S, Basu R, DeNicola N. Association of Air Pollution and Heat Exposure With Preterm Birth, Low Birth Weight, and Stillbirth in the US: A Systematic Review. JAMA Netw Open. 2020 Jun 1;3(6):e208243. doi:10.1001/jamanetworkopen.2020.8243 PubMed PMID: 32556259; PubMed Central PMCID: PMC7303808.

205. Jiao A, Reilly AN, Benmarhnia T, Sun Y, Avila C, Chiu V, et al. Fine Particulate Matter, Its Constituents, and Spontaneous Preterm Birth. JAMA Netw Open. 2024 Nov 13;7(11):e2444593. doi:10.1001/jamanetworkopen.2024.44593

206. Picciotto S, Huang S, Lurmann F, Pavlovic N, Ying Chang S, Mukherjee A, et al. Pregnancy exposure to PM2.5 from wildland fire smoke and preterm birth in California. Environ Int. 2024 Apr;186:108583. doi:10.1016/j.envint.2024.108583

207. Morgan ZEM, Bailey MJ, Trifonova DI, Naik NC, Patterson WB, Lurmann FW, et al. Prenatal exposure to ambient air pollution is associated with neurodevelopmental outcomes at 2 years of age. Environ Health. 2023 Jan 24;22(1):11. doi:10.1186/s12940-022-00951-y

208. Perera F, Miao Y, Ross Z, Rauh V, Margolis A, Hoepner L, et al. Prenatal exposure to air pollution during the early and middle stages of pregnancy is associated with adverse neurodevelopmental outcomes at ages 1 to 3 years. Environ Health Glob Access Sci Source. 2024 Oct 30;23(1):95. doi:10.1186/s12940-024-01132-9 PubMed PMID: 39478594; PubMed Central PMCID: PMC11526525.

209. Loftus CT, Ni Y, Szpiro AA, Hazlehurst MF, Tylavsky FA, Bush NR, et al. Exposure to ambient air pollution and early childhood behavior: A longitudinal cohort study. Environ Res. 2020 Apr;183:109075. doi:10.1016/j.envres.2019.109075 PubMed PMID: 31999995; PubMed Central PMCID: PMC8903039.

210. McGuinn LA, Bellinger DC, Colicino E, Coull BA, Just AC, Kloog I, et al. Prenatal PM2.5 exposure and behavioral development in children from Mexico City. Neurotoxicology. 2020 Dec;81:109–15. doi:10.1016/j.neuro.2020.09.036 PubMed PMID: 32950567; PubMed Central PMCID: PMC7708408.

211. Volk HE, Lurmann F, Penfold B, Hertz-Picciotto I, McConnell R. Traffic-Related Air Pollution, Particulate Matter, and Autism. JAMA Psychiatry. 2013 Jan 1;70(1):71. doi:10.1001/jamapsychiatry.2013.266

212. Kalkbrenner AE, Windham GC, Serre ML, Akita Y, Wang X, Hoffman K, et al. Particulate Matter Exposure, Prenatal and Postnatal Windows of Susceptibility, and Autism Spectrum Disorders: Epidemiology. 2015 Jan;26(1):30–42. doi:10.1097/EDE.0000000000000173

213. Chun H, Leung C, Wen SW, McDonald J, Shin HH. Maternal exposure to air pollution and risk of autism in children: A systematic review and meta-analysis. Environ Pollut. 2020 Jan;256:113307. doi:10.1016/j.envpol.2019.113307

214. Rahman MM, Shu YH, Chow T, Lurmann FW, Yu X, Martinez MP, et al. Prenatal Exposure to Air Pollution and Autism Spectrum Disorder: Sensitive Windows of Exposure and Sex Differences. Environ Health Perspect. 2022 Jan;130(1):017008. doi:10.1289/EHP9509

215. Udagawa O, Furuyama A, Imai K, Fujitani Y, Hirano S. Effects of diesel exhaust-derived secondary organic aerosol (SOA) on oocytes: Potential risks to meiotic maturation. Reprod Toxicol. 2018 Jan;75:56–64. doi:10.1016/j.reprotox.2017.11.006

216. Vecoli C, Montano L, Andreassi MG. Environmental pollutants: genetic damage and epigenetic changes in male germ cells. Environ Sci Pollut Res. 2016 Dec;23(23):23339–48. doi:10.1007/s11356-016-7728-4

217. Yauk C, Polyzos A, Rowan-Carroll A, Somers CM, Godschalk RW, Van Schooten FJ, et al. Germ-line mutations, DNA damage, and global hypermethylation in mice exposed to particulate air pollution in an urban/industrial location. Proc Natl Acad Sci U S A. 2008 Jan 15;105(2):605–10. doi:10.1073/pnas.0705896105 PubMed PMID: 18195365; PubMed Central PMCID: PMC2206583.

218. Liao J, Yan W, Zhang Y, Berhane K, Chen W, Yang Z, et al. Associations of preconception air pollution exposure with growth trajectory in young children: A prospective cohort study. Environ Res. 2025 Feb 15;267:120665. doi:10.1016/j.envres.2024.120665 PubMed PMID: 39706320; PubMed Central PMCID: PMC11878012.

219. Chen Y, Kuang T, Zhang T, Cai S, Colombo J, Harper A, et al. Associations of air pollution exposures in preconception and pregnancy with birth outcomes and infant neurocognitive development: analysis of the Complex Lipids in Mothers and Babies (CLIMB) prospective cohort in Chongqing, China. BMJ Open. 2024 Jul 2;14(7):e082475. doi:10.1136/bmjopen-2023-082475 PubMed PMID: 38960456; PubMed Central PMCID: PMC11227797.

220. Jo H, Eckel SP, Chen JC, Cockburn M, Martinez MP, Chow T, et al. Gestational diabetes mellitus, prenatal air pollution exposure, and autism spectrum disorder. Environ Int. 2019 Dec;133(Pt A):105110. doi:10.1016/j.envint.2019.105110 PubMed PMID: 31610366; PubMed Central PMCID: PMC7250244.

221. McGuinn LA, Windham GC, Kalkbrenner AE, Bradley C, Di Q, Croen LA, et al. Early Life Exposure to Air Pollution and Autism Spectrum Disorder: Findings from a Multisite Case-Control Study. Epidemiology. 2020 Jan;31(1):103–14. doi:10.1097/EDE.0000000000001109 PubMed PMID: 31592868; PubMed Central PMCID: PMC6888962.

222. Basilio E, Chen R, Fernandez AC, Padula AM, Robinson JF, Gaw SL. Wildfire Smoke Exposure during Pregnancy: A Review of Potential Mechanisms of Placental Toxicity, Impact on Obstetric Outcomes, and Strategies to Reduce Exposure. Int J Environ Res Public Health. 2022 Oct 22;19(21):13727. doi:10.3390/ijerph192113727 PubMed PMID: 36360613; PubMed Central PMCID: PMC9657128.

223. Luglio DG, Yu X, Lin JC, Chow T, Martinez MP, Chen Z, et al. Prenatal Exposure to Wildfire and Autism in Children. Environ Sci Technol. 2026 Feb 3;60(4):2907–16. doi:10.1021/acs.est.5c08256

224. O'Sharkey K, Mitra S, Chow T, Goodrich AJ, Conlon KC, Nuño M, et al. Prenatal exposure to wildfire-related PM2.5 and autism spectrum disorder in children born in California between 2001–2019. Environ Int. 2026 Feb;208:110131. doi:10.1016/j.envint.2026.110131

225. Xu R, Li S, Wu Y, Yue X, Wong EM, Southey MC, et al. Wildfire-related PM2.5 and DNA methylation: An Australian twin and family study. Environ Int. 2023 Jan;171:107704. doi:10.1016/j.envint.2022.107704

226. Brown AP, Cai L, Laufer BI, Miller LA, LaSalle JM, Ji H. Long-term effects of wildfire smoke exposure during early life on the nasal epigenome in rhesus macaques. Environ Int. 2022 Jan;158:106993. doi:10.1016/j.envint.2021.106993 PubMed PMID: 34991254; PubMed Central PMCID: PMC8852822.

227. Janssen BG, Godderis L, Pieters N, Poels K, Kiciński M, Cuypers A, et al. Placental DNA hypomethylation in association with particulate air pollution in early life. Part Fibre Toxicol. 2013 Dec;10(1):22. doi:10.1186/1743-8977-10-22

228. Ladd-Acosta C, Feinberg JI, Brown SC, Lurmann FW, Croen LA, Hertz-Picciotto I, et al. Epigenetic marks of prenatal air pollution exposure found in multiple tissues relevant for child health. Environ Int. 2019 May;126:363–76. doi:10.1016/j.envint.2019.02.028 PubMed PMID: 30826615; PubMed Central PMCID: PMC6446941.

229. Ghazi T, Naidoo P, Naidoo RN, Chuturgoon AA. Prenatal Air Pollution Exposure and Placental DNA Methylation Changes: Implications on Fetal Development and Future Disease Susceptibility. Cells. 2021 Nov 5;10(11):3025. doi:10.3390/cells10113025

230. Achenbach T, Rescorla L. Manual for the ASEBA preschool forms & profiles: An integrated system of multi-informant assessment; Child Behavior Checklist for Ages 1 1/2–5; Language Development Survey; Caregiver-teacher Report Form. Burlington: University of Vermont.; 2000.

231. Hertz-Picciotto I, Schmidt RJ, Walker CK, Bennett DH, Oliver M, Shedd-Wise KM, et al. A Prospective Study of Environmental Exposures and Early Biomarkers in Autism Spectrum Disorder: Design, Protocols, and Preliminary Data from the MARBLES Study. Environ Health Perspect. 2018 Nov;126(11):117004. doi:10.1289/EHP535

232. Lord C, Risi S, Lambrecht L, Cook EH, Leventhal BL, DiLavore PC, et al. The Autism Diagnostic Observation Schedule—Generic: A Standard Measure of Social and Communication Deficits Associated with the Spectrum of Autism. J Autism Dev Disord. 2000 Jun;30(3):205–23. doi:10.1023/A:1005592401947

233. Mullen E. Mullen scales of early learning. Circle Pines, MN: AGS; 1995.

234. Hu J, Zhang H, Chen SH, Wiedinmyer C, Vandenberghe F, Ying Q, et al. Predicting Primary $PM_{2.5}$ and $PM_{0.1}$ Trace Composition for Epidemiological Studies in California. Environ Sci Technol. 2014 May 6;48(9):4971–9. doi:10.1021/es404809j

235. Venecek MA, Yu X, Kleeman MJ. Predicted ultrafine particulate matter source contribution across the continental United States during summertime air pollution events. Atmospheric Chem Phys. 2019 Jul 23;19(14):9399–412. doi:10.5194/acp-19-9399-2019

236. Yu X, Venecek M, Kumar A, Hu J, Tanrikulu S, Soon ST, et al. Regional sources of airborne ultrafine particle number and mass concentrations in California. Atmospheric Chem Phys. 2019 Dec 5;19(23):14677–702. doi:10.5194/acp-19-14677-2019

237. Yao J, Brauer M, Henderson SB. Evaluation of a Wildfire Smoke Forecasting System as a Tool for Public Health Protection. Environ Health Perspect. 2013 Oct;121(10):1142–7. doi:10.1289/ehp.1306768

238. Kleeman MJ, Robert MA, Riddle SG, Fine PM, Hays MD, Schauer JJ, et al. Size distribution of trace organic species emitted from biomass combustion and meat charbroiling. Atmos Environ. 2008 Apr;42(13):3059–75. doi:10.1016/j.atmosenv.2007.12.044

239. Liang L, Engling G, Liu C, Xu W, Liu X, Cheng Y, et al. Measurement report: Chemical characteristics of $PM_{2.5}$ during typical biomass burning season at an agricultural site of the North China Plain. Atmospheric Chem Phys. 2021 Mar 3;21(4):3181–92. doi:10.5194/acp-21-3181-2021

240. Committee on the Chemistry of Urban Wildfires, Board on Chemical Sciences and Technology, Division on Earth and Life Studies, National Academies of Sciences, Engineering, and Medicine. The Chemistry of Fires at the Wildland-Urban Interface [Internet]. Washington, D.C.: National Academies Press; 2022 [cited 2026 Jan 13]. Available from: https://www.nationalacademies.org/publications/26460 doi:10.17226/26460

241. Zhu Y, Gomez JA, Laufer BI, Mordaunt CE, Mouat JS, Soto DC, et al. Placental methylome reveals a 22q13.33 brain regulatory gene locus associated with autism. Genome Biol. 2022 Feb 16;23(1):46. doi:10.1186/s13059-022-02613-1

242. Haghani V. Epigenerator: A Practical Workflow for Whole Genome Bisulfite Sequencing (WGBS) Analysis [Shell] [Internet]. 2025 [cited 2025 Mar 5]. Available from: https://github.com/vhaghani26/epigenerator

243. Yuan V. wvictor14/planet v2.2.34 [Internet]. Zenodo; 2020 [cited 2026 Jan 12]. Available from: https://zenodo.org/record/4321633 doi:10.5281/ZENODO.4321633

244. Aryee MJ, Jaffe AE, Corrada-Bravo H, Ladd-Acosta C, Feinberg AP, Hansen KD, et al. Minfi: a flexible and comprehensive Bioconductor package for the analysis of Infinium DNA methylation microarrays. Bioinforma Oxf Engl. 2014 May 15;30(10):1363–9. doi:10.1093/bioinformatics/btu049 PubMed PMID: 24478339; PubMed Central PMCID: PMC4016708.

245. Mordaunt CE, Mouat JS, Schmidt RJ, LaSalle JM. Comethyl: a network-based methylome approach to investigate the multivariate nature of health and disease. Brief Bioinform. 2022 Mar 10;23(2):bbab554. doi:10.1093/bib/bbab554

246. Leek JT, Storey JD. Capturing Heterogeneity in Gene Expression Studies by Surrogate Variable Analysis. Gibson G, editor. PLoS Genet. 2007 Sep 28;3(9):e161. doi:10.1371/journal.pgen.0030161

247. McLean CY, Bristor D, Hiller M, Clarke SL, Schaar BT, Lowe CB, et al. GREAT improves functional interpretation of cis-regulatory regions. Nat Biotechnol. 2010 May;28(5):495–501. doi:10.1038/nbt.1630 PubMed PMID: 20436461; PubMed Central PMCID: PMC4840234.

248. Smedley D, Haider S, Ballester B, Holland R, London D, Thorisson G, et al. BioMart – biological queries made easy. BMC Genomics. 2009 Dec;10(1):22. doi:10.1186/1471-2164-10-22

249. Cavalcante RG, Sartor MA. annotatr: genomic regions in context. Valencia A, editor. Bioinformatics. 2017 Aug 1;33(15):2381–3. doi:10.1093/bioinformatics/btx183

250. Ernst J, Kellis M. ChromHMM: automating chromatin-state discovery and characterization. Nat Methods. 2012 Mar;9(3):215–6. doi:10.1038/nmeth.1906

251. Wilcox RR. Introduction to robust estimation and hypothesis testing. 3rd ed. Amsterdam Boston: Academic Press; 2012. (Statistical modeling and decision science).

252. Laufer B, Charles M, Hyeyeon H. DMRichR [R] [Internet]. Available from: https://github.com/ben-laufer/DMRichR?tab=readme-ov-file

253. Mouat JS, Krigbaum NY, Hakam S, Thrall E, Kuodza GE, Mellis J, et al. Sex-specific DNA methylation signatures of autism spectrum disorder from whole genome bisulfite sequencing of newborn blood. Biol Sex Differ. 2025 Apr 30;16(1):30. doi:10.1186/s13293-025-00712-9

254. Mouat JS, Li X, Neier K, Zhu Y, Mordaunt CE, La Merrill MA, et al. Networks of placental DNA methylation correlate with maternal serum PCB concentrations and child neurodevelopment. Environ Res. 2023 Mar;220:115227. doi:10.1016/j.envres.2023.115227

255. Wenger DA, Rafi MA, Luzi P. Molecular genetics of Krabbe disease (globoid cell leukodystrophy): diagnostic and clinical implications. Hum Mutat. 1997;10(4):268–79. doi:10.1002/(SICI)1098-1004(1997)10:4%3C268::AID-HUMU2%3E3.0.CO;2-D PubMed PMID: 9338580.

256. Borgal L, Habbig S, Hatzold J, Liebau MC, Dafinger C, Sacarea I, et al. The ciliary protein nephrocystin-4 translocates the canonical Wnt regulator Jade-1 to the nucleus to negatively regulate β-catenin signaling. J Biol Chem. 2012 Jul 20;287(30):25370–80. doi:10.1074/jbc.M112.385658 PubMed PMID: 22654112; PubMed Central PMCID: PMC3408186.

257. Schwarting GA, Kostek C, Ahmad N, Dibble C, Pays L, Püschel AW. Semaphorin 3A is required for guidance of olfactory axons in mice. J Neurosci Off J Soc Neurosci. 2000 Oct 15;20(20):7691–7. doi:10.1523/JNEUROSCI.20-20-07691.2000 PubMed PMID: 11027230; PubMed Central PMCID: PMC6772895.

258. Acevedo LM, Barillas S, Weis SM, Göthert JR, Cheresh DA. Semaphorin 3A suppresses VEGF-mediated angiogenesis yet acts as a vascular permeability factor. Blood. 2008 Mar 1;111(5):2674–80. doi:10.1182/blood-2007-08-110205 PubMed PMID: 18180379; PubMed Central PMCID: PMC2254547.

259. Uchida Y, Ohshima T, Sasaki Y, Suzuki H, Yanai S, Yamashita N, et al. Semaphorin3A signalling is mediated via sequential Cdk5 and GSK3β phosphorylation of CRMP2: implication of common phosphorylating mechanism underlying axon guidance and Alzheimer's disease. Genes Cells. 2005 Feb;10(2):165–79. doi:10.1111/j.1365-2443.2005.00827.x

260. Chardin P. Function and regulation of Rnd proteins. Nat Rev Mol Cell Biol. 2006 Jan;7(1):54–62. doi:10.1038/nrm1788

261. Jiang CL, Jin SG, Pfeifer GP. MBD3L1 Is a Transcriptional Repressor That Interacts with Methyl-CpG-binding Protein 2 (MBD2) and Components of the NuRD Complex. J Biol Chem. 2004 Dec;279(50):52456–64. doi:10.1074/jbc.M409149200

262. Jiang CL, Jin SG, Lee DH, Lan ZJ, Xu X, O'Connor TR, et al. MBD3L1 and MBD3L2, Two New Proteins Homologous to the Methyl-CpG-Binding Proteins MBD2 and MBD3: Characterization of MBD3L1 as a Testis-Specific Transcriptional Repressor. Genomics. 2002 Dec;80(6):621–9. doi:10.1006/geno.2002.7001

263. Peng Z, Gong Y, Liang X. Role of FAT1 in health and disease (Review). Oncol Lett. 2021 Mar 18;21(5):398. doi:10.3892/ol.2021.12659

264. Ozdinler PH, Erzurumlu RS. Slit2, a branching-arborization factor for sensory axons in the Mammalian CNS. J Neurosci Off J Soc Neurosci. 2002 Jun 1;22(11):4540–9. doi:10.1523/JNEUROSCI.22-11-04540.2002 PubMed PMID: 12040061; PubMed Central PMCID: PMC4260804.

265. Lim R, Lappas M. Slit2 Exerts Anti-Inflammatory Actions in Human Placenta and is Decreased with Maternal Obesity. Am J Reprod Immunol. 2015 Jan;73(1):66–78. doi:10.1111/aji.12334

266. Liao W xiang, Wing DA, Geng JG, Chen D bao. Perspectives of SLIT/ROBO signaling in placental angiogenesis. Histol Histopathol. 2010 Sep;25(9):1181–90. doi:10.14670/HH-25.1181 PubMed PMID: 20607660; PubMed Central PMCID: PMC8900672.

267. Zhu Y, Gomez JA, Laufer BI, Mordaunt CE, Mouat JS, Soto DC, et al. Placental methylome reveals a 22q13.33 brain regulatory gene locus associated with autism.

Genome Biol. 2022 Feb 16;23(1):46. doi:10.1186/s13059-022-02613-1 PubMed PMID: 35168652; PubMed Central PMCID: PMC8848662.

268. Postolow F, Dakshinamurti S. Fetal Oxygenation during Maternal Hypoxic Illness. In: Hypoxic Respiratory Failure in the Newborn [Internet]. 1st ed. Boca Raton: CRC Press; 2021 [cited 2026 Jan 28]. p. 51–6. Available from: https://www.taylorfrancis.com/books/9780367494018/chapters/10.1201/9780367494018-10 doi:10.1201/9780367494018-10

269. Bosio A, Binczek E, Stoffel W. Functional breakdown of the lipid bilayer of the myelin membrane in central and peripheral nervous system by disrupted galactocerebroside synthesis. Proc Natl Acad Sci. 1996 Nov 12;93(23):13280–5. doi:10.1073/pnas.93.23.13280

270. Hori K, Shimaoka K, Hoshino M. AUTS2 Gene: Keys to Understanding the Pathogenesis of Neurodevelopmental Disorders. Cells. 2021 Dec 21;11(1):11. doi:10.3390/cells11010011 PubMed PMID: 35011572; PubMed Central PMCID: PMC8750789.

271. Tanaka AJ, Cho MT, Willaert R, Retterer K, Zarate YA, Bosanko K, et al. De novo variants in EBF3 are associated with hypotonia, developmental delay, intellectual disability, and autism. Cold Spring Harb Mol Case Stud. 2017 Nov;3(6):a002097. doi:10.1101/mcs.a002097 PubMed PMID: 29162653; PubMed Central PMCID: PMC5701309.

272. Christian SL, Brune CW, Sudi J, Kumar RA, Liu S, Karamohamed S, et al. Novel submicroscopic chromosomal abnormalities detected in autism spectrum disorder. Biol Psychiatry. 2008 Jun 15;63(12):1111–7. doi:10.1016/j.biopsych.2008.01.009 PubMed PMID: 18374305; PubMed Central PMCID: PMC2440346.

273. Abrahams BS, Arking DE, Campbell DB, Mefford HC, Morrow EM, Weiss LA, et al. SFARI Gene 2.0: a community-driven knowledgebase for the autism spectrum disorders (ASDs). Mol Autism. 2013 Dec;4(1):36. doi:10.1186/2040-2392-4-36

274. Gao Z, Lee P, Stafford JM, Von Schimmelmann M, Schaefer A, Reinberg D. An AUTS2–Polycomb complex activates gene expression in the CNS. Nature. 2014 Dec;516(7531):349–54. doi:10.1038/nature13921

275. Matsuda M, Ubels JL, Edelhauser HF. A larger corneal epithelial wound closes at a faster rate. Invest Ophthalmol Vis Sci. 1985 Jun;26(6):897–900. PubMed PMID: 4008202.

276. Lukin K, Fields S, Hartley J, Hagman J. Early B cell factor: Regulator of B lineage specification and commitment. Semin Immunol. 2008 Aug;20(4):221–7. doi:10.1016/j.smim.2008.07.004 PubMed PMID: 18722139; PubMed Central PMCID: PMC2577021.

277. Green YS, Vetter ML. EBF factors drive expression of multiple classes of target genes governing neuronal development. Neural Develop. 2011 Apr 30;6(1):19. doi:10.1186/1749-8104-6-19

278. Alto LT, Terman JR. Semaphorins and their Signaling Mechanisms. Methods Mol Biol. 2017;1493:1–25. doi:10.1007/978-1-4939-6448-2_1 PubMed PMID: 27787839; PubMed Central PMCID: PMC5538787.

279. Xu L, Li YH, Zhao WJ, Sang YF, Chen JJ, Li DJ, et al. RhoB Promotes Endometrial Stromal Cells Decidualization Via Semaphorin3A/PlexinA4 Signaling in Early Pregnancy. Endocrinology. 2022 Oct 11;163(11):bqac134. doi:10.1210/endocr/bqac134

280. Chen X, Qi L, Zhao C, Xue J, Chen M, Diao L, et al. Decreased expression of SEMA4D in recurrent implantation failure induces reduction of trophoblast invasion and migration via the Met/PI3K/Akt pathway. J Reprod Immunol. 2022 Sep;153:103657. doi:10.1016/j.jri.2022.103657

281. Wilson C, González-Billault C. Regulation of cytoskeletal dynamics by redox signaling and oxidative stress: implications for neuronal development and trafficking. Front Cell Neurosci. 2015;9:381. doi:10.3389/fncel.2015.00381 PubMed PMID: 26483635; PubMed Central PMCID: PMC4588006.

282. Vornic I, Buciu V, Furau CG, Gaje PN, Ceausu RA, Dumitru CS, et al. Oxidative Stress and Placental Pathogenesis: A Contemporary Overview of Potential Biomarkers and Emerging Therapeutics. Int J Mol Sci. 2024 Nov 13;25(22):12195. doi:10.3390/ijms252212195 PubMed PMID: 39596261; PubMed Central PMCID: PMC11594287.

283. Wu F, Tian FJ, Lin Y. Oxidative Stress in Placenta: Health and Diseases. BioMed Res Int. 2015;2015:293271. doi:10.1155/2015/293271 PubMed PMID: 26693479; PubMed Central PMCID: PMC4676991.

284. Chiarello DI, Ustáriz J, Marín R, Carrasco-Wong I, Farías M, Giordano A, et al. Cellular mechanisms linking to outdoor and indoor air pollution damage during pregnancy. Front Endocrinol. 2023 Feb 15;14:1084986. doi:10.3389/fendo.2023.1084986

285. Martin EM, Fry RC. A cross-study analysis of prenatal exposures to environmental contaminants and the epigenome: support for stress-responsive transcription factor occupancy as a mediator of gene-specific CpG methylation patterning. Environ Epigenetics. 2016 Jan;2(1):dvv011. doi:10.1093/eep/dvv011 PubMed PMID: 27066266; PubMed Central PMCID: PMC4824001.

286. Ladd-Acosta C, Feinberg JI, Brown SC, Lurmann FW, Croen LA, Hertz-Picciotto I, et al. Epigenetic marks of prenatal air pollution exposure found in multiple tissues relevant for child health. Environ Int. 2019 May;126:363–76.

doi:10.1016/j.envint.2019.02.028 PubMed PMID: 30826615; PubMed Central PMCID: PMC6446941.

287. Brose K, Bland KS, Wang KH, Arnott D, Henzel W, Goodman CS, et al. Slit Proteins Bind Robo Receptors and Have an Evolutionarily Conserved Role in Repulsive Axon Guidance. Cell. 1999 Mar;96(6):795–806. doi:10.1016/S0092-8674(00)80590-5

288. Rebecchi MJ, Pentyala SN. Structure, Function, and Control of Phosphoinositide-Specific Phospholipase C. Physiol Rev. 2000 Jan 10;80(4):1291–335. doi:10.1152/physrev.2000.80.4.1291

289. Bohnekamp J, Schöneberg T. Cell adhesion receptor GPR133 couples to Gs protein. J Biol Chem. 2011 Dec 9;286(49):41912–6. doi:10.1074/jbc.C111.265934 PubMed PMID: 22025619; PubMed Central PMCID: PMC3234928.

290. Ikenouchi J, Umeda M. FRMD4A regulates epithelial polarity by connecting Arf6 activation with the PAR complex. Proc Natl Acad Sci. 2010 Jan 12;107(2):748–53. doi:10.1073/pnas.0908423107

291. Shallie PD, Naicker T. The placenta as a window to the brain: A review on the role of placental markers in prenatal programming of neurodevelopment. Int J Dev Neurosci. 2019 Apr;73(1):41–9. doi:10.1016/j.ijdevneu.2019.01.003

292. Leni Z, Künzi L, Geiser M. Air pollution causing oxidative stress. Curr Opin Toxicol. 2020 Apr;20–21:1–8. doi:10.1016/j.cotox.2020.02.006

293. Milani C, Farina F, Botto L, Massimino L, Lonati E, Donzelli E, et al. Systemic Exposure to Air Pollution Induces Oxidative Stress and Inflammation in Mouse Brain, Contributing to Neurodegeneration Onset. Int J Mol Sci. 2020 May 24;21(10):3699. doi:10.3390/ijms21103699 PubMed PMID: 32456361; PubMed Central PMCID: PMC7279458.

294. Graziano ACE, Cardile V. History, genetic, and recent advances on Krabbe disease. Gene. 2015 Jan;555(1):2–13. doi:10.1016/j.gene.2014.09.046

295. Sherchan P, Travis ZD, Tang J, Zhang JH. The potential of Slit2 as a therapeutic target for central nervous system disorders. Expert Opin Ther Targets. 2020 Aug;24(8):805–18. doi:10.1080/14728222.2020.1766445 PubMed PMID: 32378435; PubMed Central PMCID: PMC7529836.

296. Lim YC, Li J, Ni Y, Liang Q, Zhang J, Yeo GSH, et al. A complex association between DNA methylation and gene expression in human placenta at first and third trimesters. PloS One. 2017;12(7):e0181155. doi:10.1371/journal.pone.0181155 PubMed PMID: 28704530; PubMed Central PMCID: PMC5509291.

297. Schroeder DI, Blair JD, Lott P, Yu HOK, Hong D, Crary F, et al. The human placenta methylome. Proc Natl Acad Sci. 2013 Apr 9;110(15):6037–42. doi:10.1073/pnas.1215145110

298. Sibley CP. Understanding placental nutrient transfer--why bother? New biomarkers of fetal growth. J Physiol. 2009 Jul 15;587(Pt 14):3431–40. doi:10.1113/jphysiol.2009.172403 PubMed PMID: 19417095; PubMed Central PMCID: PMC2742272.

299. Schröder HJ. Comparative aspects of placental exchange functions. Eur J Obstet Gynecol Reprod Biol. 1995 Nov;63(1):81–90. doi:10.1016/0301-2115(95)02206-M

300. Brown AP, Cai L, Laufer BI, Miller LA, LaSalle JM, Ji H. Long-term effects of wildfire smoke exposure during early life on the nasal epigenome in rhesus macaques. Environ Int. 2022 Jan;158:106993. doi:10.1016/j.envint.2021.106993

301. Laufer BI, Hasegawa Y, Zhang Z, Hogrefe CE, Del Rosso LA, Haapanen L, et al. Multi-omic brain and behavioral correlates of cell-free fetal DNA methylation in macaque maternal obesity models. Nat Commun. 2022 Sep 21;13(1):5538. doi:10.1038/s41467-022-33162-7

302. Alberry M, Maddocks D, Jones M, Abdel Hadi M, Abdel-Fattah S, Avent N, et al. Free fetal DNA in maternal plasma in anembryonic pregnancies: confirmation that the origin is the trophoblast. Prenat Diagn. 2007 May;27(5):415–8. doi:10.1002/pd.1700

303. Leibovitz Z, Lerman-Sagie T, Haddad L. Fetal Brain Development: Regulating Processes and Related Malformations. Life. 2022 May 29;12(6):809. doi:10.3390/life12060809 PubMed PMID: 35743840; PubMed Central PMCID: PMC9224903.

304. Bakulski KM, Dou JF, Feinberg JI, Aung MT, Ladd-Acosta C, Volk HE, et al. Autism-Associated DNA Methylation at Birth From Multiple Tissues Is Enriched for Autism Genes in the Early Autism Risk Longitudinal Investigation. Front Mol Neurosci. 2021;14:775390. doi:10.3389/fnmol.2021.775390 PubMed PMID: 34899183; PubMed Central PMCID: PMC8655859.

305. Masi A, DeMayo MM, Glozier N, Guastella AJ. An Overview of Autism Spectrum Disorder, Heterogeneity and Treatment Options. Neurosci Bull. 2017 Apr;33(2):183–93. doi:10.1007/s12264-017-0100-y

306. Siegel M, Beaulieu AA. Psychotropic Medications in Children with Autism Spectrum Disorders: A Systematic Review and Synthesis for Evidence-Based Practice. J Autism Dev Disord. 2012 Aug;42(8):1592–605. doi:10.1007/s10803-011-1399-2

307. Uljarević M, Phillips JM, Schuck RK, Schapp S, Solomon EM, Salzman E, et al. Exploring Social Subtypes in Autism Spectrum Disorder: A Preliminary Study. Autism Res. 2020 Aug;13(8):1335–42. doi:10.1002/aur.2294

308. Bohane L, Maguire N, Richardson T. Resilients, overcontrollers and undercontrollers: A systematic review of the utility of a personality typology method in understanding adult mental health problems. Clin Psychol Rev. 2017 Nov;57:75–92. doi:10.1016/j.cpr.2017.07.005

309. Agelink van Rentergem JA, Deserno MK, Geurts HM. Validation strategies for subtypes in psychiatry: A systematic review of research on autism spectrum disorder. Clin Psychol Rev. 2021 Jul;87:102033. doi:10.1016/j.cpr.2021.102033

310. Wolfers T, Floris DL, Dinga R, van Rooij D, Isakoglou C, Kia SM, et al. From pattern classification to stratification: towards conceptualizing the heterogeneity of Autism Spectrum Disorder. Neurosci Biobehav Rev. 2019 Sep;104:240–54. doi:10.1016/j.neubiorev.2019.07.010

311. Casanova MF, Casanova EL, Frye RE, Baeza-Velasco C, LaSalle JM, Hagerman RJ, et al. Editorial: Secondary vs. Idiopathic Autism. Front Psychiatry. 2020 Apr 14;11:297. doi:10.3389/fpsyt.2020.00297

312. Palladino VS, McNeill R, Reif A, Kittel-Schneider S. Genetic risk factors and gene–environment interactions in adult and childhood attention-deficit/hyperactivity disorder. Psychiatr Genet. 2019 Jun;29(3):63–78. doi:10.1097/YPG.0000000000000220

313. Schiele MA, Domschke K. Epigenetics at the crossroads between genes, environment and resilience in anxiety disorders: Epigenetics in anxiety disorders. Genes Brain Behav. 2018 Mar;17(3):e12423. doi:10.1111/gbb.12423

314. Lee EC, Hu VW. Phenotypic Subtyping and Re-Analysis of Existing Methylation Data from Autistic Probands in Simplex Families Reveal ASD Subtype-Associated Differentially Methylated Genes and Biological Functions. Int J Mol Sci. 2020 Sep 19;21(18):6877. doi:10.3390/ijms21186877

315. Brett D, Warnell F, McConachie H, Parr JR. Factors Affecting Age at ASD Diagnosis in UK: No Evidence that Diagnosis Age has Decreased Between 2004 and 2014. J Autism Dev Disord. 2016 Jun;46(6):1974–84. doi:10.1007/s10803-016-2716-6

316. Neimy H, Pelaez M, Carrow J, Monlux K, Tarbox J. Infants at risk of autism and developmental disorders: Establishing early social skills. Behav Dev Bull. 2017 Apr;22(1):6–22. doi:10.1037/bdb0000046

317. Malik-Soni N, Shaker A, Luck H, Mullin AE, Wiley RE, Lewis MES, et al. Tackling healthcare access barriers for individuals with autism from diagnosis to adulthood. Pediatr Res. 2021 Mar 25. doi:10.1038/s41390-021-01465-y PubMed PMID: 33767375; PubMed Central PMCID: PMC7993081.

318. Kodak T, Bergmann S. Autism Spectrum Disorder. Pediatr Clin North Am. 2020 Jun;67(3):525–35. doi:10.1016/j.pcl.2020.02.007

319. Blanc R, Latinus M, Guidotti M, Adrien JL, Roux S, Dansart P, et al. Early Intervention in Severe Autism: Positive Outcome Using Exchange and Development Therapy. Front Pediatr. 2021 Dec 15;9:785762. doi:10.3389/fped.2021.785762

320. Pierce K, Gazestani V, Bacon E, Courchesne E, Cheng A, Barnes CC, et al. Get SET Early to Identify and Treatment Refer Autism Spectrum Disorder at 1 Year and Discover Factors That Influence Early Diagnosis. J Pediatr. 2021 Sep;236:179–88. doi:10.1016/j.jpeds.2021.04.041

321. Green J, Pickles A, Pasco G, Bedford R, Wan MW, Elsabbagh M, et al. Randomised trial of a parent-mediated intervention for infants at high risk for autism: longitudinal outcomes to age 3 years. J Child Psychol Psychiatry. 2017 Dec;58(12):1330–40. doi:10.1111/jcpp.12728

322. Whitehouse AJO, Varcin KJ, Pillar S, Billingham W, Alvares GA, Barbaro J, et al. Effect of Preemptive Intervention on Developmental Outcomes Among Infants Showing Early Signs of Autism: A Randomized Clinical Trial of Outcomes to Diagnosis. JAMA Pediatr. 2021 Nov 1;175(11):e213298. doi:10.1001/jamapediatrics.2021.3298

323. Janšáková K, Kyselicová K, Ostatníková D, Repiská G. Potential of Salivary Biomarkers in Autism Research: A Systematic Review. Int J Mol Sci. 2021 Oct 8;22(19):10873. doi:10.3390/ijms221910873

324. Wang Y, Zhang J, Song W, Tian X, Liu Y, Wang Y, et al. A proteomic analysis of urine biomarkers in autism spectrum disorder. J Proteomics. 2021 Jun;242:104259. doi:10.1016/j.jprot.2021.104259

325. Bjørklund G, Meguid NA, El-Ansary A, El-Bana MA, Dadar M, Aaseth J, et al. Diagnostic and Severity-Tracking Biomarkers for Autism Spectrum Disorder. J Mol Neurosci. 2018 Dec;66(4):492–511. doi:10.1007/s12031-018-1192-1

326. Génin E. Missing heritability of complex diseases: case solved? Hum Genet. 2020 Jan;139(1):103–13. doi:10.1007/s00439-019-02034-4

327. Gui A, Jones EJH, Wong CCY, Meaburn E, Xia B, Pasco G, et al. Leveraging epigenetics to examine differences in developmental trajectories of social attention: A proof-of-principle study of DNA methylation in infants with older siblings with autism. Infant Behav Dev. 2020 Aug;60:101409. doi:10.1016/j.infbeh.2019.101409

328. Lo YMD, Han DSC, Jiang P, Chiu RWK. Epigenetics, fragmentomics, and topology of cell-free DNA in liquid biopsies. Science. 2021 Apr 9;372(6538):eaaw3616. doi:10.1126/science.aaw3616

329. Chiu RWK, Lo YMD. Cell-free fetal DNA coming in all sizes and shapes. Prenat Diagn. 2021 Sep;41(10):1193–201. doi:10.1002/pd.5952

330. Laufer BI, Hasegawa Y, Zhang Z, Hogrefe CE, Del Rosso LA, Haapanan L, et al. Multi-omic brain and behavioral correlates of cell-free fetal DNA methylation in macaque maternal obesity models [preprint] [Internet]. Genomics; 2021 Aug [cited 2022 Apr 29]. Available from:

http://biorxiv.org/lookup/doi/10.1101/2021.08.27.457952
doi:10.1101/2021.08.27.457952

331. Lei XY, Li YJ, Ou JJ, Li YM. Association between parental body mass index and autism spectrum disorder: a systematic review and meta-analysis. Eur Child Adolesc Psychiatry. 2019 Jul;28(7):933–47. doi:10.1007/s00787-018-1259-0 PubMed PMID: 30470952.

332. Grosswendt S, Kretzmer H, Smith ZD, Kumar AS, Hetzel S, Wittler L, et al. Epigenetic regulator function through mouse gastrulation. Nature. 2020 Aug 6;584(7819):102–8. doi:10.1038/s41586-020-2552-x

333. Michowski W, Chick JM, Chu C, Kolodziejczyk A, Wang Y, Suski JM, et al. Cdk1 Controls Global Epigenetic Landscape in Embryonic Stem Cells. Mol Cell. 2020 May;78(3):459-476.e13. doi:10.1016/j.molcel.2020.03.010

334. Dimitrova E, Turberfield AH, Klose RJ. Histone demethylases in chromatin biology and beyond. EMBO Rep. 2015 Dec;16(12):1620–39. doi:10.15252/embr.201541113

335. Wu Z, Connolly J, Biggar KK. Beyond histones - the expanding roles of protein lysine methylation. FEBS J. 2017 Sep;284(17):2732–44. doi:10.1111/febs.14056

336. Morgan MAJ, Shilatifard A. Reevaluating the roles of histone-modifying enzymes and their associated chromatin modifications in transcriptional regulation. Nat Genet. 2020 Dec;52(12):1271–81. doi:10.1038/s41588-020-00736-4

337. Stricker SH, Köferle A, Beck S. From profiles to function in epigenomics. Nat Rev Genet. 2017 Jan;18(1):51–66. doi:10.1038/nrg.2016.138

338. Liu XS, Wu H, Krzisch M, Wu X, Graef J, Muffat J, et al. Rescue of Fragile X Syndrome Neurons by DNA Methylation Editing of the FMR1 Gene. Cell. 2018 Feb;172(5):979-992.e6. doi:10.1016/j.cell.2018.01.012

339. Nuñez JK, Chen J, Pommier GC, Cogan JZ, Replogle JM, Adriaens C, et al. Genome-wide programmable transcriptional memory by CRISPR-based epigenome editing. Cell. 2021 Apr;184(9):2503-2519.e17. doi:10.1016/j.cell.2021.03.025

340. Xu X, Tan X, Tampe B, Wilhelmi T, Hulshoff MS, Saito S, et al. High-fidelity CRISPR/Cas9- based gene-specific hydroxymethylation rescues gene expression and attenuates renal fibrosis. Nat Commun. 2018 Dec;9(1):3509. doi:10.1038/s41467-018-05766-5

341. Gomez JA, Beitnere U, Segal DJ. Live Animal Epigenome Editing: Convergence of Novel Techniques. Trends Genet TIG. 2019 Jul;35(7):527–41. doi:10.1016/j.tig.2019.04.007 PubMed PMID: 31128888; PubMed Central PMCID: PMC6608710.

342. Deverman BE, Ravina BM, Bankiewicz KS, Paul SM, Sah DWY. Gene therapy for neurological disorders: progress and prospects. Nat Rev Drug Discov. 2018 Sep;17(9):641–59. doi:10.1038/nrd.2018.110 PubMed PMID: 30093643.

343. Ripamonti L. Disability, Diversity, and Autism: Philosophical Perspectives on Health. New Bioeth. 2016 Jan 2;22(1):56–70. doi:10.1080/20502877.2016.1151256

344. Schuck RK, Tagavi DM, Baiden KMP, Dwyer P, Williams ZJ, Osuna A, et al. Neurodiversity and Autism Intervention: Reconciling Perspectives Through a Naturalistic Developmental Behavioral Intervention Framework. J Autism Dev Disord. 2021 Oct 13. doi:10.1007/s10803-021-05316-x

345. Bey AL, Jiang Y. Overview of Mouse Models of Autism Spectrum Disorders. Curr Protoc Pharmacol. 2014 Sep;66(1). doi:10.1002/0471141755.ph0566s66

346. Qin L, Ma K, Wang ZJ, Hu Z, Matas E, Wei J, et al. Social deficits in Shank3-deficient mouse models of autism are rescued by histone deacetylase (HDAC) inhibition. Nat Neurosci. 2018 Apr;21(4):564–75. doi:10.1038/s41593-018-0110-8

347. Clark DF, Schmelz R, Rogers N, Smith NE, Shorter KR. Acute high folic acid treatment in SH-SY5Y cells with and without MTHFR function leads to gene expression changes in epigenetic modifying enzymes, changes in epigenetic marks, and changes in dendritic spine densities. Chiariotti L, editor. PLOS ONE. 2021 Jan 7;16(1):e0245005. doi:10.1371/journal.pone.0245005

348. Shen T, Ji F, Wang Y, Lei X, Zhang D, Jiao J. Brain-specific deletion of histone variant H2A.z results in cortical neurogenesis defects and neurodevelopmental disorder. Nucleic Acids Res. 2018 Mar 16;46(5):2290–307. doi:10.1093/nar/gkx1295

349. Lu Z, Liu Z, Mao W, Wang X, Zheng X, Chen S, et al. Locus-specific DNA methylation of Mecp2 promoter leads to autism-like phenotypes in mice. Cell Death Dis. 2020 Feb;11(2):85. doi:10.1038/s41419-020-2290-x

350. Chen J, Lambo ME, Ge X, Dearborn JT, Liu Y, McCullough KB, et al. A MYT1L syndrome mouse model recapitulates patient phenotypes and reveals altered brain development due to disrupted neuronal maturation. Neuron. 2021 Dec;109(23):3775-3792.e14. doi:10.1016/j.neuron.2021.09.009

351. Nicolini C, Fahnestock M. The valproic acid-induced rodent model of autism. Exp Neurol. 2018 Jan;299:217–27. doi:10.1016/j.expneurol.2017.04.017

352. Haddad FL, Patel SV, Schmid S. Maternal Immune Activation by Poly I:C as a preclinical Model for Neurodevelopmental Disorders: A focus on Autism and Schizophrenia. Neurosci Biobehav Rev. 2020 Jun;113:546–67. doi:10.1016/j.neubiorev.2020.04.012

353. Meyza KZ, Blanchard DC. The BTBR mouse model of idiopathic autism – Current view on mechanisms. Neurosci Biobehav Rev. 2017 May;76:99–110. doi:10.1016/j.neubiorev.2016.12.037